



# pennsylvania

DEPARTMENT OF TRANSPORTATION

## Storm Water Control Management & Monitoring

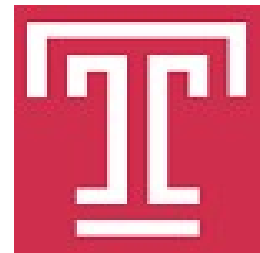
FINAL REPORT

November 30, 2017

By Laura Toran  
Temple University

COMMONWEALTH OF PENNSYLVANIA  
DEPARTMENT OF TRANSPORTATION

CONTRACT # 4400011166  
WORK ORDER # TEM 006



<b>1. Report No.</b> FHWA-PA-2017-005-TEM WO 06	<b>2. Government Accession No.</b>	<b>3. Recipient's Catalog No.</b>	
<b>4. Title and Subtitle</b>  Storm Water Control Management & Monitoring		<b>5. Report Date</b> 11/30/2017	
		<b>6. Performing Organization Code</b>	
<b>7. Author(s)</b> Laura Toran, Sasha Eisenman, Joshua Caplan, Benoit van Aken, Erica McKenzie, Jonathan Nyquist, Robert Ryan, John Kelley, Robert Traver, Min-Cheng Tu, Nora Schmidt, Elizabeth Calt		<b>8. Performing Organization Report No.</b>	
<b>9. Performing Organization Name and Address</b>  Temple University 1801 N Broad St Philadelphia, PA 19122		<b>10. Work Unit No. (TRAIS)</b>	
		<b>11. Contract or Grant No.</b> 4400011166, TEM WO 6	
<b>12. Sponsoring Agency Name and Address</b>  The Pennsylvania Department of Transportation Bureau of Planning and Research Commonwealth Keystone Building 400 North Street, 6 <sup>th</sup> Floor Harrisburg, PA 17120-0064		<b>13. Type of Report and Period Covered</b>  Final Report 12/01/2016 – 11/30/2017	
		<b>14. Sponsoring Agency Code</b>	
<b>15. Supplementary Notes</b> Technical advisor is Daryl St. Clair, Special Assistant, Highway Administration, Deputy Secretary's Office, PA Dept of Transportation, 400 North Street – 8 <sup>th</sup> Floor, Harrisburg, PA 17120 717-787-9512; dstclair@pa.gov			
<b>16. Abstract</b> Temple and Villanova universities collected monitoring and assessment data along the I-95 corridor to evaluate the performance of current stormwater control design and maintenance practices. An extensive inventory was developed that ranks plants in the basins according to their health and location. Three plant species performed poorly in bioretention design and alternatives are proposed. Grab samples were collected for storms approximately monthly and analyzed for a variety of road runoff constituents. Although a full year of data was not yet available, annual loading for total suspended solids (TSS) and nutrients were estimated. LiDAR data helped show that variations in basin performance occurred due to changes in stormwater capture during construction. Simulated runoff tests (SRTs) were conducted to study response during a large volume event. These SRTs were valuable in quantifying drainage areas and improving monitoring strategies. Recommendations are provided on hydrologic design, potential contaminant mobility, planting, and maintenance.			
<b>17. Key Words</b>  Stormwater, bioswale, I-95, infiltration, hydrologic monitoring, simulated runoff test, trace metals, TSS, LiDAR, SWMM, plant characterization, maintenance practices		<b>18. Distribution Statement</b> No restrictions. This document is available from the National Technical Information Service, Springfield, VA 22161	
<b>19. Security Classif. (of this report)</b>  Unclassified	<b>20. Security Classif. (of this page)</b>  Unclassified	<b>21. No. of Pages</b>  335	<b>22. Price</b>  N/A



**Disclaimer:**

The contents of this report reflect the views of the authors who are responsible for the facts and the accuracy of the data presented herein. The contents do not necessarily reflect the official views or policies of the US Department of Transportation, Federal Highway Administration, or the Commonwealth of Pennsylvania at the time of publication. This report does not constitute a standard, specification or regulation.

**Statement of credit:**

This work was sponsored by the Pennsylvania Department of Transportation and the U.S. Department of Transportation, Federal Highway Administration.

# **Storm Water Control Management and Monitoring**

Temple University Master Agreement

Contract No. 4400011166

Work Order TEM 006

## **Task 9: Final Report**

November 30, 2017

### **Prepared By:**

Laura Toran

Sasha Eisenman

Joshua Caplan

Benoit van Aken

Erica McKenzie

Jonathan Nyquist

Robert Ryan

John Kelley

### **Temple University**

Robert Traver

Min-Cheng Tu

Nora Schmidt

Elizabeth Calt

### **Villanova University**

## Table of Contents

Table of Contents .....	iv
Executive Summary .....	ix
Chapter 1: Report Organization .....	1
Chapter 2: Baseline monitoring for groundwater conditions.....	3
Methods.....	3
Baseline Monitoring Well Construction .....	3
Baseline Monitoring Well Locations .....	6
Hydrologic Monitoring .....	6
Spatial and Statistical Analyses .....	8
Results.....	9
Precipitation records .....	9
Water level records .....	9
Tidal response .....	16
Differences between wells .....	17
Patterns in Groundwater Temperature and Conductivity Data.....	20
Implications.....	23
Distance Between SMP and Water Table.....	23
Seasonal Variation in Conductivity .....	25
Influence of Historic Stream Channels and Urban Legacies .....	26
References.....	26
Chapter 3: Hydrologic monitoring.....	28
Introduction.....	28
History of Site .....	30
Size & Drainage Area .....	30
Monitoring Design .....	35
Data Acquisition .....	36
Weather Sensors.....	37
Inflow Sensors .....	40
Flow Measurement.....	42
SMP Hydrologic Monitoring Results .....	58

Weather Station Data .....	58
SMP Runoff Tracking.....	60
SMP Rainfall Response .....	66
Simulated Runoff Test .....	68
Future Work and SMP Functionality.....	72
References.....	73
Chapter 4: Water Quality Monitoring.....	76
Introduction.....	76
Methods.....	78
Stormwater Sampling – Grab Samples .....	78
Groundwater Sample Collection.....	79
Simulation Runoff Tests (SRTs).....	80
Lysimeter Installation .....	81
Installation of Stormwater Sampling Bottles and Autosamplers.....	84
Monitoring plan .....	87
Sample Handling, Preservation, and Storage.....	87
Analyses.....	88
Load Calculation .....	90
Results and Discussion .....	90
Influent Water Quality – General Parameters.....	90
Influent Water Quality – Metals .....	101
Subsurface Water Quality .....	107
Simulated Runoff Tests (SRTs).....	121
Contaminant Loads .....	123
Quality assurance and quality control.....	126
Chapter 5: LiDAR Scanning and Data Processing .....	131
Methods for Digital Elevation Models .....	131
LiDAR Scanning to Map Stormwater Basins .....	134
Calculation of I-95 Storm Drain Capture Areas .....	137
Remarks on Terrestrial LiDAR Utility .....	142
Chapter 6: SMP Computer Modeling .....	144
Introduction.....	144

Methods.....	144
SWMM Modeling.....	144
Model Calibration Procedure.....	164
Model Evaluation.....	169
Site Data to Date .....	171
SWMM Results.....	172
Inflow Calibration.....	173
Pond Calibration and Discussion.....	188
SWMM Modeling Conclusions .....	196
Coupling the Hydrologic Model with the Fate of Contaminants.....	200
Observed Pollutant Removal Rates .....	200
Total Suspended Solids Removal Algorithm.....	203
Total Phosphorus Removal Algorithm .....	204
Nitrogen removal algorithm.....	205
Evaluation of Computational Water Quality Models .....	207
SWMM (Storm Water Management Model).....	207
WASP (Water Quality Assessment Program) .....	207
AQUATOX.....	208
EFDC (Environmental Fluid Dynamics Code).....	209
Infoworks ICM (Integrated Catchment Model).....	209
MATLAB.....	209
Water Quality Modeling Summary.....	210
Computational Models.....	210
Refinement of Algorithms for Water Quality Modeling .....	210
Model Calibration and Comparison to Design Expectations.....	212
References.....	212
Chapter 7: Plant monitoring.....	220
Introduction.....	220
Methods.....	222
Plant Survival and General Health.....	222
Gradient Approach.....	225
Topographic Variation in Plant Health .....	229

Spontaneous Vegetation.....	232
Contaminant Uptake .....	232
Soil Contaminants .....	233
Results and Discussion .....	234
Plant Survival and General Health.....	234
Taxonomic Discrepancies .....	240
Spontaneous Vegetation.....	241
Topographic Variation in Plant Health .....	242
Leaf-level Physiology .....	245
Soil Contaminants.....	258
References.....	262
Chapter 8: Maintenance and SMP Functionality .....	264
Introduction.....	264
Methods.....	264
Results.....	266
Maintenance requirements and evaluation.....	266
Drainage and erosion .....	274
Trash issues .....	274
Soil amendments .....	275
References.....	276
Chapter 9:.....	278
Recommended Changes to Future SMP Designs and Placement Plan.....	278
Recommendations on Hydrologic Design .....	278
Watershed drainage design – temporary phases .....	278
SMP construction evaluation .....	279
Instrumentation in support of SMP monitoring.....	280
Observations on hydrologic monitoring and modeling .....	280
Recommendations on Contaminant Accumulation and Mobility.....	281
Contaminant remobilization.....	282
Preferential flow paths in SMPs and lesson from the use of tracers.....	283
Recommendations on Planting Designs.....	284
Avoid intolerant plants.....	284

Expand the use of stress-tolerant plants.....	285
Overplanting .....	286
Other recommendations.....	286
Alternative design strategies .....	287
Improvements to the amended soil .....	288
Recommendations for SMP Maintenance .....	288
Weed removal .....	288
Removal of litter and dog waste .....	289
Erosion reduction .....	290
Drainage.....	291
Recommendations of Community Adoption .....	292
Final Observations .....	292
Appendix 1: Baseline well drilling logs.....	294
Appendix 2: Monitoring and modeling of SMP A .....	296
Appendix 3: Calculation of loads in SMPs C and D .....	311

## Executive Summary

### Statement of task

The Pennsylvania Department of Transportation (PennDOT) is incorporating extensive green stormwater infrastructure into the redesign of the I-95 corridor in Philadelphia, which will take place over the next 25 years. These stormwater management practices (SMPs) are designed to capture the first inch or more of stormwater that falls on the highway and allow it to infiltrate rather than enter the storm sewer network. The use of SMPs to manage stormwater runoff stems from requirements of the Pennsylvania Department of Environmental Protection and the Philadelphia Water Department's *Green City, Clean Waters* program, which were designed to address combined sewer overflow problems in Philadelphia. SMPs are also expected to improve runoff water quality and mitigate spills on roadways. The latter will help PennDOT comply with the permitting requirements of the National Pollutant Discharge Elimination System (NPDES) of the Clean Water Act.

Scientists and engineers at Temple and Villanova Universities collected monitoring and assessment data along the Girard Avenue Interchange (GIR) to evaluate the performance of current stormwater control, design and maintenance practices. This group has worked together since 2005 to advance the knowledge base of stormwater management in the Philadelphia region and nationally. The research program includes monitoring, modeling, and assessment, with the goal of providing data-driven recommendations to PennDOT and its consultants for improving SMP design and maintenance practices. While SMPs have been used in transportation projects throughout the United States, the technology is still evolving. The magnitude of the I-95 stormwater infrastructure design, which will contain as many as 75-80 SMPs, presents an opportunity to conduct a rigorous evaluation of the first phase of construction to ensure that future SMPs are located, designed, and maintained to function optimally.

This report covers the first year of study on the I-95/GIR SMPs, specifically SMPs A, C, D, and G (also known as basins A, C, D, and G). The Temple and Villanova teams addressed the following critical areas: (1) characterization of the groundwater table along the corridor, (2) impact of urban soil and fill, (3) hydrologic performance and stormflow characterization, (4) geochemical characterization of stormwater runoff, (5) plant performance, and (6) maintenance strategies. The initial period involved monitoring design and installation of equipment. Approximately seven months of hydrologic monitoring is described, together with nine months of plant monitoring and maintenance; periods vary by basin. In addition, to supplement natural storm events, simulated runoff tests (SRTs) were conducted in three basins to evaluate their response to a large volume event. The runoff was simulated by releasing water from fire hydrants at the SMP inlet pipes. These tests were conducted in cooperation with the Philadelphia Water Department.

This executive summary provides highlights of findings and recommendations from the first year of study; more detailed data and discussion are included in the main report. While a great deal has been learned in this initial monitoring period, there are also limitations to the study. The



findings are based on short-term behavior in the basins; additional understanding of basin behavior will require a longer period of monitoring.

### **Storms monitored and estimated capture areas**

This executive summary provides an overview of the observed rainfall, observed inflows spanning the monitoring period, and different estimates of basin capture areas. Every SMP is designed to capture and infiltrate a specific quantity of water. The performance of a basin can in part be evaluated by comparing the planned and realized capture (or drainage) areas. Actual capture areas are calculated by dividing measured inflow by rainfall amounts (Table E-1) and assuming a uniform distribution of rain during an event. The actual capture areas for individual inlet structures is presented as a percentage of the designed drainage areas for each inlet to evaluate how much water was received for each storm.

Almost all of the basins monitored received lower volumes than expected. A consequence of lower capture volumes was 100% removal efficiency (no outflow) in SMPs C and D during the monitoring period (as discussed in the next section). With the exception of inlet N9 (within SMP A), realized capture areas were substantially smaller than their designed capture areas. Percentages ranged from 1-80% for SMP A (Table E-1a) and from 2-50% for SMPs C, D, and G (Table E-1b, also reported in Chapter 6). Inlet N9 sometimes had volumes greater than 100%, probably as a result of water from N8 being redirected to N9.

The large variation in captured volumes for each inlet across storms suggests that the drainage areas were not constant through the period of study. It is likely that this variation was due to changing conditions in the drained region of the highway. For example, the grate over one of the highway inlets draining to SMPs D and G was blocked by construction equipment, but the length of time it was blocked is unknown. For N8 the observed drainage area was less than 7% of what was expected for ten of the reported 12 storms, leading to the conclusion that the piping system was blocked as a temporary construction measure or leaking. Values were 20% and 13.8% for the remaining two events. Both of these are larger rain events, suggesting changes in stormwater capture area may have increased flow. As mentioned above, flow recorded at N9 exceeds the volumes expected from the drainage areas based on design plans in some cases (showing capture areas >100%). It may be that water crossed a flow divide or piping restrictions were overcome in these storm events. Clearly, monitoring is important to evaluate such changes during and after construction to identify and remove blockages and to take into account variations in system performance.

A detailed microtopographical analysis was conducted to more precisely determine why observed stormwater capture areas differed from those expected from planning documents. Accurate drainage area values were also needed to carry out sediment and contaminant loading estimates (next section) and provide watershed areas for modeling. LiDAR surveys of the highway provided elevation data that were used together with updated inlet coordinates to calculate flow routing and estimate capture areas with ArcGIS (Figures E-1-4). These were then compared to areas from design plans (Table E-2). The data presented here supersede values presented in Chapter 6 of the report. However, design plans were used for modeling SMPs C, D, and G in Chapter 6.

The maps of capture area show separate drainage to the N inlets along the sidewall and M inlets in the center of the highway due to the variation in microtopography mapped with LiDAR. In SMP A (Figure E-1 and E-2), several small drainage areas leading to several of the M inlets connect to the N8 inlet before entering SMP A. According to the LiDAR-based flow paths, a substantial area bypasses the inlets for SMP A. Note that the drainage area of the small ramp traveling down the embankment to SMP A has not yet been evaluated, and could raise the capture area by another 0.1 acre. In Figures E-3 and E-4, the large maroon area is piped to N7 (SMP C), and the smaller pale blue area is piped to N5 (SMP G). AECOM recently discovered that a revised plan set showed this blue drainage was split between two pipes, which would reduce the area by about half.

Barriers placed on the highway during construction have openings that allow stormwater runoff to reach drains, but these openings can easily become clogged. Thus, the highway rainfall capture areas were calculated both without barriers (Figures E1 and E-3) and with the barriers restricting flow (Figures E-2 and E-4). Diversion of stormwater due to the barriers had the largest effect on Basin A, reducing the capture area from 0.39 to 0.24 acres (summing N8, N9, and N10 in Table E-2). The arrangement of the barriers near Basin C lead to a slight increase in capture area from 0.24 to 0.29 acres as water diverted from Basin D flowed into Basin C instead (Figure E4, enlarged green area). There was no diversion near Basin G.

The largest difference between design and LiDAR-derived capture areas occurred for Basin A which captured about one third of the designed stormwater. The estimated drainage areas were closer to design in SMPs C, D, and G, but were still smaller. These capture areas should be reevaluated using LiDAR after construction is finished and compared to observed inflow monitoring data.

While surface grading reduced effective capture areas, this does not entirely account for the lower observed inflows to the basin (Table E-1). Adjusting the stormwater capture area estimates by eliminating piping from the center drains provides a closer match to measured volumes. As mentioned above, it is possible that drains in the middle of the highway are blocked as a temporary construction practice or they may be leaking. However, the drains cannot be physically checked without shutting down the highway. Further exploration by remote monitoring will be conducted. Note that the roadway surface will not receive final grading until sometime in the future, when it is expected that the drainage areas will be more similar to those specified in the design plans.

For loading calculations, areas included only the LiDAR estimated surfaces that drain directly to the N inlets (LiDAR\_DA directly to inlet reduced by barriers in Table E-2) without the central drainage pipes. The areas reduced by barriers reflect the best estimate of drainage areas during the construction phase conditions during most of the monitoring period. Using an area less than the designed capture areas is based on: (a) the low flows observed in the basin (Table E-1, Chapter 3, Appendix 2), (b) flow storm routing accumulations predicted by digital elevation models from the LiDAR surveys (Chapter 5 and updated in this section), and (c) direct observations of stormwater runoff rerouting during rain events. These results emphasize the

importance of understanding the construction effect on the drainage areas. Small changes in road cross slope, temporary pipe obstructions, and barriers such as washing structures placed on inlets effect drainage patterns. It also highlights the importance of monitoring, which will be continued under the District 6 funding through AECOM.

*Table E-1a: Contributing areas from measured flow in Basin A compared to the design drainage area for individual storms.*

Date	Rainfall (inches)	N10 Contributing Area (%)	N9 Contributing Area (%)	N8 Contributing Area (%)
07/22/2017	0.53	5.4	23.6	4.8
07/23/2017	1.16	8.3	28.3	1.0
07/24/2017	0.54	60.4	155.0	20.0
08/02/2017	0.65	13.2	47.9	5.2
08/05/2017	0.94	15.2	42.7	6.4
08/18/2017	0.73	16.4	31.7	2.8
08/22/2017	0.75	29.6	53.4	5.6
08/29/2017	0.76	79.9	148.1	4.3
09/02/2017	0.41	69.3	153.4	4.1
09/06/2017	0.74	60.2	138.0	6.2
09/16/2017	1.14	12.4	21.6	5.5
10/29/2017	2.61	25.7	39.7	13.8

*Table E-1b: Contributing areas from measured flow in Basin C, D, and G compared to the design drainage area for individual storms.*

Date	Rainfall (mm)	C Contributing Area (%)	D Contributing Area (%)	G Contributing Area (%)
03/30/2017	1.67	2	36	1
04/25/2017	0.71	14	47	5
05/05/2017h	1.12	24	33	8
05/13/2017	1.90	30	13	5
05/25/2017 (B2B)*	1.71	28	7	7
06/06/2017	0.57	20	10	7
06/24/2017	1.10	14	7	8

\* B2B Stands for a combined back to back storm.

*Table E-2: Drainage area (DA) estimates for each basin based on LiDAR surveys and design plans.*

SMP	Inlet	LiDAR_DA Directly to inlet without barriers (acres)	LiDAR_DA Directly to inlet reduced by barriers (acres)**	LiDAR_DA Piped from M inlets (acres)	Sum LiDAR Areas reduced by barriers (acres)	AECOM DA Estimates (ROAD ONLY)*
A	N8	0.21	0.12	0.34	0.46	1.50
	N9	0.15	0.09	--	0.09	0.22
	N10	0.03	0.03	--	0.03	0.17
C	N7	0.24	0.29	0.66	0.95	0.98
D	N6	0.24	0.18	--	0.18	0.24
G	N5	0.18	0.18	0.07***	0.25	0.30

\* AECOM DA Estimates are based on Drawing SHEET#92B OF129 and drawing titled DRAINAGE AREA 2 -POST DEVELOPMENT STORMWATER MANAGEMENT SHEET#

\*\* Used in loading estimates

\*\*\* Adjusted by 50% to match revised plans

Figure E-1: Drainage areas for Basin A calculated from flow routing of LiDAR elevation surveys without consideration of highway barriers. The location of the highway drains was used as the capture point for outflow. The central highway drains currently appear to be blocked so those areas are not included in operational (construction-phase) capture areas.

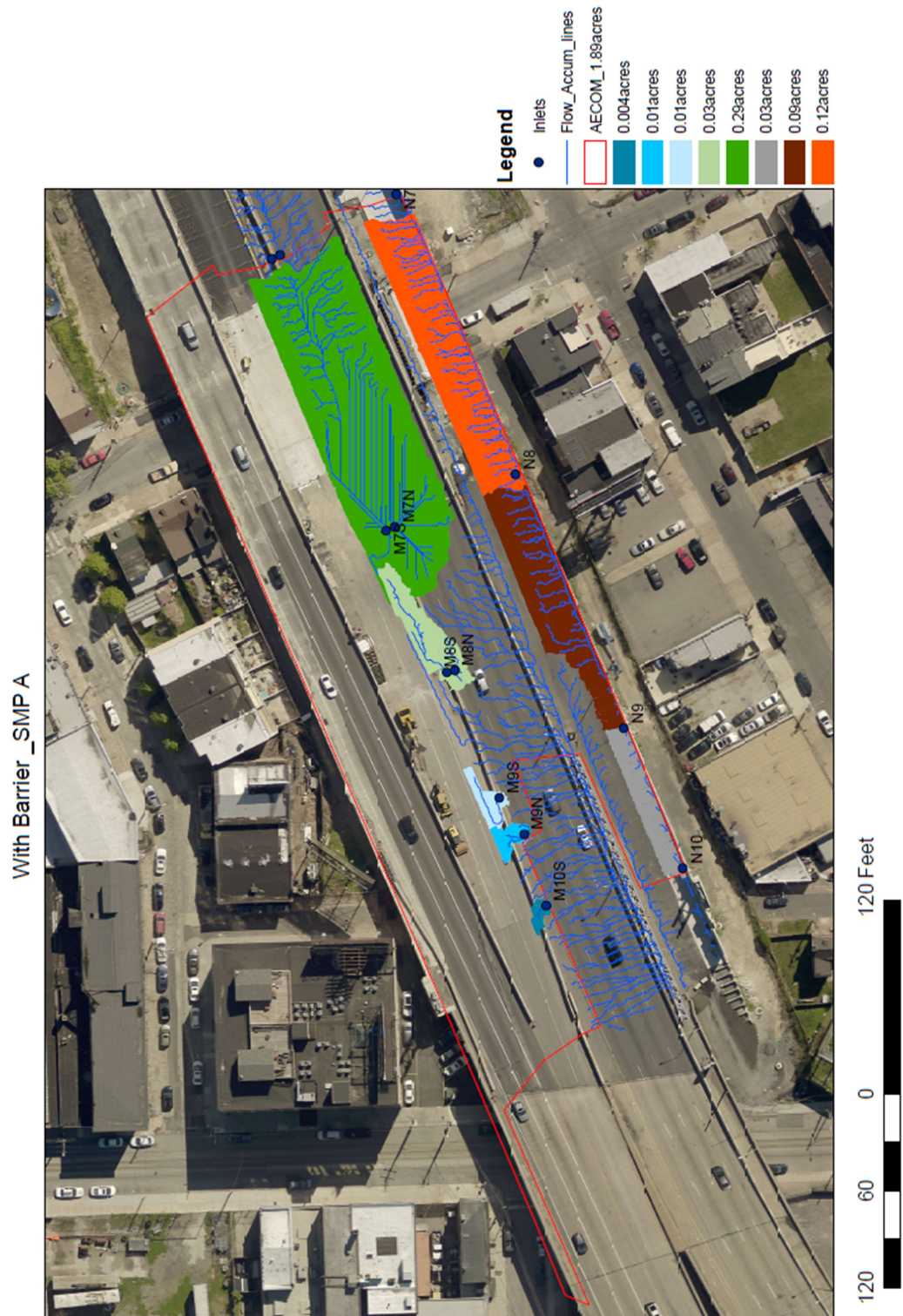




Figure E-2: Drainage areas for Basin A calculated from flow routing of LiDAR elevation surveys including rerouting due to highway barriers. These barriers were in place for most of the storms in the monitoring period. The location of the highway drains was used as the capture point for outflow. The central highway drains currently appear to be blocked so those areas are not included in operational (construction-phase) capture areas.

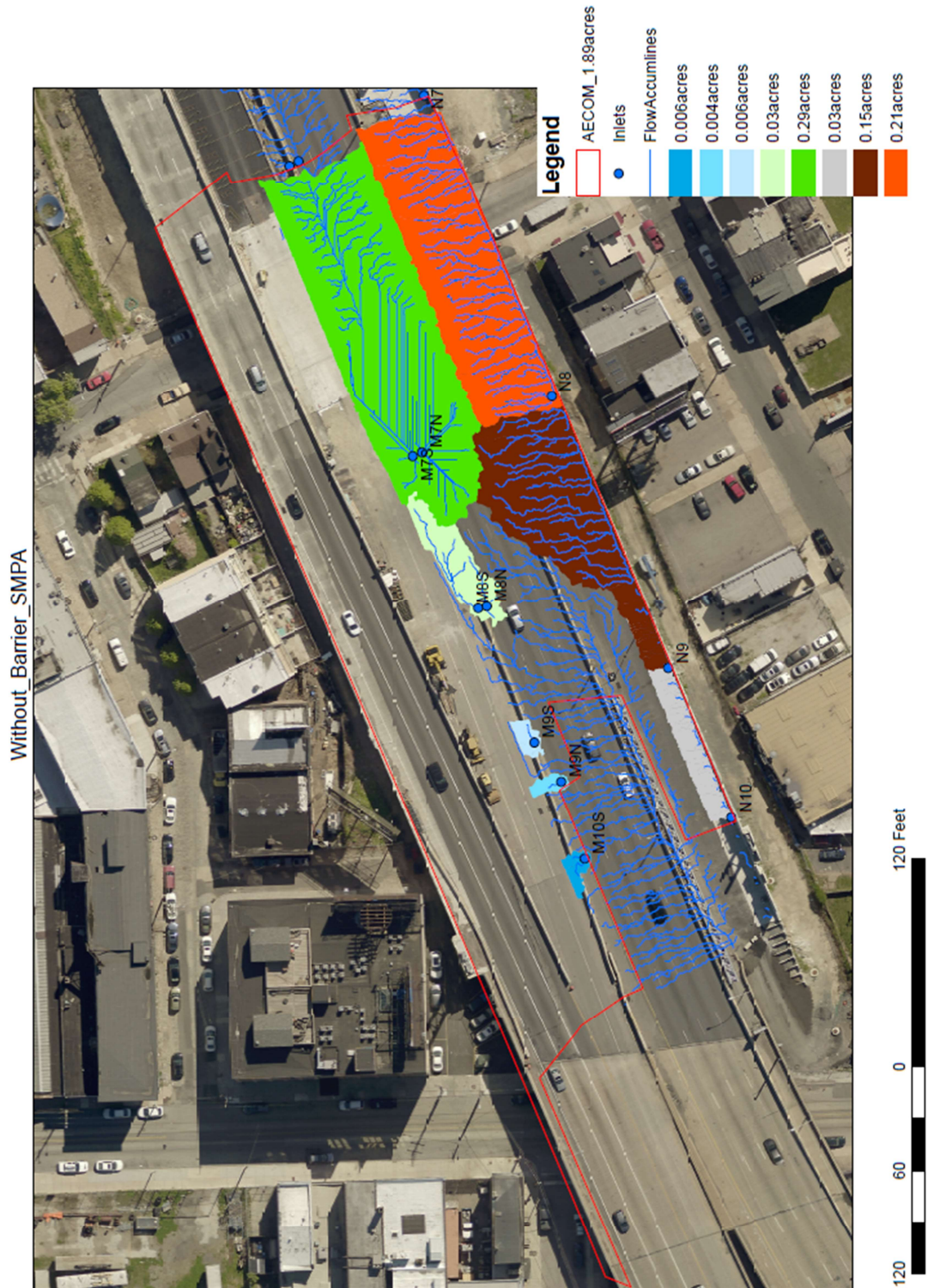




Figure E-3: Drainage areas for Basins C, D, and G, calculated from flow routing of LiDAR elevation surveys without consideration of highway barriers. The location of the highway drains was used as the capture point for outflow. The central highway drains currently appear to be blocked so those areas are not included in operational (construction-phase) capture areas.

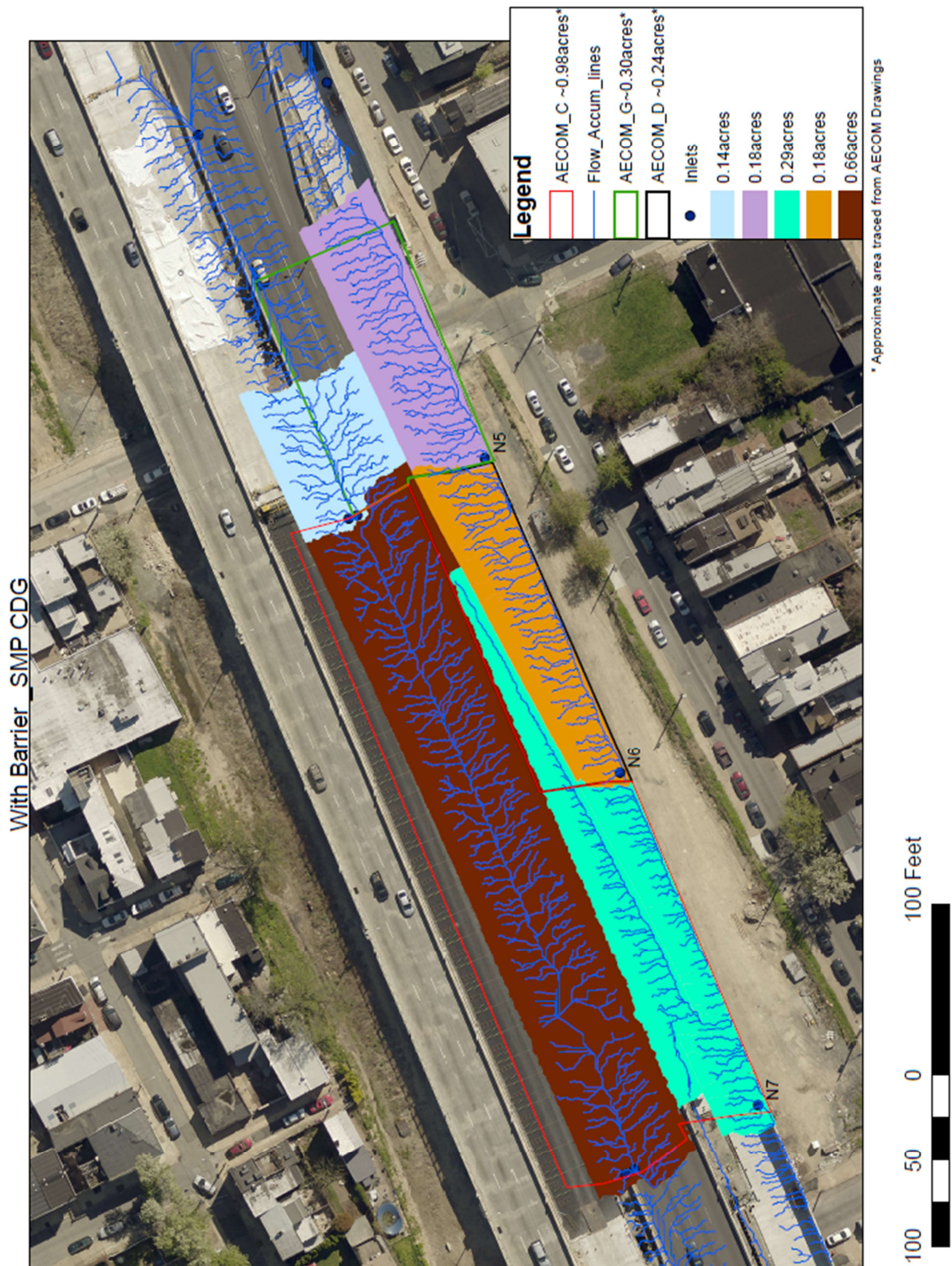
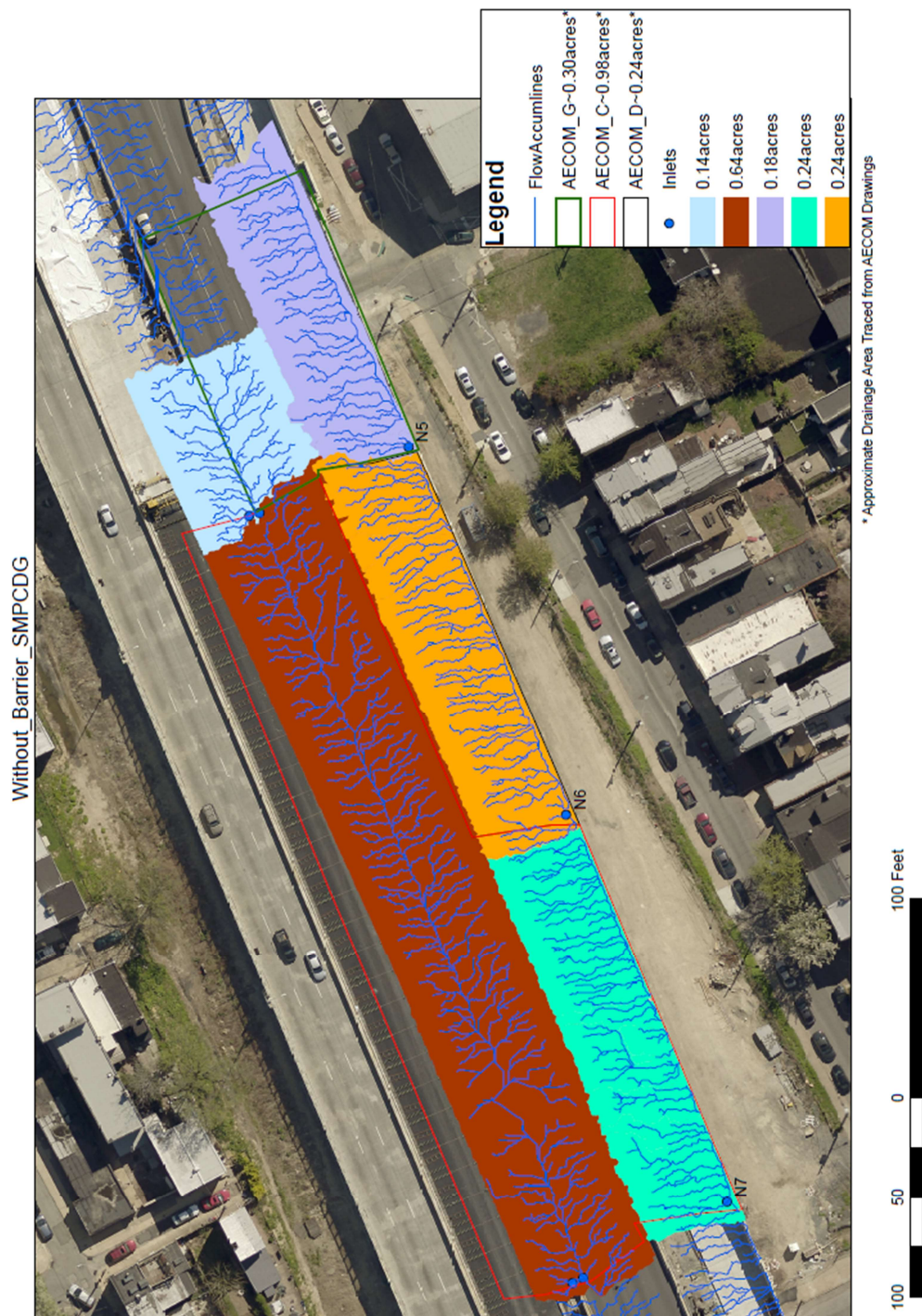




Figure E-4: Drainage areas for Basins C, D, and G, calculated from flow routing of LiDAR elevation surveys including rerouting due to highway barriers. These barriers were in place for most of the storms in the monitoring period. The location of the highway drains was used as the capture point for outflow. The central highway drains currently appear to be blocked so those areas are not included in operational (construction-phase) capture areas.





## Loading calculations

Loading calculations were updated and summarized for the first year of study. Along with the ranges in influent concentrations, these data help evaluate initial performance in the basins and provide comparisons with literature values. The total loads (mass) for each storm sampled in Basins C and D were calculated using an estimated event mean concentration (EMC), total rainfall depth and runoff area (Eq. E-1).

$$\text{Storm Load} = \text{EMC} \times \text{Rainfall} \times \text{Area} \quad \text{Eq. E-1}$$

The EMC is the flow-weighted average concentration sampled over the course of a storm (Appendix 3). In this equation, the drainage area for each basin was the capture area for corresponding inlet pipes (N7 to Basin C and N6 to Basin D; Table E-2 and Figure E-4). This table updates previous calculations in the main report. The annual load (mass per year) was estimated by summing the loads of the sampled storms then normalizing the rainfall of the sampled storms to the annual rainfall (Eq E-2). Normalization was needed because not all storms in the year were measured. The annual loads were divided by the basin surface areas for comparison with literature values reported in load per unit area.

$$\text{Annual Load} = \sum \text{Storm Load} \times \frac{\text{Average Annual Rainfall}}{\text{Rainfall for Storms Sampled}} \quad \text{Eq. E-2}$$

Contaminant concentrations measured in influent to the SMPs were compared with values reported in the literature (International BMP Database, 2016). The concentrations of suspended solids and total phosphorous measured in the study were within the range reported in the literature, and within the lowest quartile. The nitrate concentration exceeded the values reported in the literature, presumably because of the particular nature of the influent at this site. Nitrate in stormwater runoff from highways is reported to be higher than in residential areas (Burton and Pitt, 2002).

The calculated annual loadings were compared to literature values for urban runoff (EPA, 1976) and to loads per unit area reported in Burton and Pitt (2002) and Shaver et al., (2007). The loads per unit area reported in these studies were multiplied by the Basin C and D basin areas similar to Eq E-2 for comparison (Appendix 3). Note that the units for the EPA data base were ambiguous in that they reported Total N, but did not specify whether it was inorganic N only (which would be mostly nitrate) or both inorganic and organic. The more recent data on nitrate loadings from Burton and Pitt and Shaver fell in the same range, so it may be that the EPA data are inorganic N and comparable. However, given this uncertainty caution is needed in comparing the literature loading values for nitrogen. Suspended solids and total phosphorus loads in Basin C were on the lower end of the reported range while nitrate loads exceeded the maximum reported value. In Basin D, suspended solids were below the minimum reported value, total phosphorus was on the low end of the reported range and nitrate was in the middle of the reported range.

Typical removal efficiencies for bioswales (National Pollutant Removal Performance Database, 2007) are provided for context only because the absence of outlet flows from the SMPs precludes the calculation of removal efficiencies. In effect, the resulting removal efficiency in Basins C and D was 100%. Literature values for removal efficiency range up to 65 to 98%, but can be much lower. Note that negative efficiency occurs when the outlet concentration (or load) is greater than the inlet concentration (or load).

Table E-3: Median concentrations and annual loads observed in Basins C and D, based on storms captured between Oct 27, 2016 to Aug 29, 2017. Literature values for concentration and efficiency reported from the International BMP database.

Contaminant	Conc. measured in SMP <sup>a</sup> (mg/L) <i>median</i> [min-max]	Conc. reported in literature <sup>b</sup> (mg/L) <i>median</i> [min-max]	Load measured in SMP <sup>c</sup> (lbs) <i>median</i> [min-max]	Total load measured in SMP <sup>d</sup> (lbs)	Predicted annual load <sup>e</sup> (lbs/yr)	Annual load per surface area measured in SMP (lbs/yr/ac)	Annual load per area reported in literature for urban runoff <sup>f</sup> (lbs/yr/ac) <i>mean</i> [min-max]	Efficiency reported in literature <sup>g</sup> (mg/L) <i>median</i> [min-max]
<b>SMP C Contributing Drainage Area<sup>h</sup> = 0.29 ac Basin Surface Area = 0.1 ac</b>								
<b>Suspended Solids</b>	80 [0.0-845]	40.6 [2-1200]	0.54 [0.02-2.7]	7.7	79.5	274.2	1784 [441-4461]	59 [-100-98]
<b>Nitrate or TN</b>	1.83 [0.63-7.17] Nitrate	0.35 [0.06-1.2] Nitrate	0.01 [0.001-0.04] Nitrate	0.1  Nitrate	1.3  Nitrate	4.7  Nitrate	4.5 [1.8-18] TN	43 [0-76] Nitrate
<b>Total Phosphorus</b>	0.22 [0.066-0.83]	0.13 [0.01-2.0]	0.001 [0.00007-0.004]	0.01	0.2	0.7	0.7 [0.2-4.5]	5 [-100-65]
<b>SMP D Contributing Drainage Area<sup>h</sup> = 0.18 ac Basin Surface Area = 0.05 ac</b>								
<b>Suspended Solids</b>	41 [0.0-600]	40.6 [2-1200]	0.22 [0.009-1.7]	3.4	35.7	198.5	1784 [441-4461]	59 [-100-98]
<b>Nitrate or TN</b>	1.07 [0.13-6.63] Nitrate	0.35 [0.06-1.2] Nitrate	0.004 [0.0006-0.01] Nitrate	0.04  Nitrate	0.5  Nitrate	2.7  Nitrate	4.5 [1.8-18] TN	43 [0-76] Nitrate
<b>Total Phosphorus</b>	0.11 [0.057-0.83]	0.13 [0.01-2.0]	0.0006 [0.00004-0.002]	0.005	0.1	0.5	0.7 [0.2-4.5]	5 [-100-65]

a. Influent concentrations for storms sampled from Oct 27, 2016 to Aug 29, 2017.

b. Source: International BMP Database (2016).

c. Median [minimum-maximum] load for storms sampled from Oct 27, 2016 to Aug 29, 2017 and calculated using the operational (construction phase) contributing drainage areas.

d. Total load for the storms sampled from Oct 27, 2016 to Aug 29, 2017.

e. Annual load estimated based on average annual rainfall in the Philadelphia area.

- f. Source: EPA (1976), Burton and Pitt (2002), Shaver et al., (2007) Nitrogen concentrations reported in the EPA report did not specify whether they included organic nitrogen or inorganic only so numbers are gray to indicate literature values may be higher than for nitrate alone.
- g. Source: National Pollutant Removal Performance Database (2007).
- h. Drainage area determined by LiDAR measurement.

## **Plants and maintenance**

Species selection and placement are critical to maximizing plant performance (i.e., survival, growth, health, and flowering) in vegetated SMPs. We conducted two sets of studies assessing plant performance in the SMPs within GR2. First, we inventoried the intentionally planted vegetation in basins A, C, D, G, E and part of F to assess survival and health of the 56 species present. Over 8100 plants were included in the inventories, which occurred twice: approximately one year after planting and then after the plants had experienced two winters in the SMPs. The overall survival rate was approximately 80%, though varied considerably across plant life forms, species, and locations within the SMPs.

Second, we conducted in-depth investigations of the growth and physiological health of nine species that spanned the gradient of exposure to stormwater within the basins. Based on the information from the two studies (detailed in Chapter 7) and additional reports of the species' preferences from other sources, we report here ratings of the suitability of each species for placement in low elevation and mid to high elevation areas within PennDOT's SMPs (Table E-4). We rate suitability separately by elevation because environmental conditions can vary substantially within basins, with low elevation areas experiencing much greater inundation and exposure to salts, trace metals, and other contaminants, and higher elevation areas experiencing limited water availability. Continued monitoring would make it possible to evaluate the effects of long-term exposure to environmental stressors and to differentiate the effects of stressors on widely used species.

Temple University hired a landscaping contractor (Terraquabor, LLC) to carry out the maintenance and inspection needs of the five SMPs in GR2. Maintenance included weeding, pruning, trash and debris removal, as well as re-mulching as needed. The cost of their services provides a means of projecting maintenance and inspection costs into the future (Table E-5). However, one of the recommendations we make is to increase the frequency of some aspects of maintenance, including weeding and trash collection, which will inevitably increase the cost. We also recommended adjusting the timing of some maintenance tasks (Table E-6). We note that cost estimates do not account for reconstruction or major replanting, which will be necessary intermittently.

Table E-4: Species rankings and suggested species for different environments within the basin. The rating system includes well suited (green), moderately suited (yellow) and not well suited (red) to the conditions listed.

Inventoried Plant Species						
Code	Plant type	Scientific name	Common name	Suitability at mid to high elevation	Suitability at low elevation	Notes
N	Bulb	<i>Narcissus</i> 'Ice follies'	Daffodil			
KA	Graminoid	<i>Calamagrostis</i> × <i>acutiflora</i> 'Karl Foerster'	Karl foerstern feather reed grass			
CL	Graminoid	<i>Carex lupulina</i>	Hop sedge			
CVA	Graminoid	<i>Carex muskingumensis</i> 'Oehme'	Variegated palm sedge			
CV	Graminoid	<i>Carex vulpinoidea</i>	Fox sedge			
PA	Graminoid	<i>Pennisetum alopecuroides</i> 'Hameln'	Dwarf fountain grass			
AC	Perennial	<i>Achillea millefolium</i> 'Coronation gold'	Yellow yarrow			
AF	Perennial	<i>Achillea millefolium</i> 'Fireland'	Fireland yarrow			
AI	Perennial	<i>Asclepias incarnata</i> 'Ice ballet'	Swamp milkweed			
AN	Perennial	<i>Aster novae-angliae</i> 'Purple dome'	New england aster			
CH	Perennial	<i>Cimicifuga ramosa</i> 'Hillside black beauty'	Autumn snakeroot			
EP	Perennial	<i>Echinacea purpurea</i>	Purple cone flower			
GG	Perennial	<i>Gaillardia</i> × <i>grandiflora</i> 'Kobold'	Indian blanket			
GM	Perennial	<i>Geranium maculatum</i>	Wild geranium			
HM	Perennial	<i>Helenium autumnale</i> 'Mardi gras'	Mardi gras perennial sunflower			
HHR	Perennial	<i>Hemerocallis</i> 'Happy returns'	Happy returns daylily			
HRR	Perennial	<i>Hemerocallis</i> 'Rosy returns'	Rosy returns daylily			
HI	Perennial	<i>Hosta</i> 'Ice follies'	Ice follies hosta			Requires some shade
HR	Perennial	<i>Hosta</i> 'Royal standard'	Royal standard standard hosta			Requires some shade
IP	Perennial	<i>Iris pseudacorus</i> 'Variegata'	Variegated water iris			
IS	Perennial	<i>Iris sibirica</i> 'Caesar's brother'	Caesar's brother iris			
IV	Perennial	<i>Iris versicolor</i>	American blue flag iris			
LS	Perennial	<i>Liatris spicata</i>	Blazing star			
MA	Perennial	<i>Matteuccia struthiopteris</i>	Ostrich fern			
MC	Perennial	<i>Monarda</i> 'Cambridge scarlet'	Cambridge scarlet beebalm			
RF	Perennial	<i>Rudbeckia fulgida</i> var. <i>sullivantii</i> 'Goldsturm'	Black-eyed Susan			
TO	Perennial	<i>Tradescantia ohimensis</i>	Ohio spiderwort			
AM	Shrub	<i>Aronia melanocarpa</i> 'Autumn magic'	Autumn magic black chokeberry			Good candidate for low areas
BT	Shrub	<i>Berberis thunbergii atropurpurea</i>	Crimson pygmy barberry			Potential invasive
LB	Shrub	<i>Calycanthus floridus</i>	Carolina allspice			
CA	Shrub	<i>Cornus alba</i> 'Sibirica'	Red twig dogwood			
CS	Shrub	<i>Cornus sericea</i> 'Cardinal'	Red-osier dogwood			

Table E-4 (continued)

Inventoried Plant Species						
Code	Plant type	Scientific name	Common name	Suitability at mid to high elevation	Suitability at low elevation	Notes
FS	Shrub	<i>Forsythia suspensa sieboldii</i>	Siebold weeping forsythia	●	●	Potential invasive
HV	Shrub	<i>Hamamelis vernalis</i>	Vernal witchhazel	●	●	
IH	Shrub	<i>Itea virginica</i> 'Little Henry'	Virginia sweetspire dwarf	●	●	
JH	Shrub	<i>Juniperus horizontalis</i> 'Blue chip'	Blue chip juniper	●	●	
KJ	Shrub	<i>Kerria japonica</i> 'Pleniflora'	Japanese kerria	●	●	
RH	Shrub	<i>Rhus aromatica</i>	Fragrant sumac	●	●	
RR	Shrub	<i>Rosa rugosa</i>	Rugosa rose	●	●	Known to be invasive
VT	Shrub	<i>Viburnum trilobum</i> 'Wentworth'	American cranberrybush	●	●	
YB	Shrub	<i>Yucca</i> × 'Bright edge'	Variegated adam's needle	●	●	
AP	Tree	<i>Acer platanoides</i> 'Crimson king'	Crimson king maple	●	●	
AA	Tree	<i>Amelanchier arborea</i>	Common serviceberry	●	●	
AG	Tree	<i>Amelanchier</i> × <i>grandiflora</i> 'Autumn brilliance'	Autumn brilliance serviceberry	●	●	
BN	Tree	<i>Betula nigra</i> 'Heritage'	Heritage river birch	●	●	
CC	Tree	<i>Cercis canadensis</i>	Redbud	●	●	
CP	Tree	<i>Crataegus phaenopyrum</i>	Washington hawthorne	●	●	
CW	Tree	<i>Crataegus viridis</i> 'Winter king'	Winter king hawthorne	●	●	
FJ	Tree	<i>Juniperus chinensis</i> 'Hetzii columnaris'	Fairview juniper	●	●	
PP	Tree	<i>Picea pungens</i>	Colorado spruce	●	●	
PN	Tree	<i>Pinus nigra</i>	Austrian pine	●	●	
TE	Tree	<i>Thuja occidentalis</i> 'Emerald green'	Emerald green arborvitae	●	●	
TH	Tree	<i>Thuja occidentalis</i> 'Holmstrup'	Holmstrup arborvitae	●	●	
TW	Tree	<i>Thuja occidentalis</i> 'Wintergreen'	Wingergreen arborvitae	●	●	

Table E-4 (continued)

Suggested Plant Species					
Species type	Scientific name	Common name	Suitability at mid to high elevation	Suitability at low elevation	Notes
Graminoid	<i>Acorus calamus</i>	Sweetflag	●	●	Requires frequent inundation and partial shade
Graminoid	<i>Ammophila brevifolula</i>	Beach grass	●	●	Requires sandy soil; Salt tolerant
Graminoid	<i>Carex stricta</i>	Tussock sedge	●	●	
Graminoid	<i>Juncus effusus</i>	Common rush	●	●	
Graminoid	<i>Panicum amarum</i>	Bitter panic grass	●	●	Salt tolerant
Graminoid	<i>Panicum virgatum</i>	Switch grass	●	●	Salt tolerant
Graminoid	<i>Scirpus cyperinus</i>	Woolgrass	●	●	
Perennial	<i>Chelone glabra</i>	Turtlehead	●	●	
Perennial	<i>Helianthus angustifolius</i>	Swamp sunflower	●	●	
Perennial	<i>Hibiscus moscheutos</i>	Rose mallow	●	●	Salt tolerant
Perennial	<i>Lobelia siphilitica</i>	Great blue lobelia	●	●	
Perennial	<i>Physostegia virginiana</i>	Obedient plant	●	●	
Perennial	<i>Pycnanthemum virginianum</i>	Virginia mountain mint	●	●	
Perennial	<i>Solidago sempervirens</i>	Seaside goldenrod	●	●	Salt tolerant
Shrub	<i>Baccharis halimifolia</i>	Eastern baccharis	●	●	
Shrub	<i>Clethra alnifolia</i>	Sweet pepperbush	●	●	Salt tolerant
Shrub	<i>Myrica pensylvanica</i>	Bayberry	●	●	Salt tolerant
Shrub	<i>Physocarpus opulifolius</i>	Ninebark	●	●	
Shrub	<i>Prunus maritima</i>	Beach plum	●	●	Salt tolerant
Shrub	<i>Rhododendron viscosum</i>	Swamp azalea	●	●	
Shrub	<i>Rhus copallinum</i>	Winged sumac	●	●	Salt tolerant
Shrub	<i>Rosa palustris</i>	Swamp rose	●	●	
Shrub	<i>Salix discolor</i>	Pussy willow	●	●	Salt tolerant
Shrub	<i>Sambucus canadensis</i>	Elderberry	●	●	Salt tolerant
Tree	<i>Salix nigra</i>	Black willow	●	●	





Table E-5: Maintenance costs for landscaping contractor working on five basins.

	Current	Projected
Annual cost	\$70,000	\$100,000
Weeding frequency	1/month	2/month, April-Sept
Trash collection frequency	1/month	2/month, Year-round

Table E-6: Recommended maintenance schedule by month.

Task Type	Jan	Feb	Mar	Apr	May	Jun	Jul	Aug	Sep	Oct	Nov	Dec
Trash & Debris Removal												
Weeding												
Plant Health Inspection												
Watering (as needed)												
Fertilizing (as needed)												
Pruning and tree maintenance (as needed)												
Plant Inspection & Replacement												
Mulch Inspection & Replacement												
Sediment Removal												
Retilling of Site												
Upgradient Inlets Inspection & Cleanout												
Inspection & Maintenance of Inlet / Outlet Structures												
Inspection & Maintenance of SMP Stability (outlet structures, berms, & embankments)												

Optimal time for task  Acceptable time for task 

## Highlights of recommendations after the first year of study

- We recommend that drainage system design include consideration of performance during the intermediate construction stages for long term projects, and not just the final design requirements.
- We recommend that designers locate inlets where slight changes of slope will not cause stormwater to bypass inlets.
- We recommend that LiDAR and monitoring be used to demonstrate that constructed surfaces are within tolerance before project acceptance, and for adjustments to correct for construction changes.
- We recommend that SRTs or rain event monitoring be required as part of SMP acceptance.
- We recommend that SMP's be designed to support instrumentation for temporary monitoring of performance and maintenance activities.
- SMP media can be replaced or managed to prioritize infiltration performance and underlying water quality rather than concerns of remobilization within the SMP
- The observation of preferential flow paths emphasizes the importance of planting vegetation in the basins to reduce preferential flow paths and render the flow more turbulent, thereby increasing mixing and reducing the magnitude of surface water hotspots.
- Based on the plant survival data collected thus far, there are three species whose use should be avoided or reserved for shaded and minimally stressful regions of the SMPs. These are *Cimicifuga ramosa*, *Geranium maculatum*, and *Matteuccia struthiopteris*
- Given the difficult growing conditions found at the lowest elevations within SMPs, we recommend planting additional species that are known to tolerate periodic inundation.
- Regardless of the reason, many installers will replace individuals that die within a year of planting; we recommend that this provision be noted when contracting with installers and that it be enforced.
- We recommend avoiding the use of known invasives in SMP plantings
- We recommend accommodating foot traffic in the design strategy to reduce erosion, soil compaction, and damage to plants.
- We recommend that the depth of amended soil in upper areas of SMPs be increased, which could be accomplished by ensuring that the current design specification is enacted.
- We recommend that weeding be conducted every two weeks, and that the maintenance manual be updated to reflect this. However, frequent weeding (perhaps even weekly) along the fences of neighboring residences and businesses could be an important way to maintain positive relations with neighbors.
- We recommend that motorized weeding devices be allowed during restricted hours of the day in certain cases where weed removal is prohibitively difficult with manual tools and hand pulling and that targeted herbicide application be used.
- We recommend that inflow pipes continue to be elevated where possible, and that a low-cost, maintenance-friendly trash collection system be developed to capture small pieces of trash.
- With respect to larger litter and debris items, the maintenance manual currently specifies that they should be removed monthly; we recommend increasing the frequency to at least every two weeks in this highly urban setting.

- Adding signage about dog waste negatively impacting water quality would inform the community and making it as easy as possible for dog owners to collect and dispose of their dog's waste could also help mitigate the problem
- We recommend modifying inlet spillways to be able to dissipate energy and reduce water velocities.
- We recommend decreasing the slopes of SMP sidewalls when they are initially dug out to better support root establishment.
- In future installations, we recommend that a more thorough evaluation of subsoil conditions be conducted prior to the installation of amended soil
- Actively engaging the community in SMP management could be an effective strategy for both increasing the person-hours dedicated to maintaining the vegetation and litter in BMPs and decreasing the labor costs.

The SMPs along the Girard Avenue Interchange have proven to be successful in many ways. They are capturing stormwater together with the contaminants it carries, thereby preventing either from entering the municipal stormwater system and being released into the Delaware River. Moreover, much of the vegetation has successfully established and promises to beautify the neighborhood for years to come. Our data-intensive investigation has highlighted several ways in which the design and maintenance of SMPs can be improved while minimizing the associated costs. The analyses and recommendations provided here are an initial synthesis of our ongoing effort; we expect the empirical and modeling processes that we have developed to facilitate many further insights and suggestions that can be put into practice in future phases of SMP design, installation, and management.

## References

- EPA. 1976. *Areawide Assessment Procedures Manuals*. Vol. I. Municipal Environ. Res. Lab., Cincinnati, Ohio. EPA-600/9-76-014.
- Burton, G.A. and Pitt, R.E. 2002. *Stormwater Effects Handbook: A Toolbox for Watershed Managers, Scientists, and Engineers*. Lewis Publishers.
- Shaver, E., Horner, R., Skupien, J., May, C. and Ridley, G. 2007. *Fundamentals of Urban Runoff Management: Technical and Institutional Issues*. 2<sup>nd</sup> Edition. North American Lake Management Society, Madison, WI
- International BMP Database. 2016. *2016 Summary Statistics*. Water Environment and Reuse Foundation
- Center for Watershed Protection. 2007. *National Pollutant Removal Performance Database*. Version 3

## **Chapter 1: Report Organization**

This report represents Deliverable 10 for TEM 006 “Stormwater Control Management and Monitoring.” It is a final report on work conducted at the I-95 stormwater management projects (SMPs) in GR2, specifically basins A, C, D, and G. The work under this deliverable commenced December 1, 2016. The first few months were taken up with instrument installation, basin maintenance, some initial plant characterization, and some grab sampling of storms. There was minimal monitoring during this period, except in the baseline monitoring wells, which were installed under a complementary grant through AECOM. This final report was drafted in September 2017. Thus, this project covers SMP monitoring from March 2017 to September 2017, or approximately seven months.

A great deal has been learned in this initial monitoring period. This report is organized by work plan task, summarizing the results from each. Chapter 2 describes the baseline well monitoring, which includes data collected in the earlier monitoring period funded by AECOM to provide a full year of data. Chapter 3 covers the hydrologic monitoring program. The extensively instrumented basins allow us to monitor storms as well as simulated runoff tests (SRTs). Two SRTs were conducted, which provided key findings about basin performance. Chapter 4 provides a summary of data collected for chemical monitoring in wells, lysimeters (unsaturated zone), stormwater samples, and runoff during the SRTs. This dataset only provides information on the short-term behavior in the basin; long-term behavior will require a longer monitoring period. Chapter 5 describes the LiDAR scans that supported hydrology and plant characterization. Chapter 6 is a description of modeling conducted to date, including some results of modeling of the recent SRTs. Chapter 7 summarizes the plant characterization,

including a list of plants with high and low survival rates along with assessment of why certain species performed better. Chapter 8 is a description of maintenance activities in the basin.

Recommendations are provided in Chapter 9, based on analysis of the findings to date, as of the final report deliverable on November 30, 2017. The executive summary at the beginning of the report provides summary tables, and highlights of the recommendations.

The report was co-written by Temple University and Villanova University.

## **Chapter 2: Baseline monitoring for groundwater conditions**

### **Methods**

#### *Baseline Monitoring Well Construction*

Seven monitoring wells (MW1-MW7) were installed in March 2016 to evaluate baseline groundwater conditions, both hydrological and chemical (see Chapter 4 for details on the results of the chemical analyses), along the I-95 corridor. The well construction design of all monitoring wells was based on the standard Philadelphia Water Department (PWD) monitoring well program (Fig. 2-1). All wells were cased with 2-inch polyvinyl chloride (PVC) schedule 40 casing. Three wells (MW5-7) have 4-inch steel. The remaining four wells (MW1-4) were installed flush with the sidewalk, and thus did not require above ground casing. To protect against vandalism and unauthorized access, all well caps have locking mechanisms.

A well boring report was completed by Susquehanna Civil Inc. for each well. Each boring report records both sedimentological (e.g., Unified Soil Classification System soil texture) and hydrological (e.g., relative moisture content) properties (Appendix 1). Table 2-1 provides the general well construction details. Monitoring well land surface elevations were initially surveyed during well installation. However, to ensure that the relative elevations in closely spaced wells were correct, the land surface elevations were resurveyed at MW1-3 in April 2017 using a total station (Nikon NPR-332) to verify previously collected elevation data. Resurveying determined that the relative elevations previously surveyed were correct.

*Table 2-1. Monitoring well construction details, including the land surface elevation (in ft above sea level or asl), the well depth (ft below land surface), and the screened well depths (ft below land surface).*

Well	Land Surface Elevation (ft asl)	Well Depth (ft below land surface)	Screened Depths (ft below land surface)
MW1	21.2	30.0	24.0 – 29.0
MW2	19.7	30.0	23.0 – 28.0
MW3	19.0	30.0	23.5 – 28.5
MW4	14.5	25.5	12.0 – 17.0
MW5	16.5	30.0	24.0 – 29.0
MW6	10.6	16.5	11.5 – 16.5
MW7	25.2	35.0	26.0 – 31.0

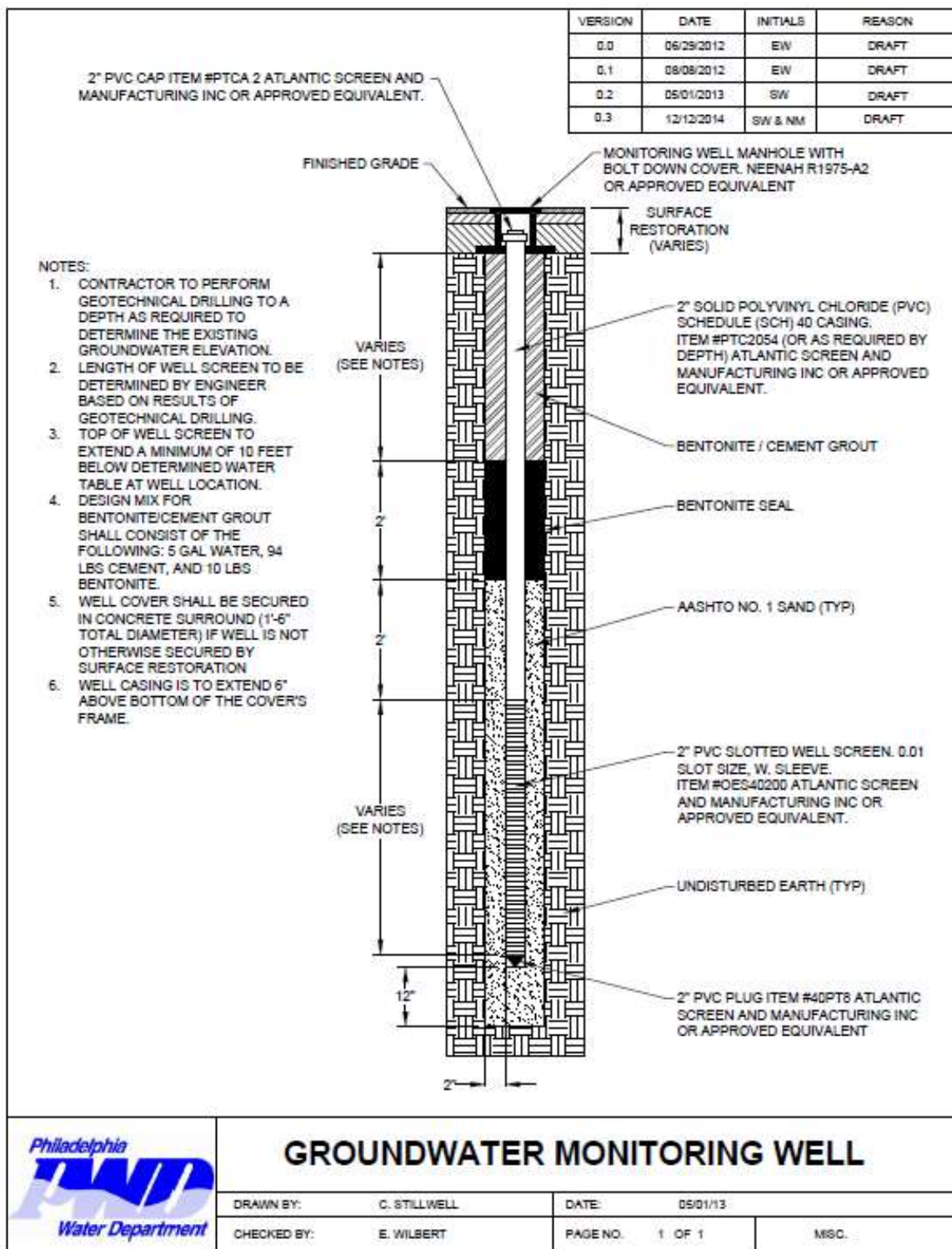


Fig. 2-1. Standard Philadelphia Water Department (PWD) groundwater monitoring well design specifications.



### *Baseline Monitoring Well Locations*

The plan for siting and installing the seven monitoring wells was developed in conjunction with right of way and utility locations (Fig. 2-2). In general, the monitoring wells extend along a southeast – northeast transect that parallels I-95. The northernmost well (MW5) is located near Melvale St and the southernmost well (MW7) is located near Callowhill St. Additionally, three wells (MW1-3) were installed along a transect perpendicular to I-95 to monitor the impact of infiltration from the SMP on the local water table and the variation in groundwater level response as a function of distance from the Delaware River. All monitoring wells tap an unconfined aquifer contained within the Pleistocene age Trenton gravel (Paulachok, 1991).

### *Hydrologic Monitoring*

The hydrologic monitoring of the baseline wells is conducted using submersible loggers that continuously measure groundwater levels and conductivity at fifteen minute intervals. Water level loggers (Onset Hobo U20L-001-04 with plastic casing) were installed in all monitoring wells in April 2016 and have an operational range of 0-13 ft water depth, measure changes in water levels with a resolution of 0.007 ft, and measure water levels with an accuracy of 0.015ft. One conductivity logger (Onset Hobo U24-001) was installed alongside the water level logger in MW3, and has a range of 0-1000  $\mu\text{S}/\text{cm}$ , an accuracy of 5  $\mu\text{S}/\text{cm}$  and resolution of 1  $\mu\text{S}/\text{cm}$ . Data from these loggers was used to record storm events, tidal conditions, and steady state water level and water quality. Data from submersible loggers was downloaded approximately every other month and compiled in Microsoft Access.

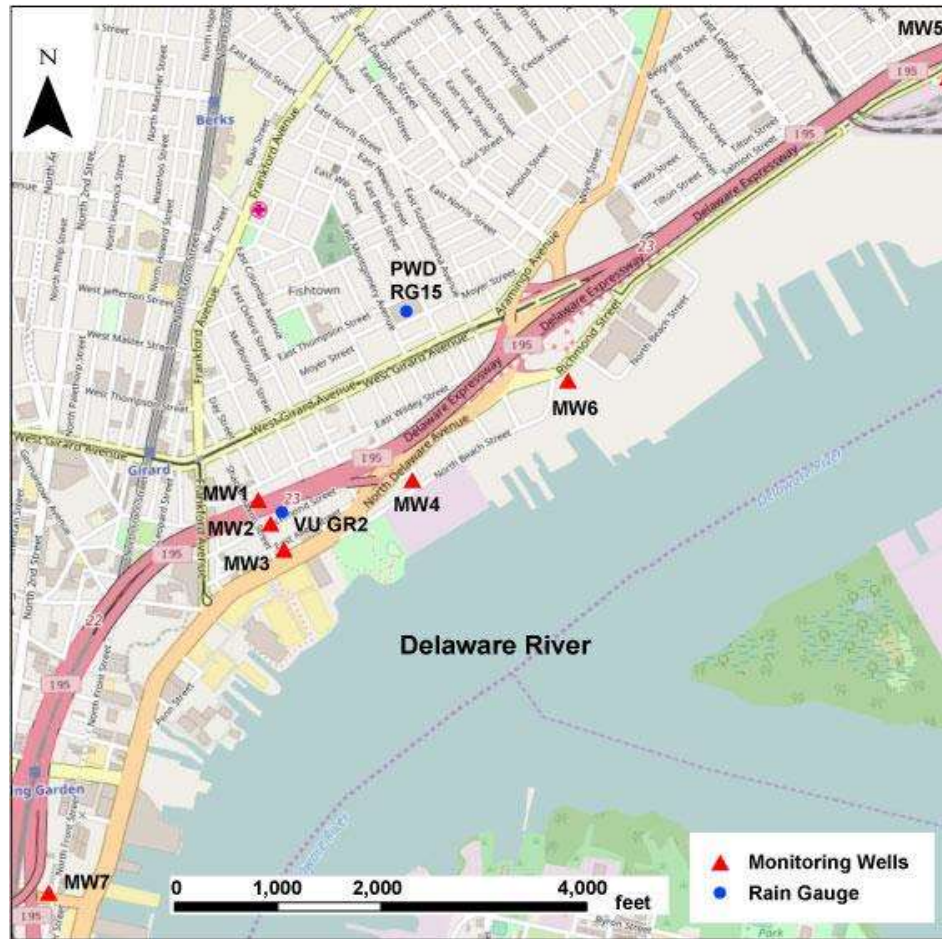


Fig. 2-2. Map of monitoring well (triangles), and rain gauge (circles) locations.

Because loggers determine the changes in water levels by measuring changes in the overlying water pressure, it is necessary to have an accurate measurement of the local barometric pressure. Barometric pressure was measured with an additional Onset Hobo U20L-001-04 logger installed in the air at MW1.

The hydrologic conductivities of aquifer sediments in monitoring wells were measured between May and June 2017 well using the Hvorslev slug test analysis method (Hvorslev 1951). The slug used consisted of a 4 cm by 55 cm long PVC schedule 40 pipe filled with sand. During the slug test water levels were logged with an Onset Hobo U20L-001-04 plastic casing logger set to 10 second logging intervals.

Rainfall data was measured with tipping bucket rain gauges, which send a signal to a data recorder for every 0.01 inch of rainfall received. The precipitation data used for rainfall event analysis was collected from gauges at two locations, a weather station installed near SMP C by Villanova University (VU GR2), and at a rain gauge operated by the Philadelphia Water Department (PWD RG15) located approximately 0.5 miles northeast of SMP C (Fig. 2-2).

Detailed specifications for the VU GR2 tipping bucket rain gauge are provided in the hydrologic monitoring chapter. Whenever possible precipitation data from the VU GR2 gauge was used for analysis; however, data from the PWD RG 15 gauge was used to fill in data gaps due to the VU GR2 gauge occasionally malfunctioning and during the period before the VU GR2 gauge was installed. Tidal data was taken from the Philadelphia, PA National Oceanic Atmospheric Association CO-OPs station (ID #8545240) (NOAA Center for Operational Oceanographic Products and Services, 2017).

#### *Spatial and Statistical Analyses*

Spatial analysis was conducted in ArcGIS 10.0. The groundwater table surface was created by using the kriging method to spatially interpolate the average recorded groundwater elevation in each monitoring well during the period of record. Statistical analyses were conducted in the R software (R Core Team, 2016). Lag times between ground water level fluctuations and tidal fluctuations were calculated using the cross correlation function in R. The coverage of the main sewerage system in the vicinity of the study area was digitized from a map included in the 1902 annual report of the city of Philadelphia (Philadelphia Department of Public Works Bureau of Surveys 1902).

## Results

### *Precipitation records*

During the first year of observation (April 2016 to March 2017) a total of 119 precipitation events occurred. Rainfall amounts during these events ranged from 0.01 to 1.35 inches, and the total rainfall over this period was 26.92 inches, an amount less than the average annual precipitation (41.53 inches) in Philadelphia (NOAA National Climatic Data Center, 2010). The duration of rainfall events ranged from 135 to 1695 minutes.

### *Water level records*

In general, during the period of record the highest observed groundwater levels occur in well MW4 (Figs. 2-3 through 2-5, Table 2-2). Spatially interpolating the average water level during the period of record (approximately one year) in all wells suggests that the water table is relatively higher near MW4, creating a mound that extends over to MW1-3. The lowest water levels were observed in well MW6 (Figs. 2-3 & 2-4, Table 2-2). Within the transect of monitoring wells (MW1-3) that runs perpendicular to I-95, water levels are generally the highest in MW2 and lowest in MW1 (Fig. 2-5, Table 2-2). This pattern is contrary to the expected slope of the local groundwater table, which should generally decrease moving towards the Delaware River (Paulachok, 1991). The exact cause of this pattern is currently unknown, but could represent heterogeneities in aquifer materials. Although groundwater mounding due to the SMP devices could be a factor (Machusick et al., 2011), there is not an observed seasonality to the mounding (e.g., mounding is not higher during wetter seasons). Note the full archive of data for the first year is available in a supplemental excel file with metadata.

The infiltration of precipitation appears to have varying levels of influence on the water levels in the monitoring wells. In particular, water levels in only three (MW2, MW3, and MW6) of the seven monitoring wells seem to be sensitive to precipitation events (Figs. 2-4 & 2-5). Moreover, these three wells display varying levels of sensitivity to precipitation events, with MW6 exhibiting the sensitivity even to small rainfall events. Specifically, MW6 displays a much flashier hydrograph than the other monitoring wells. While water levels in MW3 are also responsive to storm events, the responses are not as high as rises in the water levels of MW6 after storm events. For example, a 0.08-inch rainfall event that occurred on July 18, 2016 caused a sharp increase in the water levels of both MW3 and MW6 (Fig. 2-5, black arrows). However, two days earlier (July 16, 2016) a smaller (0.05 inch), rainfall event only caused a response in MW6 (Fig. 2-4, red arrow), thereby suggesting MW6 is relatively more sensitive to precipitation events.

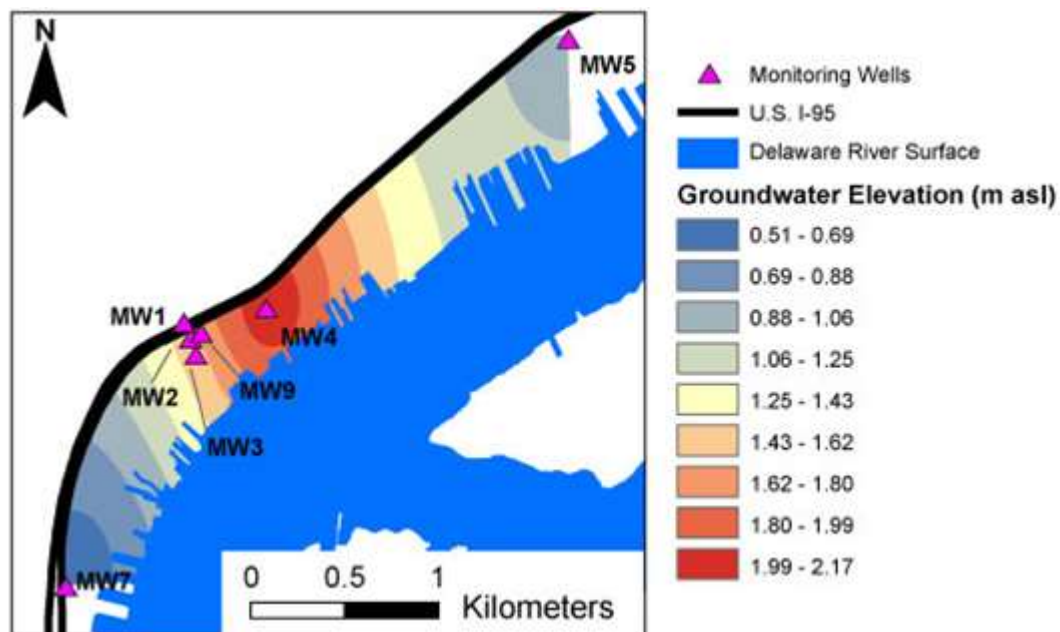


Fig. 2-3 Groundwater table surface created by interpolating the yearly average water level in each well.

*Table 2-2. Seasonal and annual mean groundwater elevations (in meters above sea level), and the measured hydraulic conductivity (K, in  $m\ s^{-1}$ ) in each well during the first year of observation (April 2016–May 2017).*

<b>Well</b>	<b>Ave Water Level  Spring</b>	<b>Ave Water Level  Summer</b>	<b>Ave Water Level  Fall</b>	<b>Ave Water Level  Winter</b>	<b>Annual Mean Water Level</b>	<b>K</b>
<b>MW1</b>	<b>1.41</b>	<b>1.52</b>	<b>1.62</b>	<b>1.57</b>	<b>1.54</b>	<b><math>1.69 \times 10^{-3}</math></b>
<b>MW2</b>	<b>1.65</b>	<b>1.70</b>	<b>1.63</b>	<b>1.62</b>	<b>1.65</b>	<b><math>2.00 \times 10^{-3}</math></b>
<b>MW3</b>	<b>1.54</b>	<b>1.63</b>	<b>1.58</b>	<b>1.55</b>	<b>1.58</b>	<b><math>1.65 \times 10^{-3}</math></b>
<b>MW4</b>	<b>2.16</b>	<b>2.17</b>	<b>2.17</b>	<b>2.20</b>	<b>2.18</b>	<b><math>8.83 \times 10^{-5}</math></b>
<b>MW5</b>	<b>1.14</b>	<b>1.09</b>	<b>0.96</b>	<b>0.96</b>	<b>1.03</b>	<b><math>9.29 \times 10^{-5}</math></b>
<b>MW6</b>	<b>0.28</b>	<b>0.36</b>	<b>0.32</b>	<b>0.09</b>	<b>0.33</b>	<b>&amp;</b>
<b>MW7</b>	<b>0.65</b>	<b>0.66</b>	<b>0.56</b>	<b>0.52</b>	<b>0.59</b>	<b><math>1.76 \times 10^{-3}</math></b>

& Results were inconsistent for MW6

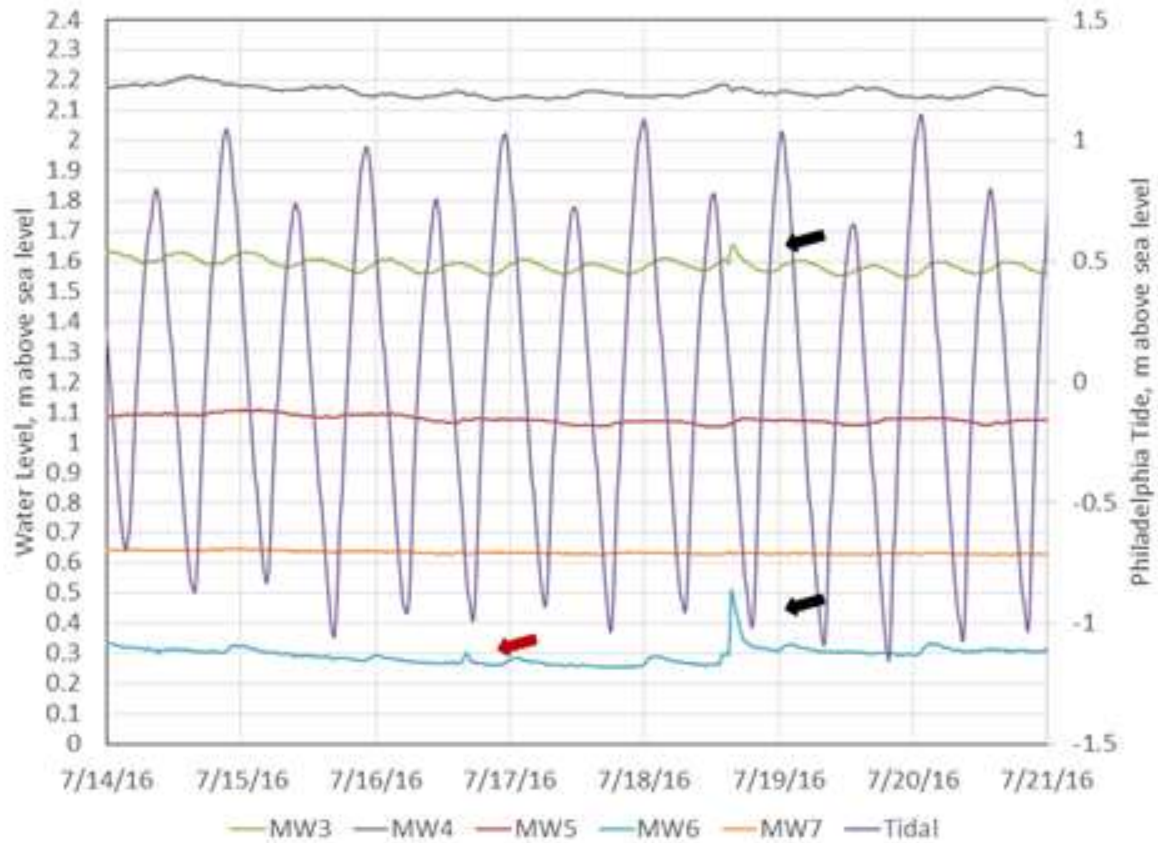
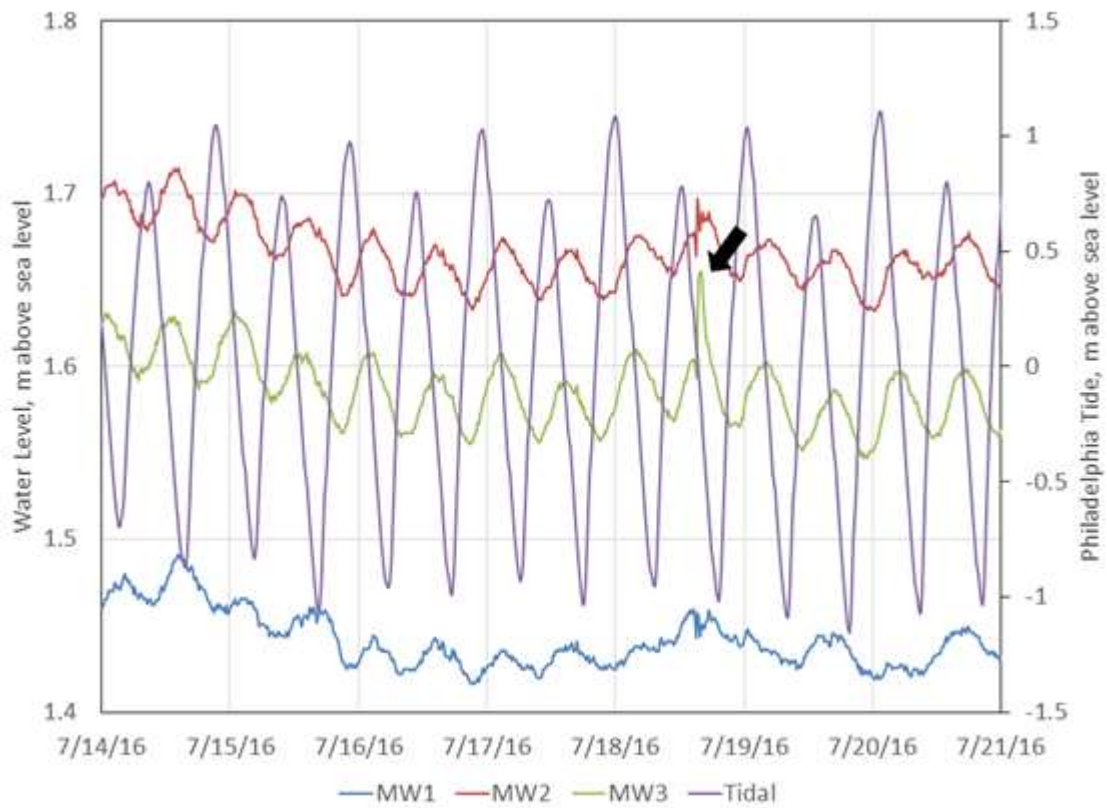


Fig. 2-4. Water level heights in baseline wells and tidal fluctuations of the Delaware River in Philadelphia (NOAA Center for Operational Oceanographic Products and Services, 2017). The black arrows indicate the response in water levels in MW3 and MW6 to a 0.08-inch rainfall event. The red arrow indicates the response of water levels in MW6 to a 0.05-inch rainfall event.



*Fig. 2-5. Water level heights in baseline wells and tidal fluctuations of the Delaware River in Philadelphia (NOAA Center for Operational Oceanographic Products and Services, 2017). The black arrow indicates the response in water levels in MW2 and MW3 to a 0.08-inch rainfall event.*





*Fig. 2-6. Excavation around MW6 showing the 19<sup>th</sup> century glassworks foundations.*

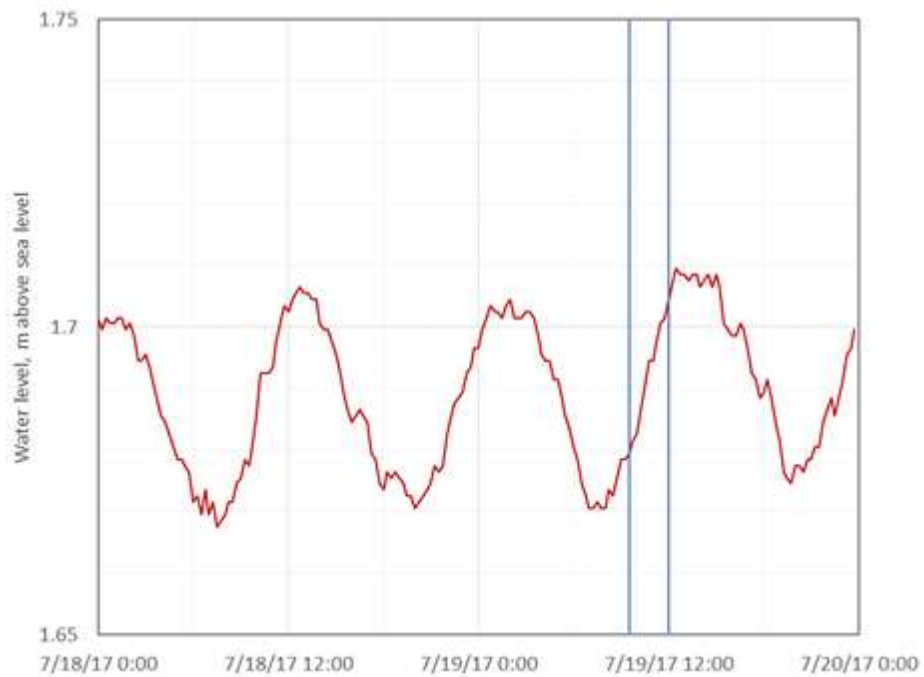


*Fig. 2-7: Water level response in MW2, adjacent to the Basin C before, during, and after the Simulated Runoff Test (SRT) on July 19, 2017. Water was injected into the basin during the period marked by vertical blue lines.*

The more rapid response in MW6 likely exists due to this well tapping a perched water table, possibly created by the buried portions of the 19<sup>th</sup> century Dyott Glass Works.

Specifically, MW6 was not drilled as deep as the other wells (Table 2-1) because an impeding layer was encountered, presumably the brickwork from the glass works (Fig. 2-6). Similarly, water levels in MW3, are more sensitive to precipitation events than the water levels in MW2 (Fig. 2-5, arrow). However, only medium or high precipitation events appear to affect water levels in these wells. At the current time the threshold value of rainfall needed to affect water levels in MW2, MW3, and MW6 is not yet quantified.

The spatial pattern of the response of well water levels to storm events is not consistent with infiltration of stormwater enhanced by the SMP. The response of water levels in MW2 and MW3 to storm events could indicate that the newly installed SMP is altering the local hydrogeological regime by infiltrating more stormwater. During construction the SMP devices were filled with amended soils in an effort to quickly infiltrate storm runoff. A relatively efficient infiltration of runoff is suggested by the relatively quick rise in the water levels in MW2 and MW3 following precipitation events. However, the spatial pattern of the response of well water levels to storm events is not consistent with an infiltration of stormwater solely from the SMP. As MW2 is adjacent to the SMP, and MW3 is located approximately 250 ft south of the SMP, the influence of infiltration from the SMP should be relatively stronger in MW2; however, MW3 is generally more responsive to storm events. Furthermore, MW1 is located adjacent to SMP E and water levels in this well do not respond to storm events. It may be that MW3 has a larger effective contributing area due to the heterogeneity (e.g., clay lenses) noted within the Trenton Gravel (Paulachok, 1991). Additionally, exfiltration from storm sewer infrastructure (Bhaskar and Welty, 2012; Ellis et al., 2004) near MW3 may be augmenting infiltrated water

from the SMP, resulting in the relatively higher increases groundwater levels. Further evidence that infiltrating water from the basin does not influence water level response is that when water was injected into Basin C for a Simulated Runoff Event (SRT), no water level increase was observed in MW2 adjacent to the basin (Fig. 2-7). The storm responses in MW6 likely are influenced more by the perched water table rather than the relatively small nearby SMP.

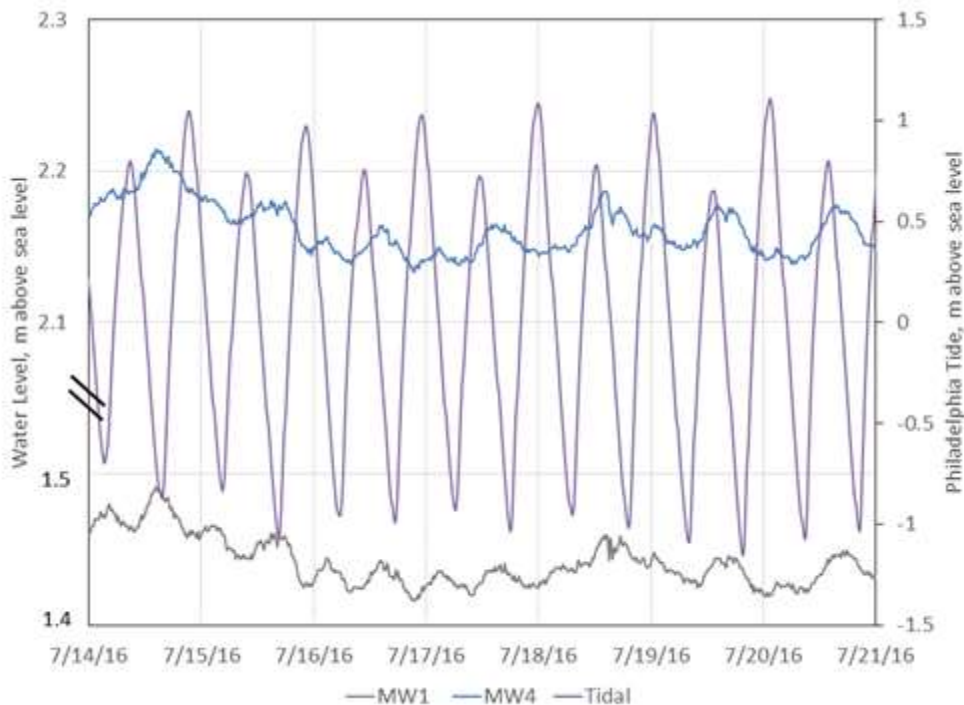


Figure 2-8. Comparison of tidal fluctuations in MW1 and MW4 plotted at the same scale (note axis discontinuity)

### *Tidal response*

A tidally forced pattern in well water levels is present only in wells MW1, 2, 3 and 4 (Figs. 2-5, 2-4, & 2-8). Signal processing analysis indicates that the fluctuations in water levels in these wells appear to lag tidal fluctuations by approximately 360 minutes in MW1 and MW4, 270 minutes in MW2, and 233 in MW3 minutes (Fig. 2-9). Unsurprisingly, the lag between fluctuations in water levels and tidal fluctuations increases with increasing distance from the

Delaware River (Fig. 2-2). Although MW4 is closer to the river than MW1, there is a similar response (Fig. 2-7), which may be due to the lower hydraulic conductivity in MW4 (Table 2-2). Furthermore, the effect of tidal influence (i.e., the amplitude) in the wells decreases as the distance to the Delaware River increases. Although the other monitoring wells (MW5-7) are installed at similar distances from the Delaware River (Fig. 2-2), no tidal signal is present in these groundwater records.

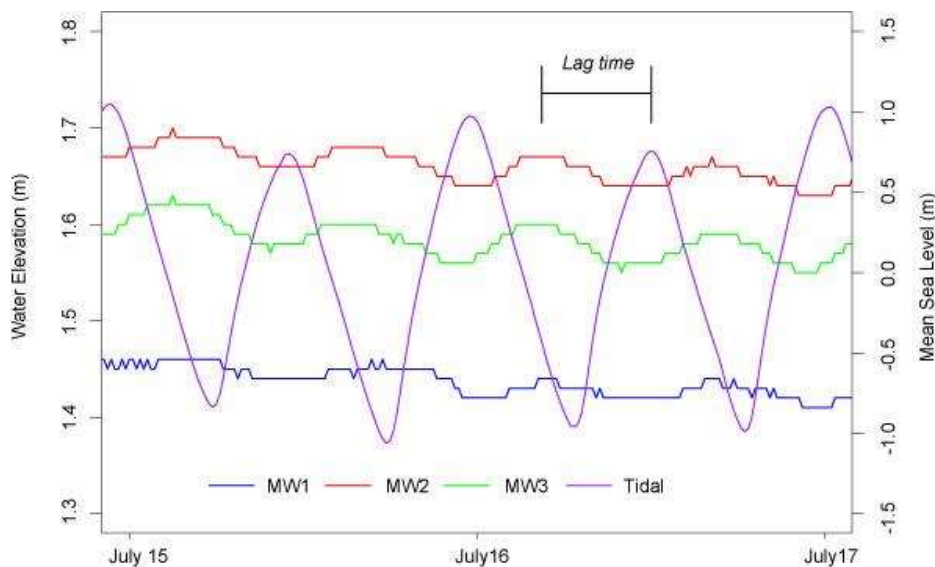
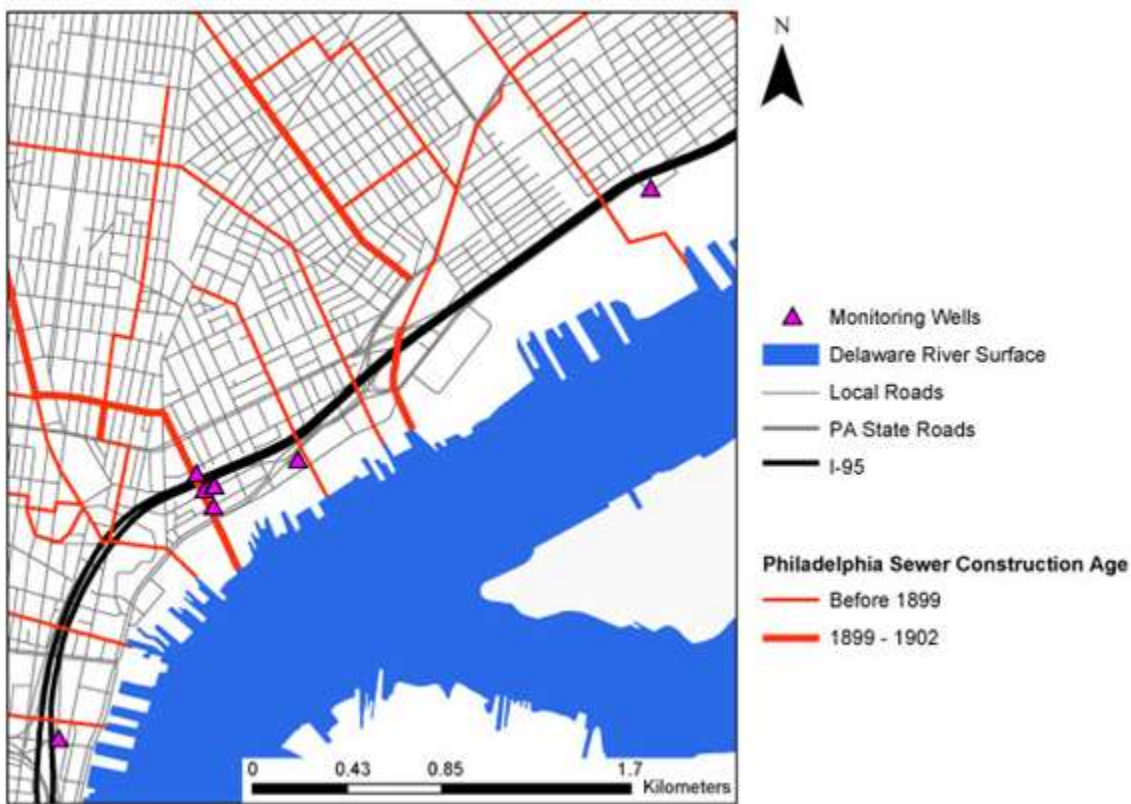


Fig. 2-9. Example of the lag time between tidal fluctuations of the Delaware River, and tidally influenced fluctuations in the water levels in MW1-3.

#### *Differences between wells*

The presence of a tidal signature in wells MW1-4 suggests there is heterogeneity within subsurface groundwater flow regimes in the I-95 study area. In particular, the waters in MW1-3 appear to experience a relatively more direct exchange with Delaware River waters. This discrepancy could result from several processes, including preferential flow paths due to bedrock fractures, the topography of the pre-European settlement landscape, or legacy impacts from urbanization such as sewer lines. For example, the historical Shackamaxon Relief Sewer is located within 5 m of wells MW1-3 (Fig. 2-10). The former sewer bed could thus serve as a

conduit, which would facilitate a relatively direct exchange of tidal fluctuations. Exfiltration of stormwater from the Shackamaxon sewer main (Ellis et al. 2004; Bhaskar and Welty 2012) has been noted as a cause of water level fluctuations. The storm and tidal responses in MW4 likely are influenced by the relatively shallow depth of the water table in addition to the relatively nearby sewer main (within 40 m).



*Fig. 2-10. The main sewerage system of Philadelphia in the study area in as of 1902. Sewer lines were digitized from a map included with the 1902 annual report of the City of Philadelphia (Philadelphia Department of Public Works Bureau of Surveys 1902).*

A related factor may be the locations of former streambeds. The analysis of high-resolution elevation data suggests MW1-3 are located in a former streambed. Specifically, flow accumulation analysis using high resolution (3.2 ft) LiDAR data (PAMAP Program PA



Department of Conservation and Natural Resources Bureau of Topographic and Geologic Survey, 2006) places a former stream near MW1-3 (Fig. 2-11). This stream appears to be the former Cohocksink creek, which was used as a canal sometime in the early 19<sup>th</sup> century (Berkeley and King, 1832), culverted, and ultimately buried in the 1860s (“Our Hidden Streams: Forgotten Watercourses Beneath the City of Philadelphia,” 1889).

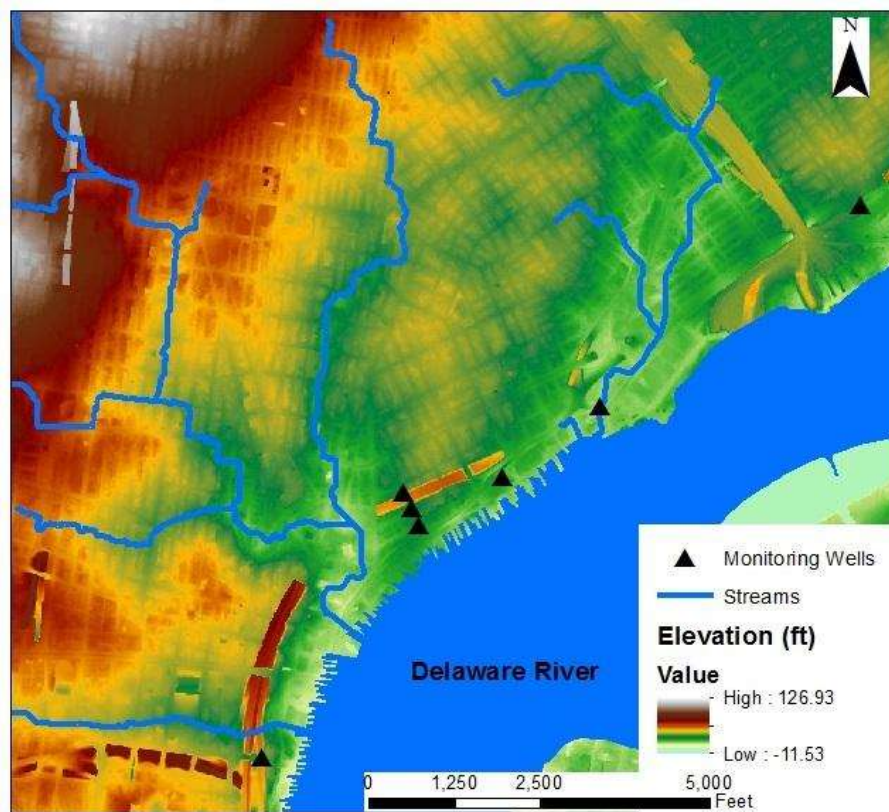


*Fig. 2-11. Historic stream channels in the vicinity of the I-95 study area. The high resolution (3.2 ft) LiDAR digital elevation model (PAMAP Program PA Department of Conservation and Natural Resources Bureau of Topographic and Geologic Survey, 2006) highlights the existence of now buried stream channels.*

Furthermore, the boring logs of MW1, MW 2, and MW3 suggest these wells are sited in a former streambed. For example, MW 1 and MW2 have corresponding sections (12.4 to 5.7 and, 13.2 to 7.7 ft asl, respectively) of sediments which consist of well sorted sand with silt and some gravel (Appendix 1). This sedimentological sequence would be consistent with fluvial

sorting and thus likely represents former alluvial sediments. Other poorly sorted units may represent valley floor colluvial deposits. Furthermore, boring logs indicate that the bedrock is mantled by silty fine sand (MW2 & 3) or sandy silt (MW1). However, the boring records in the other monitoring wells (MW4 & 5) indicate the bedrock is mantled by saprolite. This sedimentological sequence is consistent with MW1-3 being located in a former stream channel, as Lewis (1880) notes alluvial deposits in the Philadelphia vicinity do not lie upon unaltered rock except near streams. Thus, the absence of saprolite in these well borings further suggests MW1-3 are located in a buried stream valley.

The presence of this old stream channel may have led to the sewer being located along Shackamaxon Street. The relatively high permeability of these alluvial sediments, in conjunction with the conduit created by the sewage infrastructure, should increase the tidal exchange between the Delaware River and shallow groundwater, thus driving the tidal signal observed only observed in MW1-3. Thus, a combination of spatial analysis, analysis of the historical written record, and sedimentological evidence suggest that the observed discrepancy ultimately likely results from the pre-European settlement landscape.

#### *Patterns in Groundwater Temperature and Conductivity Data*

Specific conductivity in MW3 ranged between 538  $\mu\text{S}/\text{cm}$  and 751  $\mu\text{S}/\text{cm}$ , and water temperature in MW3 ranged between 13.34  $^{\circ}\text{C}$  and 17.73  $^{\circ}\text{C}$  (Fig. 2-12). During the period of record, the water temperature in MW3 gradually increases until it reaches a maximum of 17.73  $^{\circ}\text{C}$ , and then seemingly exhibits an equally gradual decrease. This pattern is likely driven by seasonality.

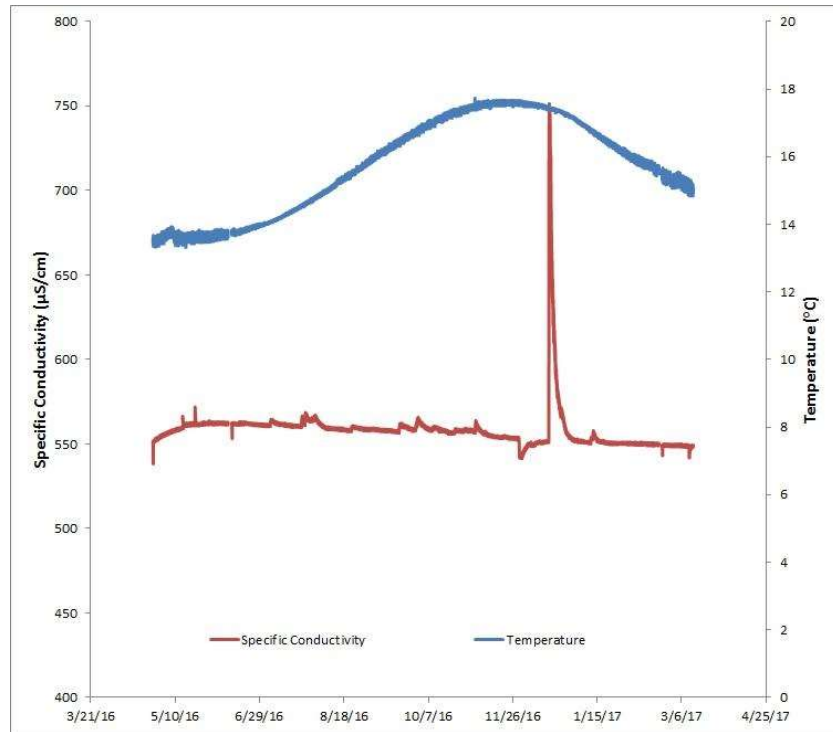


*Fig. 2-12. Groundwater specific conductivity ( $\mu\text{S}/\text{cm}$ ) and temperature ( $^{\circ}\text{C}$ ) measurements in MW3 over the period of observation.*

Contrary to the annual trend in groundwater temperatures, specific conductivity in MW3 appears to remain relatively constant throughout the year, averaging  $559 \mu\text{S}/\text{cm}$ . However, there is a brief period (December 17 – 27 2016) where specific conductivity appears to rapidly respond to an external forcing, resulting in a sharp rise in specific conductivity (Fig. 2-12). The exact cause for this rise is not entirely clear; however, it is possibly related to road salting activities.

Specifically, the dissolution of road salt ( $\text{NaCl}$ ) in roadside meltwaters generally increases loadings of  $\text{Na}^{+}$  and  $\text{Cl}^{-}$  to shallow ground waters (Labadia and Buttle, 1996), thereby increasing the electrical conductivity in these waters (Bauske and Goetz, 1993). Thus, the sharp rise in specific conductivity on December 17 could indicate the infiltration of a pulse of salt-rich meltwater.



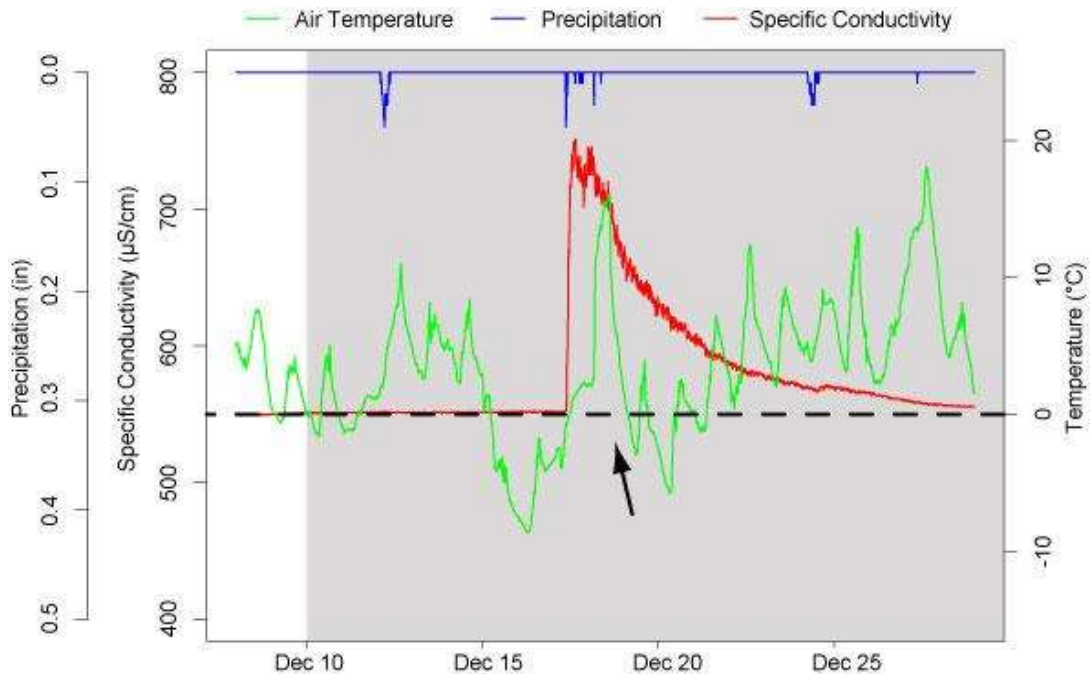


*Fig. 2-13. Specific conductivity (red) in MW3 waters, air temperature (green), and precipitation (blue) for the period of December 8 – December 28, 2016. The grey shaded box indicates the period where road deicers were likely applied to roadways. The arrow indicates the period when a melt event likely occurred.*

A pulse of meltwater is further suggested by the recorded air temperature data. Namely, a week prior to this event (i.e., December 10, 2016) marks the first time air temperatures dropped below freezing for a significant period (9.75 hours). Thus, December 10 likely represents the beginning of the period in the winter of 2016 when deicing salts were applied to roadways (Fig. 2-13, shaded grey box). Similarly, air temperatures rise above freezing on December 17, 2016 concurrent to the sharp increase in electrical conductivity (Fig. 2-13, arrow). It is then likely that this event indicates a delivery of salt-rich meltwaters to groundwater. Because well MW3 is located approximately 250 ft south of the SMP, the concurrent rise in air temperature and specific conductivity would not be consistent with subsurface delivery of salt-rich waters. Consequently, it is likely that the source of these salt-rich waters is the local streets rather than infiltrated waters from the SMP device. However, because groundwater chemistry was not sampled at this time we cannot confirm our speculations with patterns in groundwater  $\text{Na}^+$  and

Cl<sup>-</sup> concentrations. An increase in specific conductance was not observed for other snow events such as the March 14, 2017 Stella blizzard, so it is not clear why this was the only event observed to alter the conductivity signal in MW3.

## **Implications**

### *Distance Between SMP and Water Table*

Enough space for water to infiltrate is imperative to the successful operation of infiltration based green infrastructure. For this reason, the Pennsylvania Department of Environmental Protection (PADEP) stormwater BMP guidelines establish a minimum 2 ft buffer between the bottom of an infiltration basin and the seasonal high groundwater table (Pennsylvania Department of Environmental Protection, 2006). Comparing the seasonal high water levels in MW1 and MW2 (6.30 and 6.20 ft asl, respectively) to an assumed maximum depth of 2 ft of amended soils (as per AECOM design documents) below the lowest land surface elevation in SMP device E and C (21 and 18 ft asl, respectively) indicates the appropriate buffer elevations for SMP device E and C are 17 and 14 ft asl, respectively (Table 2-3). These buffer elevations are located 10.7 and 7.8 ft above the maximum water elevations observed in MW1 and MW2, respectively, and thus groundwater mounding does not appear to threaten the efficacy of the SMP devices in the near future.

While the current conditions meet the requirements established by the PADEP stormwater BMP guidelines, it is possible that sea level rise driven by global climate change could affect subsurface hydrologic flow regimes, thereby decreasing the efficiency of these SMP devices. In particular, the tidal signature in wells MW1-3 suggest that rises in sea level, and by extension the surface of the Delaware River, could raise the water table in the study area.

Table 2-3. Maximum observed water level in the two monitoring wells located nearest to SMP devices. Also provided is the elevation of the lowest land surface in each SMP device, and the appropriate 2 ft buffer as defined by PADEP stormwater BMP guidelines.

Well	Seasonal Max Water Table (ft asl)	Nearby SMP Device	Lowest Elevation of SMP Device (ft asl)	Buffer Elevation (ft asl)	Space Between Water Table and Buffer (ft)
MW1	6.30	E	21	17	10.7
MW2	6.20	C	18	14	7.8

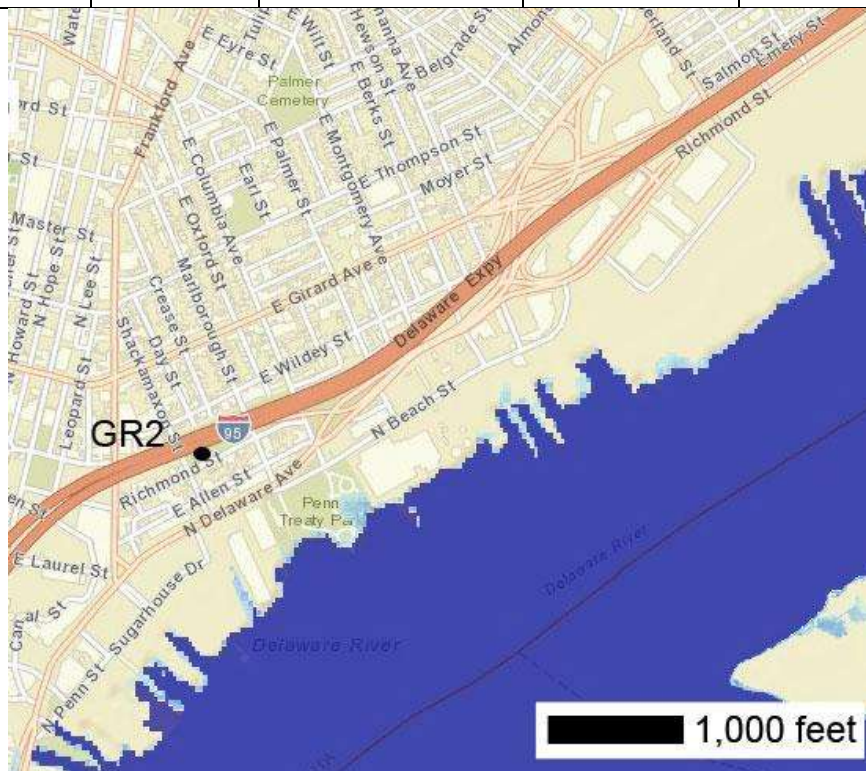


Fig. 2-14. Predicted inundation (light blue) in the area surrounding GR2 caused by a 3ft rise in sea level (NOAA Coastal Services Center, 2017).

predict that sea level in Philadelphia will rise by approximately 0.01 ft per year (Miller et al., 2013). Extrapolating this increase to 20 years from now suggests a total sea level rise of 0.20 ft, which would not be enough of a raise to inundate the studied SMP devices (Fig. 2-14). Thus, it appears that long term (i.e., 20 years from now) changes in local sea level, and by extension, the

local water table will have a minimum influence on the long-term operation of the SMP devices installed.

Future groundwater monitoring will incorporate data collected from the three monitoring wells installed by Villanova University. Including water level data from these wells would allow for higher resolution mapping of the local water table, and would further refine the spatial pattern of groundwater monitoring. Furthermore, the chemical analysis of water samples collected from these extra wells could ascertain if there is any subsurface transport of contaminants associated with infiltrated road runoff.

#### *Seasonal Variation in Conductivity*

Contrary to expectations, the relatively large winter storm Stella, which occurred on March 14, 2017, did not affect specific conductivity measurements in MW3. This is surprising, as it would stand to reason that deicers would be applied heavily to roadways in advance of the predicted blizzard. The absence of a response in specific conductivity measurements to this event could imply that road salt is accumulating in the SMP device, and thereby not dramatically affecting ground water conductivity levels. Conversely, it is possible the sharp rise in specific conductivity on December 17, 2016 might not indicate an infiltration of salt-rich runoff, and instead represent an anomalous event that occurred somewhere else in the groundwater shed. In the coming months, additional conductivity loggers could be installed in MW1 & 2 to help refine the spatial interpretation of future anomalous events (e.g., the sharp rise in specific conductivity on December 17, 2016), and determine if such events are due to solute rich waters infiltrating in SMP C, or the infiltration of solute-rich runoff elsewhere.

## *Influence of Historic Stream Channels and Urban Legacies*

The influence of a historic stream channel on the observed water level dynamics in MW1-3 poses important implications for the site selection of future SMPs. Specifically, the historic land surface and land use appear to influence subsurface hydrologic flow regimes. In particular, the subsurface heterogeneity caused by legacy urbanization activities (e.g., the sewerage and burying of streams) leads to unexpected patterns in groundwater dynamics, which can in turn, possibly influence runoff infiltration dynamics in unexpected ways. For example, the installation of a SMP could inadvertently connect to a legacy stream channel, thereby creating a subsurface flow path which would facilitate a relatively direct transport of infiltrated runoff to adjoining areas. Thus, future site selection should carefully assess a combination of utility records, historic maps, and high-resolution elevation data to ensure potential risks are fully constrained.

## **References**

- Bauske, B., & Goetz, D. (1993). Effects of Deicing-Salts on Heavy Metal Mobility. *Acta Hydrochimica et Hydrobiologica*, 21(1), 38–42.
- Berkeley, & King, E. F. (1832). *A digest of the acts of assembly, and of the ordinances, of the commissioners and inhabitants of the Kensington district of the Northern Liberties: for the government of that district*. Oxford University. Joseph Rakestraw.
- Bhaskar, A. S., & Welty, C. (2012). Water balances along an urban-to-rural gradient of metropolitan baltimore, 2001-2009. *Environmental and Engineering Geoscience*, 18(1), 37–50. <https://doi.org/10.2113/gseegeosci.18.1.37>
- Ellis, J. B., Revitt, D. M., Blackwood, D. J., & Gilmour, D. J. (2004). Leaky sewers: assessing the hydrology and impact of exfiltration in urban sewers. In B. Webb, M. Acreman, C. Maksimovic, H. Smithers, & C. Kirby (Eds.), *hydrology: science and practices for the 21st century* (pp. 266–271). Imperial College, London: British Hydrological Society.
- Labadia, C., & Buttle, J. (1996). Road salt accumulation in highway snow banks and transport through the unsaturated zone of the Oak Ridges Moraine, southern Ontario. *Hydrological Processes*, 10, 1575–1589. Retrieved from [http://onlinelibrary.wiley.com/doi/10.1002/\(SICI\)1099-1085\(199612\)10:12%3C1575::AID-HYP502%3E3.0.CO;2-1/abstract](http://onlinelibrary.wiley.com/doi/10.1002/(SICI)1099-1085(199612)10:12%3C1575::AID-HYP502%3E3.0.CO;2-1/abstract)

- Lewis, H. C. (1880). The Surface Geology of Philadelphia and Vicinity. *Proceedings of the Academy of Natural Sciences of Philadelphia*, 32, 258–272.
- Machusick, M., Welker, A., & Traver, R. (2011). Groundwater Mounding at a Storm-Water Infiltration BMP. *Journal of Irrigation and Drainage Engineering*, 137(3), 154–160. [https://doi.org/10.1061/\(ASCE\)IR.1943-4774.0000184](https://doi.org/10.1061/(ASCE)IR.1943-4774.0000184)
- Miller, K. G., Kopp, R. E., Horton, B. P., Browning, J. V., & Kemp, A. C. (2013). A geological perspective on sea-level rise and its impacts along the U.S. mid-Atlantic coast. *Earth's Future*, 1(1), 3–18. <https://doi.org/10.1002/2013EF000135>.Received
- NOAA Center for Operational Oceanographic Products and Services. (2017). Observed Water Levels. Retrieved March 13, 2017, from <https://tidesandcurrents.noaa.gov/waterlevels.html?id=8545240>
- NOAA Coastal Services Center. (2017). Sea Level Rise and Coastal Flooding Impacts. Retrieved April 21, 2017, from <http://54.243.129.238/SLR.html#%5Cnhttps://coast.noaa.gov/slr/>
- NOAA National Climatic Data Center. (2010). PHILADELPHIA INTERNATIONAL AIRPORT, PA US 1981-2010 Normals. Retrieved April 27, 2017, from <https://www.ncdc.noaa.gov/cdo-web/datatools/normals>
- Our Hidden Streams: Forgotten Watercourses Beneath the City of Philadelphia. (1889, August 11). *The Times - Philadelphia*, p. 7. Philadelphia, PA.
- PAMAP Program PA Department of Conservation and Natural Resources Bureau of Topographic and Geologic Survey. (2006). PAMAP Program 3.2 ft Digital Elevation Model of Pennsylvania. Retrieved from <http://www.pasda.psu.edu>
- Paulachok, G. N. (1991). Geohydrology and ground-water resources of Philadelphia. *United States Geological Survey Water-Supply Paper*, 2346.
- Pennsylvania Department of Environmental Protection. (2006). *Pennsylvania Stormwater BMP Manual*.
- R Core Team. (2016). R: A language and environment for statistical computing. Vienna, Austria: R Foundation for Statistical Computing. Retrieved from <https://www.r-project.org/>

## Chapter 3: Hydrologic monitoring

### Introduction

Villanova and Temple Universities are currently monitoring 4 SMPs along the Northbound section of Interstate 95 in the Northern Liberties neighborhood of Philadelphia. Monitoring is occurring within two city blocks consisting of 4 separate SMPs; these are along Richmond Avenue between Frankford Avenue and Marlborough Street (Figure 3-1). The three SMPs located between Shackamaxon and Marlborough Streets are linearly adjacent, but hydrologically independent (SMPs C, D, and G). The SMP between Shackamaxon and Frankford (SMP A), is a single, long, narrow SMP with three inlets and two outlets; it is further characterized by the absence of maintenance. SMPs C, D, and G will be compared with A, which is about the size of C, D, and G combined. Task 3 is split into two parts, water quantity monitoring (led by Villanova University; Chapter 3) and water quality monitoring (led by Temple University; Chapter 4). The two teams have shared data and coordinated activities in conducting the empirical and modeling efforts described in the corresponding chapters. Note that the majority of the content in Chapter 3 was recently synthesized in the Master's Thesis of Nora Schmidt, entitled *Bioswale Modeling in a Transitive Urban Transportation Setting: Green Infrastructure Instrumentation, Challenges, and Lessons Learned*.

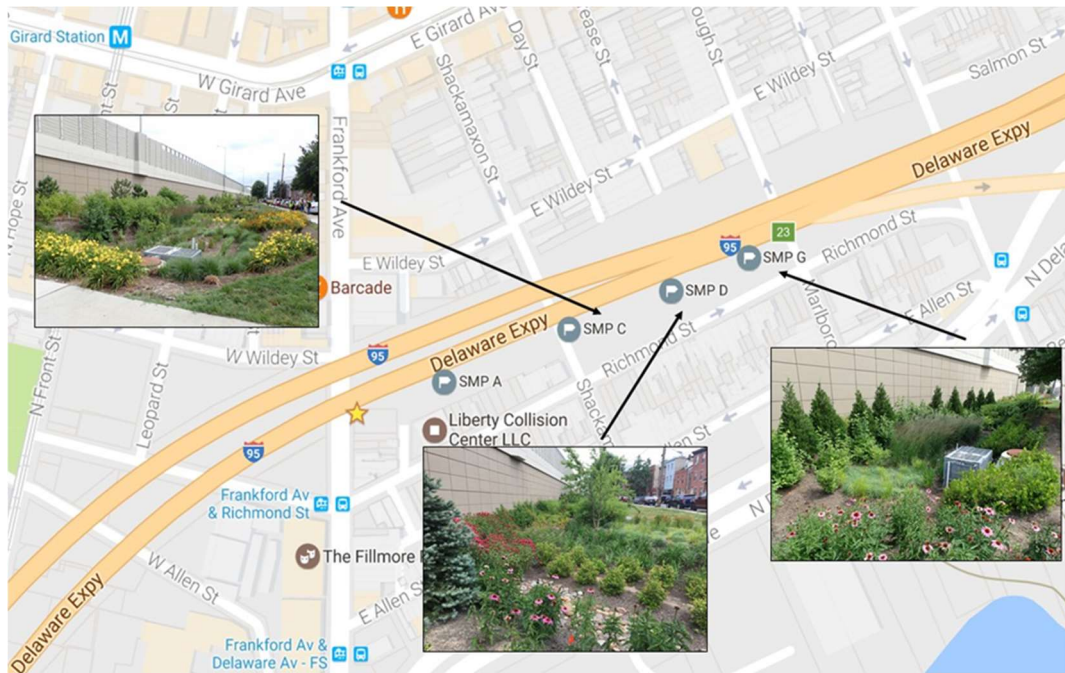


*Figure 3-1: SMP A, C, D, and G locations, large weather station location is denoted by yellow star (Google 2017).*

Over the course of this project, the team designed and implemented an extensive monitoring design. SMPs C, D, and G were the initial primary focus of monitoring; SMP A followed. Two significant challenges limited the data record and should be noted at the outset: The drainage area was significantly smaller than the design, primarily due to slopes of the temporary roadway and NJ barriers that directed the flow away from these SMPs; this was by the monitoring itself. The reduced drainage area meant that the runoff from most storms was smaller than designed, such that it could not be measured accurately by the inflow meters. Note that this reduced water volume could still be recorded by the depth and soil meters. The second challenge was sensor failure; some sensors had to be returned to the manufacturer to be replaced or repaired.

Both to test instrumentation and to simulate a larger storm, the Villanova and Temple teams worked with PennDOT and the Philadelphia Water Department to conduct a Simulated Runoff Test (SRT); this involved opening fire hydrants and filling the SMPs. The SRT provided data



that allowed the teams to evaluate SMP performance under conditions similar in magnitude to expected design events. In addition, the actual size of the drainage areas that contribute to the SMPs are being determined using LiDAR.

### **History of Site**

Prior to reconstruction, the highway was built on an embankment with single span bridges over each intersection with streets throughout Philadelphia. The original construction lacked stormwater management controls and the runoff from the highway was discharged directly into the combined sewer system. In the recent reconstruction, the embankment system was replaced with a retaining wall to add wider shoulders. To meet Philadelphia's stormwater regulations, roadway runoff is now managed before discharging to the sewer system through the constructed bioswales and other SMPs. The bioswales are designed to meet the Philadelphia Water Department and the PADEP NPDES Phase II permit regulations.

### **Size & Drainage Area**

Bioswales in GR2 were designed given constraints including space, available sunlight, drainage area, and regulatory guidelines. The drainage area for each bioswale is intended to cover the highway's directly connected impervious area (DCIA). Figures 3-2 through 3-4 show drainage areas as planned; (see Chapter 5 for the drainage areas active during the construction phase). The SMPs also receive some water from small grassy areas adjacent to them (between the sidewalk and landscaped areas); these are shown in Figure 3-5a and b. Further, the highway's drainage area is bounded by New Jersey barriers that separate the two directions of traffic. The northbound lanes are sloped such that flow is directed to the inlets in the center of the northbound lanes as well as to an inlet on the edge of the Girard Street exit ramp, directly above the exit into the bioswales. Additional New Jersey barriers currently form the Girard Street exit

ramp (i.e., the lane closest to the bioswales), blocking runoff from parts of the roadway; these barriers are intended to be removed after the completion of GR3.

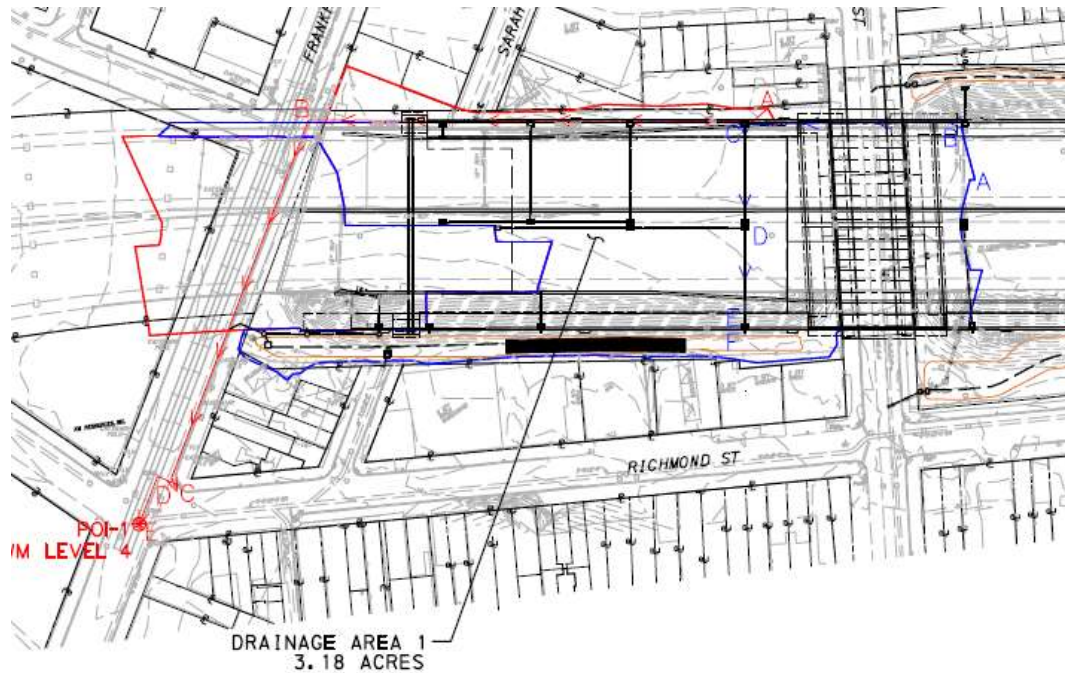


Figure 3-2. SMP A drainage area defined by AECOM (AECOM/URS 2015).

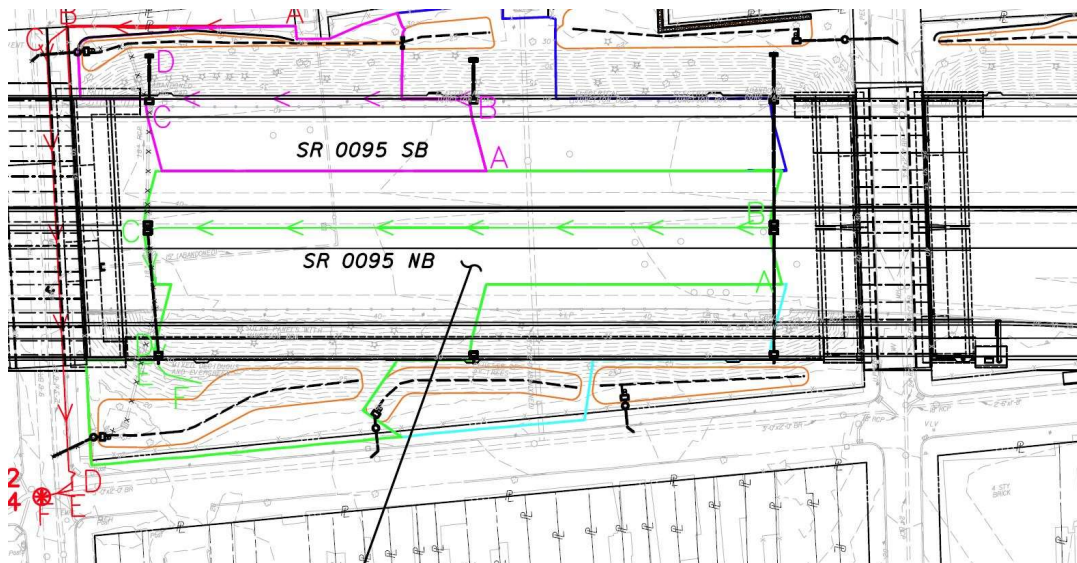


Figure 3-3. SMP C and D drainage area defined by AECOM (AECOM/URS 2015).

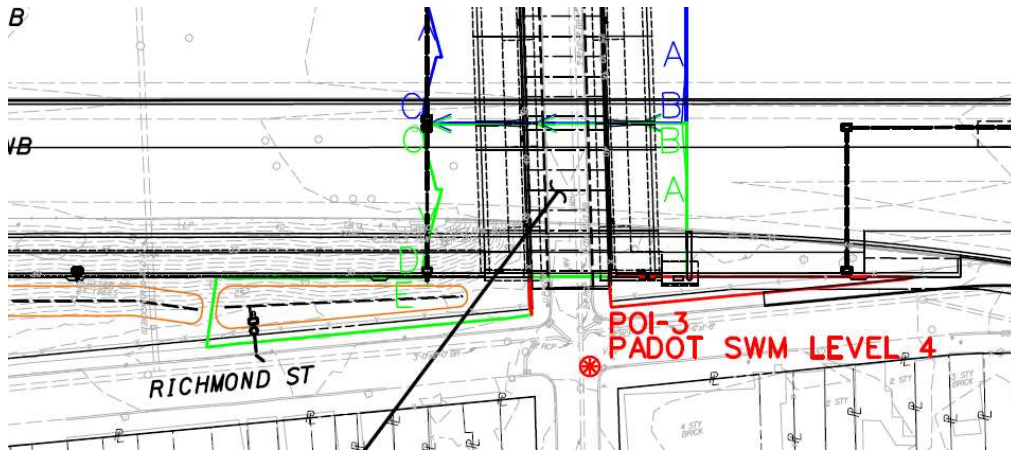
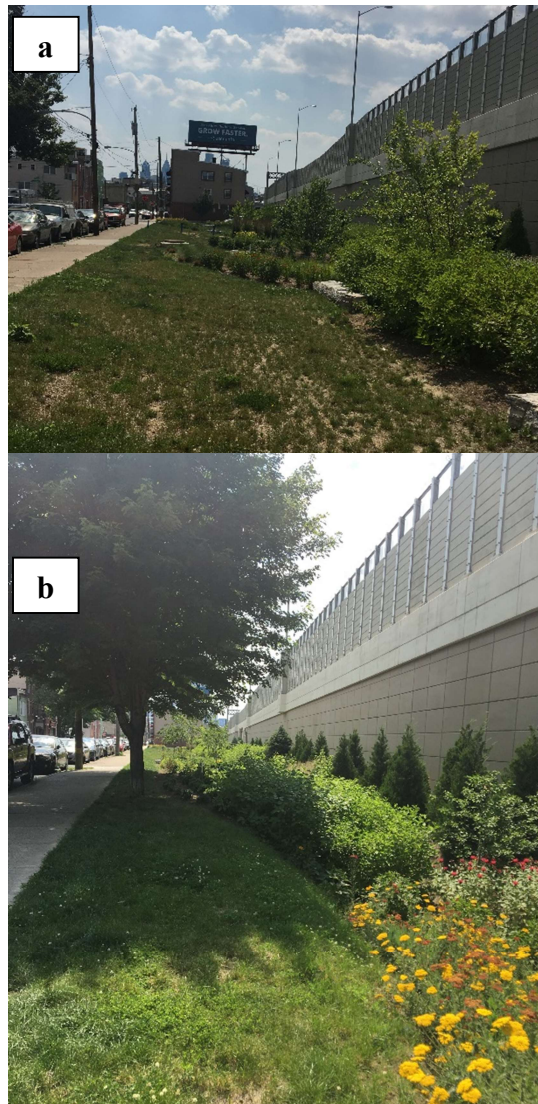


Figure 3-4. SMP G Drainage Area Delineation (AECOM/URS 2015).



*Figure 3-5. Pervious drainage areas for (a) SMPs D, C and (b) G.*

The bioswales in GR2 were designed by AECOM to reduce the peak rate of two-year storms to the pre-development one-year peak rate. PWD requires SMPs to be able to manage one-year, 24 hour, NRCS Type II storm events (Philadelphia Planning & Research and PWD 2014). Further, recent regulations have increased the minimum design to the 1.5-inch storm (PWD 2015), which has been incorporated into the new SMP designs accompanying future roadway reconstruction. SMP plans created by AECOM were submitted to Philadelphia Water Department (PWD) for approval and then to PennDOT. The loading ratios are all below the

suggested 16:1 ratio set forth by PWD (PWD 2015); SMPs A, C, D, and G have loading ratios (DCIA/SMP Area) of 8.5, 3.8, and 7.0, respectively. The maximum capacity of each bioswale is that corresponding to a 100-year storm (8.4 inches of rainfall on the DCIA); this would require the outlet structure not exceed the discharge rate set by PWD. Also, there is a 6-inch berm above the 100- year storm volume to prevent overflow onto sidewalks and residential properties. The bioswales' outlet structures have a variety of overflow orifices and weirs. These design features were incorporated to accommodate the City's Long Term Control Plan (LTCP) that restricts releases into the combined sewer system to 1-year, 24 hour storm volumes, at an average rate of 0.12 cfs per acre and with a maximum rate of 0.24 cfs per acre in 24 to 72 hours (Philadelphia Planning & Research and PWD 2014; PWD 2009).

Each bioswale has a six-inch corrugated pipe underdrain laid at a slope of 0.5 %. A two-foot-thick layer of amended soil was installed above the underdrain, with geotextile lining the soil and backfilled with Type I backfill. The design schematic below (Figure 3-6) shows the underdrain placement in the bioswale as well as the inlet and stilling basin. The underdrains were left uncapped for one growing season to allow the plants to establish, then they were sealed with a metal plate screwed onto the outlet structure. If the basin does not infiltrate as predicted, then the underdrain can be uncapped, allowing flow from the underdrain to convey stormwater directly to the outlet structure. If the structure is uncapped, the release rate into the combined sewer system is limited to by the values described above from PWD.

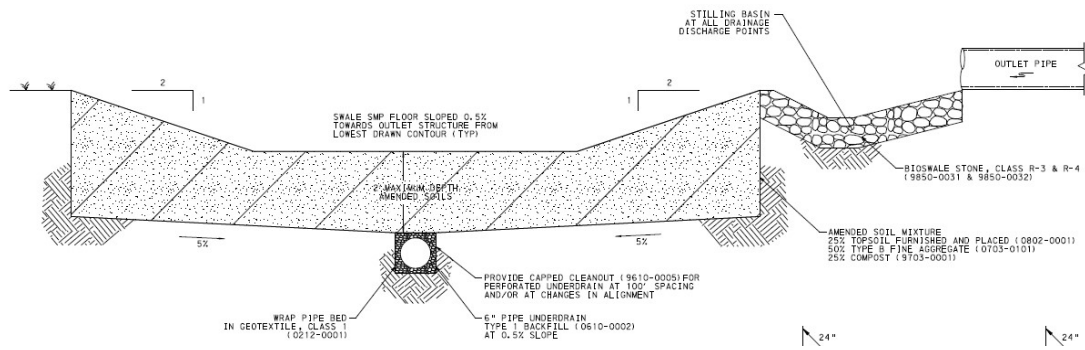


*Figure 3-6. Side view of a bioswale showing the underdrain and amended soil together with a pipe that conveys stormwater from the highway and its associated stilling basin (AECOM/URS 2015).*

## Monitoring Design

Villanova is monitoring the quantity of water entering and exiting each of the bioswales, which requires quantifying flow through the system. This begins with measuring the volume and timing of runoff coming from the highway and its ponding depth throughout the bioswale. These data describe the rates of hydraulic and hydrologic processes as water moves off the drainage area, through piping and into the bioswale, and out via infiltration or overflow to the sewer.

When monitoring green infrastructure, sensor choice is critical. The parameters monitored, as well as the precision and accuracy of sensors determine the validity of the measurements. In many cases, monitoring is used to show regulatory compliance, so the accuracy and precision of the monitoring equipment is of utmost importance. Moreover, the resolution and accuracy specifications provided by the manufacturer were determined under laboratory settings, so field testing and calibration are necessary to ensure that data collected outside the laboratory are of acceptable quality.

Figure 3-7 details the monitoring scheme for SMP C; the other SMPs in GR2 have a similar monitoring scheme but do not have groundwater observation wells. Flow is recorded at the inlet pipe to the bioswale using area velocity sensors (Blue Siren); there are also soil moisture sensors



at different depths at the bottom of the pond (Stevens Hydraprobe). Ponding water level is recorded with pressure transducers at the outlet (Campbell Scientific), and flow leaving over the outlet structure is measured with a V-notch weir. Observation wells equipped with Decagon Devices CTD-10 sensors are used to measure local groundwater mounding and changes in electrical conductivity. All sensors selected for measurement have variable ranges to accommodate the expected flows and depths ranging from smaller, more frequent storms (0.5-1.5 inches of precipitation) up to the maximum 100-year storm. More detailed descriptions of the monitoring equipment are provided below, including accuracy and precision specifications.

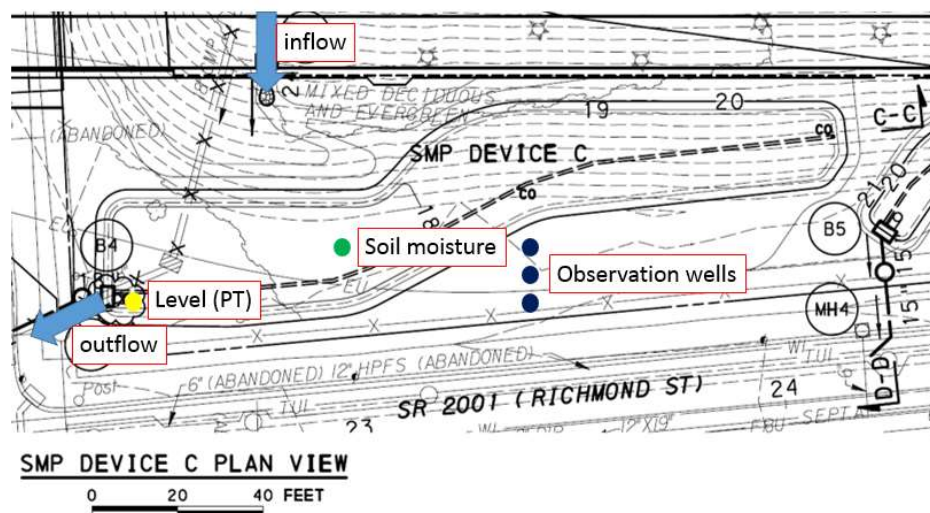


Figure 3-7. Configuration of instrumentation for monitoring water quantity in SMP C.

### Data Acquisition

Each sensor was tested in the lab to verify that it functioned before it was installed in the field. All sensors for SMP C, D, and G, as well as a weather station, were hardwired to a Campbell Scientific CR-6 datalogger. This logger is housed in an equipment box that is attached to a 10-foot wooden utility pole installed between SMPs C and D. The system is powered by a

solar panel, which is regulated with a charge regulator (CH-150; Campbell Scientific) and charges a 12 volt battery. Data were collected continuously to facilitate measurements of response times and related properties of water movement in each bioswale (described further in Chapter 4). Data were collected every five minutes from all sensors, as this interval is sufficient to capture peak flow and other point measurement values critical for stormwater modeling and research (Urbonas 2007). The system was further designed so sensors could communicate with each other and send their data at scheduled times to Villanova. Specifically, the data are transmitted by radio (Campbell Scientific RF407) to the large weather station at the intersection of the northbound lanes of I-95 and Frankford Avenue (Figure 3-3); data are transmitted to a computer on Villanova's campus every six hours through a Verizon cellular modem (Sierra Wireless, AirLink Raven XT). The data are reviewed and uploaded monthly onto a database stored on Villanova's servers.

#### *Weather Sensors*

The weather sensors installed on the pole between SMPs C and D are shown in Figure 3-8:

- Solar radiation sensor (model PYR from FTS Inc.). This was previously a LI-200RX Pyranometer (LI-COR)
- Photosynthetically active radiation sensor (model PAR from FTS Inc.)
- Wind monitor (R.M. Young 05103)
- Temperature sensor (Campbell Scientific CS109)
- Rain gage tipping bucket with an eight-inch orifice (Texas Electronics TE525)

The instrumentation follows the analytical methods outlined in the Quality Assurance Project Plan (QAPP) set forth under the grant terms.





*Figure 3-8. Weather station installed between SMPs C and D.*

In October 2016, a weather station was installed at the top of 50-foot utility pole above I-95, at the intersection of Frankford Ave and I-95 Northbound (Figure 3-9). This larger weather station is installed above the highway to monitor the weather over a wider area and without the influence of shade from the highway's retaining wall. The equipment box and solar panel are located at ground level for ease of access. This station is similar to the one between SMPs C and D, but is also equipped with a Raven Cellular modem with a 21831-dipole cellular antenna to transmit the data back to Villanova. The sensors are similar to those between SMPs C and D, but there is also a barometric pressure sensor (Campbell Scientific CS100), a temperature and relative humidity sensor (Campbell Scientific HC2S3-L55-PT) and a second rain gage (Campbell Scientific CS700).

There are two rain gauges to facilitate comparison of differences between sensors and to provide a backup system in case one is not working. The accuracy of the rain gauges is important

when quantifying and analyzing the inflow and ponding results. Both rain gages have the same resolution but differ slightly in their accuracy. The stated resolution is important as it defines how precise the measurement readings are. The accuracy of rainfall and other parameters are important because errors can compound during modeling and data manipulation. The Texas Electronics TE525 tipping bucket has a precision of 0.254 mm (0.01 in) increments and an accuracy of  $\pm 1$  percent at rates up to 50.8 mm/hr (2 in/hr) (Campbell Scientific Inc. 2017). The accuracy of the CS700 rain gage is  $\pm 2$  percent for under 250 mm/hr (9.8 in/hr) and the resolution is 0.254 mm (0.01 inches) (Campbell Scientific Inc. 2016b). The weather station with both rain gauges is shown in Figure 3-9 and 3-10.

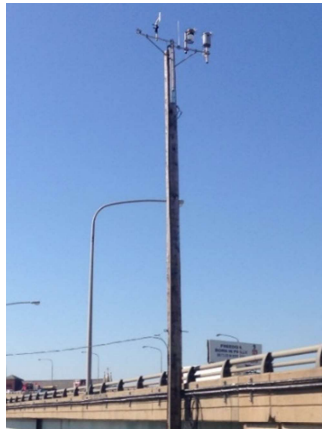


*Figure 3-9. Weather station above I-95 with rain gauges and wind monitor*



*Figure 3-10: Bird's eye view of large weather station above I-95*

Data from the rain gauges at the two elevations make it possible to (a) compare precipitation received by the I-95 road surface with rain entering bioswales and (b) evaluate spatial variation in rainfall so that the correct hydrological response can be simulated in our modeling effort. The variation in rainfall amounts and intensities are particularly important to evaluate how sharp peaks in rainfall affect soil infiltration rates, as these are particularly difficult for bioswales to accommodate (Phillips and Buchanan 2011).

### *Inflow Sensors*

SMP A has three inlets (N8, N9, and N10) while the other SMPs have one inlet each (N5, N6, and N7 for SMPs C, D, and G, respectively); all of these convey stormwater runoff from the highway above. SMPs C and G have an extra pair of inlets in the middle of the northbound travel lanes that are piped approximately 80 feet under the roadway to the third inlet. Inlets entering into SMPs C and G have lateral inflow and are specifically functioning as ‘drop manholes’; they allow local energy dissipation and thus lower velocity (Christodoulou 1991). In SMP D, inlet N6 only receives water from the roadway surface that enters through the grates since it only receives water from the Girard Street exit ramp. The inlet schematic is shown in Figure 3-11, with a

PennDOT Standard Type M inlet box on the roadway that drops around ten feet before making a 90-degree bend to enter the bioswale. After making the 90-degree turn, there is a 6-foot length of pipe before the water drops to a rock stilling basin prior to the bioswale.

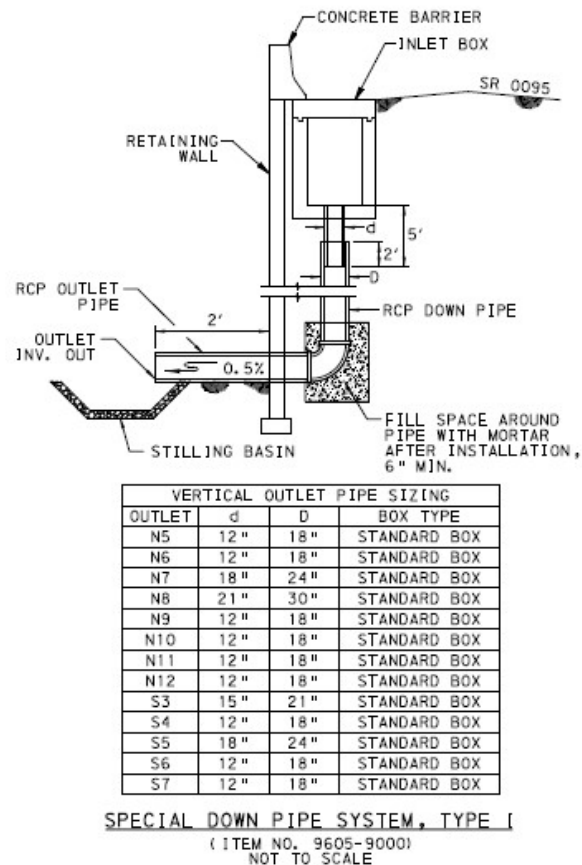


Figure 3-11. Inlet schematic and sizes (AECOM/URS 2015)

Each bioswale receives a small amount of runoff from the surrounding grassy areas. Table 3-1 shows the area of directly connected impervious area (DCIA) draining to each bioswale, as well as the area of the bioswale. The pervious drainage area is not measured by a flow meter, as the flow is distributed across the edge of the bioswale.

Table 3-1. Drainage areas of the three focal SMPs in GR2 and the areas of the SMPs themselves

	DCIA -ac (m <sup>2</sup> )	Pervious Drainage -ac (m <sup>2</sup> )	Bioswale Area - ft <sup>2</sup> (m <sup>2</sup> )
<b>SMP C</b>	0.954 (3860)	0.285 (1150)	4889 (454)
<b>SMP D</b>	0.220 (892)	0.156 (631)	2529 (235)
<b>SMP G</b>	0.417 (1690)	0.009 (35.6)	2587(240)

## *Flow Measurement*

Hydrologic and hydraulic models depend on water depth and velocity measurements to calibrate models to the specific system. Inlets are a very critical location for recording water depth, velocity, and flow as they are a concentrated location where most of the drainage area drains to before entering each bioswale. Understanding and correctly calculating the flow through these pipes is the first step to gauging the impact of a storm and calibrating any model. Thus, these measurements need to be accurate, accessible and effective in order to accurately portray urban stormwater drainage systems (Aguilar et al. 2015). Errors in data are often introduced in the field, when the calibrated flow devices do not meet the conditions in which their rating curves were developed, when the device is improperly installed, or not maintained enough or properly (Quigley et al. 2002). Each sensor chosen for monitoring was carefully chosen for accuracy to minimize modeling errors.

An analysis using the program Green Infrastructure Flow Measurement Evaluation Tool (GIFMET) was performed to determine the best flow measurement device to install. The input for the program included the impervious watershed area, impervious watershed abstractions, pervious watershed area, pervious curve number, basin top area, basin bottom area, basin porosity, infiltration rate, sensor accuracy and device specific information. GIFMET is a program developed by Ryan Lee, PhD for estimating the effectiveness of flow measurement devices and hydrologic capture of SMPs during large storm events (Lee 2015). The model is run with Excel and based off rainfall from the Bio infiltration Traffic Island (BTI) rain garden rain gage at Villanova between 2011 and 2015 (Lee 2015). Thelmar weirs and V-notch weirs were found to have unacceptable estimated maximum flow measurement errors and too large

estimated percent over topping. Thus, area velocity flow meters were chosen to measure and calculate flows entering the bioswale directly from the highway.

Acoustic velocity meters (AVM) or acoustic Doppler velocimeters (ADV) are systems used when other measurement methods (flumes and weirs) are not appropriate due to low velocities, improper installation environments, backwater conditions, small watersheds with “extremely peaky flows” and large variations from mean flow rates (Quigley et al. 2002; Vermeyen 2000). AVM sensors were chosen due to their small size, ease of installation and general low cost (Bonakdari and Zinatizadeh 2011). AVM sensors are additionally appealing due to their ability to accurately measure both low and high flow rates. The sensors measure velocity and depth of the water column, which are used to calculate flow rates with Equation 1.

$$Q = A\bar{V} \quad \text{Equation 1}$$

where,  $Q$  represents discharge,  $A$  represents area of the cross section of the pipe, and  $\bar{V}$  is the mean velocity of the cross section (ASTM International 2013). Depth is usually measured with a piezo-resistive chip which is submerged in the flow (Aguilar et al. 2015). A hose connected to atmospheric pressure is used to calculate the pressure difference between the air and water, translating to depth of the water column above the sensor. (Aguilar et al. 2015). To calculate velocity, AVM sensors send out an acoustic signal at a known frequency upstream. The signal is continuously transmitted into the flow volume and the signal direction is reversed after reflecting off particulates in the water. The return time and Doppler frequency shift is used to calculate the velocity of the water (Bonakdari and Zinatizadeh 2011; Vermeyen 2000). This is based on a principle that an upstream acoustic pulse takes longer than the returning travel time downstream (ASTM International 2013). Equation 2 shows that the velocity of flow is determined by sending out a signal diagonal to flow direction and calculating the response time.

$$V_L = \frac{B}{2 \cos \theta} \left[ \frac{1}{t_{CA}} - \frac{1}{t_{AC}} \right] \quad \text{Equation 2}$$

where,  $V_L$  is the line velocity, or the average water velocity at the depth of the acoustic path,  $\theta$  is the angle of departure between streamflow and the acoustic path,  $t_{AC}$  is travel time from A to C (upstream),  $t_{CA}$  is the travel time from C to A (downstream), and  $B$  is length of the acoustic path from A to C (ASTM International 2013). This type of continuous acoustic signal AVM is one of two different types of Doppler signal processing; Incoherent or continuous Dopplers, like those produced by Blue Siren and Unidata; and the second being coherent or profiling Dopplers, that are more expensive and transmit encoded pulses to specific locations (Vermeyen 2000).

Accurately installing the AVM sensor is important as mentioned above. According to the *ASTM Standard Test Method for Open-Channel Flow Measurement by AVM systems* (2013), the channel should be straight for three to ten channel widths upstream and two widths downstream of the sensor. This sensor attempts to measure velocity and depth at a hydraulically controlled location, to ensure the accuracy of the measured data. Velocity in pipes, especially stormwater pipes are known to vary widely, as the amount entering the system varies with rainfall.

Variations in velocity make data analysis difficult to see trends in flow values. Thus, velocity variations can be averaged out when compared to a time interval long enough to minimize the variations (ASTM International 2013). Some other errors that might occur during field monitoring with AVM sensors are signal errors. The ASTM D5389 test standard (2013) and Aguilar et. Al (2015) note that high suspended solids, significant entrained air bubbles, and sedimentation over the sensor have a negative effect on the signal, causing reflection and scatter.

The specific area velocity sensor chosen for each inlet is the Blue Siren Dual-Wave Doppler Digital Velocity sensor, which measures depth and velocity of water passing over the sensor. The sensor uses the ultrasonic Doppler equation below to calculate velocity,

$$V = K(F_R - F_T)$$

Equation 3

where,  $V$  is velocity,  $K$  is the calibration constant,  $F_R$  represents the frequency received, and  $F_T$  is the frequency transmitted (Krause et al. 2005). Thousands of velocity measurements are then averaged together to represent the velocity of the flow accurately (a function of sample time and echo reduction parameters). The continuity equation is used to find the flow rate, using the area of the pipe that is full of water (depth measurement) and velocity as shown in Equation 1. Blue Siren's sensor records depth to an accuracy of 1 mm and a 2-mm resolution. The sensor records velocity with a Serial TTL output at 4 samples/second. It has a range of 0-10 m/s with a resolution of 1 mm/s or 1 hz/sec (Blue Siren 2017). Prior to shipping the sensor is calibrated in the manufacturer's lab in a flow tank with velocities ranging from 0.01 m/s to 2.0 m/s and in a depth tank ranging from 140 mm to 470 mm (Blue Siren 2017). Although it is manufactured with a minimum depth specification of zero inches or millimeters, this is for the lab setting only. In a flowing pipe, the estimated minimum depth reading is around 15-20 mm (Soucheck 2017).

The sensor in the field is attached to a metal mounting band, which is tightened one foot inside the inlet, as shown in Figure 3-12. The pipe is six feet long so there is five feet of pipe prior to the sensor. A longer pipe length is desired to avoid the effects from the channel turn as mentioned above, but is considered acceptable for this situation, with lower observed depth values. The sensors are removed from the flow path in the inlets during the winter months to avoid freezing the depth sensor.





*Figure 3-12: Installed Blue Siren Area Velocity Sensor*

## Fluids Laboratory Testing

As with all the other equipment, the area velocity sensor was first tested in our lab to make sure that it complied with expected accuracy and precision criteria. The Blue Siren Dual Wave Area Velocity sensor was calibrated more cautiously and extensively due to the challenge of measuring low-flow depths and velocity in open channel flow. Lab testing was completed with the sensor in an eight-inch pipe (largest available) and compared against the four-inch (10.2 cm) flowmeter (Toshiba Electromagnetic Flowmeter LF434 Series) in the laboratory's flume. A variety of different scenarios were tested to see how the sensor reacted. It was noted that at low depths, the sensor had difficulty measuring the flow accurately. Restricting the pipe diameter to back up water over the sensor was tested as a remedy to this solution, but caused skewed results on the higher flows (with higher than 0.5 Froude number). It was concluded that it could not accurately handle backwater conditions or highly turbulent water, and needed at least one inch of depth before it could accurately measure flow.

## Field Calibration

Once the Blue Siren Area Velocity sensors were installed in the field at inlets N5, N6, and N7 as described above, they needed to be field calibrated. Calibration was necessary due to the analog signal degradation over varying amounts of wire length from each inlet to the datalogger. Each sensor was manually calibrated by adding one inch of water depth every five minutes (this time increment was set by the original datalogger code) to a bucket with the sensor at the bottom. The slope of the calibration was roughly the same for all three sensors, but with different offsets. Figure 3-13 shows how the slope and offset were determined based on the manual measurements and the datalogger measurements during the calibration period. The values from the calibration

curves were entered the datalogger code so that the raw data would reflect the accurate depth levels converted to the correct units (from mV to mm).

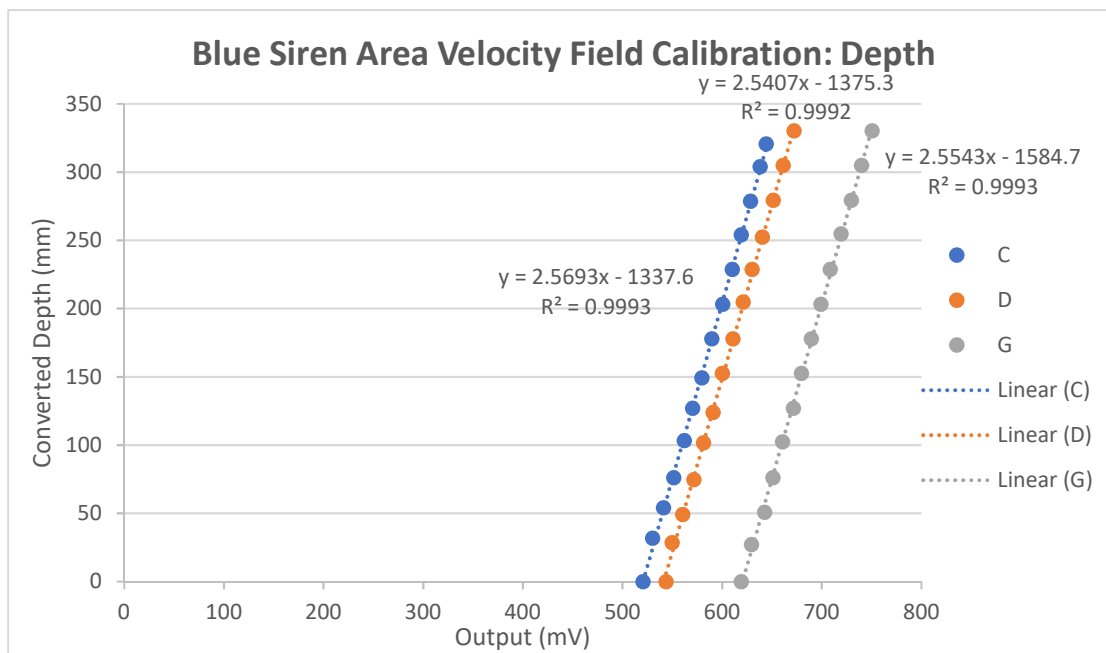


*Figure 3-13: Depth Calibration Curves for Blue Siren Area Velocity sensors installed in the field. Date of calibration: 3/29/17*

### Bioswale Sensors

Prior to reaching the pond (area of each bioswale that captures and holds water), the water entering from the piped inlet runs on and over a rock stilling basin. The stilling basins have an underlying geotextile for erosion control. After running over the rock bed, the runoff enters the bioswale area, which is vegetated and sloped towards the outlet structure at the other end of the bioswale.

Infiltration through the bioswale is a key design aspect, so understanding the infiltration in the system is an important research goal. The volume of runoff that is infiltrated can be determined using a mass balance approach, by subtracting overflow from the outlet and

estimated evapotranspiration from the total runoff. Infiltration in a bioswale, rain garden, or other pervious area is controlled by three different mechanisms: maximum entry rate of water through soil/plant surface, rate of movement through the vadose (unsaturated) zone, and rate of water movement from the vadose zone to the saturated zone (Pitt et al. 2002). Infiltration is also affected by organismal created voids (O'Bannon and Nall 2012) and root structures, which both provide pathways for water to travel. The interactions between the native soil layer and the engineered soil layer, as well as between the vegetation and the soil have an impact on the hydrological movement through the system. Vegetation has been shown previously to reduce runoff for vegetative swales, bioswales and infiltration trenches, by intercepting, infiltrating and promoting evapotranspiration (Bloorchian et al. 2016). These interactions and interceptions determine the infiltration rates which are impacted by the soil conditions and the vegetation of the site (Bloorchian et al. 2016).

Pre-construction infiltration testing locations are shown in Figure 3-14. The two locations tested were roughly located where SMP C is currently (TP-1) and where SMP D (TP-2) is currently. TP-1 had an infiltration rate of 1.8 in/hr and TP-2 had an infiltration rate of 0.25 in/hr based on tests from a double ring infiltrometer. The infiltration data is assumed to be used in the design of the bioswales, but information was not provided by AECOM on its specific integration into the bioswale design.

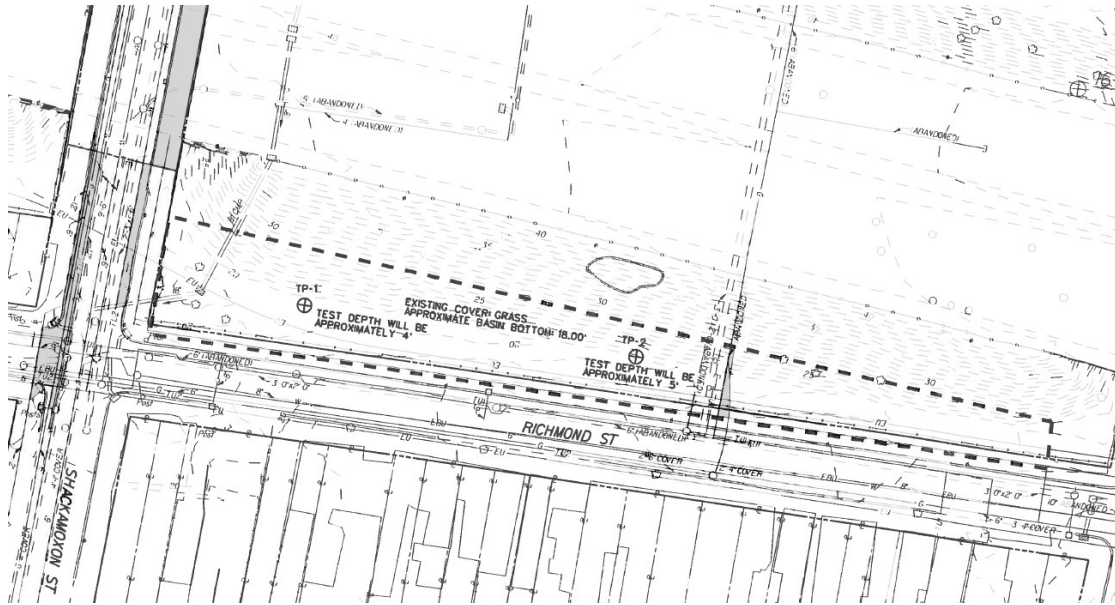


*Figure 3-14: Preconstruction Infiltration Testing Locations*

### Pond Sensors

To understand the spatial variability and timing of infiltration, soil moisture point readings can be used to get a larger understanding of how water moves through the soil. Ponding water depth in correlation with point soil moisture readings help determine infiltration rates of the soil. To measure the depth and temperature of water in the pond, there is a Campbell Scientific CS451 pressure transducer outside of each outlet, which is also the deepest part of each bioswale. SMP A in addition has two pressure transducers at V-notch weirs at the beginning and end of the gabion section. The sensor has a range of 0-2.9 psig (0-2 m), a resolution of 0.0035% full scale range, and an accuracy of 0.1% full scale range of combined errors due to nonlinearity, hysteresis, nonrepeatability, and thermal effects over the compensated temperature range (Campbell Scientific Inc. 2016a). The sensor is used to calculate recession rates after storm events and to see the volume capacity of the bioswale used per storm event. This can be used to

verify design and understand the water budget of each bioswale as effected by the different soils underlying each system.

The pressure transducers in SMP C, D, and G were installed and data was reliable as of April 2017. In May of 2017 the pressure transducer installed in the pond of SMP C was replaced with a Decagon CTD-10, which measures electrical conductivity of the ponded water, in addition to the temperature and depth of water. CTD-10 has a water depth accuracy of 0.05 % of full scale at 20° C, a resolution of 2 mm and a range of 0 to 10,000 mm. The sensor has bulk electrical conductivity accuracy of  $\pm 0.01$  dS/m or  $\pm 10$  % (whichever is greater), a resolution of 0.001 dS/m and a range of 0 to 120 dS/m (bulk) (Decagon Devices, Inc. 2016). The electrical conductivity is useful when comparing to the data within the three groundwater wells nearby, which have the same Decagon sensors. The extra parameter of electrical conductivity is useful for monitoring different SMPs. In dilute solutions, electrical conductivity, which measures the concentration of salts in solution, is highly correlated to total dissolved solids (TDS). TDS is useful to monitor in stormwater, as values of TDS indicate dissolved salts that are found from deicing procedures as well as different roadway constituents/pollutants.

### Soil Sensors

To track changes in soil moisture during precipitation and ponding events, soil moisture sensors (Steven's Hydraprobe) are installed in the deepest section of each bioswale. As described above, soil moisture data helps track the portion of the water budget that is lost to infiltration versus evaporation. The soil moisture sensors were installed in clusters with sensors at different depths. The specified depths are used to see the impact of moisture variance through the soil column. The originally planned depths are standard depths used at all our sites at Villanova and other off campus research sites. The standard depths are 10 cm, 35 cm, 60 cm, 91

cm, and a duplicate at 35 cm to confirm the validity of the values measured. The deepest sensor was supposed to be placed just below the amended soil layer so that a difference can be seen between amended and native soil layers. During installation, challenges with older foundations/construction fill caused some variance in the soil moisture depths. SMP C and D have construction fill at a depth of two feet (SMP C had gravel and SMP D had bricks), so the deepest sensor is located at 60 cm and 55 cm, respectively. SMP G has five sensors within its cluster, but the deepest sensor was shortened to 83 cm due to feasibility of installation. The soil moisture sensors used are the Stevens Hydra Probe and they have three prongs that are inserted horizontally into undisturbed soil. The hole was dug with an auger and a post-hole-digger and the sensor was inserted without wiggling them, as any non-soil contact results in measurement error. Thus, when we ran into construction fill and gravel they could not be inserted into this media and maintain enough contact on the prongs as needed to get an accurate measurement.

Installation of the soil moisture sensors within SMP D is shown in Figure 3-15 a and b. Stevens Hydra Probe soil moisture sensors measure soil temperature, soil moisture, soil electrical conductivity, and complex dielectric permittivity. The soil moisture is measured in water fraction by volume (wfv), which is a volume fraction,  $\text{m}^3\text{m}^{-3}$ , and has an accuracy of  $\pm 0.03$  wfv with a precision of  $\pm 0.003$  wfv (Stevens Water Monitoring Systems, Inc 2015). Electrical conductivity (EC) in soil is highly dependent on soil salinity and is a combined EC measurement of the soil/water/air matrix (Stevens Water Monitoring Systems, Inc 2015). The soil EC of the Hydra Probe has an accuracy of  $\pm 0.0014$  S/m or  $\pm 5\%$  if temperature corrected from 0 to 25 °C (Stevens Water Monitoring Systems, Inc 2015).





*Figure 3-15: Digging and Laying Conduit in SMP D (a). Hole prior to soil moisture probe installation (b)*

### Outflow monitoring

Each bioswale has a single Type I standard box outlet structure at the deepest part of the pond close to the berm edge (SMP C outlet structure shown in Figure 3-16). It has a metal trash rack over the top to prevent big debris from entering into the sewer system. Each outlet box also has a variety of orifices and weirs cut into the concrete to allow flow into the box at varying depths correlating to flow restrictions into the combined sewer as described previously. Flow into the box is not measured, but flow out of the bottom of the outlet structure is measured with a V-notch weir and pressure transducer. Each outlet box contains a Campbell Scientific CS451 pressure transducer and 30° v-notch weir (the v-notch is one-foot-tall, and the crest is located 9 inches from the ground, but varies slightly due to individual shape of each outlet). The angle and height of notch on the weir for the outlets in SMP A, C, D, and G were determined using GIFMET as described above. The pressure transducer measures the depth in the outlet box (the resolution and accuracy are stated above). The known height and crest of the weir are compared to the water depth and are used to determine the surface flow leaving the bioswale, using the V-notch weir equation for 25-100 degrees:

$$Q = C_d \frac{8}{15} \sqrt{2g} \tan \frac{\theta}{2} H^{5/2} \quad \text{Equation 4}$$

where,  $\theta$  is notch angle,  $C_d$  is coefficient of discharge, and  $H$  is the head over the crest of the weir. This equation has the head over the crest to the  $5/2$  power, so accurately modeling and measuring head is critical (ASTM International 2014). In a triangular weir, accuracy of the head measurement is also very critical, especially for the lower heads, where the area over the crest is very small. The V-notch weir was built to American National Standards Institute (ASTM) standards to ensure the reliability of the structure, so that the head above the crest can be measured with the highest accuracy by a high precision pressure transducer (with a stated resolution of 0.0035%, and an accuracy of 0.1% of the full-scale range).



*Figure 3-16: SMP C Outlet structure in September 2016, looking towards SMP D and G.*

The weir and pressure transducer placement is restricted by the outlet structure shape, but the pressure transducer was able to be placed within three to four times the maximum head

measurement upstream of the weir (Bos 1989). The pressure transducer is located on the opposite side of the outlet structure to ensure the accuracy of the depth measurement and not allow for interference from the flow through the weir. Bos (1989) also recommended that the weir have tail water at least 0.16 feet (0.05 m) below the crest of the weir to allow for aeration under the nappe, which effects the discharge coefficient. Since there is no baseflow or backwater from the sewer, this is achieved in all the outlet structures where the weirs were installed.

Each pressure transducer is installed with a slotted PVC pipe that holds the pressure transducer upright and allows water through, but prevents trash and big debris from interfering with the sensor. All pressure transducers are calibrated to measure and account for any drift in the slope and offset of the sensor with the same procedure used for the Blue Siren Area Velocity sensor. Pressure transducers are also removed during the winter months as they do not tolerate being frozen. The weirs are installed with metal C-channels screwed into the wall of the outlet and then sealed with silicone caulk. The underdrains entering the outlets are also sealed with metal plates and silicone caulk. Each weir is covered with wood and sealed with silicon to prevent rain and flow from entering above the weir and not being measured by flowing over the weir, as shown in Figure 3-17.



*Figure 3-17: Outlet V-Notch Weir, Weir Cover, and slotted pipe for pressure transducer (top left).*

### Monitoring Wells

Groundwater wells close to SMP C are used to track the influence of the bioswale on the localized groundwater table. The water table is significantly below the bioswales, so it does not interfere with the infiltration of the bioswale. Thus, groundwater is not modeled in the SWMM model, but the data is included for future studies. There are three wells (8, 9, and 10) shown in Figure 3-18 and Figure 3-19, each containing one Decagon CTD-10 pressure transducer (discussed previously). Well 8 is located closest to I-95 and Well 10 is closest to the sidewalk on Richmond Street. The sensor is hung below the water table and a calculation in the database converts the depth of water above the sensor to depth from the ground to the water table. Each sensor was tested in the lab to ensure its accuracy and data collection initiated in February of 2017. Starting in March 2017 it was noted that the well data was not logical in Well 9. The sensor was sent back to the manufacturer and replaced with a HOBO water level sensor. It was



noted in May that the Decagon in SMP C pond was also not responding accurately and was also replaced with a HOBO water level sensor.

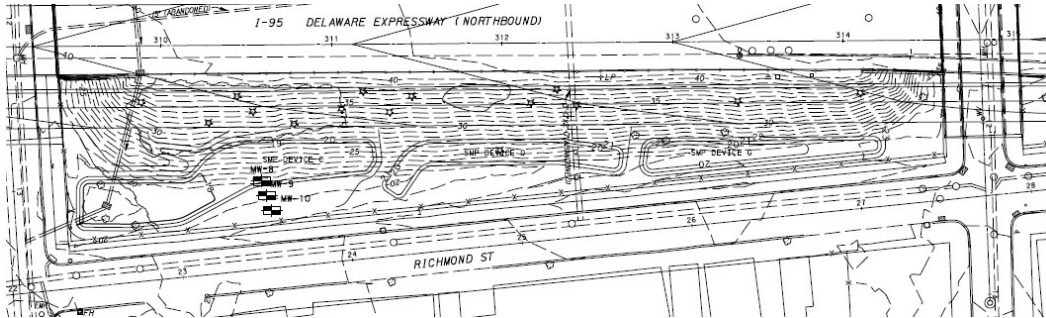


*Figure 3-18: Monitoring Well locations (MW-8, MW-9, MW-9)*



*Figure 3-19: Wells with Decagon CTD-10 Pressure Transducers*

### Simulated Runoff Tests

It is important to verify SMP performance in reducing impervious surface runoff water quantity and improving water quality (Li 2015) using both continuous water level monitoring (CWL) and simulated runoff testing (SRT) (Heffernan et al. 2016). CWL monitoring is event driven, where the water level is recorded before, during and after storms to see the response of the system to the storm event. SRTs are on a unique form of monitoring as they simulate a storm

event but with controlled timing and volume. Flow is added with a fire hydrant to SMPs to observe the behavior of the system to a controlled inflow. SRTs are useful for raingardens as they help verify the drainage area of the system, as well as to verify that the instrumentation is functioning. An SRT was performed for SMPs C and G on July 19<sup>th</sup>, by placing a fire hose next to the inlet to simulate where the water would enter the garden (we were unable to access the highway to have water flow through the inlet as it would do during a storm). A second SRT was performed for SMPs A on Aug 18, where we could put the hose down two different inlets. The instantaneous flow rate and total amount of flow through the hose was recorded every five minutes. The inflow from the hydrant was kept at a constant intensity (maximum of 31 cfm for SMP A, 40 cfm for SMP C and 30 cfm for SMP G) to see the basic response of the bioswale to the input of water and to fill up the gardens. The results and data gained from these SRTs were used to evaluate the performance the instrumentation, the SMP, and calibrate the SWMM model.

### **SMP Hydrologic Monitoring Results**

Despite limitations in the data record described above (e.g., errors in drainage area), we were able to collect a number of valuable datasets. The essential datasets are described here; details on their analysis and incorporation into modeling is described in Chapter 6.

#### *Weather Station Data*

The two rain gauges in SMP A yielded datasets that corresponded closely to each other (Figure 3-20). In contrast, the rain gage from SMP C (below the elevation of the sound wall) yielded a very different dataset (Figure 3-21) to that from the SMP A rain gauges. This latter result highlights the importance of using data from an appropriate weather station to describe conditions at each contributing drainage area (e.g., the highway vs. pervious areas).

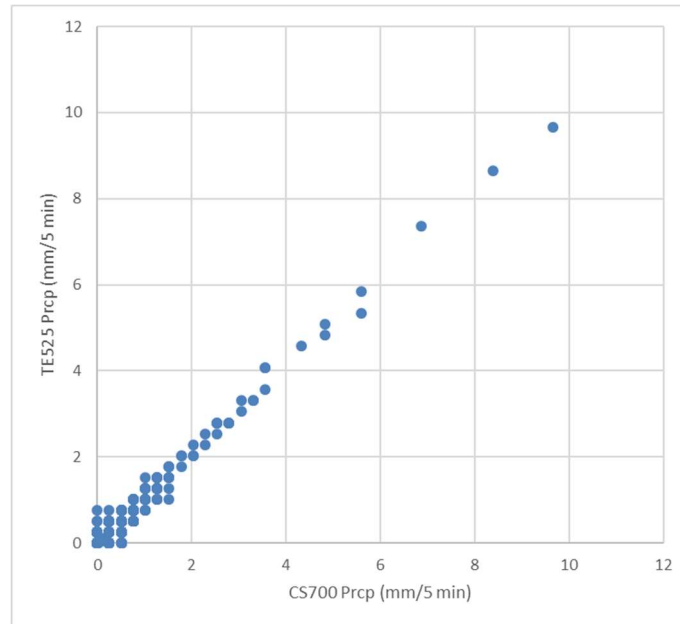


Figure 3-20. Comparison of data from the pair of rain gauges at the weather station in SMP A.

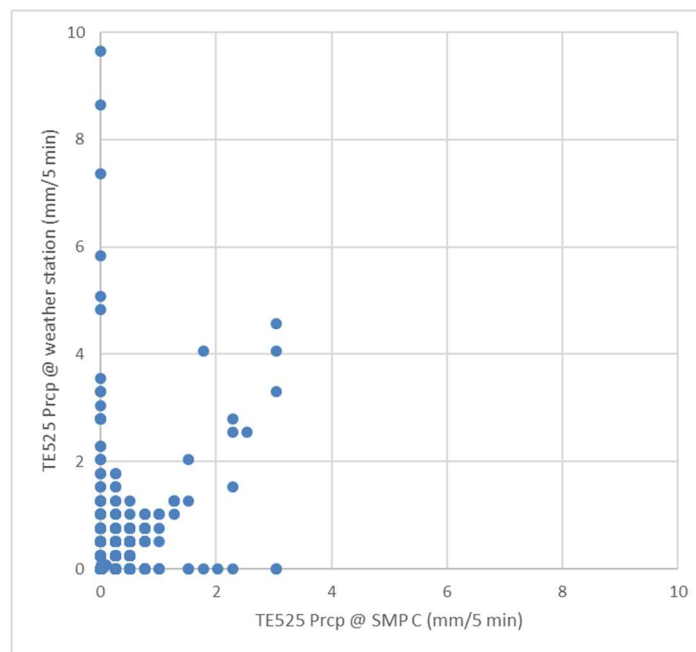


Figure 3-21: Comparison of SMP A to SMP C Rain Gage

Other data recorded is used by both the Temple and Villanova teams for evapotranspiration studies. Figure 3-22 explores the relationship between air temperature and solar energy, and



illustrates the correlation between solar energy and temperature, and how temperature is affected by short-term weather events (e.g. see the snow event in mid-March).

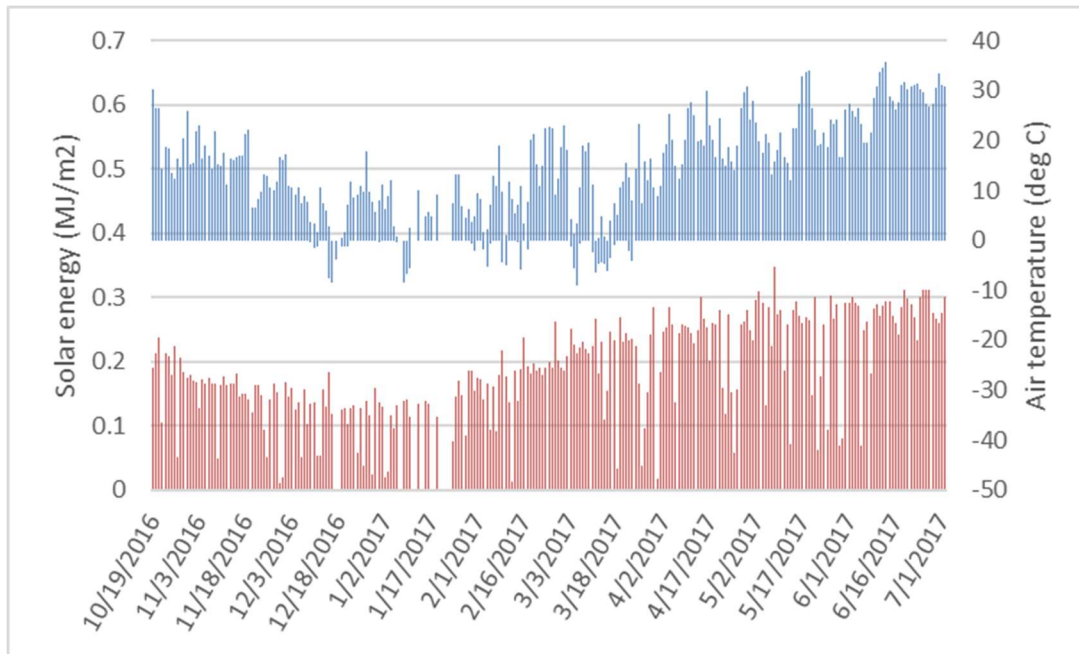
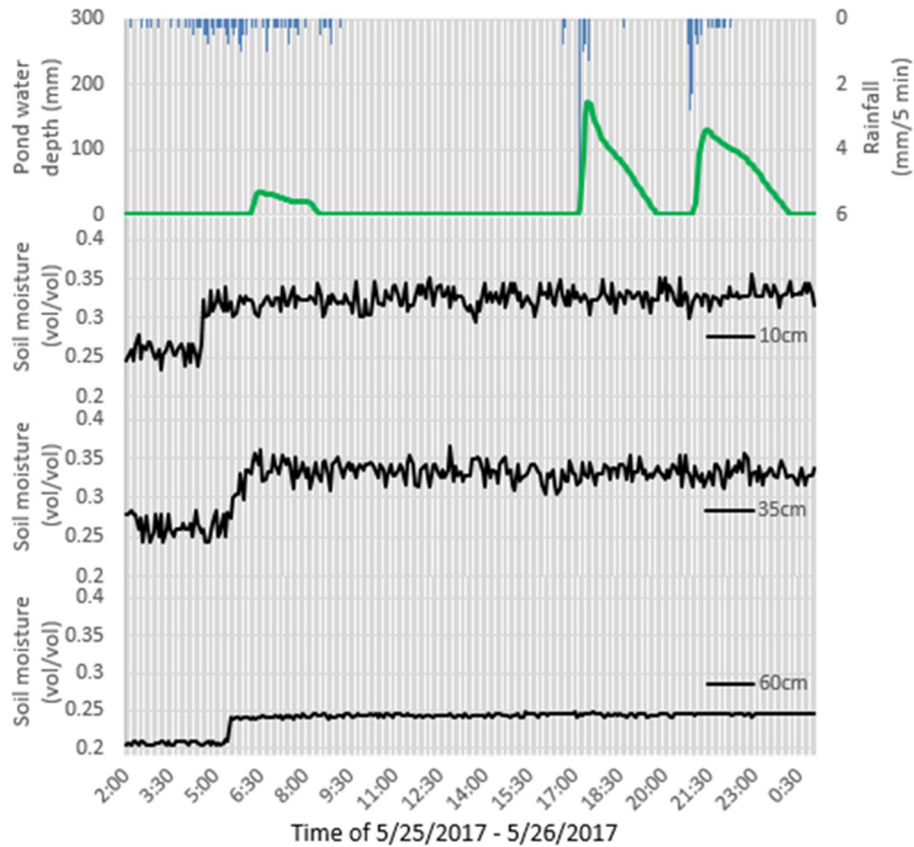


Figure 3-22: Compare recorded data of solar energy (bottom) and air temperature (top)

### *SMP Runoff Tracking*

The next several figures relate rainfall to SMP water depths and soil moisture sensors from the two storms that occurred on May 25, 2017. Figure 3-23 shows that the vertical water transfer from the surface to 60 cm depth takes about 1 hour, which is much faster than might be expected. Moreover, soil moisture starts rising at the 60-cm depth before ponding occurs.



*Figure 3-23. Summary of data collected for SMP A during the back-to-back storms on 5/25/2017.*

Figure 3-24 shows data collected from SMP C for the same pair of storms, but also includes the well data (#8) response with respect to conductance and ground water levels. As in SMP A, vertical movement of water is rapid, and soil remains saturated throughout the two storms. The time required for water to reach a 60-cm depth is shorter than needed in SMP A. The groundwater response and the change in groundwater conductance are fast as well. Note that the data described pertain to the well closest to the SMP.

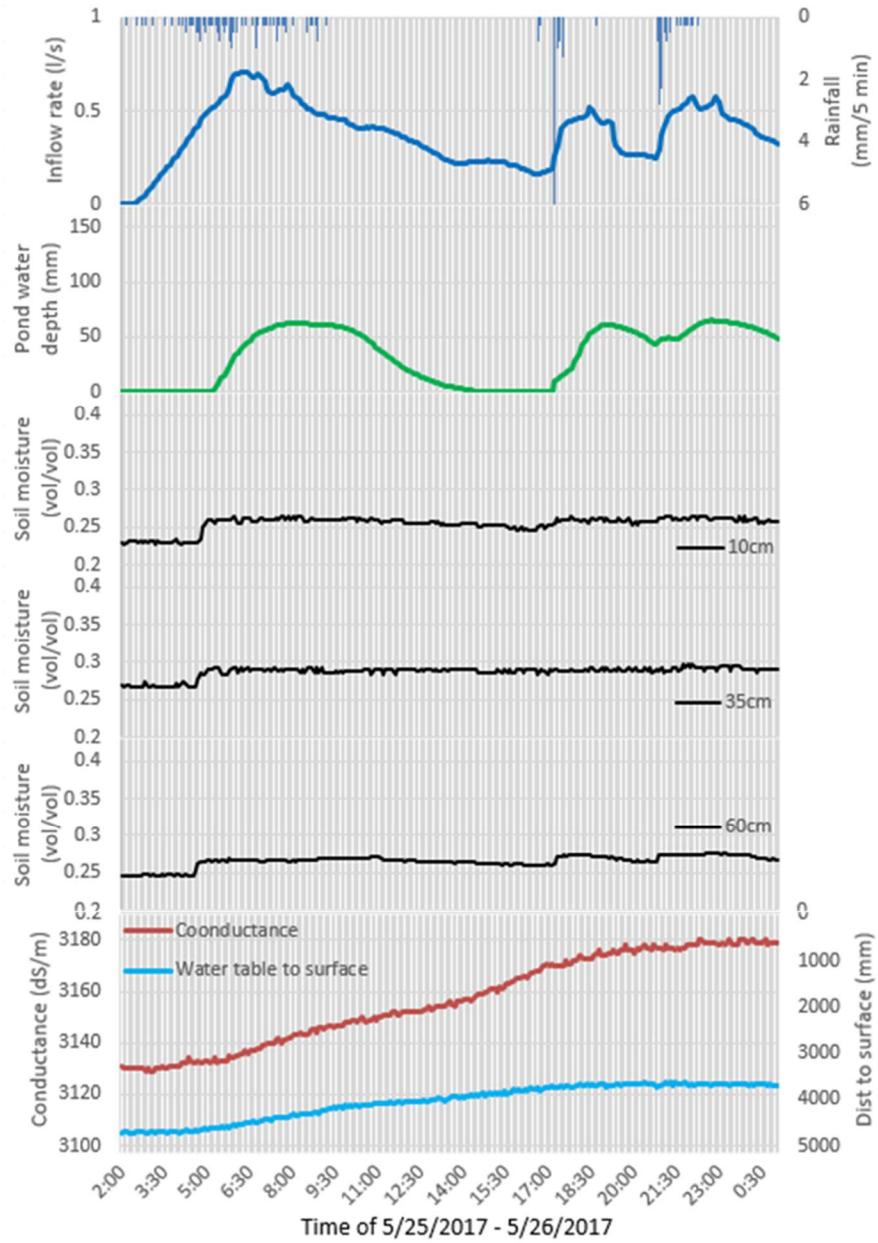


Figure 3-24: Summary of data collected for SMP C during the back-to-back storms on 5/25/2017

When expanding the range of data, you can also see the recession of both the ground water levels and conductivity over time (Figure 3-25).

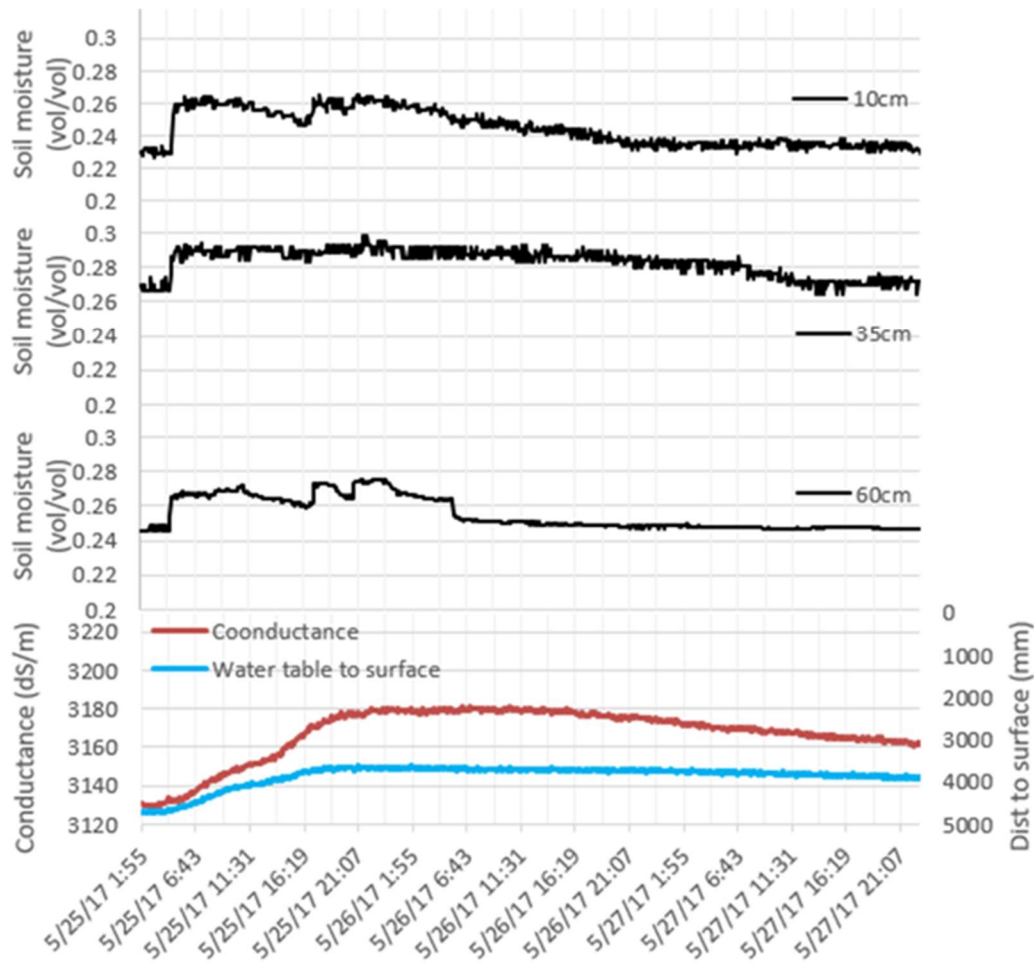


Figure 3-25: Soil moisture and groundwater data from SMP C for the longer time frame (5/25/17-5/27/17)

The soil moisture response in SMP D (Figure 3-26) is quite different from that in SMPs A and C. For one, soil moisture was not at saturation after storms began. Also, water infiltrates quickly and soil moisture returns to pre-storm conditions during the short dry time (about 6 hours) between the two storms. These patterns indicate that SMP D has a rapid water level recession rate. However, the soil moisture responses at 35 cm and 60 cm are like that of SMPs A and C.

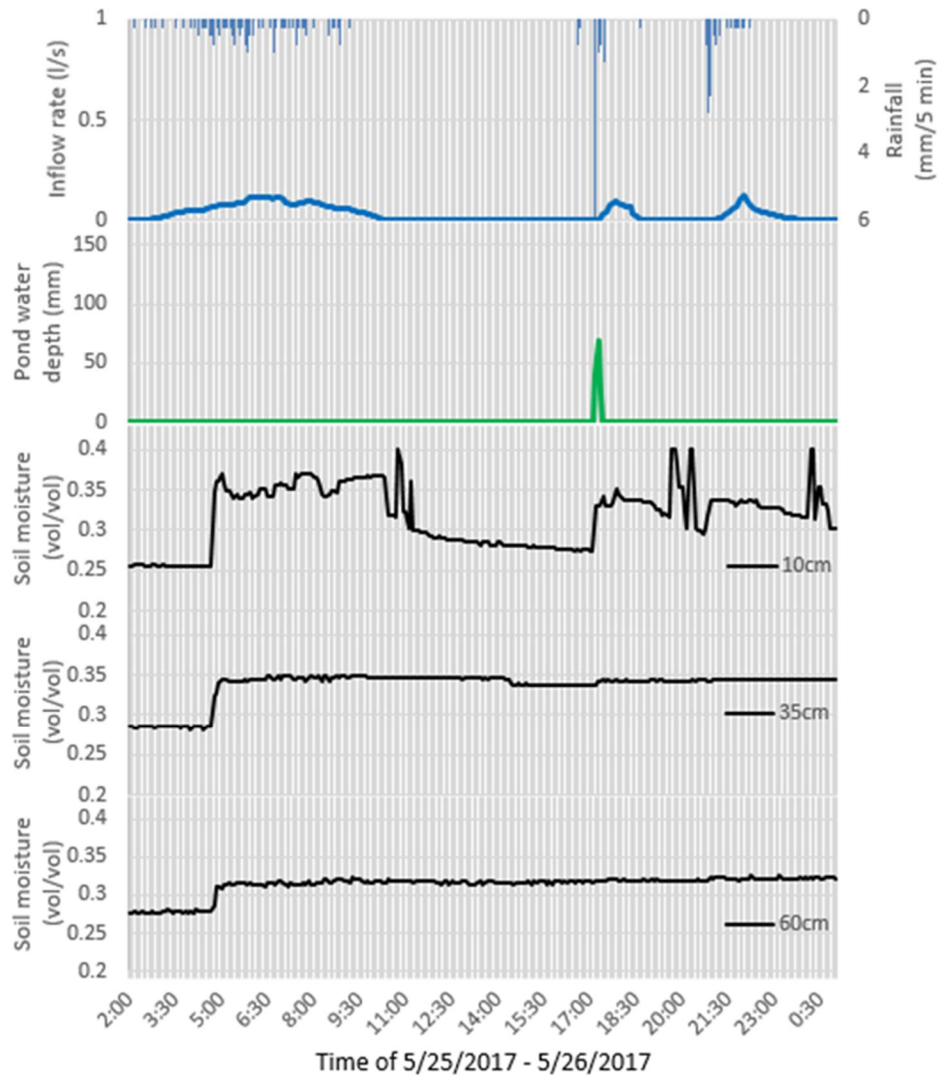


Figure 3-26: Summary of data collected for SMP D during the back-to-back storms on 5/25/2017

SMP G (Figure 3-27) had a slightly different soil moisture response than the other SMPs. The surface layers (10 cm and 35 cm) remained at a high soil moisture levels and the rate of decrease was slow, as observed in SMPs A and C. However, the first storm did not fully saturate the surface layers and the second storm further increased the soil moisture content. It became apparent during the SRT that the underdrain leaks in this SMP, so some runoff may have leaked into the outlet rather than ponding as intended. It is worth noting that deeper soils (60 cm and 83 cm) became saturated quickly and remained saturated for a time before draining quickly after the

storm. Given that bricks were found during soil moisture sensor installation, it is possible that water infiltrates to the deeper soil layers rapidly via macropores.

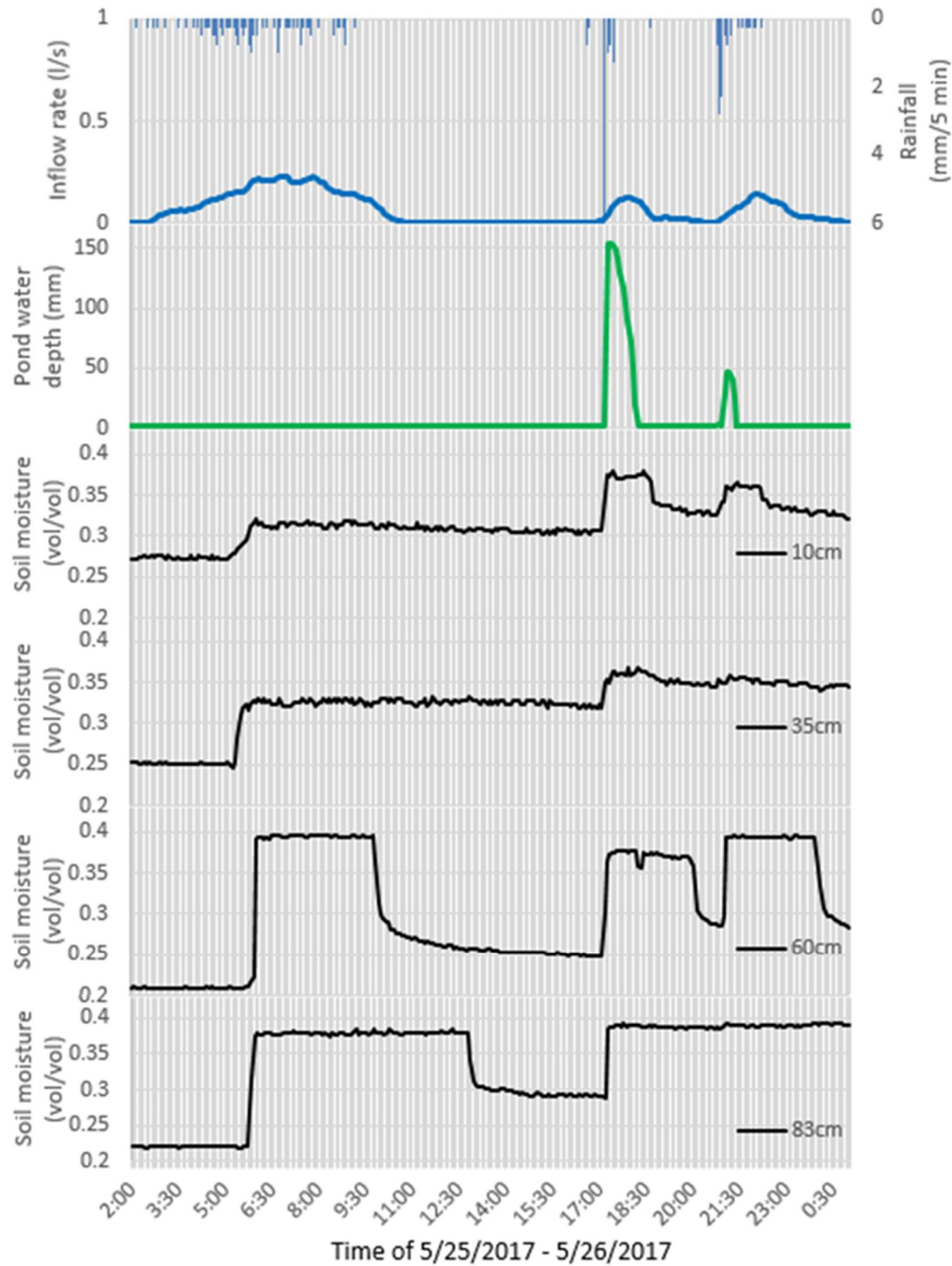
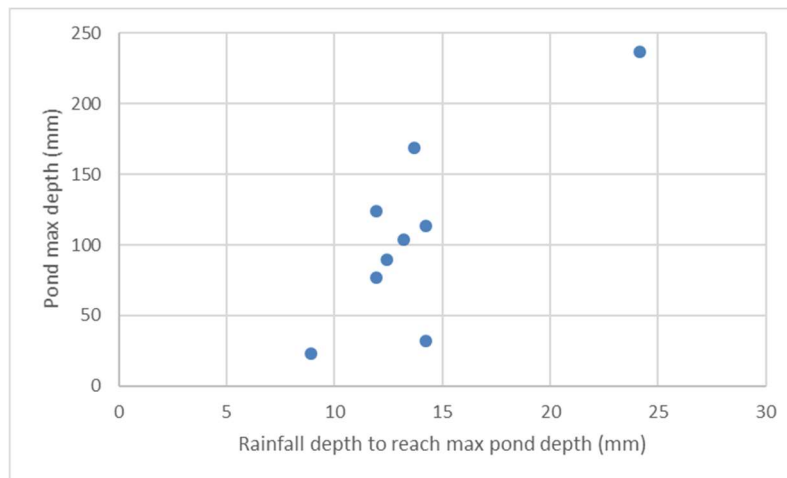


Figure 3-27. Summary of data collected in SMP G during back-to-back storms on 5/25/2017

These results demonstrate that the instrumentation is capturing the relationships of pond level and soil moisture.

### *SMP Rainfall Response*

Another approach to understanding the hydrological dynamics of the SMPs is to examine their responses to rainfall. SMP A appears to receive more runoff and is thus a suitable SMP to examine how rainfall volumes (Figure 3-28) and intensities (Figure 3-29) influence maximum pond depths. It should be noted that uncertainty in the drainage area for SMP A and its later instrumentation date than SMPs C, D, and G have resulted in a smaller data record.



*Figure 3-28: Event rainfall depth (before reaching max ponding depth) vs. max ponding depth for SMP A*

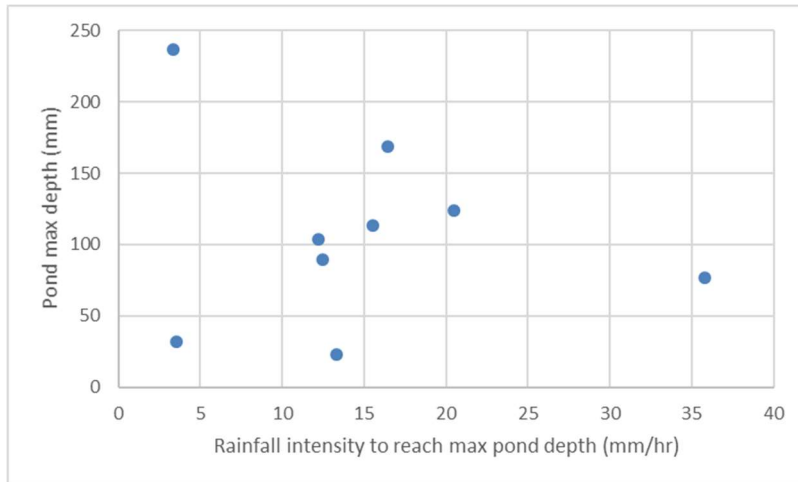


*Figure 3-29: Event rainfall intensity (before reaching max ponding depth) vs. max ponding depth for SMP A*

Similar plots of rainfall and ponding in C, D, G provide limited data due to the small contributing drainage area and low depths (Figures 3-30 and 3-31). When the drainage area is increased after construction, the data will be more informative about high flow events. Fortunately, the data collected so far does prove the value of the monitoring approach for when the site watershed flows are corrected.

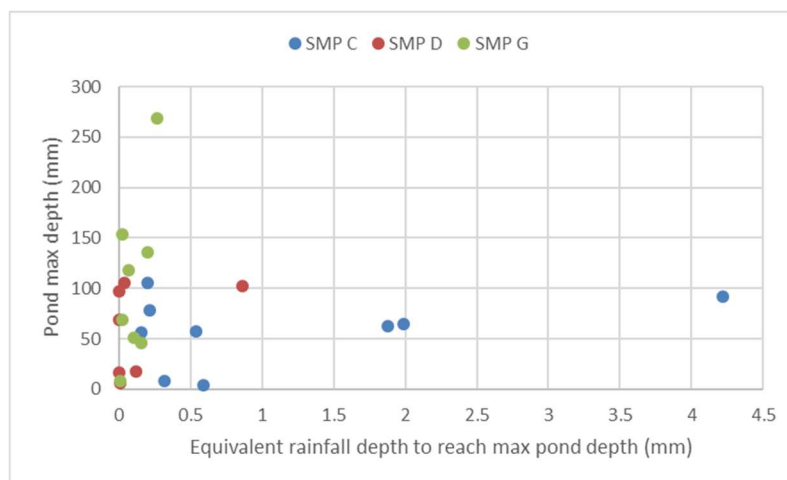


*Figure 3-30: Event rainfall depth (before reaching max ponding depth) vs. max ponding depth for SMPs C, D, and G*



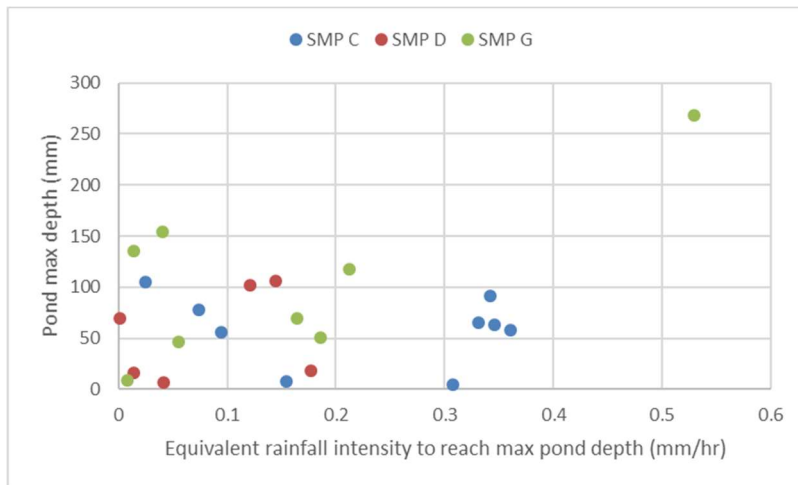


*Figure 3-31: Event rainfall intensity (before reaching max ponding depth) vs. max ponding depth for SMPs C, D, and G*

### Simulated Runoff Test

A simulated runoff test (SRT) was performed on July 17, 2017 in SMPs C and G. The SRT was intended to deliver sufficient water to the bioswale that it would enter the outlet structure. The primary objectives of the SRT were to generate data needed to calibrate the SWMM model describing these bioswales, to identify any issues with bioswale design and construction, and to calibrate the instrumentation in the bioswale. The SRT for SMP C took 2.5 hours to complete and entailed constant flow (40 cfm or 1,133 liters/s) entering the rock bed next to the inlet. The total volume discharged into the bioswale via the stilling basin in SMP C was 5858 ft<sup>3</sup> (165,880 liters). Note that this flow greatly exceeded any of the measured volume events that entered the SMP during rainstorms. If this volume of water had been applied to the drainage area in a precipitation event, it would have been equal to a constant intensity storm of 0.69 in/hr (17.5 mm/hr), equaling 1.69-inch (42.9 mm) storm over the design drainage area. Based on Pennsylvania Region 5 interpolation of the intensity duration frequency curves (IDF), the

volume of water that entered the bioswale was a little under a 2-year storm (1.69 inches in 120 minutes versus the 150 minutes of the actual test). This demonstrated that the bioswale design goal of holding the 2-year storm before overflow into the outlet was achieved.

Overflow from the pond into the outlet box in SMP C occurred after approximately 1.5 hours. Water also overflowed the V-notch weir shortly after. Even once the ponding depth reached the first orifice of the outlet box, it continued to increase slightly. This was likely due to the first overflow occurring in a four-inch orifice that is used to regulate the overflow rate out of the outlet structure. The SRT continued for an additional 20 minutes after the V-notch weir in the outlet overflowed, at which point the hydrant was turned off. Pondered water then receded over the course of a few hours. The pond or “bowl” of the bioswale is approximately 3,400 ft<sup>3</sup> at the height of the first overflow orifice (i.e., the designed two-year storm basin volume). Since the water level wasn’t significantly higher than the first overflow orifice, we can assume that roughly 2,400 ft<sup>3</sup> of water exfiltrated through the media before the hydrant inflow was shut off. This is a significant “loss” of runoff that infiltrated during the two-and-a-half-hour event, equaling roughly 40 percent of the total water that was discharged onto the rock stilling basin.

Figure 3-3 compares the inflow and outflow of water to SMP C during the SRT on July 19, 2017. The peak outflow was 0.19 l/s, which is 1% of the constant hydrant inflow of 19 l/s (40 cfm). The volume of overflow was 267 liters (9.4 ft<sup>3</sup>), which is 0.19% of the inflow volume of 165,880 liters (5858 ft<sup>3</sup>). This outflow rate and volume is minimal and well under the limit set by the City of Philadelphia for discharge to the combined sewer system (CSS). The flow over the weir in the outlet occurred soon after the ponding depth exceeded that of the outlet, while peak overflow occurred after the peak ponding depth occurred and immediately after the hydrant

inflow was turned off. That the peak pond depth seemed to occur slightly before the hydrant was turned off could be due to measurement error as the SRT inflow data is manually collected.

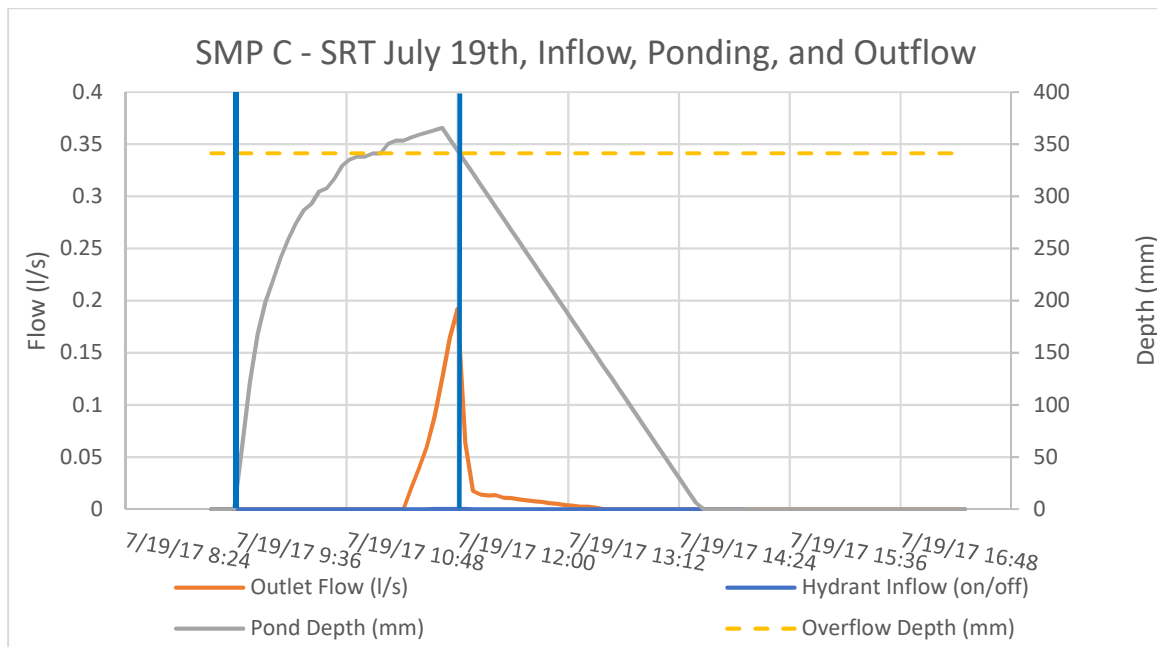


*Figure 3-32. SRT ponding depth versus inflow and outflow from SMP C. Since flow was significantly larger at the inflow than at the outflow, the inflow is depicted with two blue lines that signify when the hydrant inflow was turned on and off.*

When comparing the ponding depth in SMP C during the SRT to the soil moisture volumes (Figure 3-33), it is clear that ponding and the spike in soil moisture occur around the same time. The sensor at 10 cm peaked the most rapidly and at the greatest magnitude due to its low depth. The deepest sensor (60 cm) had a slow increase and then peaked suddenly almost an hour after the flow into the bioswale had ceased. The peak and then rapid decline in soil moisture may have been due to water entering the deepest layer and peaking only for a short time due to the pond emptying at roughly the same time. The fast restoration of void space is of great interest.

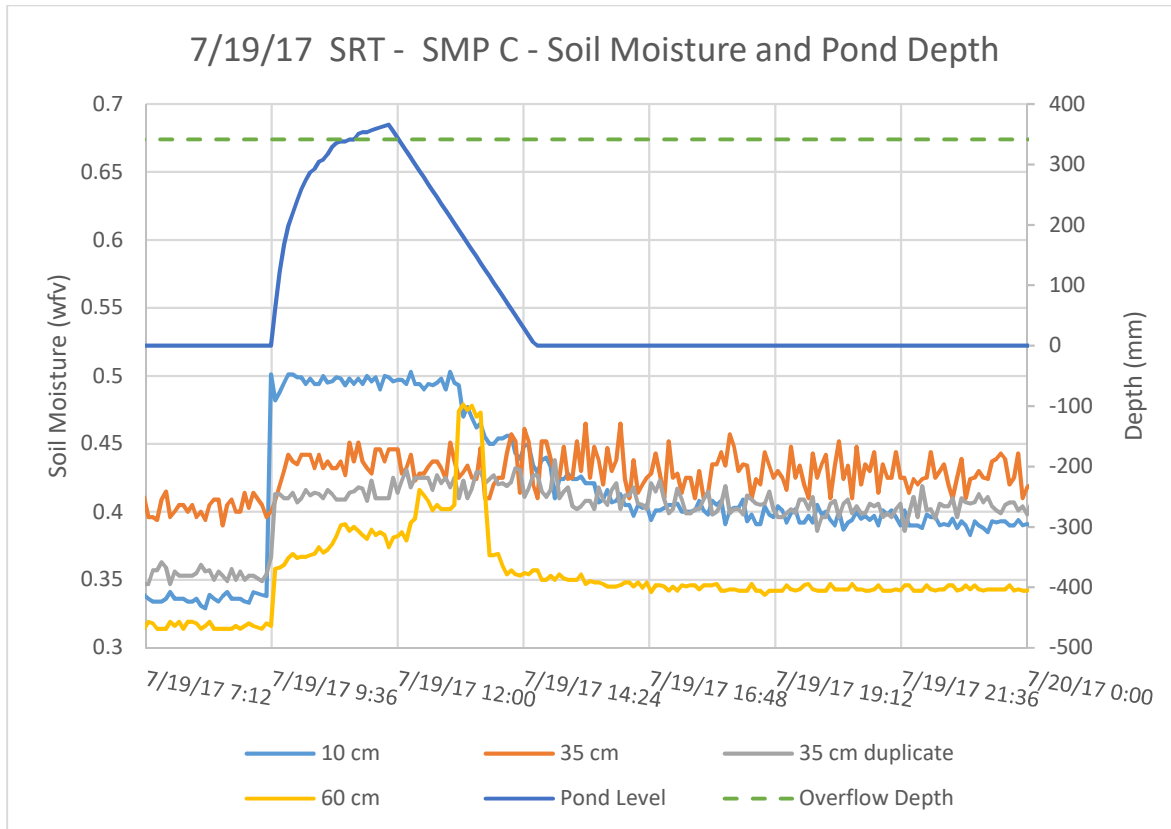


*Figure 3-33: Soil moisture readings in SMP Pond C during SRT on 7/19/17*

The SRT on SMP G lasted approximately two hours, had a constant flow rate of 30 cfm (14 l/s), and discharged 3500 ft<sup>3</sup> (99,109 liters) into the stilling basin of SMP G. During the SRT in SMP G, the outlet was found to have a large leak from the underdrain, so this basin was not calibrated to data from actual storms. It should be possible to calculate the flow rate out of the leaking underdrain and apply this flow correction to all prior storms, but this has not yet been attempted. Since the leak was discovered, the underdrain has been sealed. The data for the SRT in SMP A in late August has not yet been fully processed, but we expect to have a description of the test and results for a future report.

## **Future Work and SMP Functionality**

Results of the SRTs in SMPs C and A provided insights into their operation and identified construction problems that need to be addressed. As the watershed drainage area changes in future phases of this research, it will be possible to develop a more mechanistic understanding of the site's hydrologic performance; this will ultimately be needed to inform future design standards.

Some options to improve SMP functionality and monitoring of hydrologic performance have been recommended (see Chapter 8). A number of these recommendations involve the design of the outlet structures. In particular, adjacent basins could be linked (such as SMPs C, D, and G in GR2) such that they drain to a single outlet; this would reduce construction costs and may allow for increased water infiltration in the basin. Reduced monitoring costs would be an additional benefit of combining basins.

Additionally, the overflow openings in outlet structures should be redesigned to allow sharp crested weirs to be mounted. Although V-notch weirs are appropriate for smaller outflows, slightly raised broad crested weirs can be used for higher flows. In addition to facilitating outflow monitoring, these weirs would aid inspection and maintenance of the inlet boxes. This change has already been implemented in the existing inlets in GR2 and will be included in future designs. Also, moving the steps used for access away from the outlet pipe would facilitate the installation of internal weirs. Finally, incorporation of a plugged hole in the structures below ground level to allow for cabling would assist installation of monitoring equipment; these would not affect functionality. The inlet pipes should be slightly raised to allow for measurement of outflow. These and other recommendations are included in Chapter 8.

## References

- AECOM/URS. (2015). "Post-Construction Stormwater Management Plans; Philadelphia County, SR 0095, Section GR 2."
- Aguilar, M. F., McDonald, W. M., and Dymond, R. L. (2015). "Laboratory Evaluation of Flow Sensor Technology for Use in Storm Sewer Measurements." World Environmental and Water Resources Congress: Floods, Droughts, and Ecosystems, ASCE, 2579–2589.
- ASTM International. (2013). "ASTMD5389.11562.pdf." Standard Test Method for Open-Channel Flow Measurement by Acoustic Velocity Meter Systems.
- ASTM International. (2014). "ASTMD5640.27290.pdf." Standard Guide for Selection of Weirs and Flumes for Open-Channel Flow Measurement of Water.
- Bloorchian, A. A., Ahiablame, L., Osouli, A., and Zhou, J. (2016). "Modeling BMP and Vegetative Cover Performance for Highway Stormwater Runoff Reduction." Procedia Engineering, 145, 274–280.
- Blue Siren. (2017). "Dual Wave Doppler Digital Velocity Sensor." Blue-Siren Inc.
- Bonakdari, H., and Zinatizadeh, A. A. (2011). "Influence of position and type of Doppler flow meters on flow-rate measurement in sewers using computational fluid dynamic." Flow Measurement and Instrumentation, 22(3), 225–234.
- Bos, M. G. (1989). Discharge measurement structures. ILRI, Wageningen, the Netherlands.
- Campbell Scientific Inc. (2016a). "Instruction Manual: CS451/CS4556 Submersible Pressure Transducer." Campbell Scientific, Inc.
- Campbell Scientific Inc. (2016b). "Instruction Manual: CS700 Tipping Bucket Rain Gage and CS700H Heated Rain Gage." Campbell Scientific, Inc.
- Campbell Scientific Inc. (2017). "Instruction Manual: TE525 Tipping Bucket Rain Gage." Campbell Scientific, Inc.
- Christodoulou, G. C. (1991). "Drop manholes in supercritical pipelines." Journal of Irrigation and Drainage Engineering, 117(1), 37–47.

- Decagon Devices, Inc. (2016). “CTD-10 Electrical Conductivity, Temperature & Depth Sensor: Operators Manual.” Decagon Devices, Inc.
- Google. (2017). “Google Maps.” <<https://www.google.com/maps/@39.9673391,-75.1321521,18z>> (Aug. 30, 2017).
- Heffernan, T., White, S., Krechmer, T., Manna, N., Bergerson, C., Olsen, M., and Cruz, J. (2016). “Green Stormwater Infrastructure Monitoring of Philadelphia’s Green City, Clean Waters Program.” Proceedings of the World Environmental and Water Resources Congress, 115.
- Krause, P., Boyle, D. P., and Bäse, F. (2005). “Comparison of different efficiency criteria for hydrological model assessment.” *Advances in Geosciences*, 5, 89–97.
- Lee, R. S. (2015). Green Infrastructure Flow Measurement Evaluation Tool (GIFMET). Villanova University, Villanova, PA.
- Li, H. (2015). “Green Infrastructure for Highway Stormwater Management: Field Investigation for Future Design, Maintenance, and Management Needs.” *Journal of Infrastructure Systems*, 21(4), 05015001.
- O’Bannon, D., and Nall, J. (2012). “Detailed Rain Garden Flow Monitoring.” *World Environmental and Water Resources Congress 2012: Crossing Boundaries*, 3565–3572.
- Philadelphia Planning & Research, and PWD. (2014). “Stormwater Management Guidance Manual, Version 2.1.” City of Philadelphia.
- Phillips, J., and Buchanan, P. (2011). “Green Stormwater Infrastructure Use to Control Combined Sewer Overflows.” *Pipelines 2011: A Sound Conduit for Sharing Solutions*, 1463–1476.
- Pitt, R., Chen, S.-E., and Clark, S. (2002). “Compacted urban soils effects on infiltration and bioretention stormwater control designs.” *Global Solutions for Urban Drainage*, 1–21.
- PWD. (2009). “Green City Clean Waters: The City of Philadelphia’s Program for Combined Sewer Overflow Control, A Long Term Control Plan Update.” <[http://www.phillywatersheds.org/ltcpu/LTCPU\\_Complete.pdf](http://www.phillywatersheds.org/ltcpu/LTCPU_Complete.pdf)> (Aug. 26, 2017).
- PWD. (2015). “Stormwater Management Guidance Manual; Version 3.0.” Philadelphia Water.

Quigley, M. M., Strecker, E. W., and Urbonas, B. (2002). "Overview of the Urban Stormwater BMP Performance Monitoring: A Guidance Manual for Meeting the National Stormwater BMP Database Requirements." *Global Solutions for Urban Drainage*, 1–14.

Soucheck, P. (2017). "Blue Siren Specifications Discussion."

Stevens Water Monitoring Systems, Inc. (2015). "The Hydra Probe® Soil Sensor, Comprehensive Stevens Hydra Probe Users Manual, Rev. IV." Stevens Water Monitoring Systems, Inc.

Urbonas, B. (2007). "Stormwater Runoff Modeling; Is it as Accurate as We Think?" Keynote Address, Humboldt State Univ., Arcata, CA.

Vermeyen, T. B. (2000). "A Laboratory Evaluation of Unidata's Starflow Doppler Flowmeter and MGD Technologies' Acoustic Doppler Flow Meter." *Building Partnerships*, 1–10.



## **Chapter 4: Water Quality Monitoring**

### **Introduction**

This chapter primarily constitutes an update the water quality study presented in the May 2017 report. It includes data from monitoring water in SMPs during selected storm events, as well as data collected during two simulated runoff tests (SRTs) conducted over the summer 2017. The report also includes information on the installation of additional monitoring equipment on the sites: lysimeters for subsurface water monitoring (in SMPs C, D, G, and A), stormwater sampling bottles for accumulation water and outfall monitoring (in SMPs C, D, G, and A), and autosamplers for collection of inlet water (in SMPs C, D, and G). Two SMPs in the GR-2 area, referred to as SMP C and SMP D, were sampled during selected storms at an average frequency of one storm per month starting in October 2016. No storms were recorded during June and July 2017, because of the frequent lightning accompanying the storms and the preparation and conduction of the two SRTs. The purpose of this first phase of field monitoring was to assess the field conditions during actual storms (e.g., delay between the onset of rain and inlet flow, water accumulation in the SMPs, overflow, etc.) and to test analytical methods and sampling operations in the field.

At this stage, only grab samples were collected. Samples were then collected from the inlet of two SMPs, from the initial flow shortly after the onset of rain and periodically during the following two hours (Figure 4-1, A). Six samples were collected per SMP and per storm. In addition, samples of ponded water were collected when water accumulated in the SMPs (Figure 4-1, B & C). Starting in October 2017, inlet water will be collected using autosamplers and stormwater sampling will be coordinated with collection of other samples (infiltration

accumulation, and outfall water). No large accumulation of water and no overflows were observed during any of the storms sampled during the first phase. This observation highlights the need for water quality modeling to predict SMP performance under extreme events.

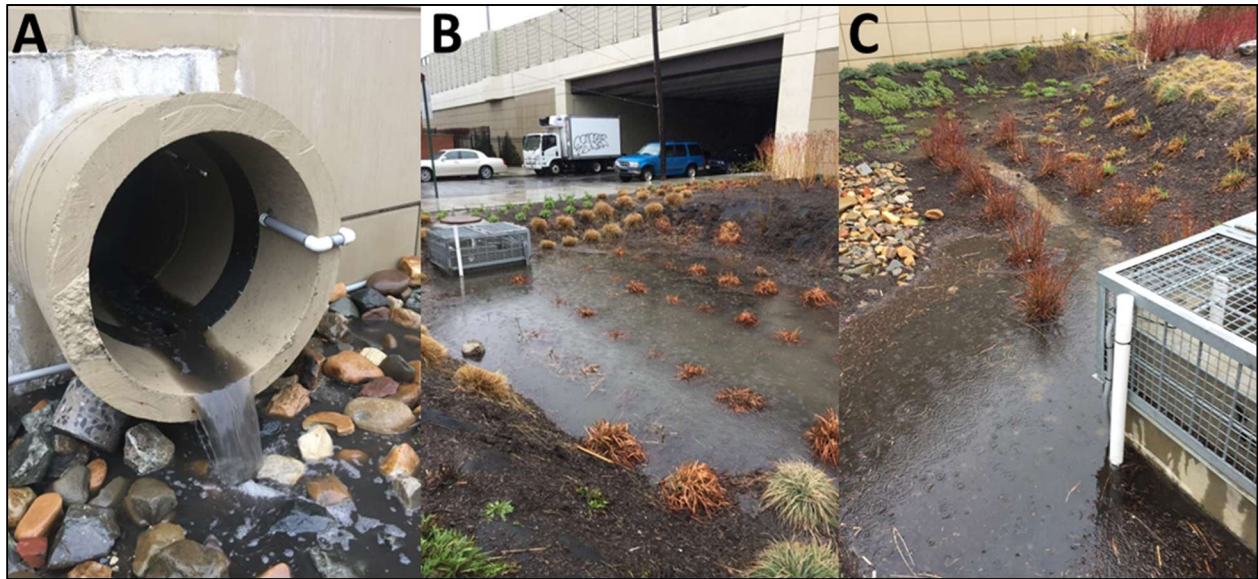


*Figure 4-1. Pictures taken on GR-2 site during an intense storm on March 31. A: First flush from the inlet of SMP C. B: Ponding water in SMP C. C: Ponding water in SMP D.*

Contaminant dynamics in SMPs is frequently evaluated using a mass balance approach. For a non-degrading contaminant, this approach assumes that the mass of contaminants entering the SMP is equal to the mass leaving the SMP plus the change in the contaminant mass stored in the SMP. Contaminants enter the SMP primarily with the stormwater, and can leave the SMP either via the outlet or transport into the subsurface with the infiltrating water. Infiltrating water may transport contaminants into the subsurface, where contaminant mobility will depend on the contaminant, hydraulic characteristics, basin fill material, and time. While infiltration of water is a desired outcome to prevent contamination of surface water, it may cause potential problems if the contaminants are transported into the underlying groundwater, particularly if the groundwater is being used as a drinking water source – which is not the case in the Philadelphia

area. If a greater contaminant mass is entering the SMP than leaving the SMP, then contaminants are accumulating in the SMP. Additionally, some stormwater constituents may be utilized or degraded – for example, plants may utilize nutrients, and soil microbes may biotransform trace organic contaminants – while other contaminants cannot be degraded (e.g., metals and inorganic particles). To account for all of these factors, the study design includes sampling inflow, ponded water, water in the unsaturated zone, water in the groundwater zone. In addition, plant and soil analysis is underway as reported in Chapter 7.

The capacity of the SMPs to collect and infiltrate all runoff water ensures the containment of contaminants in the structure, helping protect surface water. To date, there have not been any natural storm events resulting in water exiting the outlet structure. Plant and soil analysis is currently being conducted, which is expected to help address questions regarding the long-term fate and transport of the contaminants within the SMPs.

## **Methods**

The sampling and analytical methods used were as described in the January 2017 QAPP and summarized here. Additional activities included the acquisition of new autosamplers and the upgrade of an existing one owned by Temple University's Department of Civil and Environmental Engineering.

### *Stormwater Sampling – Grab Samples*

Grab samples were collected in 500-mL or 1-L plastic bottles (polypropylene). Sampling bottles were rinsed 2 times with flowing water before sample collection (except when collecting the first flush). Temperature and DO were recorded immediately after sample collection. Grab samples were stored chilled until and during transportation to the lab within four hours after collection.

Sampling started at the beginning of the storm: the first sample (time 0:00) consisted of the first 500 or 1,000 mL falling from the inlet pipe. Additional samples were then collected after 15, 30, 60, 90, and 120 min.

#### *Groundwater Sample Collection*

During the initial months of the study, the sampling and analytical method were being refined, so some elements were not measured in the earlier samples. To date, three rounds of groundwater sampling have been collected and two rounds have been analyzed, which are described below:

Nov 2016: the wells were not developed and were not purged prior to sampling. Samples were collected using a bailer. The sampling protocol included recording depth to water (DTW), visual observations, and collecting samples for metals analysis.

Feb/April 2017: to collect more representative samples, it was decided that the wells should be developed (to remove standing water or water introduced during the drilling process). The wells were purged prior to sampling; 4 well volumes were removed. Due to pump failure (overheating) and the time-intensive nature of well development, well development efforts were spread over a number of days and two wells (MW 4 and MW5) were not developed; samples were collected in spite of incomplete development efforts. Generally, the sampling effort included: measuring DTW; well development/purging; on-site analysis of pH, conductivity, and dissolved oxygen (DO); collection of a sample for metals analysis. Sampling tools and analytical probes were rinsed between uses with nanopure water and well water.

June 2016: the wells were not developed and were not purged prior to sampling. Samples were collected using a bailer. The sampling protocol included recording depth to water (DTW),

visual observations, on-site analysis of pH, conductivity, and dissolved oxygen (DO), and collecting samples for metals analysis.

#### *Simulation Runoff Tests (SRTs)*

Three SRTs were conducted in June 2017 in SMPs C and D, and in August 2017 in SMP A. Three tracers were applied during the tests: a colorimetric tracer, fluorescein, and two conservative tracers, lithium ( $\text{Li}^+$ ), intended to simulate the behavior of cationic contaminants (e.g.,  $\text{NH}_4^+$ , metals), and bromide ( $\text{Br}^-$ ), intended to simulate the behavior of anionic contaminants (e.g.,  $\text{NO}_3^-$ ,  $\text{SO}_4^{2-}$ ,  $\text{PO}_4^{3-}$ ) (Figure 4-2). Fluorescein was applied as a single pulse addition at the beginning of the test (SMP C) or during the course of the test (SMP G and A). Lithium ( $\text{Li}^+$ ) and bromide ( $\text{Br}^-$ ) were added continuously (through pulse additions every minute) during the entire duration of the test as a LiBr-saturated solution (Figure 4-2, B). A total of 300 g of fluorescein and 1,500 g of LiBr were added in each SMPs monitored. The tracer amounts were estimated based on the detection limit of the analyte (i.e., fluorescein,  $\text{Li}^+$ ,  $\text{Br}^-$ ) – which was multiplied by a factor 10, and the maximum volume of dilution (volume of the SMP and estimated infiltration volume, based on the substrate porosity and depth).

Samples were collected from different locations in the SMPs, including the inlet pipe, accumulation water at different distances from the inlet, and from the outfall water, when it occurred.



*Figure 4-2. Left panel: fluorescein in SMP C. Right panel: near-continuous addition of LiBr.*

### *Lysimeter Installation*

Lysimeters are wells in the unsaturated zone that sample pore water through suction. They are included in the study to sample subsurface SMP media pore water at designated depths. Lysimeters allow for the determination of contaminant transport into the subsurface, and potentially into the underlying groundwater. Twenty lysimeters were installed in SMP C, A, G, and D during June and July 2017 (6/14/2017, 6/22/2017, and 7/20/2017). Soil Moisture Equipment Corp 1900L Surface Samplers were installed at two depths: 15 centimeters (shallow) and 30 centimeters (deep). The different depths were selected to assess if contaminants originating at the surface (i.e., in the stormwater) are being transported through the porous media. The locations of the lysimeters were determined relative to the inlet and outlet of the SMPs. SMP C is the largest and most complex; ten lysimeters (three shallow, seven deep) were installed in SMP C. SMP A is the longest and includes two weirs; six lysimeters (three shallow, three deep) were placed in SMP A along the longitudinal axis. Both SMP D and G are smaller and less complex; each had two lysimeters installed, one shallow and one deep in approximately



the middle of the SMP. The lysimeters were placed in locations that were expected to routinely be inundated with stormwater.

At each selected site, characterization efforts were undertaken which included: depth to rejection (depth probe), bulk density (soil cores), and texture analysis. Soil samples were assessed, dependent on soil quality and lysimeter depth, at 5 centimeters, 15-20 centimeters, and 30 centimeters. The lysimeters were installed while taking note of potential soil depth profiles; when refilling, care was taken to keep soil depths consistent and to exclude debris. Bentonite was added around the lysimeter to prevent the development of a preferential flow path from the surface into the sampling zone. The remaining space around the lysimeter was filled with soil and tamped down with PVC pipe; the final height of the lysimeters was measured to determine true lysimeter depth. For protection, larger-diameter PVC casings and lids were installed. Approximate lysimeter locations are shown below for SMP C, D, and G. Installation details are shown in Figure 4-3 and Table 4-1.



Figure 4-3. Approximate lysimeter locations in SMP C (top), G (lower left), and D (lower right). Red marks indicate deep lysimeters.

Table 4-1. Lysimeter installation details.

Installation Data			Depth (cm)		Bulk Density*	
Label	SMP	Location	Intended	Actual	(g/cm <sup>3</sup> )	Texture
C-R1	C	Elevated Bank	30	28	1.038	-
C-O1	C	Outlet	15	16.5	1.219	Loamy Sand
C-O2	C	Outlet	30	31	0.8812	Loamy Sand
C-M1	C	Middle	30	28	1.391	Sandy Loam
C-M2	C	Middle	15	17.5	1.401	Sandy Loam
C-M3	C	Middle	30	27	1.668	Sandy Loam
C-M4	C	Middle	30	28	1.035	Sandy Loam
C-I1	C	Inlet	15	17.5	1.694	Sandy Clay Loam
C-I2	C	Inlet	30	27	2.224	Sandy Clay Loam
C-U1	C	Above Inlet	30	29	1.668	Sandy Loam
A-N1	A	Inlet	15	15.5	-	Loamy Sand
A-N2	A	Inlet	30	33	-	Loamy Sand
A-M1	A	Below Gabion	30	28	-	-
A-M2	A	Below Gabion	15	15	-	Loamy Sand
A-F1	A	Outlet	15	16.5	-	-



A-F2	A	Outlet	30	31	-	Loamy Sand
D-D1	D	Inlet	30	29.5	-	Sandy Clay Loam
D-D2	D	Inlet	15	17.5	-	Sandy Clay Loam
G-G1	G	Middle	15	13.5	-	Sandy Clay Loam
G-G2	G	Middle	30	28	-	Sandy Clay Loam

\*Bulk density samples have only been analyzed for SMP C.

#### *Installation of Stormwater Sampling Bottles and Autosamplers*

The objective of this task was to equip the SMPs in order to monitor storms without the physical presence of personnel in the field, which has been an issue several times over the summer 2017 due to the frequent occurrence of lightning storms. Ten stormwater sampling bottles (Nalgene™ Storm Water Sampler) were installed in SMP C, G, and A (Figure 4-4). Stormwater sampling bottles were installed inside the outfall boxes to collect outfall water and inside the SMP basin (e.g., by the outfall box wall or the weirs) to collect ponding water.



*Figure 4-4. Stormwater sampling bottles.*

Also, three autosamplers were installed in SMPs C, D, and G. Autosamplers consisted in two Global Water GS750 autosamplers (SMPs C and D) and one ISCO 6712 autosampler (Figure 4-5). The GS750 two-bottle samplers will be used to collect a first-flush during the first 30 min of the storm and a flow-weighted composite sample for the following of the storm. The ISCO 6712 autosamplers will allow collecting up to 24 samples during one storm and will provide a more detailed profile of the contaminants washed from the highway. The suction lines and strainers are positioned into receiving boxes installed directly beneath the inlet pipe and filling quickly with drainage water during a storm event. Additional samplers will be installed in SMP A during the fall 2017. Currently, the autosamplers are operated via water level actuators located in the receiving box installed by the inlet pipe (Figure 4-6). The autosamplers will be

operated through the flowmeter network installed by Villanova University, and if the approach is not possible, through mounted rain gages.



*Figure 4-5. ISCO 6712 (left) and Global Water GS750 (right) autosamplers*



*Figure 4-6. Receiving box to collect inlet water.*

### *Monitoring plan*

Sampling will be performed using a combination of autosamplers and grab samples. Inlet water in SMP C, D, G, and A (one to three inlets) will be sampled during selected storm events using the Global Water GS750 autosamplers. The sampling pattern (e.g., sampling type, sampling time, volumes, etc.) will be pre-programmed based on the storm predictions and sampling purposes. Again, the sampling pattern will be pre-programmed: for instance, six first-flush samples will be collected during the first hour of the storm and 18 samples every 30 min during the rest of the storm. The autosamplers will be filled with ice at the time of installation to ensure constant chilling of the samples until their removal and transportation to the lab.

Ponding water will also be collected by positioning containers or trays at selected locations at the bottom of the SMPs. In addition, shallow vacuum lysimeters (e.g., Toro Shallow Ceramic Cup Lysimeter) will be installed in selected SMPs to collect infiltration water.

### *Sample Handling, Preservation, and Storage*

#### Surface Water Samples

Upon arrival in the lab, the raw samples were analyzed for pH, conductivity, and turbidity. Samples were centrifuged to remove solids (1000 Gs for 8 minutes; operationally defined as dissolved). A 50-mL aliquot of sample was collected for metal analysis. The samples were preserved by acidification ( $\text{pH} < 2$ ) and stored at  $4^{\circ}\text{C}$  until analysis. In some cases, oil and grease analysis was performed after the 28 days of storage, in which cases the samples were kept frozen at  $-20^{\circ}\text{C}$  until analysis.

#### Lysimeter Samples

Care was taken during installation and sampling procedures to minimize contamination potential. Additionally, a bottle blank, field blank, and sampling method blank are created for

each sampling effort to assess contamination. Conductivity, pH, and the total volume of water in each lysimeter is measured during sampling efforts. Trace metal samples from each lysimeter are collected, as well as bromide samples as appropriate following Simulated Runoff Tests (SRTs; applicable for SMP C, A, and G). Any remaining water in the lysimeters is purged. The trace metals samples (blanks and lysimeter samples) are acidified within 48 hours; all samples were stored in the dark at 4°C.

### *Analyses*

Analytical methods and quality control were extensively described in the QAPP. The table below summarizes the methods used.

*Table 4-2. Analytical methods for water quality monitoring.*

Parameter	Method	Materials & Equipment
pH	Combined glass bulb electrode (sensitive to hydrogen ions) and reference electrode	Accumet Basic AB 15 with Accumet 3-in-1 pH/ATC combination electrode (Fisher Scientific Corporation)
Dissolved oxygen	LDO (luminescent dissolved oxygen)	HQd Portable Meter with LDO probe (Hach)
Conductivity	Conductivity	HQd Portable Meter with Graphite, 4 pole conductivity probe (Hach)
Turbidity	Nephelometry	Turbidimeter 2020 we (LaMotte)
Solids (total, suspended)	Evaporation, filtration and gravimetry	Crucibles, glass fiber filters, filtration device, analytical balance (precision 0.1 mg/L)
Total nitrogen	Persulfate digestion	Nitrogen Total 'N Tube Low Range 0.5-25.0 mg/L (Hach) and DR5000 Spectrophotometer

Nitrate	Dimethylphenol	Nitrate, Nitrogen TNTplus Low Range 0.23-13.5 mg/L (Hach) and DR5000 Spectrophometer
Ammonia	Salicylate	Ammonia TNTplus 0.015-2.0 mg/L (Hach) and DR5000 Spectrophometer
Total Kjeldahl nitrogen	Simplified TKN (sTKN)	Simplified TKN TNTplus 0.0-16 mg/L (Hach) and DR5000 Spectrophometer
Total phosphorous	PhosVer 3 with acid persulfate digestion	Total Phosphorous Test 'N Tube 0.06-3.50 mg/L (Hach) and DR5000 Spectrophometer
COD	Dichromate	TNTplus Ultra Low Range 1–60 mg/L (Hach) and DR5000 Spectrophometer
Metals (Zn, Cu, Pb, Cr, Cd)	Inductively Coupled Plasma Mass Spectrometer (ICP-MS)	Agilent 7900 ICP-MS with collision reaction cell
Oil & grease	Solid phase extraction (SPE) and gravimetry	SPE apparatus, analytical balance (precision 0.1 mg/L)

Metal concentrations were analyzed using an inductively coupled plasma mass spectrometer (ICP-MS; Agilent 7900). Analysis details were provided in the previous report, in brief, 56 elements were generally measured, and based on previous analyses, reports in the literature, and regulatory limits, the following elements are considered high priority: Cr, Fe, Co, Cu, Zn, As, Cd, and Pb. ICP-MS analysis quality control procedures are described with more details at this end of this report section.

An additional method optimized for the determination of fluorescein tracer in water samples. In short, unfiltered samples were kept refrigerated at 4 C for no more than 72 hours before processing. After vigorous shaking, 200  $\mu$ m of samples were collected and introduced in a standard 96-well microplate for fluorescence reading. Fluorescence was then recorded on a

Tecan 200 Pro spectrophotometer (excitation 490 nm, emission 520 nm). A standard curve was established with fluorescein solutions of known concentrations. Background fluorescence was recorded in background samples collected in the field prior to fluorescein addition and subtracted from the readings.

### *Load Calculation*

Contaminants loads into the SMPs were estimated for the different storms monitored using measured contaminant concentrations and flow data recorded on the site and/or estimated from catchment surface area and rain intensity. Loads were estimated for the most significant contaminants, including suspended solids (SS), nitrate ( $\text{NO}_3^-$ ), total nitrogen (totN), total phosphorus (totP), and selected metals. Results obtained from different flow estimation methods are presented in parallel and compared. Detailed onsite flow data have been obtained for the February, March, April and May storms. Other flow data were estimated using the catchment area multiplied by the rainfall intensity.

## **Results and Discussion**

### *Influent Water Quality – General Parameters*

The tables and figures below present the results of analysis of selected water parameters for eight storms occurring from October 2016 to August 2017. Data for the April 2017 storm includes only metals, analyses of other parameters are still ongoing. Oil and grease data are only available for the October 2016 storm, analyses for subsequent storms are still ongoing.

### Sampled Storms: Intensity

Rainfall data were used to estimate the intensity of the storm. The storm intensities were estimated from rainfall data collected from the Northeast Philadelphia Airport (KPNE) weather station because local rain data were not available at the time of sample collection (Table 4-3).



These rainfall data will be compared with local weather station and updated when an understanding about the travel time for stormwater to flow from the drainage area to the collection point at the inlet pipe is obtained. Some storms did not show rainfall initiating before the first samples collected and there was a data gap in the GR2 station for one storm.

*Table 4-3. Summary of storm data (during the time of sampling) collected from the Northeast Philadelphia Airport (KPNE)*

Date	Starting Sampling Time	Average Intensity (mm/h)	Total During Sampling (mm)	Time since last event (h)	Avg. Temp (°C)
10/27/2016	1:06 PM	0.508	1.016	124	10.9
11/30/2016	9:45 AM	2.159	4.318	13	14.6
1/20/2017	12:35 PM	0.762	1.524	59	5.0
2/7/2017	9:56 AM	2.921	5.842	287	7.0
3/27/2017	8:45 AM	1.016	3.048	41	7.4
4/6/2017	11:15 AM	0.169	0.508	54	9.6
5/22/2017	10:40 AM	2.286	6.858	50	16.0
8/29/2017	10:30 AM	1.185	3.556	154	18.3

The rainfall or flow intensity is expected to impact the concentration of contaminants in the stormwater by different ways: mechanical washing of particles and colloids adsorbed to the surface, dissolution of soluble materials, or dilution of contaminants. Three of the monitored events (October, February, and August 2017) had considerable antecedent dry periods (ADP) potentially allowing for greater accumulation on the road surface, which is reflected by the higher level of some of the water parameters during the first flush (e.g., SS, nitrate, ammonia). Generally speaking, ADP seems to have lower than expected impact on the recorded water quality parameters.

### General Observations

No clear correlation was observed between the profiles of contaminants in stormwater (i.e., concentrations) and stormwater flow (estimated at this stage by the rainfall intensity).

Reasons for the lack of a correlation include incomplete data records for some storms, the



absence of significant rainfall recording at the early stage of the storm, and the unknown lag time between the onset of rainfall and sample collection at the inlet pipe. Generally speaking, intensive parameters (e.g., temperature) were consistent between SMP C and D, although extensive parameters (e.g., suspended solids) were much higher for stormwater from SMP C than SMP D, likely reflecting the respective drainage area.

### Temperature

The temperature of the water reflects the ambient temperatures at the time of sampling (Figure 4-7). The temperature shows little variation with the time of sampling and between the two SMPs sampled for a given storm. Some of the storms show an increase of temperature with time, reflecting the morning warming of the ambient air and/or pavement surface (e.g., October, March).

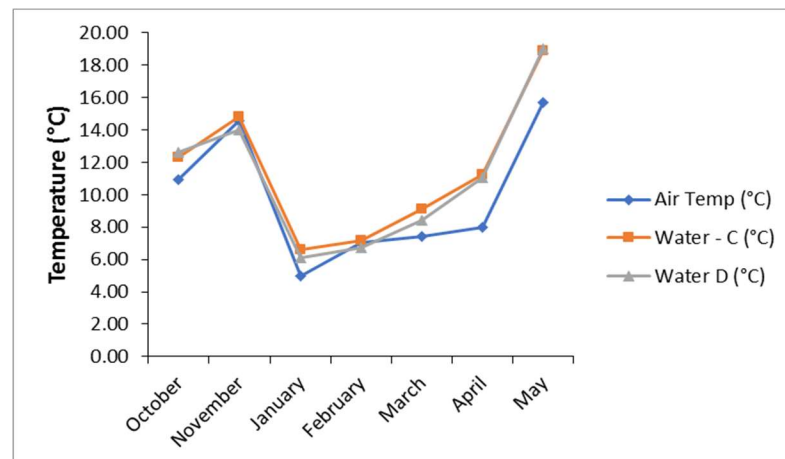


*Figure 4-7. Ambient air temperature and temperature measured in runoff water for the two SMPs C and D for the eight storms.*

### Dissolved Oxygen (DO)

DO data revealed that the stormwater runoff was always near oxygen saturation, which also reflects the ambient temperatures at the time of sampling. A very good correlation was observed between the temperature and measured DO and between measured DO and predicted

DO based on temperature, with Pearson's rank correlation coefficients for all storms,  $r = 0.98$  in both cases (Figure 4-8 and 4-9). Again, the DO shows little variation with the time of sampling and between the two SMPs for a given storm.

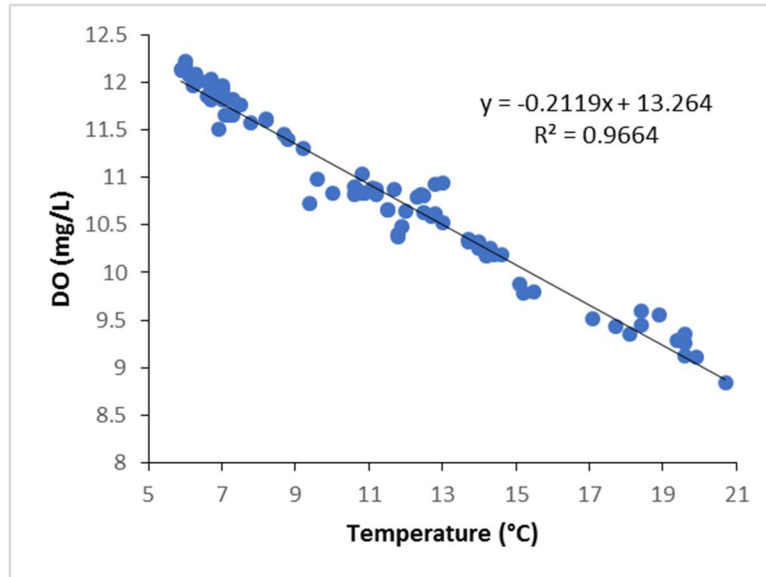


Figure 4-8. Correlation between water temperature and DO in runoff water for the eight storms.

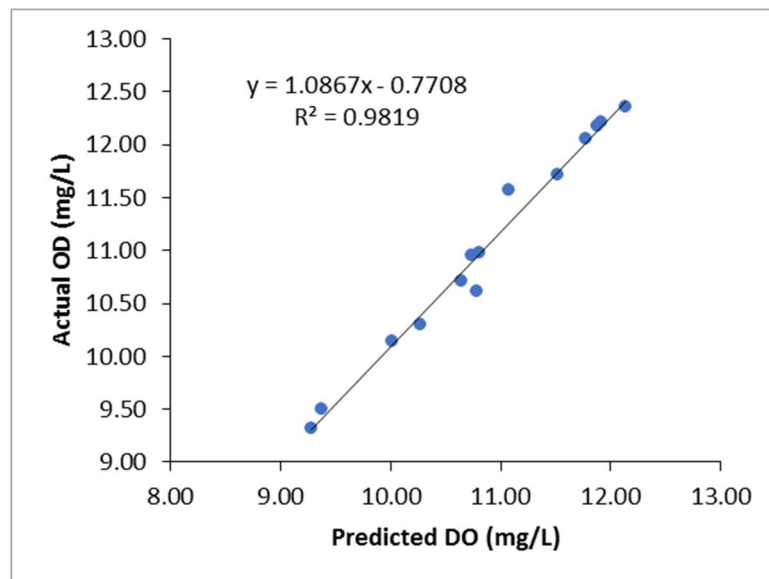


Figure 4-9. Correlation between predicted (theoretical) and actual (measured) average DO in runoff water for the eight storms.

### Proton Activity (pH)

The pH data revealed that the stormwater runoff was generally alkaline ( $\text{pH} = 7.2 - 10.0$ ) and fairly consistent between the two SMPs sampled for a given storm, although SMP D shows consistently higher reading than SMP C. The pH showed both an increase or decrease over the time of sampling, likely reflecting changes in water composition. No clear correlations were observed between pH and other water parameters that might explain these trends.

### Specific Conductivity

Specific conductivity (conductivity at  $25^{\circ}\text{C}$ ) was also highly variable across the storms ( $71 - 6,460 \mu\text{S}/\text{cm}$ , depending on the time of sampling) (Figure 4-10). The highest conductivity was observed in March after a significant snowfall event on March 14, 2017. For some storms, we observed a general decrease of the conductivity with the time of sampling, reflecting the gradual dissolution of salts (March, swale C). In some other cases, we observed an increase of conductivity with the time of sampling (March, swale D). Conductivity levels observed in January – March were much higher than during October and November, likely due to application of winter road salt. We also observed a much higher value of conductivity for the March storm in SMP C as compared with SMP D.

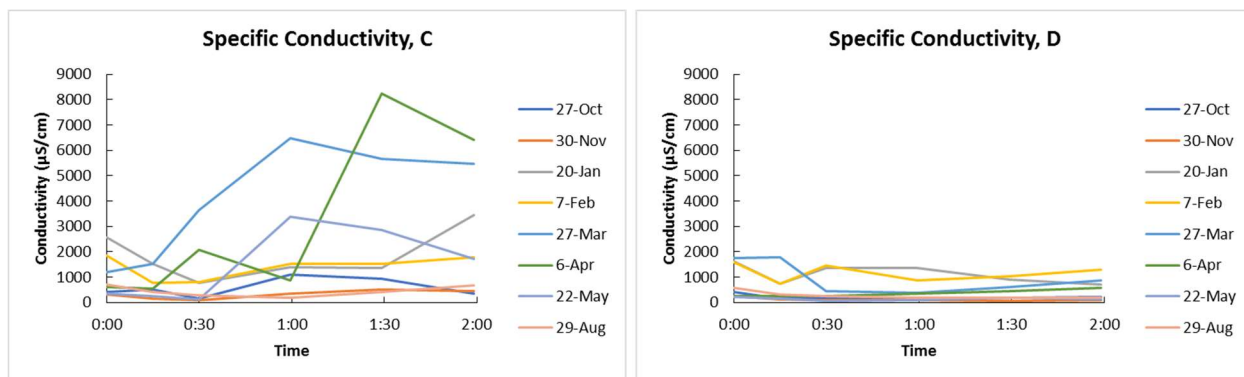


Figure 4-10. Conductivity measured in runoff water for the two SMPs C and D for the eight storms.

## Turbidity

Turbidity was highly variable across the storms (2.6 – 113 NTU, depending on the time of sampling) (Figure 4-11). For some storms, we observed a general decrease of the turbidity with the time of sampling, reflecting the gradual washing of particles and colloids from the pavement surface (October, March). In some other cases, we observed an increase of turbidity with the time of sampling (November). These different patterns are likely to be explained by the flow intensity, i.e., a high flow mechanically desorb particles and colloids from the surface.

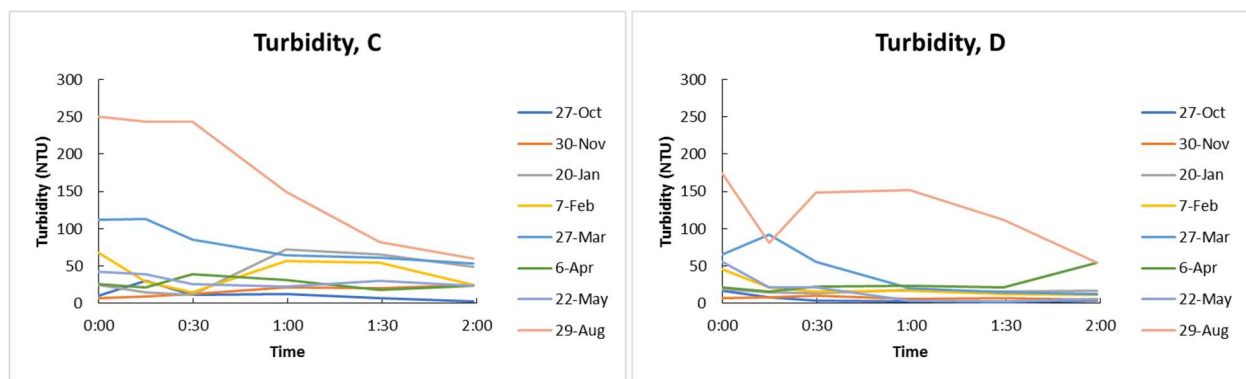


Figure 4-11. Turbidity measured in runoff water for the two SMPs C and D for the eight storms.

## Suspended Solids (SS)

For most of the storms, we observed a gradual decrease of SS with the time of sampling, reflecting the washing or desorption of suspended particles (Figure 4-12). Often, the first flush (0.5 – 1 L) was lower than the second or third sample collected (e.g., November), which is explained by the increasing flow rate, increasing the mechanical action of water to carry particles. SS correlates well with turbidity (Figure 4-13), with Pearson's rank correlation coefficient for all storms,  $r = 0.74$ .

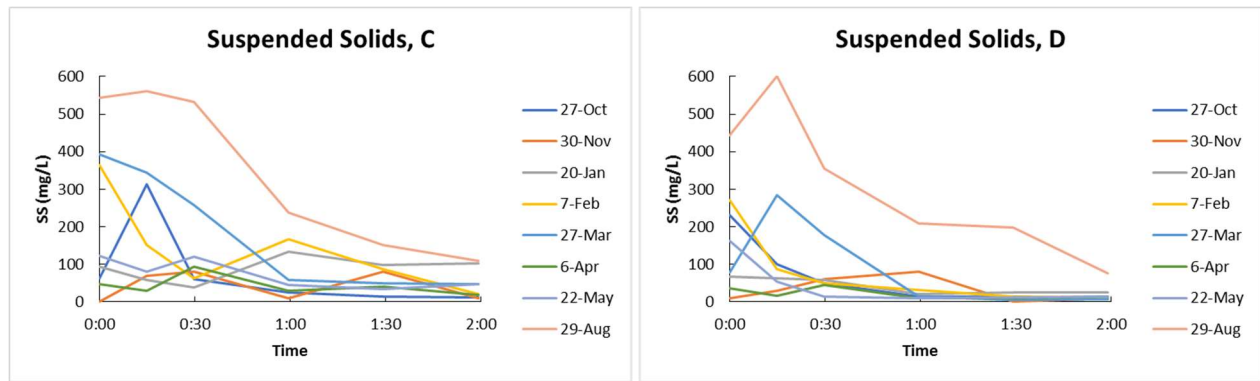


Figure 4-12. Suspended solids measured in runoff water for the two SMPs C and D for the eight storms.

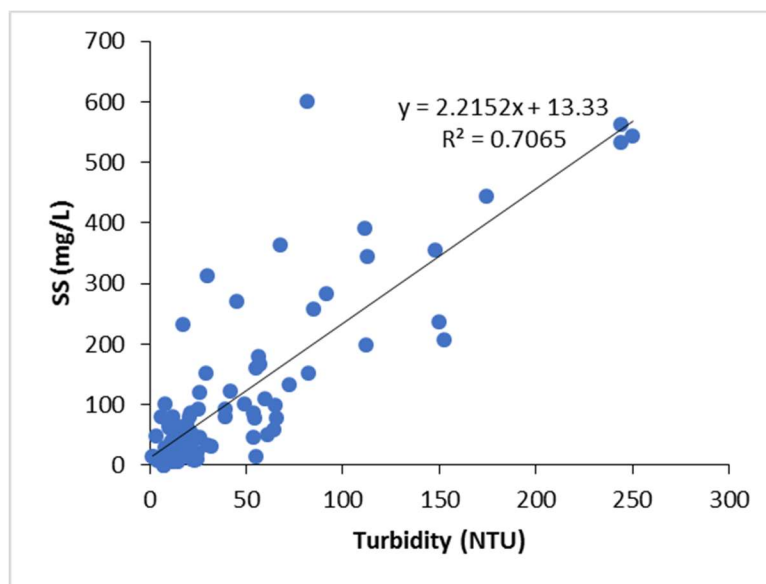


Figure 4-13. Correlation between suspended solids and turbidity in runoff water for the eight storms.

### Dissolved and Total Solids (DS and TS)

For some storms, we observed a general decrease of the DS (and TS) with the time of sampling, possibly reflecting the gradual dissolution of soluble material (March, swale D) (Figure 4-14). Conductivity levels observed in January – March were much higher than during October and November, likely due to application of winter road salt. Often, the first flush (0.5 – 1 L) DS level was lower than the second or third sample collected (e.g., November), which is explained by the increasing flow rate, increasing the mechanical action of water to wash

dissolved solids from the surface. DS correlates well with conductivity (Figure 4-15), with Pearson's rank correlation coefficient for all storms,  $r = 0.93$  (after removal of a few outliers).

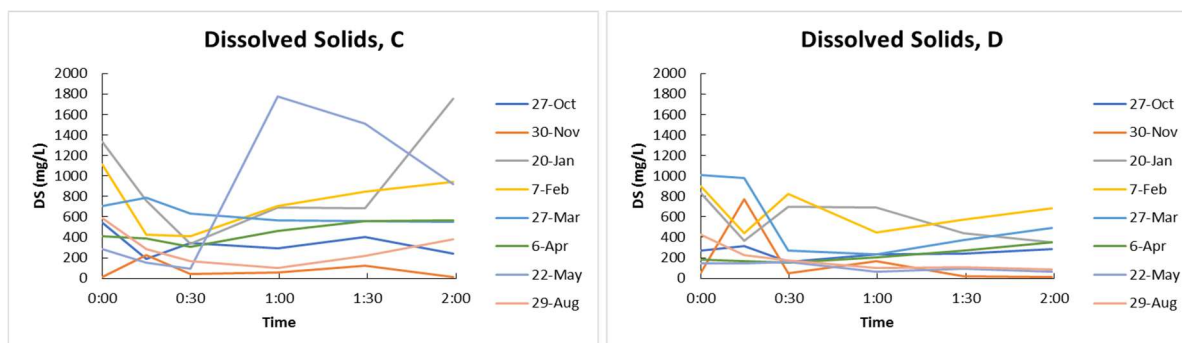


Figure 4-14. Dissolved solids measured in runoff water for the two SMPs C and D for the eight storms.

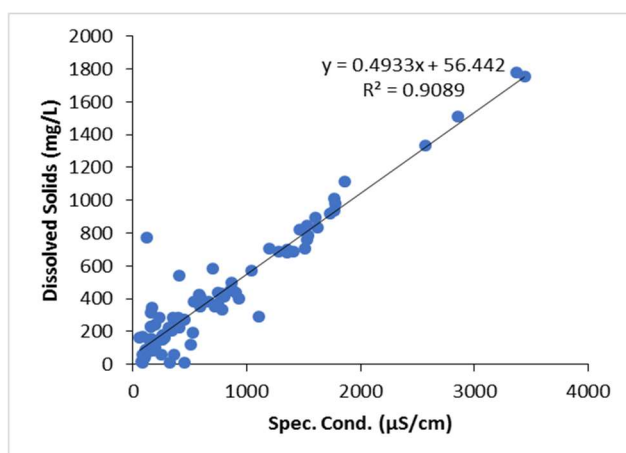


Figure 4-15. Correlation between dissolved solids and conductivity in runoff water for the eight storms (four outliers visually identified were removed).

### Total Nitrogen and Nitrate

Total nitrogen and nitrate generally decreased with the time of sampling, which was expected with these generally soluble species (Figure 4-16). In one case (February, SMP C), we observed an increase of total nitrogen with the time of sampling, which may be explained by an increase of particulate matter (i.e., increase of turbidity and SS). Total nitrogen correlates well with nitrate (Figure 4-17), with Pearson's rank correlation coefficient for all storms,  $r = 0.67$ , which was expected as nitrate is the primary form of nitrogen present in stormwater runoff.

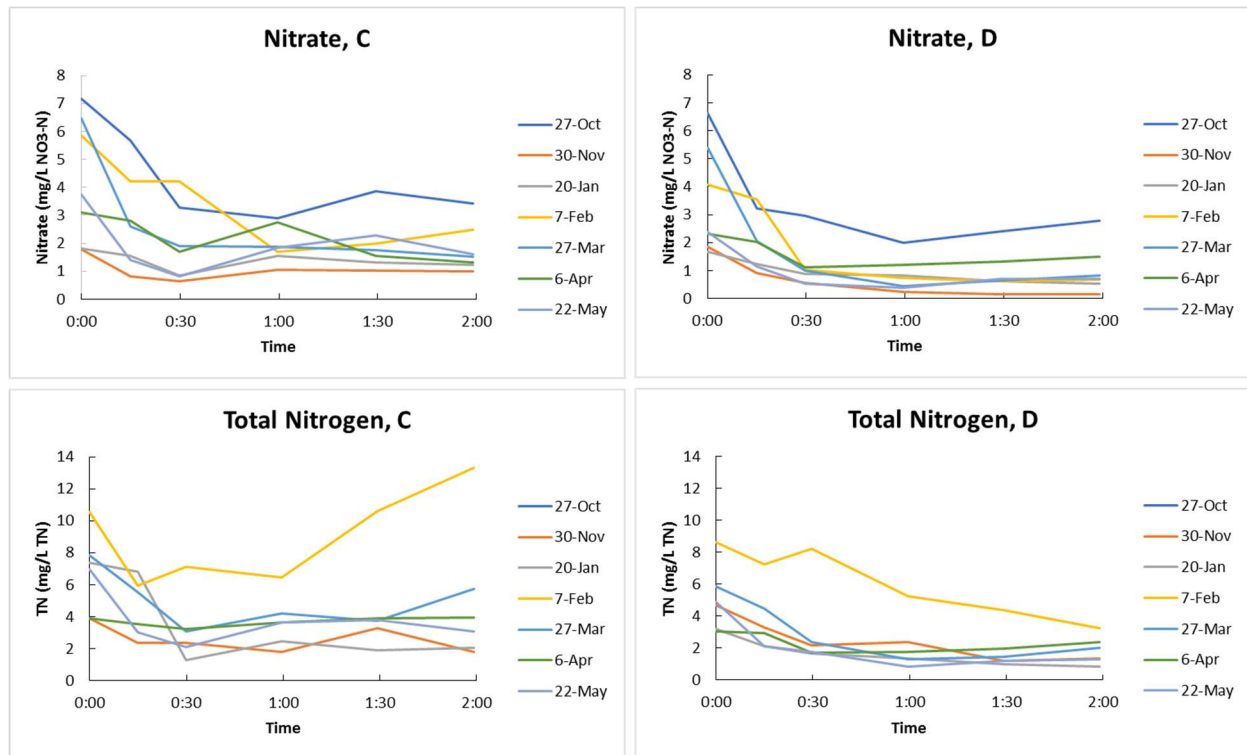


Figure 4-16. Nitrate and total nitrogen measured in runoff water for the two SMPs C and D for the seven storms.

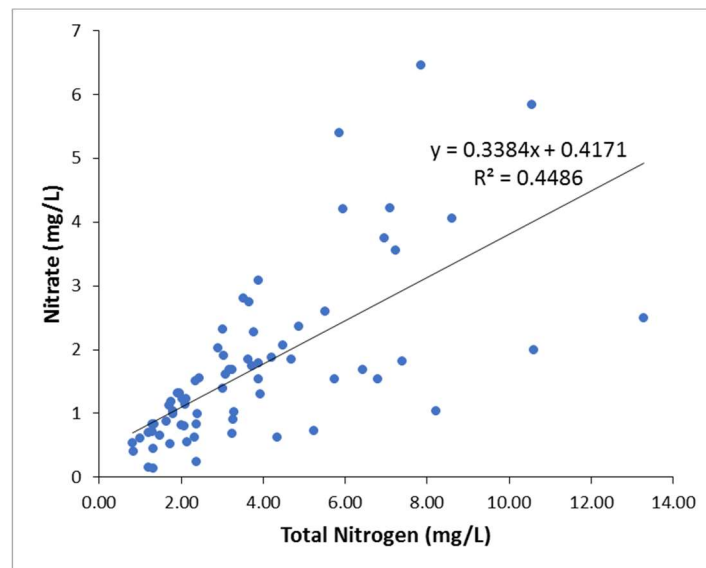


Figure 4-17. Correlation between nitrate and total nitrogen in runoff water for the seven storms.

#### Ammonia and Total Kjeldahl Nitrogen (TKN)

Ammonia and Total Kjeldahl nitrogen (TKN) do not show a specific pattern across the storms (Figure 4-18). Little correlation was observed between the two parameters. However,

TKN gave consistently higher concentration than ammonia, suggesting that a large portion of reduced nitrogen is organic.

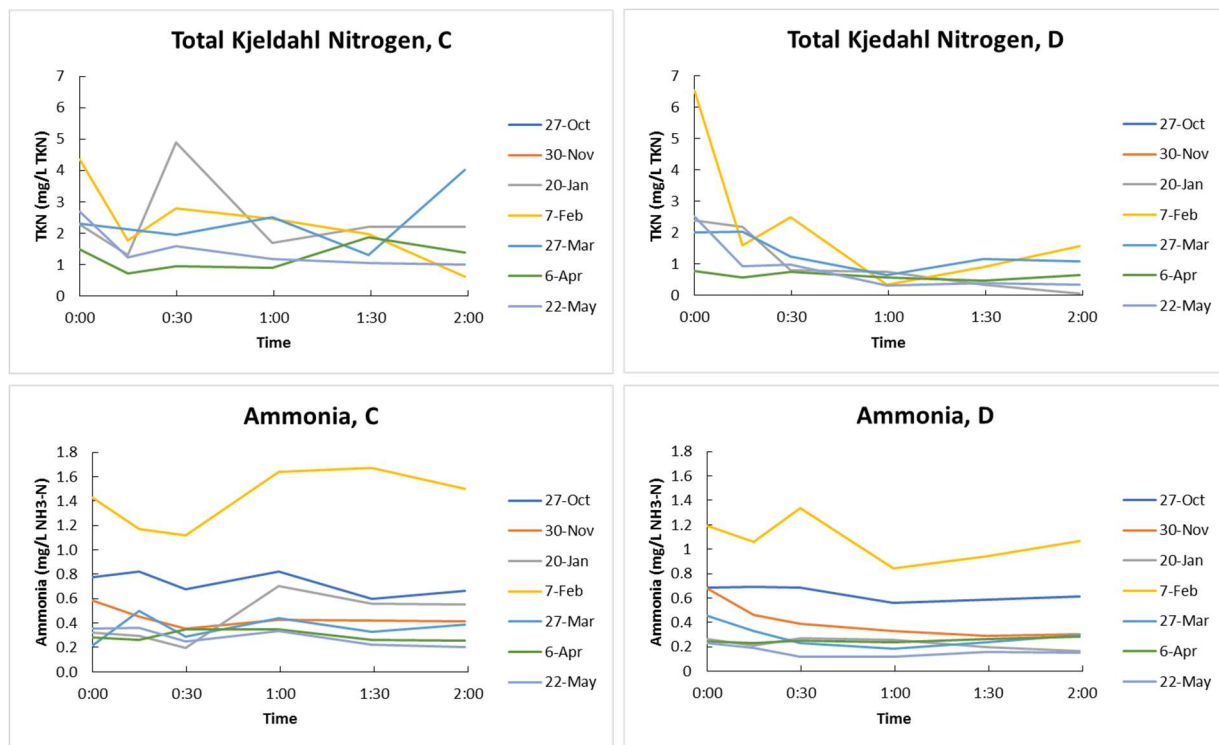


Figure 4-18. Ammonia and total Kjeldahl nitrogen measured in runoff water for the two SMPs C and D for the seven storms.

### Total Phosphorous

Total phosphorous shows a general decrease with the time of sampling, suggesting that total phosphorous is significantly washed from the surface by runoff water (Figure 4-19). Total phosphorous correlates well with turbidity and SS, with Pearson's rank correlation coefficient for all storms,  $r = 0.89$  and  $0.87$  (after removal of one outlier), respectively, which indicates that phosphorus was present mostly as particulate phosphorous (Figure 4-20).



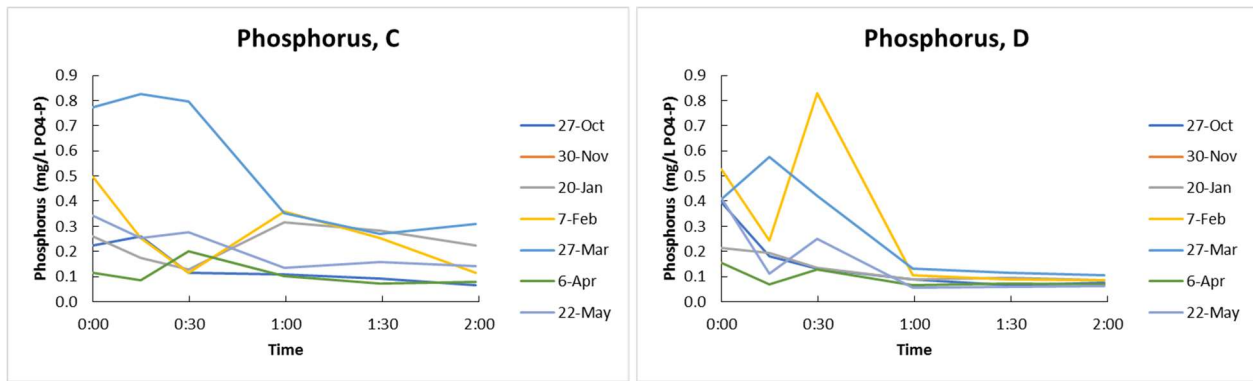


Figure 4-19. Total phosphorus measured in runoff water for the two SMPs C and D for the seven storms.

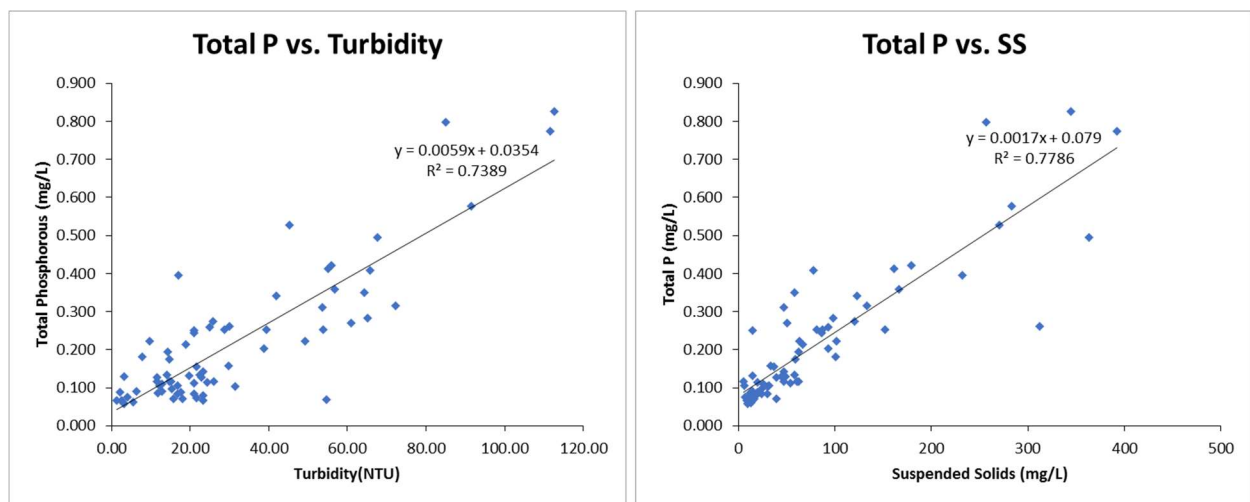


Figure 4-20. Correlation between total phosphorous and turbidity and SS in runoff water for the seven storms (a few outliers visually identified were removed).

### Chemical Oxygen Demand (COD)

Chemical oxygen demand (COD) shows a general decrease with the time of sampling in SMP D, but a rather indistinct pattern in SMP C (Figure 4-21).

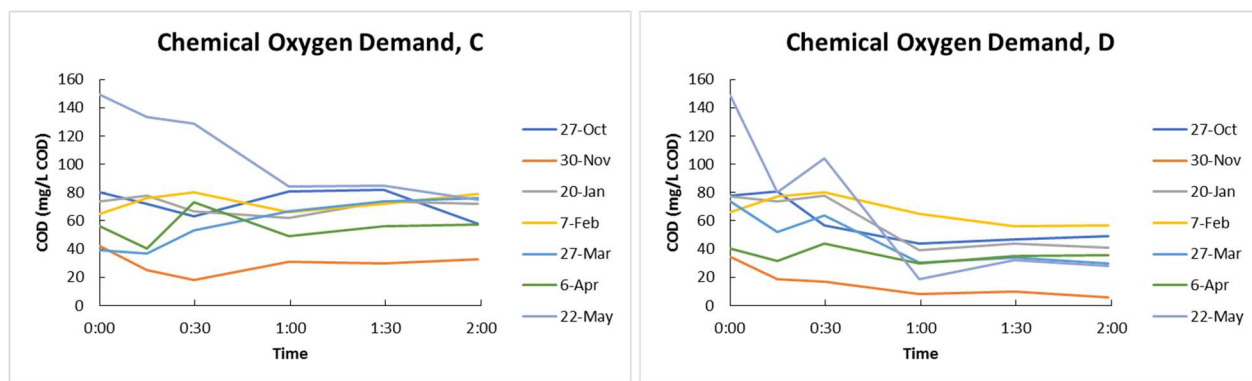


Figure 4-21. Chemical oxygen demand measured in runoff water for the two SMPs C and D for the seven storms.

### Oil and Grease

Oil and grease analyses were only finalized for the first storm (October) and shows a significant decrease with the time of sampling (Figure 4-22). Technical problems have been experienced for the analysis of oil and grease. The team is looking for alternative ways to analyze reliably hydrocarbons, such as HPCL and GC.

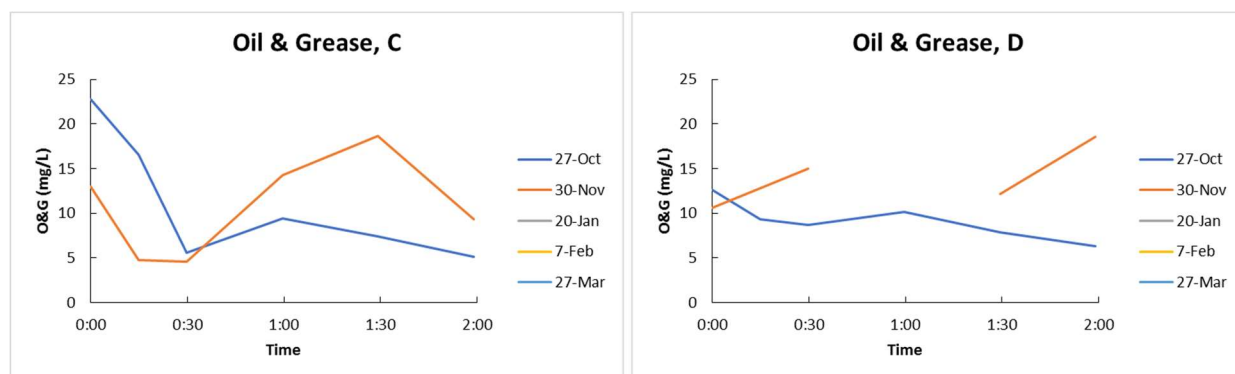


Figure 4-22. Oil and grease measured in runoff water for the two SMPs C and D for the five storms.

### Influent Water Quality – Metals

#### Metals Prioritization

Based on samples collected between October 2016 - April 2017 (71 SMP influent samples and seven SMP ponded water samples), the elements were screened to identify which elements should be the focus of reporting efforts. The screening process reflected quality

assurance measures, regulatory relevance, reports in published literature, and measured values in the current research effort. Further details are included in the previous report. Based on this assessment, the following elements are considered high priority: Cr, Fe, Co, Cu, Zn, As, Cd, and Pb. Event-based descriptive statistics are shown in Table 4-4.

*Table 4-4. Description statistics for the concentrations of high priority elements in SMP influent water for the eight collected storms.*

Runoff/ SMP Influent concentration (ug/L)												
Element	Cr			Fe			Co			Cu		
Storm	% Quant	Ave	Stdev	% Quant	Ave	Stdev	% Quant	Ave	Stdev	% Quant	Ave	Stdev
28-Oct	92	5.79	4.52	92	825	1034	92	1.09	1.01	83	54.61	47.26
30-Nov	17	4.46	7.66	92	608	387	92	0.50	0.29	75	20.39	11.86
20-Jan	82	19.21	24.68	91	944	791	91	0.95	0.50	91	48.76	30.16
7-Feb	33	14.63	17.53	92	769	666	92	768.51	666.31	83	81.79	49.41
27-Mar	92	74.61	74.26	92	4504	4168	92	3.14	2.64	92	87.57	63.35
6-Apr	92	12.14	13.79	100	668	313	92	0.72	0.46	92	28.05	11.65
22-May	0	20.80	32.30	0	852	730	64	0.78	0.53	82	37.94	23.55
29-Aug	0	0.35	1.20	0	3159	1281	100	4.75	2.81	100	61.59	34.12
Total	51	18.98	37.43	70	1555	2122	87	1.70	2.03	86	52.78	43.28
Element	Zn			As			Cd			Pb		
Storm	% Quant	Ave	Stdev	% Quant	Ave	Stdev	% Quant	Ave	Stdev	% Quant	Ave	Stdev
28-Oct	92	254.0	309.5	92	1.02	0.64	17	0.12	0.15	92	19.57	26.55
30-Nov	0	93.1	63.8	83	0.63	0.55	17	0.06	0.03	92	7.89	5.06
20-Jan	0	179.4	136.2	91	1.33	0.42	45	0.15	0.13	91	15.60	12.50
7-Feb	0	0.0	0.0	50	1.32	0.74	0	0.24	0.18	83	21.73	19.39
27-Mar	92	490.8	452.0	92	7.39	4.83	67	0.46	0.40	92	38.24	34.61
6-Apr	92	128.4	72.3	100	1.72	0.74	33	0.08	0.06	92	8.19	5.19
22-May	0	41.2	74.1	82	1.26	1.28	0	0.10	0.09	82	9.03	8.64
29-Aug	0	331.5	462.7	82	0.87	0.56	0	0.42	0.28	100	42.88	17.26
Total	47	191.5	297.1	83	1.96	2.77	22	0.21	0.24	89	20.56	22.36

Descriptive statistics for medium, medium high, and high priority elements, based on quantitative results, are shown in Table 4-5; it should be noted that these are total metals concentrations, meaning that the concentrations reflect both dissolved and particle-associated metals (dilute acid extraction). It should also be noted that Table 4-5 contrasts all influent samples with ponded samples collected during a single event (March 31, 2017) and therefore is not a paired contrast. Because the samples are not paired, direct comparison is not possible, but the average influent concentration is almost universally noticeably higher than in the ponded (i.e., in-SMP) sample concentration; Cr is the notable exception. The in-pond sample

concentration reduction, compared to the influent concentration, is likely due to either non-paired sampling approach or sedimentation of solids, resulting in a reduction in water column concentration.

The runoff (SMP influent) profiles for high-priority elements are shown below. Note that these are total metals, meaning that the concentrations reflect both dissolved and particle-associated metals (dilute acid extraction).

Across the eight high priority elements plots that are included in Figure 4-23 & 4-24, several trends emerge. As seen with other extensive parameters (e.g., conductivity, turbidity, phosphorus), the highest concentrations were observed during the March 27, 2017 event. By contrast, the event on November 30, 2016 produced comparatively low concentration samples.

Table 4-5. Descriptive statistics for SMP influent samples and ponded SMP samples based on quantitative results; data is restricted to medium, medium-high, and high priority elements.

Element	unit	Runoff/ SMP Influent samples				SMP ponding samples			
		n	% Quant	Ave	Stdev	n	% Quant	Ave	Stdev
B	µg/L	71	20%	20.15	3.38	7	0%		
P	µg/L	59	3%	181.34	3.44	7	0%		
Ti	µg/L	59	78%	86.42	0.66	7	57%	8.60	3.59
V	µg/L	71	90%	4.87	1.17	7	71%	1.64	1.54
Cr	µg/L	71	68%	46.66	0.65	7	29%	101.68	95.96
Mn	µg/L	71	90%	50.65	0.80	7	71%	8.82	6.27
Co	µg/L	71	90%	1.55	0.89	7	71%	0.21	0.08
Ni	µg/L	71	28%	7.60	0.82	7	0%		
Cu	µg/L	71	86%	45.10	1.23	7	43%	14.33	5.02
Zn	µg/L	71	46%	354.28	0.88	7	71%	61.41	46.16
As	µg/L	71	85%	3.28	0.77	7	71%	0.81	0.60
Sr	µg/L	71	90%	656.93	1.02	7	71%	45.79	51.80
Mo	µg/L	59	88%	5.63	1.51	7	71%	1.63	1.27
Pd	µg/L	59	19%	616.03	1.14	7	0%		
Ag	µg/L	71	4%	0.04	8.21	7	0%		
Cd	µg/L	71	30%	0.34	1.02	7	14%	0.13	
Sn	µg/L	59	51%	2.93	1.13	7	0%		
Ba	µg/L	71	90%	75.38	1.12	7	71%	34.23	30.27
Pb	µg/L	71	90%	22.59	0.86	7	71%	3.66	1.95
Na	mg/L	71	76%	1339.54	0.00	7	71%	49.01	76.27
Mg	mg/L	71	93%	7.55	0.00	7	71%	0.34	0.13
Al	mg/L	71	75%	1.64	0.00	7	71%	0.27	0.13
K	mg/L	71	59%	101.61	0.00	7	0%		
Fe	mg/L	71	93%	2.26	0.00	7	71%	0.34	0.17

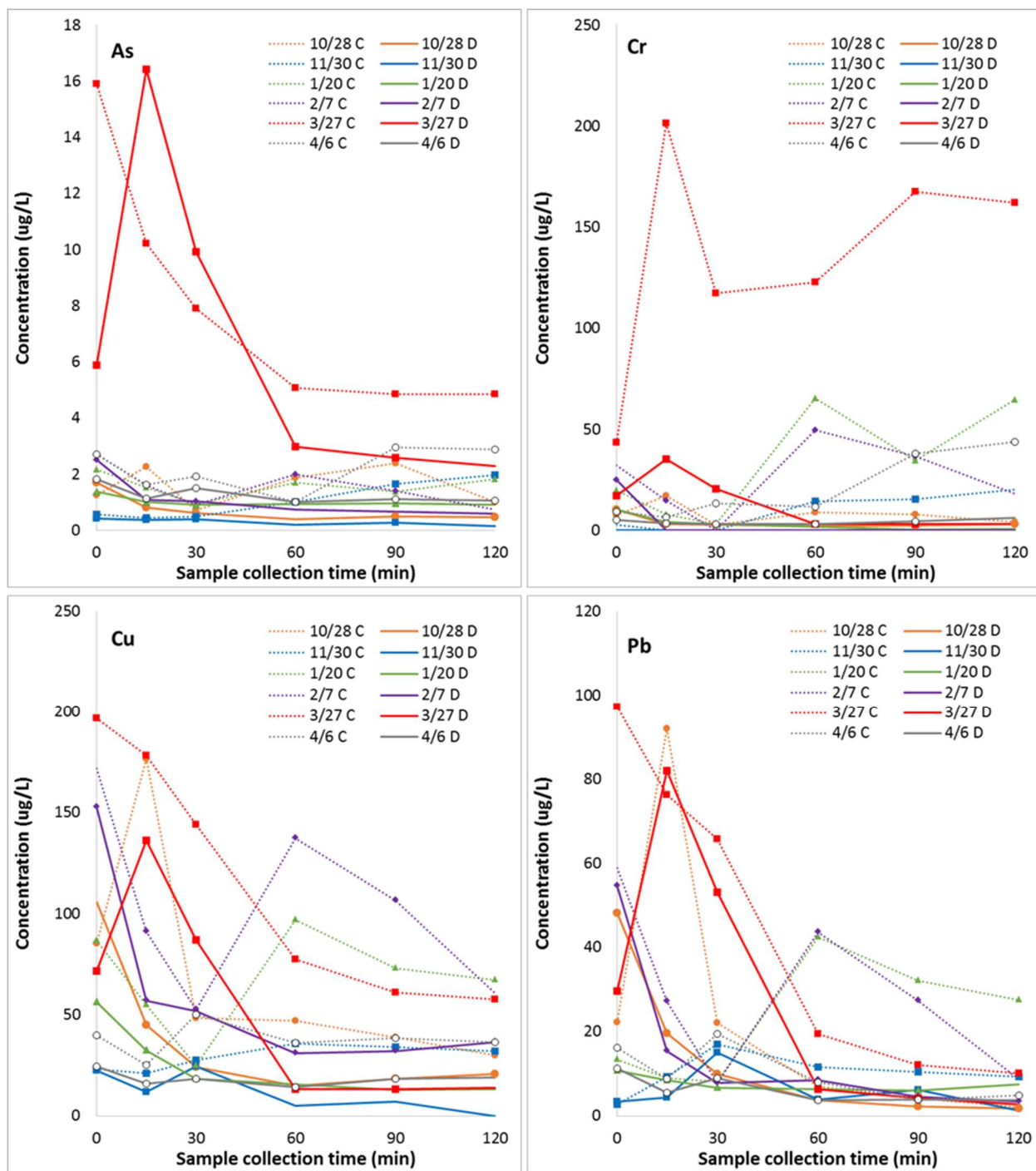


Figure 4-23. Total As, Cr, Cu, and Pb concentration for six sampling effort at SMP C and D. Samples were collected at time 0, 15, 30, 60, 90, and 120 minutes. Note that a symbol at a sampling point indicates that it is a quantitative result, while no symbol means that it is an estimate (e.g., later Cu concentrations from SMP D on 11/30 are estimates, and therefore don't include a symbol).



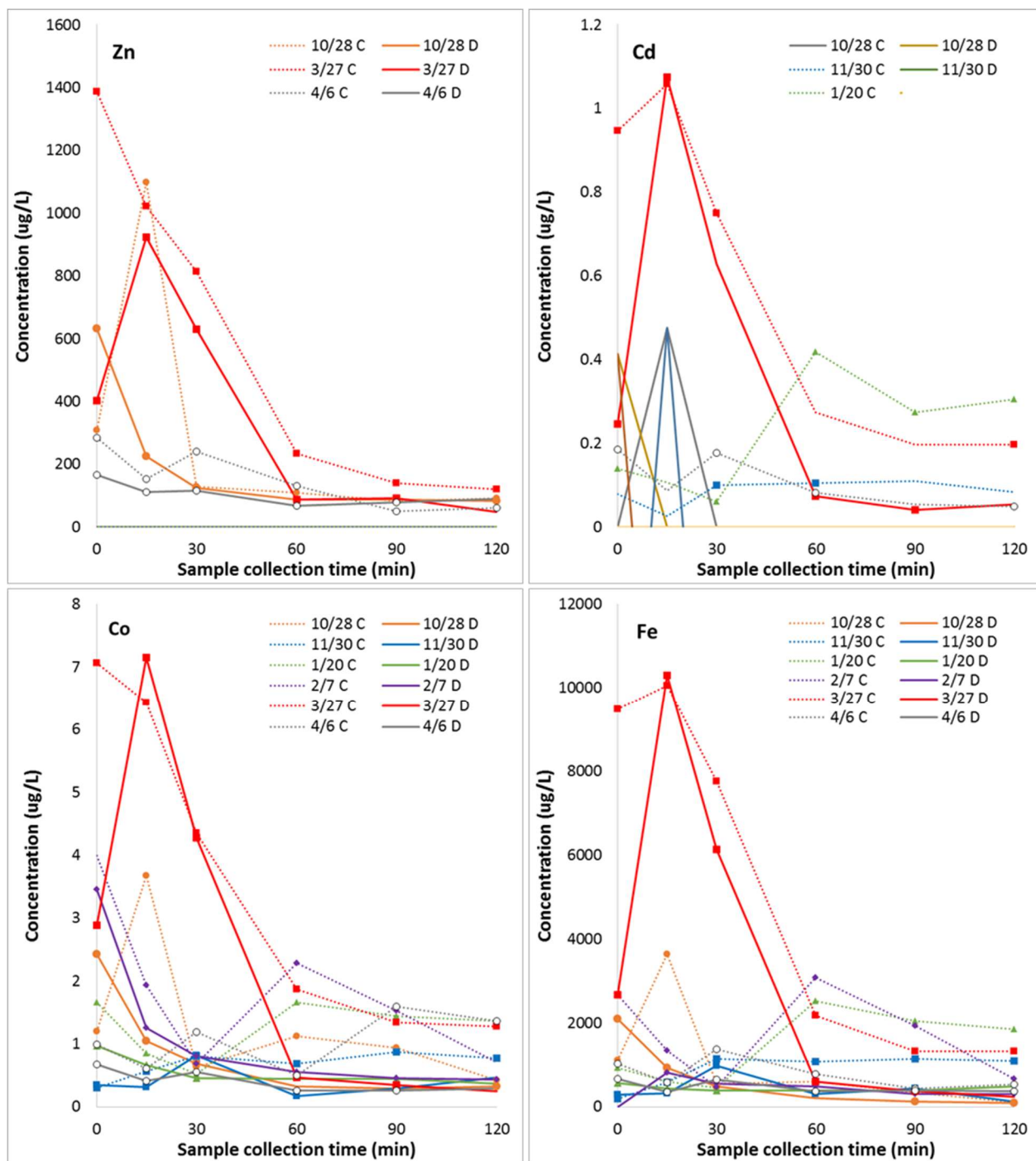


Figure 4-24. Total Zn, Cd, Co, and Fe concentration for six sampling effort at SMP C and D. Samples were collected at time 0, 15, 30, 60, 90, and 120 minutes. Note that a symbol at a sampling point indicates that it is a quantitative result, while no symbol means that it is an estimate; note that some events didn't have enough quantitative results to warrant inclusion in the plot.

For a given event and sample collection time, concentrations in SMP C samples are typically greater than concentrations in SMP D samples, and often are more than double; this is particularly true for Cr. Some metal concentrations correlate well with SS (Figure 4-25). For example, Cr (Pearson's rank correlation coefficient,  $r = 0.92$ ), Pb ( $r = 0.95$ ), Cd ( $r = 0.88$ ), and Co ( $r = 0.91$ ) are well-correlated, likely reflecting adsorption of these metals on particles and colloids.

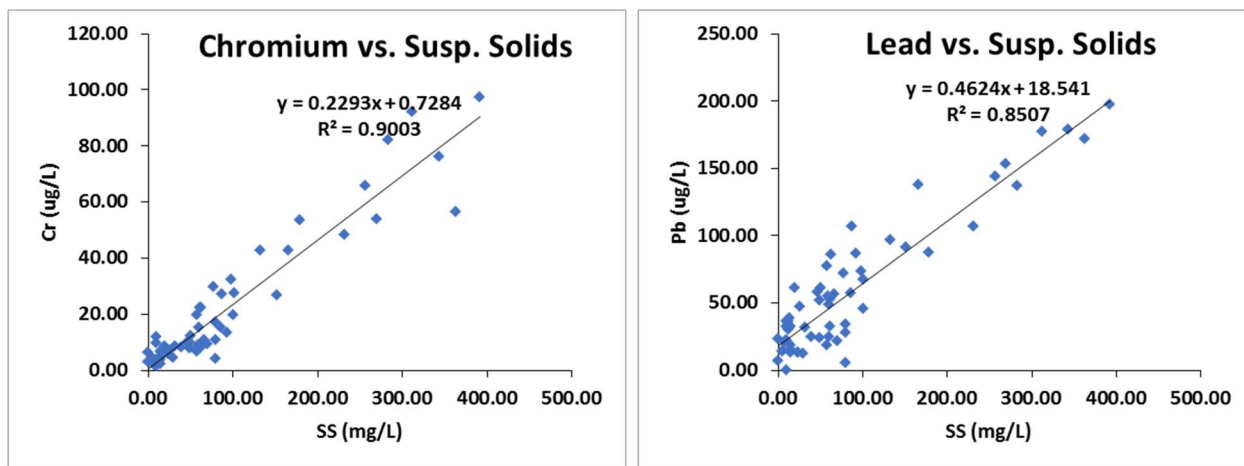


Figure 4-25. Correlation between metal concentration (Cr and Pb) and SS in runoff water for the five storms.

Lastly, the expectation of an exponential decay concentration-time curve (i.e., that the highest concentration samples will occur first, with declining concentrations at later time points) is only observed in some events (e.g., in SMP D for the events on October 28, 2016, February 7, 2017, and to a lesser extent January 20, 2017), but is not observed in other events (e.g., most SMP C profiles).

### *Subsurface Water Quality*

#### Conductivity

In SMP D and G, the conductivity values are fairly consistent and similar, around the 4500-5500  $\mu\text{S}/\text{cm}$  irrespective of depth. By contrast, in A and C a wider range of conductivity



values was observed ranging ~2000 to over 10,000  $\mu\text{S}/\text{cm}$ , and the outlets generally had lower conductivity values than locations closer to the inlet. In SMP C, the shallow lysimeters consistently has higher readings for conductivity than the deep lysimeters, while in SMP A, there were no consistent depth-based trends. A transverse transect, installed in the middle of SMP C, displayed that side lysimeters have lower conductivity values than do the central lysimeter; to-date, a sample has not been collected from the upstream location in SMP C. All lysimeters displayed fairly consistent conductivity values over the sampling record. Conductivity values for the SMPs are shown in the below figures. Taken together, there are not consistent depth-based trends; however, areas that are likely to receive less flow (along the sides and near to the outlet) appear to have lower conductivity values.

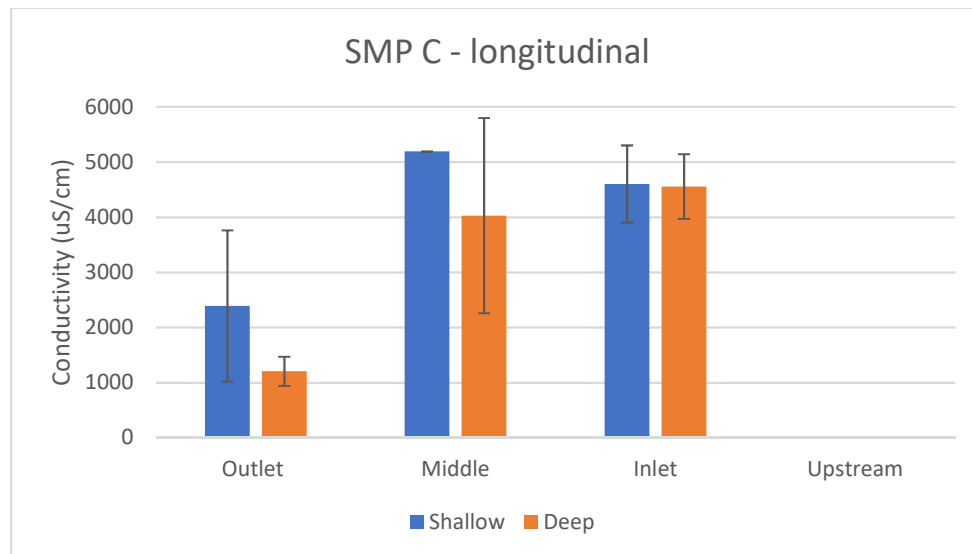


Figure 4-26. Conductivity descriptive statistics for shallow and deep lysimeters in SMP C.

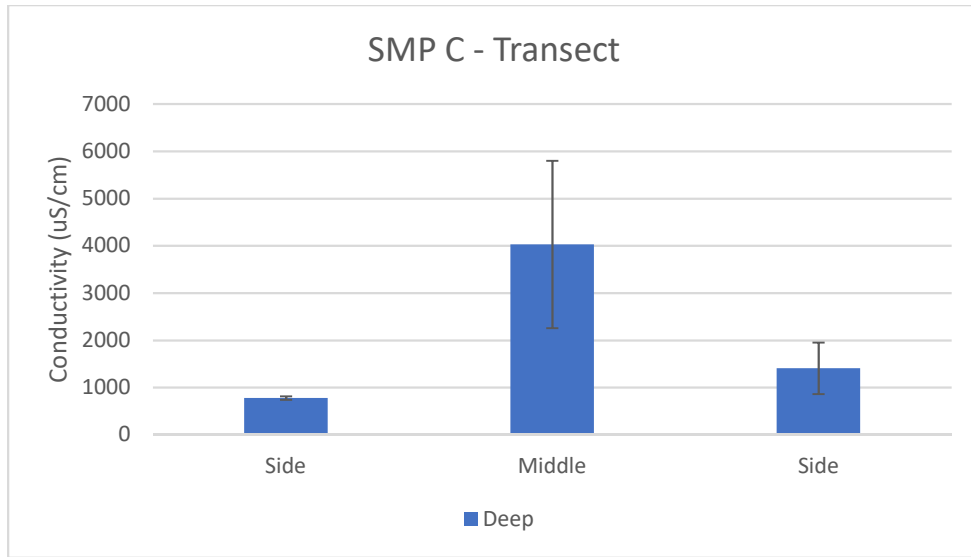


Figure 4-27. Conductivity descriptive statistics for deep lysimeters transect in SMP C.

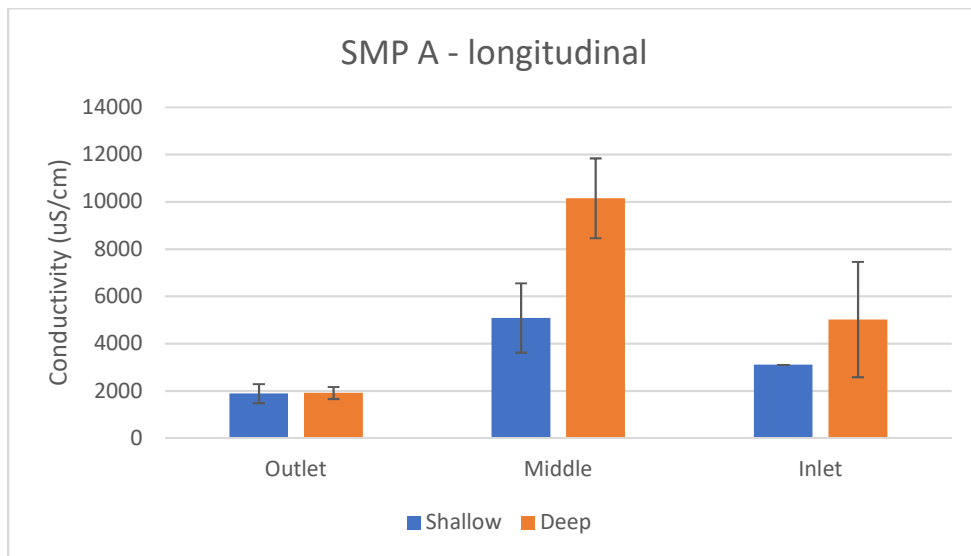


Figure 4-28. Conductivity descriptive statistics for shallow and deep lysimeters in SMP A.

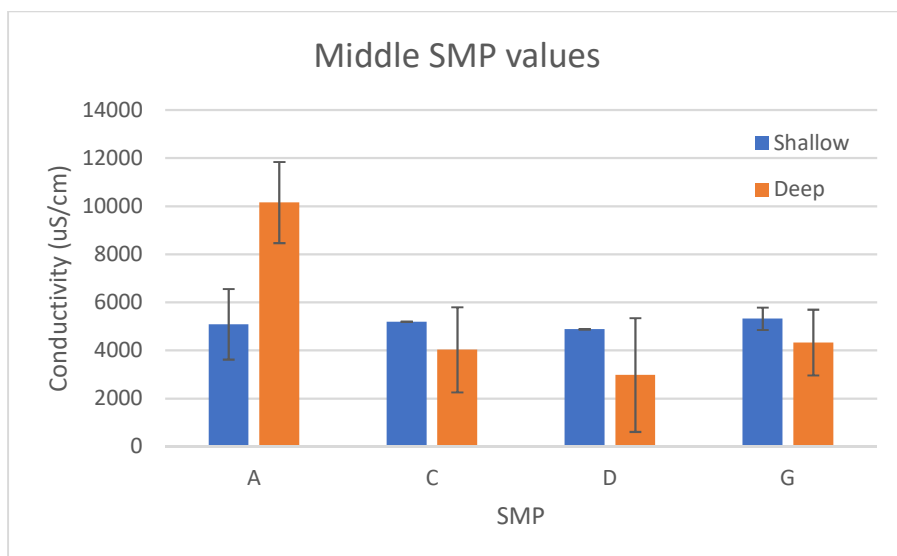


Figure 4-29. Conductivity descriptive statistics for shallow and deep lysimeters located in the middle of each SMP.

## pH

Throughout all four sites, the shallow lysimeters continually had a higher pH than the deep lysimeters. Overall, lysimeter pH ranges from 6.9 to 8.1 and generally the sampled values are relatively consistent for each lysimeter.

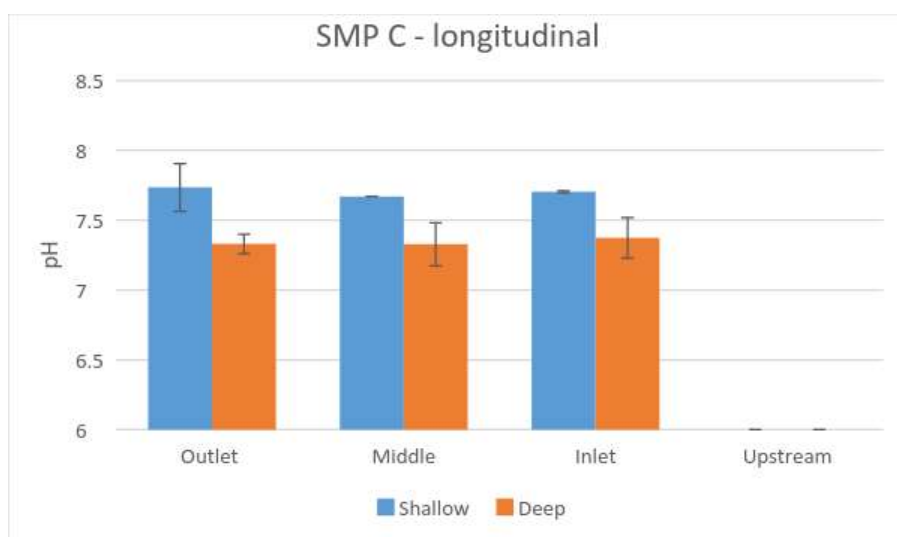


Figure 4-30. pH descriptive statistics for shallow and deep lysimeters in SMP C.

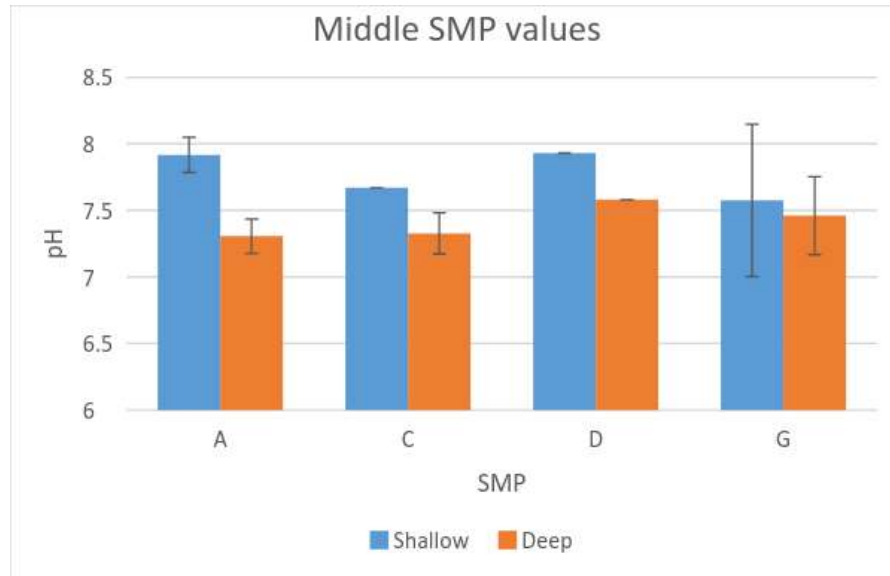


Figure 4-31. pH descriptive statistics for shallow and deep lysimeters in the middle of each SMP.

### Metals

The below discussion is based samples collected in the time since the simulated runoff tests; samples were collected prior to the simulated runoff test; however, they have not yet been analyzed. Select metals – Cd, Cu, and Pb, as well as the cationic Li tracer used in the simulated runoff test – consistently were found at higher concentrations in the shallower lysimeters. Each of these metals has a known transportation-related source, which suggests that these metals are primarily being supplied by the stormwater and are then being transported into the subsurface. The similar Li behavior further supports this hypothesis. Interestingly, among these metals, it was commonly observed the greatest concentrations were observed in the shallow lysimeter closest to the outlet.

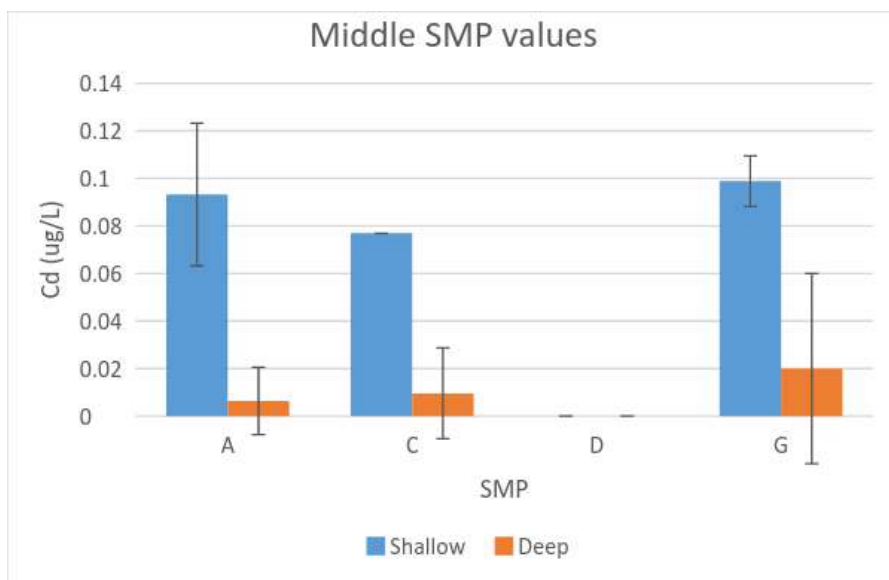


Figure 4-32. Cadmium concentrations in shallow and deep lysimeters located in the middle of each SMP.

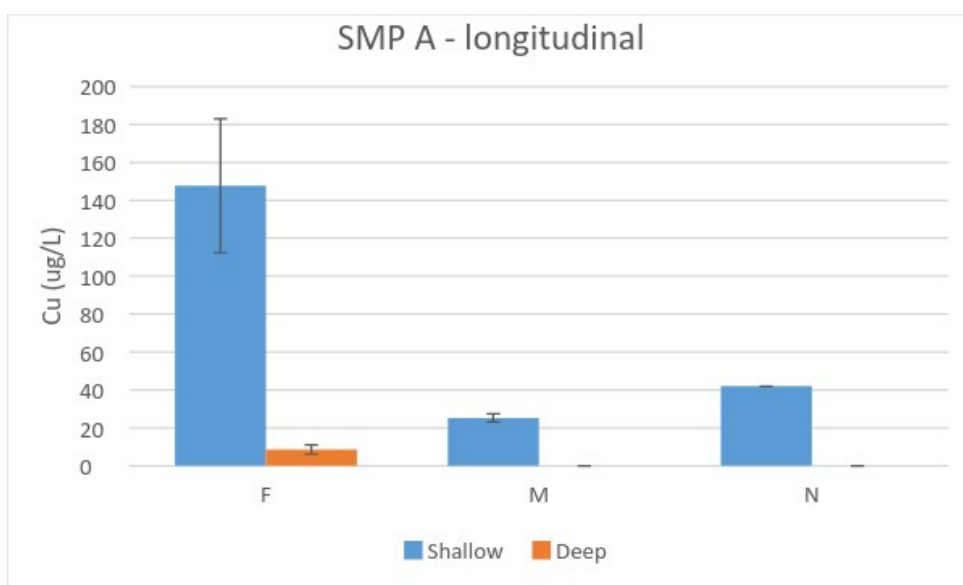


Figure 4-33. Copper concentrations in shallow and deep lysimeters in SMP A.

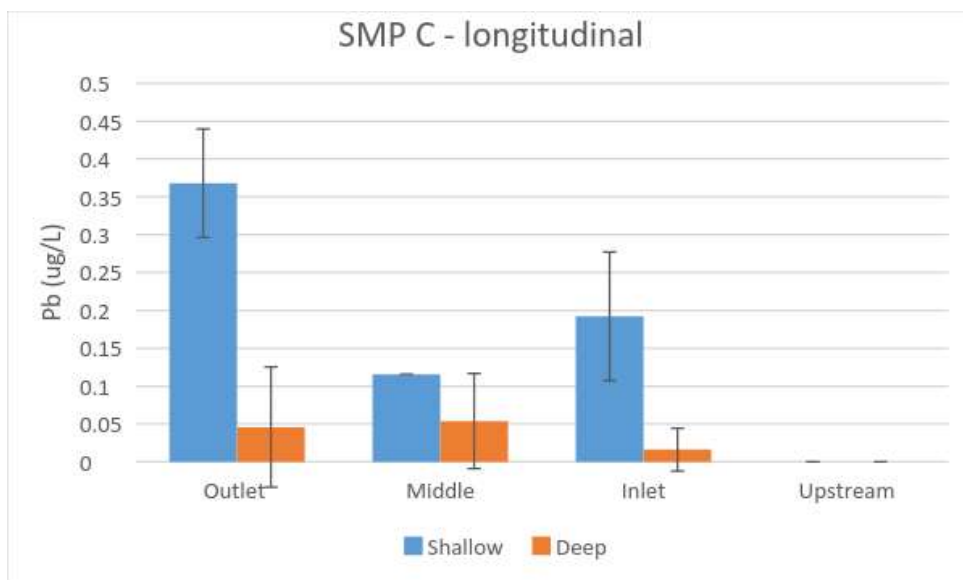


Figure 4-34. Lead concentrations in shallow and deep lysimeters in SMP C.

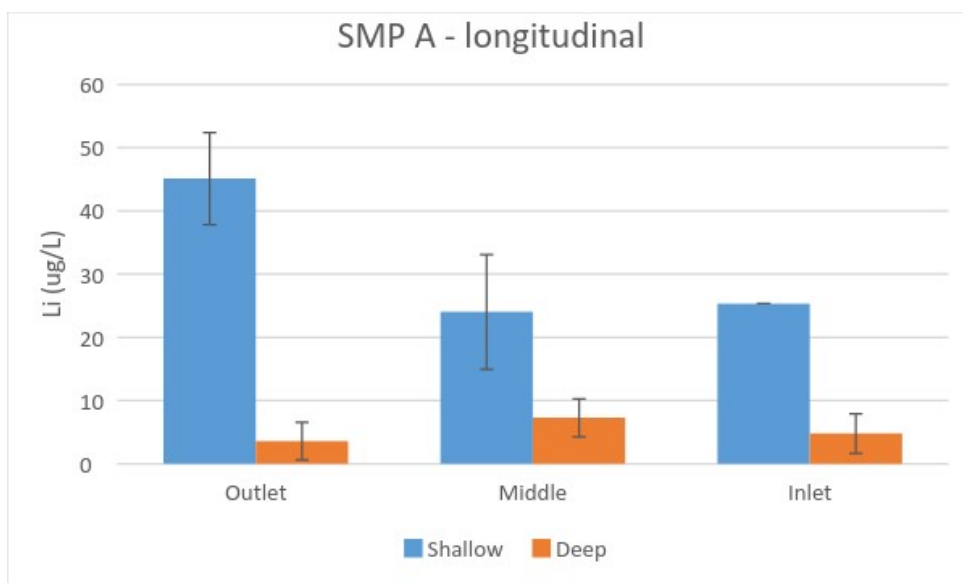


Figure 4-35. Lithium concentrations, included as a cationic tracer in the simulated runoff test, in shallow and deep lysimeters in SMP A.

By contrast, As, Co, and Fe displayed the opposite behavior and generally had greater concentrations observed in the deeper lysimeters (shown in Figure 4-36 for As). It is believed that these metals/metalloids may have originated in the SMP media and currently are being flushed out. A longer duration sampling record will be needed to further assess this hypothesis.

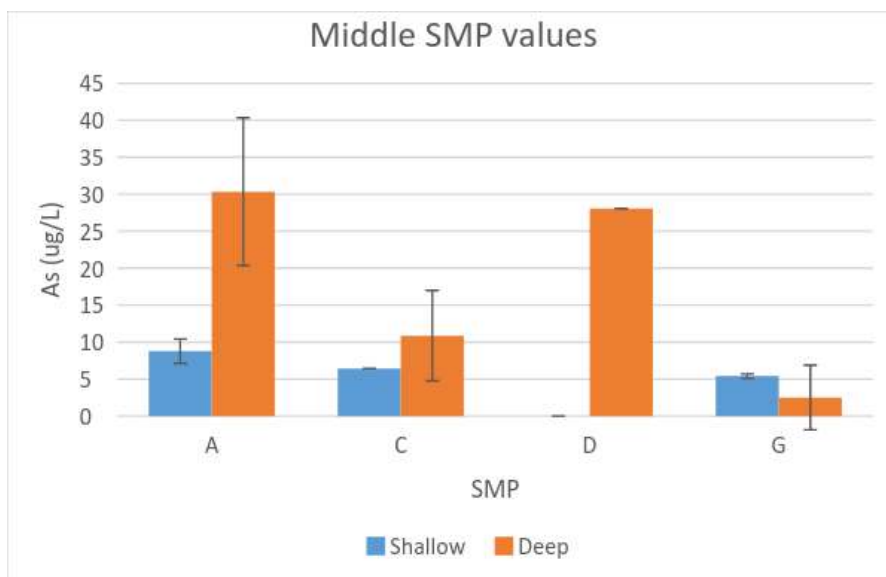


Figure 4-36. Arsenic concentrations in shallow and deep lysimeters in for the middle of each SMP.

#### Baseline Wells Groundwater Metals Concentrations

Table 4-6 shows the both quantitative and estimates of groundwater metals concentrations, including two sampling efforts at the seven wells (presented from south to north); a table excluding estimated concentrations (i.e., quantitative results only) is shown in the appendix. It is worth noting that several elements – Li, S, and Ru – were not observed to produce good calibration curves in any analysis; these elements will be excluded from future analyses. Additionally, Be, Cu, Nb, Ag, Sb, Te, Lu, Hg, and Ta were all below detection limit for all groundwater samples, and are therefore not shown in Table 4-7.

A primary goal of monitoring the groundwater is to assess the effect of water infiltration in the SMP on the underlying groundwater. At present, we do not have enough samples or a long enough sampling record to develop a real understanding of the processes. Table 4-8 shows descriptive statistics, based on the quantitative data and sample estimates, for the focal elements: Cd, Cr, Cd, Ni, Pb, and Zn (Cu was not detected in any groundwater samples).

It is hypothesized that metals that are contained in the highway runoff will accumulate in the SMP media, and be transported down into the underlying groundwater. Therefore, it is hypothesized that the groundwater metals concentrations will increase over time, influenced both by the metals mass loading to the SMP and the metals mobility as influenced by solution chemistry, porous media characteristics, and water infiltration flux. The effects on groundwater quality are presented at the set of 3 monitoring wells that are located up gradient, near, and downgradient of an SMP. For the purposes of this early and preliminary evaluation, elements that were quantitatively observed are shown below. The monitoring wells are as follows: MW 1 (up gradient), MW 2 (near the SMP), and MW 3 (downgradient). The elements were selected based on their comparatively high rates of quantitative results (generally >80% quantitative), though estimated concentrations are included as needed.



Table 4-6. ICP-MS elemental results showing both quantitative results for groundwater monitoring wells from two sampling campaigns; best estimates are parenthetically shown when not all quality assurance requirements were met. “<DL” means that it was below the detection limit

Element*	units	Rep. LOQ	Measurement 1 (Nov 2016)							Measurement 2 (Feb/Apr 2017)						
			MW7	MW1	MW2	MW3	MW4	MW6	MW5	MW7	MW1	MW2	MW3	MW4	MW6	MW5
B	µg/L	30	105	31	( 37 )	( 26 )	<DL	93	32	( 100 )	( 35 )	( 33 )	( 24 )	<DL	119	126
Al	µg/L	3	( 333 )	( 3620 )	( 85.6 )	( 32.1 )	( 36.1 )	( 6.9 )	( 18.2 )	( 32.2 )	182.6	17.4	14.1	18.7	32	( 53 )
Ti	µg/L	3								( 1.0 )	( 5.9 )	<DL	<DL	( 1.2 )	( 2.5 )	( 1.0 )
V	µg/L	0.3	1.32	4.4	( 1.19 )	( 0.71 )	<DL	( 0.19 )	( 0.16 )	<DL	( 0.56 )	<DL	( 0.49 )	( 0.21 )	0.23	( 2.52 )
Cr	µg/L	3	<DL	( 4.6 )	<DL	<DL	<DL	<DL	<DL	<DL	<DL	<DL	<DL	<DL	<DL	<DL
Mn	µg/L	1	160.1	118.4	( 550 )	248.8	( 660 )	773.6	154.2	( 1.9 )	163.8	323	268.7	547.4	1280	( 180.9 )
Fe	µg/L	10	137	5990	( 449 )	17	( 178 )	1190	50	<DL	1520	216	<DL	17200	5280	212
Co	µg/L	1	1.3	162	( 17.1 )	14.4	( 8.2 )	0.2	0.7	( 0.3 )	125.7	9.7	13.6	4.5	0.2	1.3
Ni	µg/L	0.1	1.68	131	( 12.5 )	7.91	( 15.5 )	<DL	( 2.1 )	<DL	98.8	<DL	<DL	<DL	<DL	13.7
Zn	µg/L	3	3.2	823	<DL	37.5	( 40.9 )	<DL	( 4.1 )	<DL	<DL	<DL	<DL	<DL	( 1.3 )	<DL
Ga	µg/L	0.3	( 0.11 )	( 0.88 )	( 0.06 )	( 0.03 )	<DL	<DL	<DL	<DL	( 0.09 )	( 0.06 )	( 0.04 )	<DL	<DL	<DL
Ge	µg/L	1								<DL	<DL	<DL	<DL	( 0.11 )	( 0.07 )	<DL
As	µg/L	0.3	( 0.29 )	44.68	( 0.11 )	0.5	( 0.25 )	0.53	0.74	<DL	20.05	( 0.09 )	( 0.15 )	( 2.89 )	1.65	( 0.38 )
Se	µg/L	0.3	( 1.70 )	<DL	( 10.06 )	( 1.98 )	( 0.54 )	( 0.45 )	( 3.75 )	( 1.92 )	( 0.47 )	<DL	<DL	<DL	<DL	( 3.43 )
Rb	µg/L	0.1	9.85	10.19	( 34.78 )	21.47	( 4.17 )	12.83	12.72	( 7.34 )	6.24	18.51	15.52	( 2.52 )	10.31	( 5.39 )
Sr	µg/L	3	390	207	( 563 )	168	( 337 )	442	122	( 385 )	220	275	148.9	259.9	516	( 136.1 )
Zr	µg/L	1								( 0.02 )	( 0.3 )	<DL	<DL	( 0.02 )	( 0.08 )	( 0.26 )
Mo	µg/L	0.3								<DL	<DL	<DL	<DL	<DL	0.5	1.14
Pd	µg/L	30								<DL	<DL	<DL	<DL	<DL	( 324 )	( 68 )
Cd	µg/L	0.1	( 0.03 )	( 2.95 )	( 0.22 )	( 1.22 )	( 0.03 )	<DL	<DL	<DL	( 4.67 )	( 1.29 )	( 0.87 )	<DL	<DL	<DL
Sn	µg/L	1								( 0.1 )	<DL	<DL	<DL	<DL	<DL	<DL
Cs	µg/L	0.03	0.08	0.282	( 0.183 )	( 0.269 )	( 0.016 )	0.035	( 0.327 )	( 0.011 )	( 0.035 )	( 0.078 )	( 0.081 )	<DL	( 0.031 )	( 0.022 )
Ba	µg/L	0.3	120.1	42.57	( 111 )	26.77	( 68 )	57.39	24.29	( 123 )	33.95	50.23	25.79	84.41	93.44	( 47.9 )
La	µg/L	0.01	0.225	1.598	( 1.097 )	0.908	( 0.044 )	0.016	( 0.029 )	( 0.076 )	0.793	0.815	0.932	( 0.082 )	0.039	( 0.105 )
Ce	µg/L	0.03	0.482	3.213	( 2.194 )	1.362	( 0.118 )	0.034	0.058	( 0.104 )	1.676	2.211	1.5	0.227	0.08	( 0.624 )
Pr	µg/L	0.03	0.085	0.416	( 0.283 )	0.181	( 0.011 )	( 0.004 )	( 0.004 )	( 0.017 )	( 0.199 )	( 0.341 )	( 0.188 )	( 0.025 )	0.011	( 0.047 )
Nd	µg/L	0.03	0.274	1.817	( 1.141 )	( 0.763 )	( 0.055 )	( 0.025 )	( 0.022 )	( 0.073 )	0.802	1.472	0.818	0.12	0.045	( 0.239 )
Sm	µg/L	0.3	0.05	0.38	( 0.25 )	( 0.19 )	( 0.01 )	( 0.01 )	( 0.01 )	( 0.02 )	( 0.22 )	( 0.34 )	( 0.18 )	( 0.04 )	( 0.01 )	( 0.06 )
Eu	µg/L	0.01	0.021	0.085	( 0.061 )	0.037	( 0.005 )	( 0.003 )	( 0.003 )	( 0.078 )	( 0.063 )	0.122	( 0.055 )	( 0.054 )	0.045	( 0.04 )
Gd	µg/L	0.1	( 0.07 )	0.36	( 0.35 )	( 0.22 )	( 0.02 )	<DL	<DL	( 0.02 )	( 0.23 )	( 0.49 )	( 0.29 )	( 0.05 )	( 0.03 )	( 0.08 )
Dy	µg/L	0.1	( 0.05 )	0.29	( 0.27 )	0.17	( 0.02 )	<DL	( 0.004 )	( 0.014 )	( 0.15 )	( 0.40 )	( 0.18 )	( 0.03 )	( 0.01 )	( 0.06 )
Er	µg/L	0.03	( 0.024 )	0.161	( 0.127 )	( 0.095 )	<DL	<DL	<DL	<DL	( 0.089 )	( 0.148 )	( 0.103 )	( 0.015 )	<DL	( 0.03 )
Tm	µg/L	0.01	<DL	0.015	( 0.016 )	( 0.01 )	<DL	<DL	<DL	<DL	( 0.006 )	( 0.017 )	( 0.006 )	<DL	<DL	<DL
Yb	µg/L	0.03	( 0.028 )	0.153	( 0.117 )	0.08	( 0.006 )	<DL	( 0.007 )	<DL	( 0.071 )	( 0.136 )	( 0.088 )	( 0.016 )	( 0.008 )	( 0.041 )
W	µg/L	0.3								( 1.64 )	<DL	<DL	<DL	( 0.42 )	0.29	( 17.1 )
Tl	µg/L	0.03	0.03	0.07	( 0.186 )	0.113	( 0.007 )	<DL	<DL	<DL	( 0.088 )	( 0.345 )	( 0.104 )	<DL	<DL	( 0.014 )
Pb	µg/L	0.03	0.216	1.433	( 0.235 )	0.123	( 0.199 )	0.161	0.464	<DL	0.458	<DL	<DL	<DL	0.118	( 0.846 )
Th	µg/L	1	<DL	( 0.7 )	<DL	<DL	<DL	<DL	<DL	<DL	( 0.1 )	<DL	<DL	( 0.1 )	<DL	<DL
U	µg/L	0.01	1.83	0.21	( 0.133 )	( 0.104 )	( 0.011 )	0.028	0.111	( 1.078 )	( 0.085 )	( 0.176 )	( 0.096 )	<DL	0.254	0.841
Na	mg/L	1	188.4	39.7	( 125 )	47.6	( 30 )	51.3	66.3	<DL	<DL	<DL	<DL	<DL	52.3	( 153 )
Mg	mg/L	0.1	58.38	20.09	( 46.17 )	16.46	( 8.75 )	26.05	10.44	<DL	20.41	23.25	<DL	6.06	39.84	( 25.21 )
Si	mg/L	0.03								<DL	4.318	3.868	<DL	3.169	8.1	<DL
P	mg/L	1								<DL	1.3	<DL	<DL	( 0.51 )	<DL	<DL
K	mg/L	3	10.5	2.9	( 9.9 )	9.4	( 3.1 )	10.1	5.9	( 11.8 )	3.1	7.9	9.1	2.4	<DL	<DL
Ca	mg/L	1	100.3	27.3	( 79.4 )	25	( 15.6 )	107.6	41.3	<DL	<DL	<DL	<DL	<DL	<DL	<DL

\* The following elements were analyzed but either were not detected in any groundwater samples: Be, Cu, Nb, Ag, Sb, Te, Lu, Hf, and Ta

Table 4-7. Descriptive statistics based on estimated concentrations for Cd, Cr, Ni, Pb, and Zn based on seven monitoring wells and two samples each (n=14)

Element	%ND	%Quant	Typical LOQ	Estimated concentrations (µg/L)	
				Average	Stdev
Cd	43%	0%	0.1	0.80	1.40
Cr	93%	0%	3	0.31	1.16
Ni	43%	36%	0.1	20.2	41.0
Pb	29%	50%	0.03	0.30	0.40
Zn	57%	21%	3	65	219

Two distinct trends are clear from Figure 4-34: MW 2 generally has the highest concentration, and the November 2016 concentrations are generally higher than that February

2017 samples. MW 2, which located immediately adjacent to the SMP, contains elevated concentrations compared to either the up-gradients or down-gradient sampling locations (MW 1 and MW 3, respectively); it should be noted that each of these wells shows evidence of tidal influence based on preliminary water level data. Notes from the well installation bore log indicate the following: MW 1: silty sand with clay; MW 2: silty fine sand and clayey sand; MW 3: silty fine sand. The elevated MW 2 concentrations may be due to infiltrating stormwater or other sources (e.g., legacy contaminants). For most of the presented elements, February 2017 values are less than those observed in November 2016, which may reflect well development and purging activities.

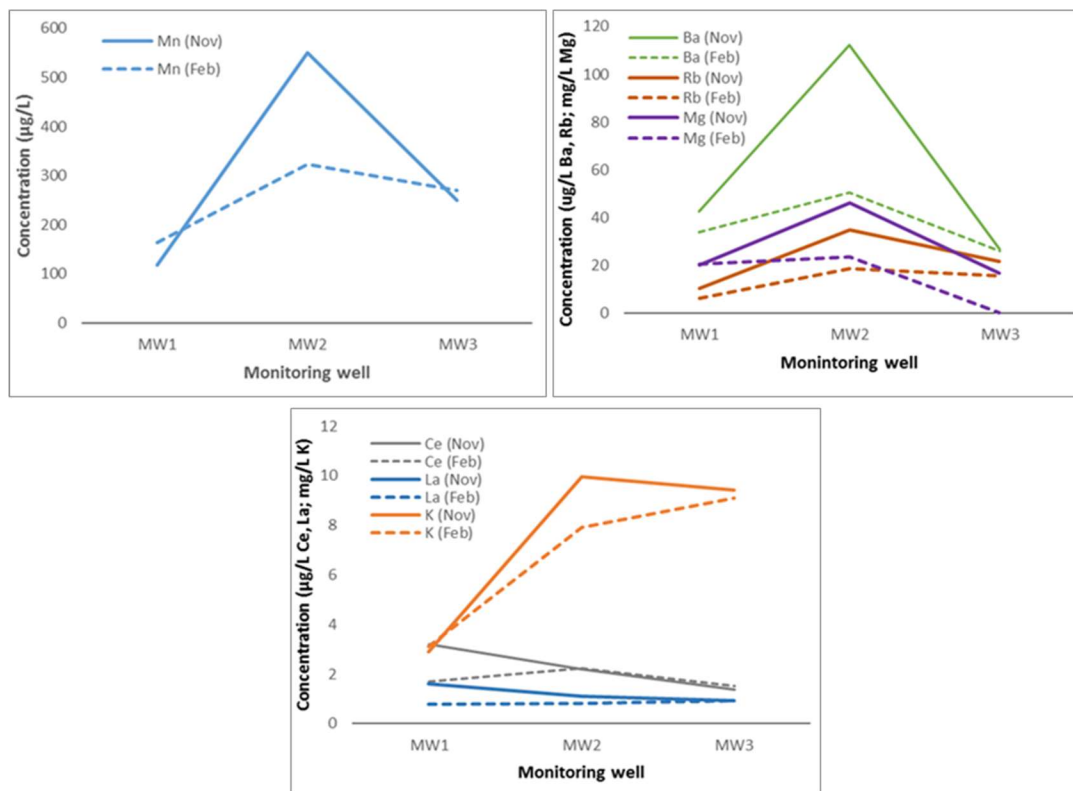


Figure 4-37. Concentrations of select elements for MW 1, MW 2, and MW 3 for the two sampling efforts. Note that the y-axis units depend on the element.

To formulate an approach to understanding SMP infiltration on groundwater quality, it is important to understand the initial similarities and differences. Table 4-8 show descriptive statistics for groundwater and SMP influent samples for the assessed elements. There are many elements that display noteworthy differences in stormwater and groundwater concentrations. For example, there are a few elements that are well quantified in both matrices and are substantially elevated in groundwater: Co, As, and Fe. However, there are several other elements that are also well quantified, but are substantially elevated in stormwater: Rb, Sr, Mo, Ba, La, Ce, Eu, Pb, Na, and K. In the future, these differences may be employed in a mixing model to determine the contributions of groundwater and infiltrating stormwater and evaluate the long-term impacts on groundwater quality.

Table 4-8. Descriptive statistics for stormwater and groundwater samples based on element quantitative concentrations

Element	unit	Groundwater samples				SMP Influent samples			
		n	% Quant	Ave	Stddev	n	% Quant	Ave	Stddev
B	µg/L	14	43%	42.79	1.97	71	20%	20.15	3.38
Al	µg/L	14	36%	72.77	0.73	71	75%	1638	1
Ti	µg/L	7	0%			59	78%	86.42	0.66
V	µg/L	14	21%	2.16	0.92	71	90%	4.87	1.17
Cr	µg/L	14	0%			71	68%	46.66	0.65
Mn	µg/L	14	71%	370.0	1.1	71	90%	50.65	0.80
Co	µg/L	14	79%	56.98	0.53	71	90%	1.55	0.89
Ni	µg/L	14	36%	59.96	0.84	71	28%	7.60	0.82
Cu	µg/L	14	0%			71	86%	45.10	1.23
Zn	µg/L	14	21%	463.9	0.6	71	46%	354.3	0.9
Ga	µg/L	14	0%			71	44%	0.68	1.39
As	µg/L	14	43%	18.05	0.63	71	85%	3.28	0.77
Se	µg/L	14	0%			71	6%	0.28	2.36
Rb	µg/L	14	64%	4.73	2.76	71	90%	26.36	0.96
Sr	µg/L	14	71%	132.7	2.1	71	90%	656.9	1.0
Zr	µg/L	7	0%			59	56%	2.78	0.82
Nb	µg/L	7	0%			59	34%	0.14	0.93
Mo	µg/L	7	29%	0.45	1.82	59	88%	5.63	1.51
Pd	µg/L	7	0%			59	19%	616.0	1.1
Ag	µg/L	14	0%			71	4%	0.04	8.21
Cd	µg/L	14	0%			71	30%	0.34	1.02
Sn	µg/L	7	0%			59	51%	2.93	1.13
Cs	µg/L	14	21%	0.13	1.01	71	75%	0.46	0.90
Ba	µg/L	14	71%	32.99	1.69	71	90%	75.38	1.12
La	µg/L	14	57%	0.54	1.23	71	89%	1.66	0.79
Ce	µg/L	14	71%	1.09	1.00	71	89%	2.93	0.76
Pr	µg/L	14	29%	0.18	0.98	71	70%	0.36	0.73
Nd	µg/L	14	50%	0.68	1.12	71	90%	1.34	0.74
Sm	µg/L	14	14%	0.23	0.94	71	24%	0.38	1.08
Eu	µg/L	14	36%	0.04	1.51	71	59%	0.11	0.85
Gd	µg/L	14	7%			71	30%	0.40	1.07
Dy	µg/L	14	14%	0.08	2.69	71	51%	0.25	0.84
Er	µg/L	14	7%			71	49%	0.13	0.78
Tm	µg/L	14	7%			71	14%	0.02	1.70
Yb	µg/L	14	14%	0.05	2.26	71	46%	0.11	0.83
W	µg/L	7	14%			59	71%	2.24	0.99
Tl	µg/L	14	21%	0.04	1.71	71	11%	0.01	2.04
Pb	µg/L	14	50%	0.47	0.89	71	90%	22.59	0.86
Th	µg/L	14	0%			71	3%	0.05	2.23
U	µg/L	14	43%	0.69	0.79	71	76%	0.21	1.44
Na	mg/L	14	43%	56.56	0.00	71	76%	1340	0
Mg	mg/L	14	64%	15.91	0.00	71	93%	7.55	0.00
Si	mg/L	7	57%	2.21	0.00	59	56%	1.63	0.00
P	mg/L	7	14%			59	3%	0.18	0.00
K	mg/L	14	64%	3.30	0.00	71	59%	101.6	0.0
Ca	mg/L	14	36%	40.41	0.00	71	45%	99.94	0.00
Fe	mg/L	14	71%	5.39	0.00	71	93%	2.26	0.00

Lead isotopic ratios may be another approach to understanding contaminant mobility and its effects on groundwater quality. Lead exists as four major isotopes:  $^{204}\text{Pb}$ ,  $^{206}\text{Pb}$ ,  $^{207}\text{Pb}$ , and  $^{208}\text{Pb}$ . In the current study, we are monitoring the later three;  $^{204}\text{Pb}$  has an isobaric interference with  $^{204}\text{Hg}$  so was not included. Previous studies have employed lead isotopes as a metric for source apportionment in the environment (e.g., Flegal et al., 2005). In the current study, there are only six well samples with quantitative Pb values for all three isotopes. As Figure 45 shows, the isotopic ratios for the stormwater are reasonably consistent which may suggest a common source (e.g., Pb in the road environment as a legacy of the leaded gasoline era). By contrast, the groundwater samples have highly variable isotopic ratios, which may be indicative of different Pb source(s). A mixing model based on Pb isotopes could also be developed to understand Pb transport into the subsurface. As more data are collected, these relationships will be further explored.

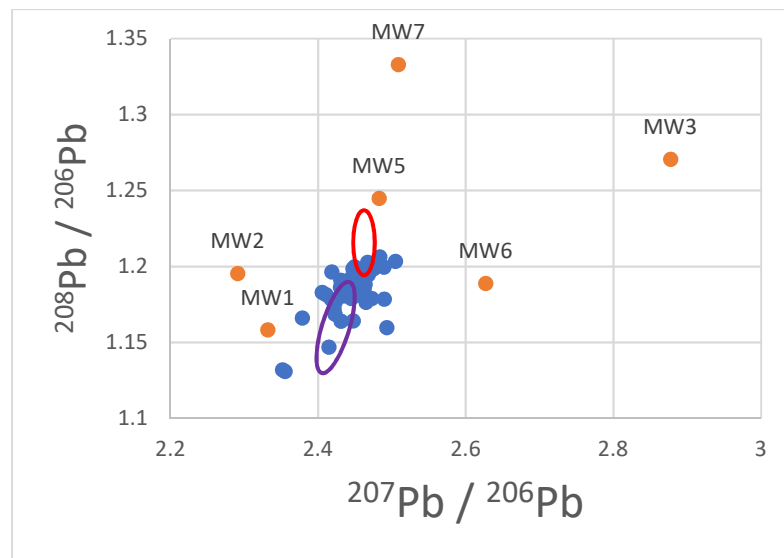
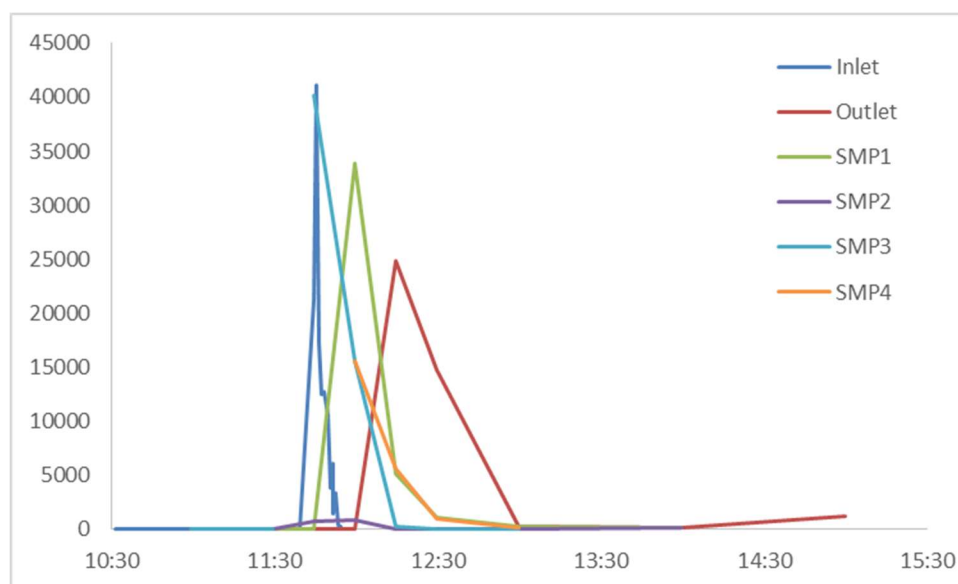


Figure 4-38. Lead isotopic ratios for stormwater (blue) and groundwater (orange samples - monitoring well labeled). The red circle is the approximate 1980's leaded gasoline isotopic ratio, and the purple circle is the 1960-70's leaded gasoline signature (approximated from Flegal et al. 2005).

### *Simulated Runoff Tests (SRTs)*

The figures below show the profile of fluorescein concentration in SMPs C and G during the SRTs conducted in June 2017. As expected, we can clearly see dispersion and dilution effects as the tracer moves from the inlet to the outlet of the SMPs.



*Figure 4-39. Profile of fluorescein concentration in SMP C presented in arbitrary units. Samples were collected at different location in the basin: Inlet, SMP1 (in front of inlet), SMP2 (at mid-distance between inlet and outfall), SMP3 (upstream the inlet), SMP4 (upstream the inlet), and outfall.*

Analysis of contaminants in various locations in the SMP C and G during the SRTs revealed generally very low concentrations, indicating low remobilization of contaminants from the SMP basin (Figure 4-40). SS were not detected. Generally speaking, average concentration in nutrients were below 2.5 mg/L with low variability, average concentration of COD and TS were 14.6 +/- 12.2 and 22.2 +/- 17.4 mg/L, pH was near neutrality, DO was near saturation, average turbidity was 9.2 +/- 15.6 NTU, and average conductivity was 339 +/- 19  $\mu$ S/cm.

The relatively low concentrations measured in the SMPs during the SRT shows a low risk of contaminant mobilization from particles due to high flow quantities in most cases. The one exception would be levels of total phosphorus, which reached a maximum of 0.92 mg/L during the test in SMP C. This concentration is about 40% of the value listed for the EPA's Aquatic Life Criteria (2.4 mg/L). Thus, phosphorus mobilization may be of interest for sensitive receiving bodies.

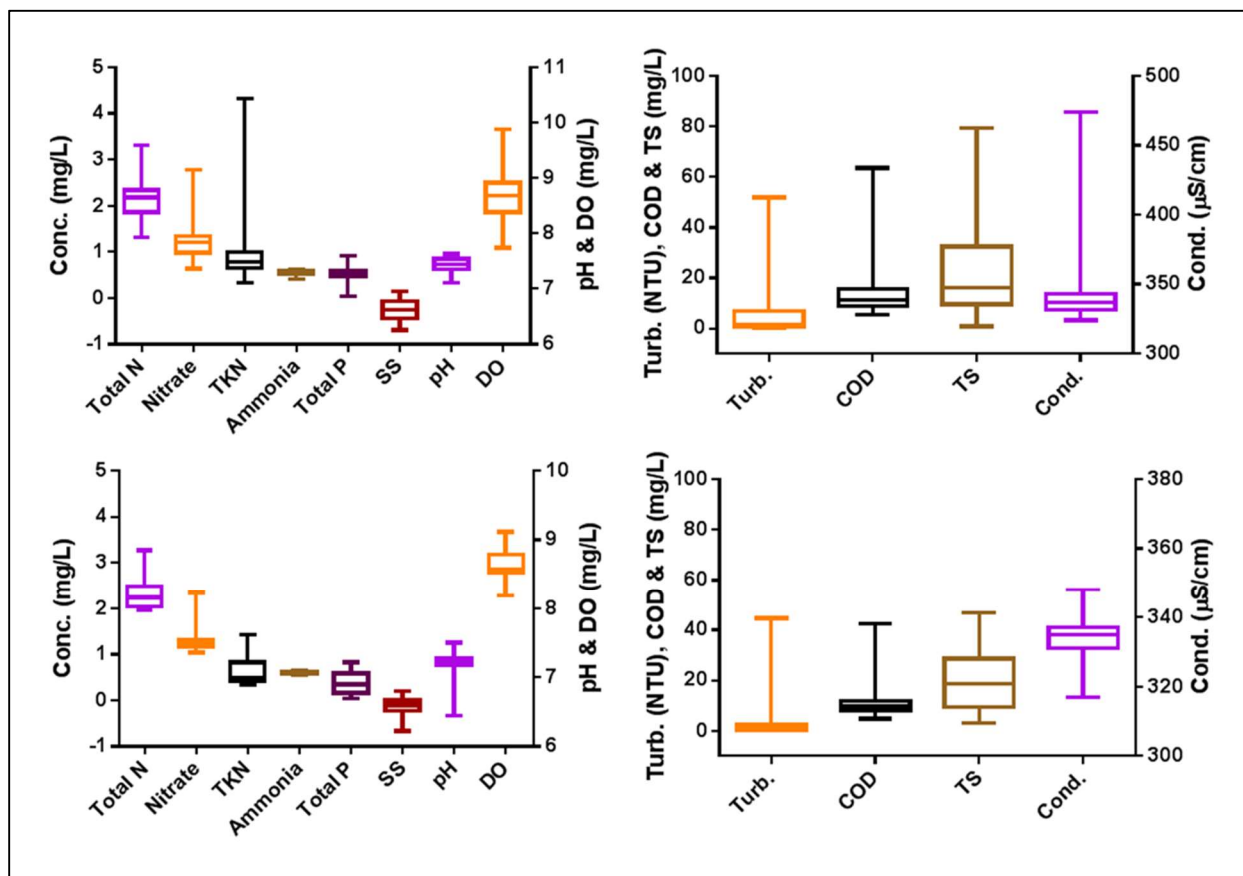


Figure 4-40. Water quality measured in SMPs during the SRTs conducted in June 2017. Upper panels: SMP C. Lower panels: SMP G. For each parameter, the box shows the median and standard deviation, and the bar shows the minimum and maximum values.

Metals were also analyzed in SRT influent water (municipal water) and in the ponded water, where ponded water samples were analyzed for total and dissolved metals. Total metals were analyzed as collected and dissolved metals, an operational definition, were syringe-filtered



in the field (0.45 um nominal pore size) to exclude particles. Influent, total, and dissolved metal descriptive statistics are shown in Table 4-9 for the high priority elements. Generally, many low concentrations were observed in both the municipal influent water and in the ponded SMP water, resulting in non-detectable concentrations, or detectable concentrations that were below the limit of quantification (shown as unbolded values in Table 4-10); descriptive statistics based on quantitative results are shown in bold. Among the priority elements, concentrations were generally low and were similar between influent and ponded SMP water for both total and dissolved samples. The low dissolved concentrations, which are generally less than the influent water, suggest that the elements of interest are not desorbing from the SMP sediments, and that they may be being removed the SMP components due to sorption. The total element concentrations, are also similar to or less than the influent concentrations; taken together with the low suspended solid concentrations observed during the SRT, this suggests that SMP sediments and the associated metals are not being resuspended during higher flow events.

*Table 4-9. Descriptive statistics for simulated runoff test high priority elements in the influent and SMP ponded water (total and dissolved; 0.45 um filtrate). Bold values are based on quantitative results, while non-bolded indicate a best estimate.*

	Concentration (ug/L)								
	Influent			SMP - total			SMP - dissolved		
	Av		Stdev	Av		Stdev	Av		Stdev
<b>As</b>	<DL			0.10		0.15	0.06		0.08
<b>Cd</b>	0.02		0.02	0.02		0.02	0.02		0.02
<b>Co</b>	<DL			0.05		0.06	<DL		
<b>Cu</b>	<DL			<DL			<DL		
<b>Fe</b>	187.78		86.69	88.00		74.57	0.96		2.05
<b>Ni</b>	<b>2.07</b>		<b>0.14</b>	<b>1.83</b>		<b>0.20</b>	<b>1.63</b>		<b>0.21</b>
<b>Pb</b>	0.18		0.22	<b>1.00</b>		<b>0.62</b>	0.02		0.03
<b>Zn</b>	<b>139.42</b>		<b>3.04</b>	<b>110.85</b>		<b>14.18</b>	<b>101.69</b>		<b>16.68</b>

### *Contaminant Loads*

The table below shows the contaminants loads in the SMPs during the monitored storms.



The loads were estimated using flow data collected on-site and by using the rainfall to drainage area relationship for the SMP. Rainfall data was taken from the nearest weather station (KPNE). Drainage areas were taken from the PennDOT plans or from the LiDAR measurements of the highway. The LiDAR measurement was approximately five times smaller than the planned drainage area for SMP C and approximately two times smaller for SMP D.

This data can be useful by estimating what the contaminant loading would be over the course of an entire year. The total rainfall over the 8 storms monitored is 101.9 mm, which represents approximately 10% of the average total annual rainfall for Philadelphia (1.05 m). Thus, the loads estimated are about 10% of what the SMPs could be exposed to in a year. Taking into account the surface area of the SMPs, this would be 60-62 g/m<sup>2</sup>-yr of SS, 0.75-1.2 g/m<sup>2</sup>-yr of nitrate and 0.2-0.3 g/m<sup>2</sup>-yr of total phosphorus.

In looking at the estimated annual loads, the mass of nitrate or phosphorus is not deemed significant in terms of benefiting the plants in the SMP. However, the plants should be capable of utilizing the nutrients if they remain in the soil for a long enough time. Metals will most likely remain trapped in the subsurface since no outflow has been observed from the basins during the monitored storms. The SS load may be the most telling, as a buildup of solids over time can be detrimental. Infiltration rates can be reduced as the media becomes clogged, causing ponding to occur earlier in the basin. Laboratory and field tests conducted with similar SS loading rates concluded that significant clogging of media could occur within 2 years, but that presence of significant vegetation can extend this by loosening the soil media and promoting infiltration.

Table 4-10. Loads of selected contaminants during the monitored storms.

Storm						Contaminant						
							Load (g) - SMP C			Load (g) - SMP D		
	Total intensity (mm)	Duration (h)	Intensity (mm/h)	Intensity during sampling (mm/h)	Dry period (d)			PennDOT				
							LiDAR (a)	(b)	VU (c)	LiDAR	PennDOT	VU
27-Oct	10.9	11	0.99	0.51	5							
						SS	84	449		42	92	
						Nitrate	3.7	20		2.1	4.6	
						Total P	0.13	0.69		0.10	0.21	
						Copper	0.07	0.35		0.02	0.05	
						Lead	0.03	0.14		0.01	0.02	
						Iron	1.0	5.3		0.38	0.83	
30-Nov	26.2	14	1.9	2.2	0.5							
						SS	198	1061		118	262	
						Nitrate	4.0	21		1.1	2.4	
						Total P						
						Copper	0.13	0.72		0.03	0.06	
						Lead	0.05	0.27		0.02	0.04	
						Iron	4.3	23		1.3	2.8	
20-Jan	2.8	3	0.94	0.76	2.5							
						SS	172	922		39	87	
						Nitrate	2.2	12		0.93	2.06	
						Total P	0.44	2.3		0.18	0.29	
						Copper	0.12	0.65		0.014	0.031	
						Lead	0.05	0.28		0.006	0.014	
						Iron	3.2	17.1		0.37	0.83	
7-Feb	5.8	2	2.9	2.9	12							
						SS	442	2371		151	334	0.11
						Nitrate	15	81		4.9	10.8	0.01
						Total P	0.95	5.1		1.7	2.8	0.001
						Copper	0.39	2		0.15	0.34	0.0003
						Lead	0.09	0.50		0.03	0.06	0.00003
						Iron	3.7	20		1.0	2.2	0.001
27-Mar	3.3	5	0.66	1	2							
						SS	526	2819	15	260	574	16
						Nitrate	6.1	32	0.32	2.2	4.9	0.30
						Total P	1.7	9.2	0.07	0.91	1.50	0.07
						Copper	0.35	1.9	0.01	0.13	0.29	0.01
						Lead	0.13	0.71	0.004	0.08	0.17	0.01
						Iron	17	89	0.47	9.5	21.0	0.62
6-Apr	26.7	14	1.9	0.18	2							
						SS	20	106	4.6	6.2	13.6	5.1
						Nitrate	0.92	4.9	0.23	0.44	0.96	0.41
						Total P	0.05	0.25	0.01	0.04	0.06	0.02
						Copper	0.02	0.09	0.004	0.005	0.012	0.005
						Lead	0.004	0.02	0.001	0.002	0.004	0.001
						Iron	0.36	1.9	0.09	0.14	0.32	0.14

Storm						Contaminant						
							Load (g) - SMP C			Load (g) - SMP D		
	Total intensity (mm)	Duration (h)	Intensity (mm/h)	Intensity during sampling (mm/h)	Dry period (d)			PennDOT LiDAR (a) (b)	VU (c)	LiDAR	PennDOT	VU
22-May	8.1	11	0.74	2.3	2							
						SS	229	1229	116	28	61	3.6
						Nitrate	4.7	25	4	1.2	2.6	0.15
						Total P	0.60	3.2	0.37	0.41	0.67	0.02
						Copper	0.18	0.99	0.11	0.05	0.11	0.004
						Lead	0.04	0.23	0.02	0.02	0.05	0.001
						Iron	4.5	24	2.2	1.7	3.7	0.08
29-Aug	18	12	1.5	1.2	6							
						SS	739	3964		615	1360	
						Nitrate						
						Total P						
						Copper	0.20	1.0		0.08	0.19	
						Lead	0.12	0.65		0.09	0.19	
						Iron	10	54		5.5	12	

(a) Load calculated based on drainage surfaces calculated using LiDAR technique (936 m<sup>2</sup> for SMP C and 696 m<sup>2</sup> for SMP D as reported in Chapter 5)

(b) Load calculated based on designed drainages surfaces (5013 m<sup>2</sup> for SMP C and 1538 m<sup>2</sup> for SMP D)

(c) Load calculated based on flow data from Villanova (500 m<sup>2</sup> for SMP C and 40 m<sup>2</sup> for SMP D)

### Quality assurance and quality control

#### General parameters

Quality control for temperature, DO, pH, turbidity, and conductivity was based primarily on the calibration of the instruments. For other parameters, including total nitrogen, nitrate, ammonia, TKN, and total phosphorous, quality control was based on the inclusion of field and laboratory blanks, standards, and replicate analyses. In some cases (total nitrogen – October, TKN, October and November, and phosphorus – November), results from the blanks and/or standards were non-satisfactory. The results for these batches of samples were then removed.

Table 4-11 summarizes the quality control results of the analysis of general water parameters. For SS and TS, the standard deviation (as percent of the mean) between replicates was between 3.5 and 10.6%. For total nitrogen, the standard deviation between replicates ranged from 0.9 to 7.5% and analysis of the standards showed an error of ranging from 1.4 to 7.7%. For

nitrate, the standard deviation between replicates was below 3.1% and the analysis of the standards showed an error of ranging from 0.7 to 12.5%. For ammonia, the standard deviation between replicates was below 3.85% and the analysis of the standards showed an error of ranging from 0.2 to 11.0%. For TKN, the standard deviation between replicates ranged from 2.7 to 10.4% and the analysis of the standards showed an error of ranging from 1.5 to 16%. For total phosphorous, the standard deviation between replicates was below 4.5% and the analysis of the standards showed an error below 5.0%. For COD, the standard deviation between replicates was below 2.2% and the analysis of the standards showed an error below 5.0%.

Quality control analysis showed that two parameters generally more problematic: total nitrogen and TKN. However, the quality of the results improved dramatically for samples collected during later storms, indicating an increased experience of the team in charge of lab experiments (graduate and undergraduate students). No changes in the methods used are proposed at this stage.

*Table 4-11. Summary of quality control results for general water quality parameters*

	SS	TS	Tot N	Nitrate	Ammonia	TKN	Total P	COD
<b>St. Dev. (mg/L)</b>	3.5 - 33.1	14.1 - 33.9	0.02 - 1.30	0.001 - 0.101	0.002 - 0.01	0.061 - 1.4	0.003 - 0.017	0.577 - 1.73
<b>St. Dev. (%)</b>	3.5 - 10.6	5.6 - 7.1	0.91 - 11.5	0.259 - 3.1	2.92E-05 - 3.85	2.66 - 30.1	0.394 - 4.46	0.320 - 2.17
<b>Blank - average (mg/L)</b>	0 - 3.0	0 - 13.0	0.04 - 1.33	0-0.075	0.005 - 0.159	0-0.298	0.005 - 0.038	1.5-1.61
<b>Blank - relative to mean (%)</b>	0 - 3.9	0 - 1.8	0.65 - 53.2	2.57-3.86	0.47 - 69.1	3.08-20.4	2.0 - 26.9	1.4-2.9
<b>Standard - average (mg/L)</b>	N/A	N/A	3.60 - 7.74	5.39 - 6.75	0.891 - 1.02	1.02 - 13.2	0.996 - 1.05	51 - 52.5
<b>Standard - error (%)</b>	N/A	N/A	1.36 - 48.1	0.667 - 12.5	0.15 - 11.0	1.50 - 122	0.376 - 5.00	2.00 - 5.00

## Metals

Metal concentrations were analyzed using an inductively coupled plasma mass spectrometer (ICP-MS; Agilent 7900). At the beginning of each daily use, the ICP-MS underwent a startup tune, to assess consistency in instrument performance. Sample analysis was generally conducted using the Agilent High Matrix Introduction system (HMI; i.e., pneumatic dilution to address elevated dissolved solids) with a gas included in the collision/reaction cell

(CRC). The gas used in the CRC was selected based on published literature and quality assurance practices; for a vast majority of elements, He was used as in the CRC to minimize polyatomic interferences. Prior to analyzing samples, the instrument was tuned to match sample matrix and quantification goals to maximize sensitivity while minimizing polyatomic interferences and doubly charged ions. In most sample analysis batches, the following elements were monitored (mass/charge;  $m/z$ ): Li (7), Be (11), Na (23), Mg (24), Al (27), Si (28), P (31), S (34), K (39), Ca (43, 44), Ti (47), V (51), Cr (52, 53), Mn (55), Fe (56, 57), Ni (58, 60), Co (59), Cu (63, 65), Zn (66, 68), Ga (71), Ge (72), As (75), Se (77, 78, 82), Rb (85), Sr (88), Zr (90), Nb (93), Mo (95, 97, 98), Ru (99, 101), Pd (105), Ag (107, 109), Cd (111), Sn (118), Sb (121, 123), Te (125), Cs (133), Ba (137), La (139), Ce (140), Pr (141), Nd (146), Sm (147), Eu (153), Gd (157), Dy (163), Er (166), Tm (169), Yb (172), Lu (175), Hf (178), Ta (181), W (182), Tl (205), Pb (206, 207, 208), Th (232), U (238). Noteworthy variations may be present within a batch, such that they affect the sample transmission into the quadrupole or the ionization of the sample; to account for variations in matrix (e.g., salts), instrument (e.g., non-steady state salt deposition), and environmental effects (e.g., room temperature and humidity), internal standard elements ( $m/z$ ) were used as follows: Li (6), Sc (45), Y (89), Rh (103), In (115), Tb (159), and Bi (209). Analyte-internal standard pairings were selected to minimize difference in first ionization energy.

Typically, batches were analyzed with 50 samples or fewer. After analysis, quality assurance measures were employed as follows: internal standard recovery was used to identify outliers; blanks were used in the determination of the detection limit; calibration curves were used to determine response and limit of quantification; standard reference materials (SRM) were used to determine accuracy. Table 4-12 shows quality assurance parameters.

Table 4-12. ICP-MS data quality assurance metrics.

Parameter	Explanation	Determination
Batch stability	Determination of batch-wide matrix has affected ICP-MS performance	Internal standard recovery: $100 \pm 30\%$
Analysis stability	Determination of instrument is stable (consistent) for a sample	Internal standard RSD $< 5\%$
Sample stability	Determination of analysis is stable (consistent) for a sample	$< 30\%$
Detection limit (DL)	Quantification of the lowest value that can be differentiated from 0	MassHunter© DL determination based on replicate analysis of calibration blank
		Analysis of seven blank vials: mean + $3 \times \text{stdev}$
Limit of quantification (LOQ)	Determination of the lowest concentration that can be quantified (30% precision)	Estimated concentration is $\pm 30\%$ of known standard concentration
Accuracy	Accurate analysis of a known sample	Measured value $\pm 10\%$ of known standard reference material concentrations*
Max concentration	Upper limit of quantification based on calibration curve	Maximum value of standard that is retained in the calibration curve
*NIST SRM 1640a was used for verification of aqueous sample accuracy; only applies to relevant elements		

In the case that an element had multiple isotopes or tune modes analyzed, then quantitative result is an average of all results that met all quality assurance measures. Ni, for which two isotopes were monitored (58 and 60), is an exception to that rule; in many instances,  $^{58}\text{Ni}$  and  $^{60}\text{Ni}$  both met all quality assurance measures, but resulted in noticeably different concentrations. In such cases,  $^{58}\text{Ni}$  value was generally greater  $^{60}\text{Ni}$  value, likely due to polyatomic interferences that formed in the complex environmental matrix; Ni quantitation is

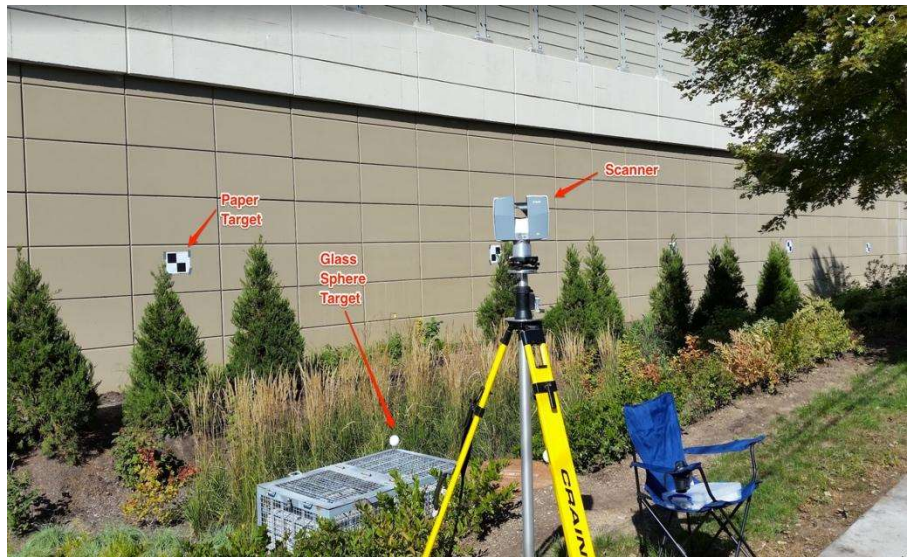
performed only on  $^{60}\text{Ni}$ . Field and bottle blanks were also employed, and showed non-detectable concentrations of elements, save low levels of Mg, Si, Zn, Sr, and W. If no quantitative results were available, then a best estimate was formed from the data that did not meet all QA/QC requirements.

## Chapter 5: LiDAR Scanning and Data Processing

### Methods for Digital Elevation Models

We collected extremely detailed data on basin microtopography, with the goal of being able to produce digital elevation models (DEMs) that can be used as input to hydrologic and water quality models. We also scanned the I-95 highway above Basins A, C, D & G to map the capture areas that drain to the basin inlets. Microtopography data were collected using a Trimble TX5 3D Laser Scanner (Fig. 5.1). This system is capable of scanning all surfaces within a 60-m radius, collecting over one million data points per second. However, LiDAR operates strictly line-of-sight; thus, dense vegetation planted within the basins complicated LiDAR data collection in some areas. Multiple scans from different angles were required to maximize the number of laser points reflecting off the ground surface.

*Fig. 5.1. Trimble TX5 3D Terrestrial LiDAR Scanner shown mounted on a tripod. Paper and glass sphere targets serve as common reference points to stitch together the point clouds from multiple scans. The photograph also shows the trees, grasses, and shrubs that interfered with the LiDAR scans, shadowing portions of the basin.*



The point clouds collected from overlapping scans can be combined provided there are at least three fixed reference points in common between each pair of scans. Reference points were created using paper and glass sphere targets (Fig. 5.1). The combined XYZ point cloud was recorded in a local coordinate system (i.e., referenced to the origin of the first scan) and required



georeferencing. To translate the coordinates to UTM (Universal Transverse Mercator), a Trimble Geo XH GPS (Global Positioning System) unit was used to record the coordinates of at least a dozen of the LiDAR targets (Fig. 5.2).

*Fig. 5.2. The Trimble Geo XH GPS used to georeference the LiDAR-derived point cloud data.*



Georeferencing involves rotation and translation of the entire point cloud without changing any of the internal distances. The scanner coordinates are accurate to  $< 1$  cm. However, the Geo XH GPS unit has a 10-cm accuracy after post-processing. Consequently, the UTM coordinates of the final DEM may be off by as much as 10 cm, but relative distances and elevations preserve the better than 1-cm internal accuracy.

The LiDAR scanner captures full-color photographs at the same time it collects XYZ point data. The red, green, blue (RGB) intensity data from the photographs can be used to color the point cloud, creating a 3D scene that can be manipulated in real time (Fig 5.3).

Once the individual scans have been merged and georeferenced, the point cloud is trimmed to remove data from areas outside the basin. All of this is accomplished using the Trimble Realworks<sup>®</sup> software package.

The next step required to produce a DEM is to remove points associated with vegetation and man-made structures such as the metal cage around the drains. For airborne LiDAR processing, ground returns are often identified using the last return from each laser pulse. This is not an option for terrestrial LiDAR because the spot size yields only a single return at each location. Considerable research has been devoted to developing algorithms used for ground filtering (Meng et al. 2010). We elected to use the *lasground\_new* filter in the LAStools® software suite (<https://rapidlasso.com/lastools/>). The *lasground\_new* algorithm is based on adaptive triangular networks (Axelsson 1999) and is quite robust.

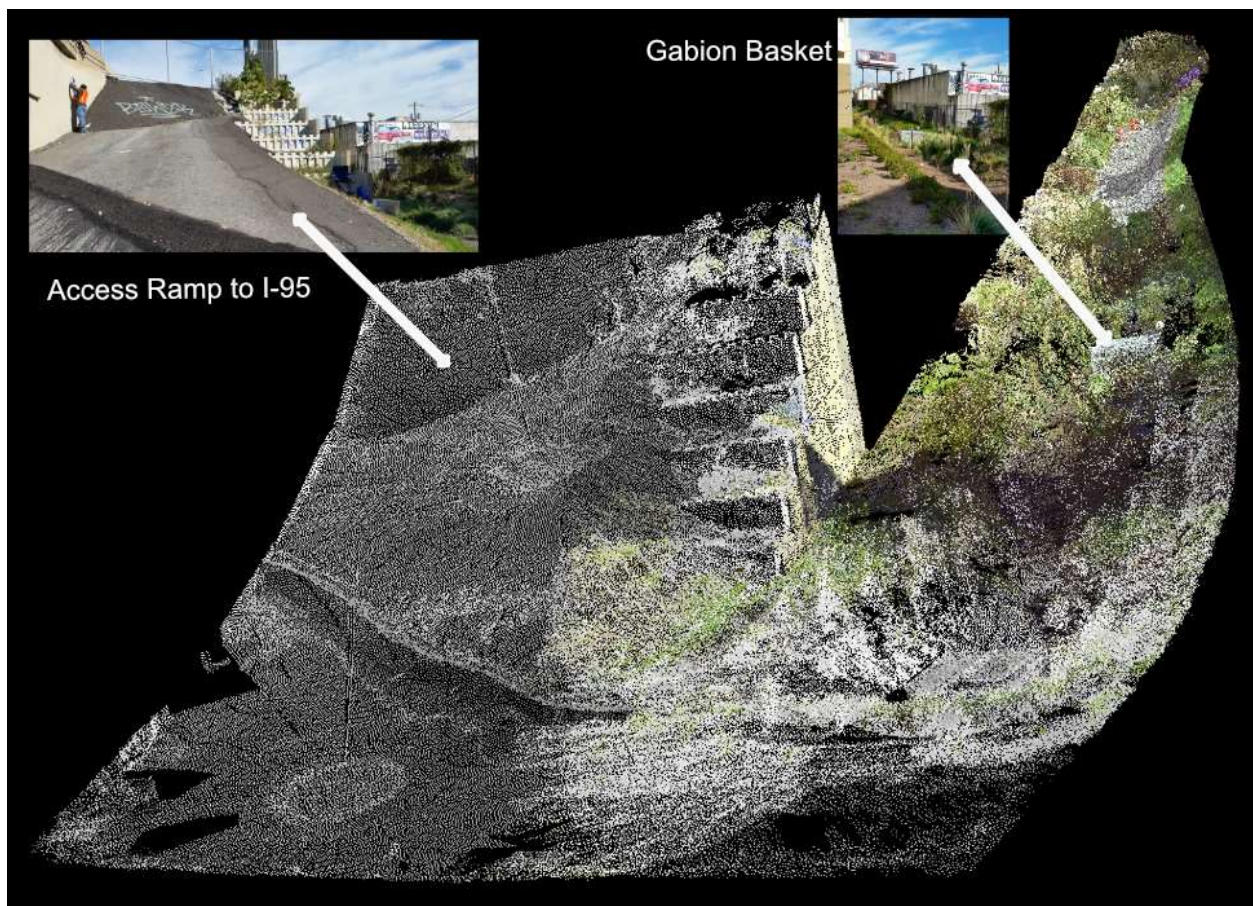


Fig. 5.3 3D point cloud for SMP A looking east-northeast at the ramp to I-95

Once the point cloud was classified into ground and above-ground points, the software package Quick Terrain Modeler<sup>®</sup> was used to grid the data (i.e., produce a raster dataset). The DEM was then exported from Quick Terrain Modeler in USGS DEM format for easy import into ArcGIS<sup>®</sup> and other cartographic/CAD software.

### **LiDAR Scanning to Map Stormwater Basins**

To date, the following basins have been scanned: (1) SMPs C, D, and G were imaged with series of 19 scans on October 4, 2016, (2) SMP A was imaged with a series of 14 scans on October 26, 2016 (one of which was an accidental duplicate). There was a small hitch in the data collection of color images for SMP A. The angle of the sun was such that high-intensity sunlight interfered with the scanner's light meter for three scans and the corresponding photographs were collected in black & white (visible at the bottom of Fig. 5.3); all other scans were in color. The loss of color information did not affect DEM production in any way, so we did not repeat the survey.

It is important to note two limitations of the DEMs produced. First, the presence surface vegetation created an obstacle to DEM production. Although multiple scans from different angles were taken in an attempt to achieve line-of-sight throughout the basins, there were still some unilluminated patches that had to be filled using interpolation. Another consequence was that the devegetation algorithm could not perfectly remove all above-ground returns, resulting in some irregularity in the DEM surface (see Fig 5.4, which is viewed from the same angle as Fig. 5.3). Note, however, that the ridge seen running diagonally across the lower left portion of the 3D view is not an artifact; it is the expression of an asphalt bump placed near the base of the I-95 service ramp to direct water flowing down the ramp into the basin. Second, the GPS uncertainty in X-Y positioning is roughly 10 cm, but the uncertainty in elevation is at least twice as large and

may be half a meter or more. While only relative elevations are important for the stormwater modeling, uncertainty in absolute elevation could potentially cause confusion if this DEM is compared with other elevation-sensitive data such as depth to the water table. If a survey elevation benchmark was established at each of the basins, it would be possible to adjust the DEM elevations to their correct values relative to mean sea level.

The final DEMs were gridded on a 10-cm spacing. This spacing was selected because experimentation showed that a finer grid spacing produced too many artifacts (pits and pinnacles) caused by the occasional misclassified point. A 10-cm grid provided some smoothing while still yielding a DEM of more than sufficient precision for stormwater modeling. The DEM for SMP A is shown in Fig 5.5, where it is displayed in ArcMap and superimposed on an aerial orthophotograph of the area.



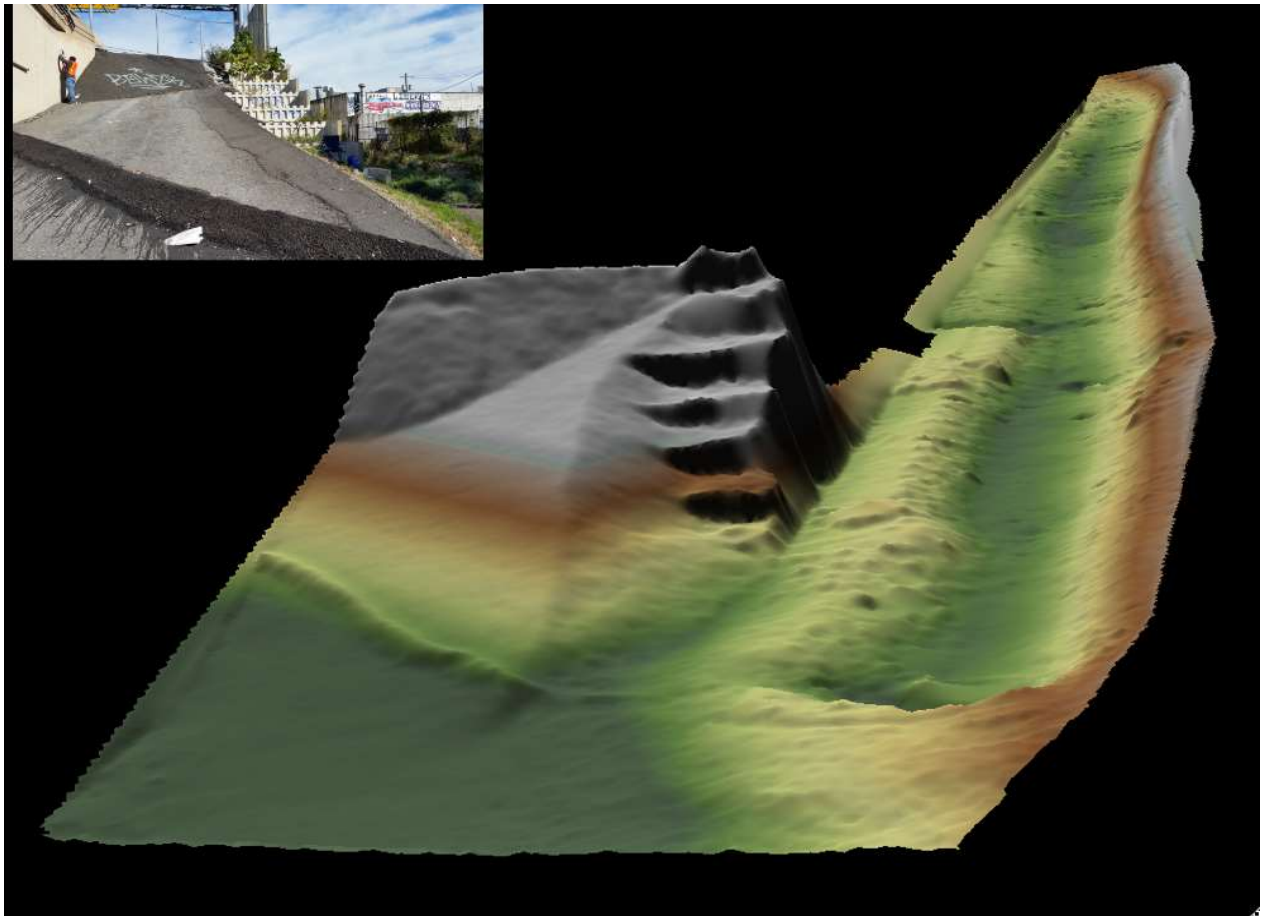


*Fig. 5.4. The 3D DEM produced from the filtered point cloud data. Inset shows a photograph of the asphalt ridge visible in the lower left corner of the DEM. The ridge was constructed to direct runoff flowing down the I-95 ramp into the stormwater basin.*

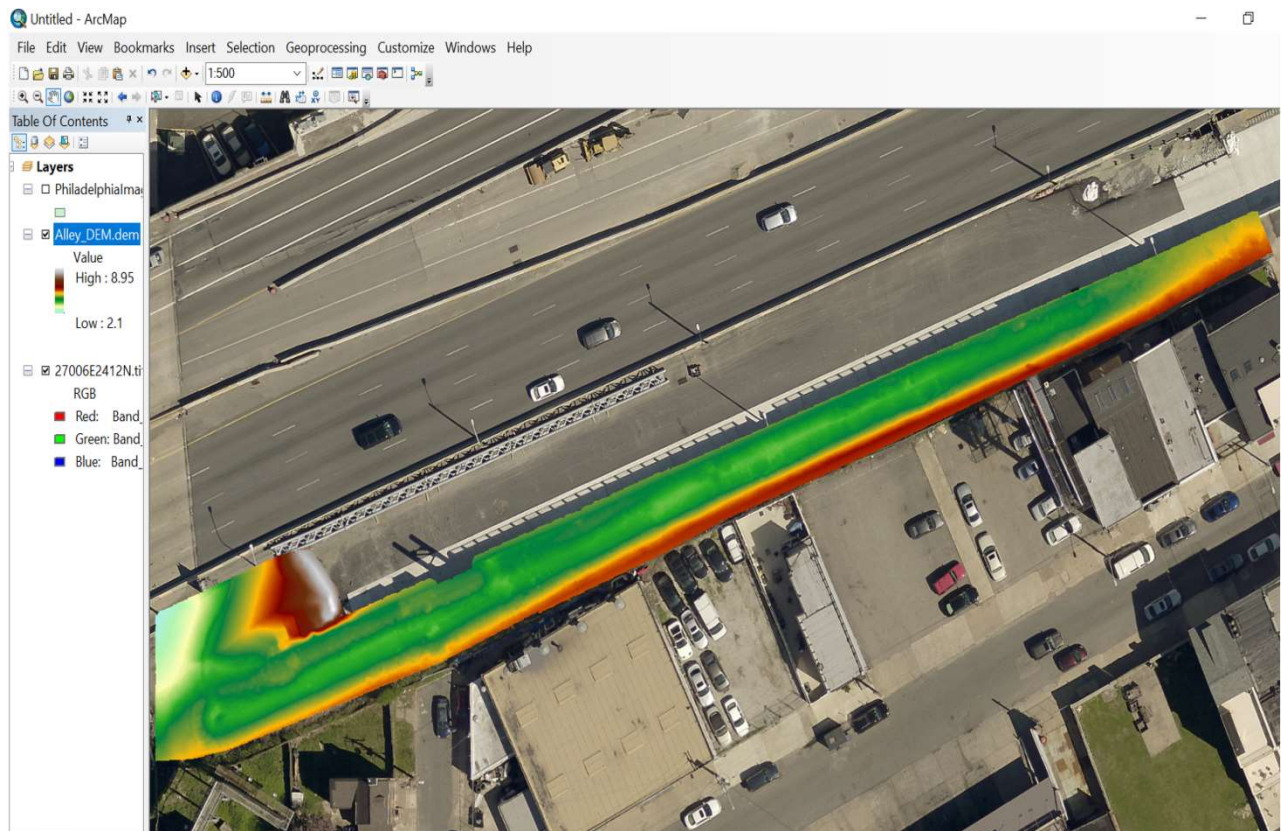


*Fig. 5.5. DEM for SMP A superimposed on an aerial orthophotograph. Data were exported in the USGS DEM format, UTM Zone 18N (meters).*

## Calculation of I-95 Storm Drain Capture Areas

Monitoring in the basins showed lower than expected flow following storms, suggesting that models of the I-95 storm drain catchments were in error. To correct this, we decided to scan the highway and create a DEM of the road surface above Basins A, C, D, and G. Safety concerns precluded placing the scanner close to traffic such that temporary concrete barriers partly occluded the scanner's view of the road in the central portion of the highway. The dense, continuous flow of cars and trucks created spurious LiDAR reflections (Fig. 5.6) that had to be removed from the data in post processing. Nevertheless, more than enough points remained to calculate catchment areas. The LiDAR point cloud was also used to extract coordinates for the storm drains adjacent to the sound barrier above the basins (Fig. 5.7).

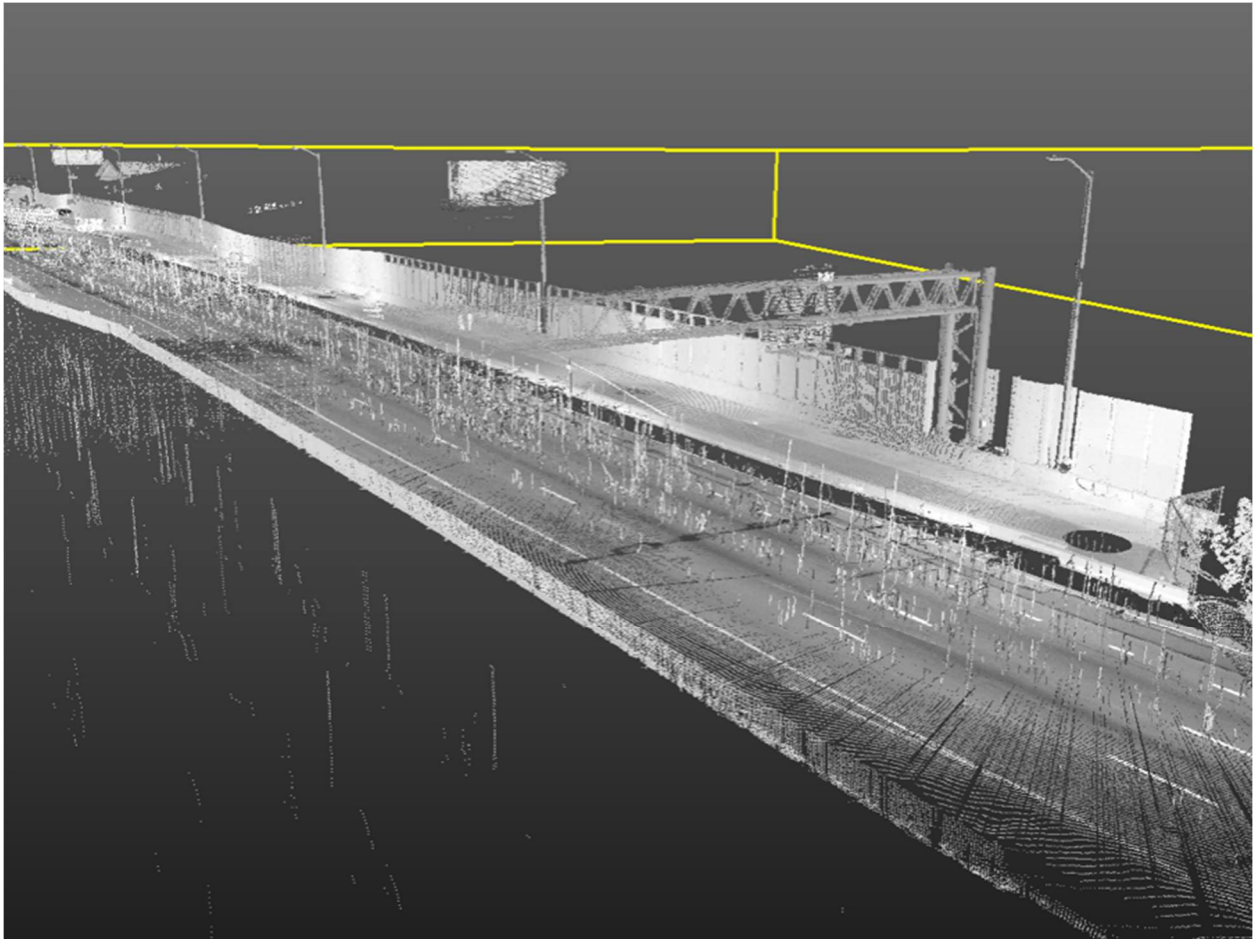


*Fig. 5.6. LiDAR point cloud with traffic noise (stray points captured from passing cars and trucks).*

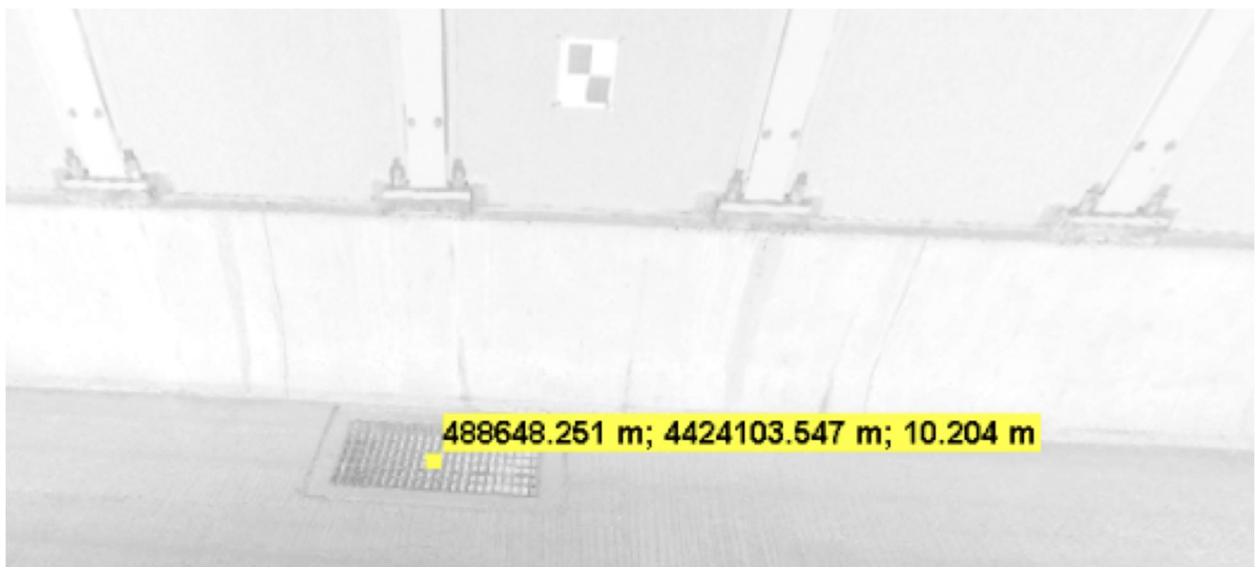


*Fig. 5.7 Example of a storm drain coordinate (UTM WGS94) picked from the LiDAR point cloud.*



In the process of removing the LiDAR points caused by traffic, the concrete barriers were also removed. To calculate drainage patterns with and without the barriers, the points associated with the barrier were added back into the point cloud (Fig. 5.8).

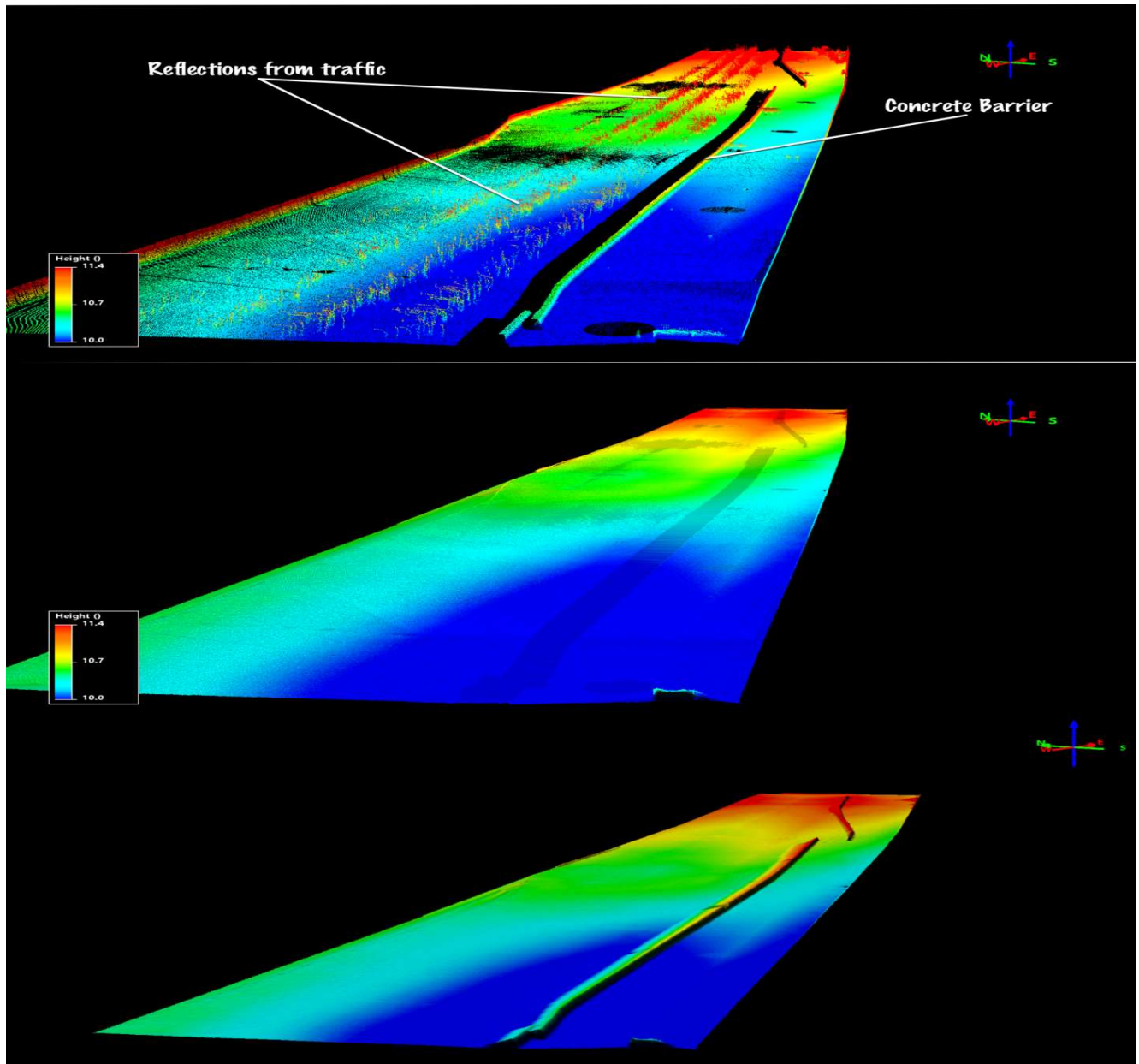


*Fig. 5.8 (Top) Point cloud for region of interest, color-coded by elevation. Note the spurious reflections from traffic. (Middle) DEM constructed only from ground surface reflections, which removed the barrier. (Bottom) DEM constructed from ground reflections with the barrier added back in. Due to the lack of LiDAR returns in the shadow of the barrier, interpolation caused the barrier to appear ramped on one side; this had a minimal effect on subsequent drainage calculations as flow is still blocked.*



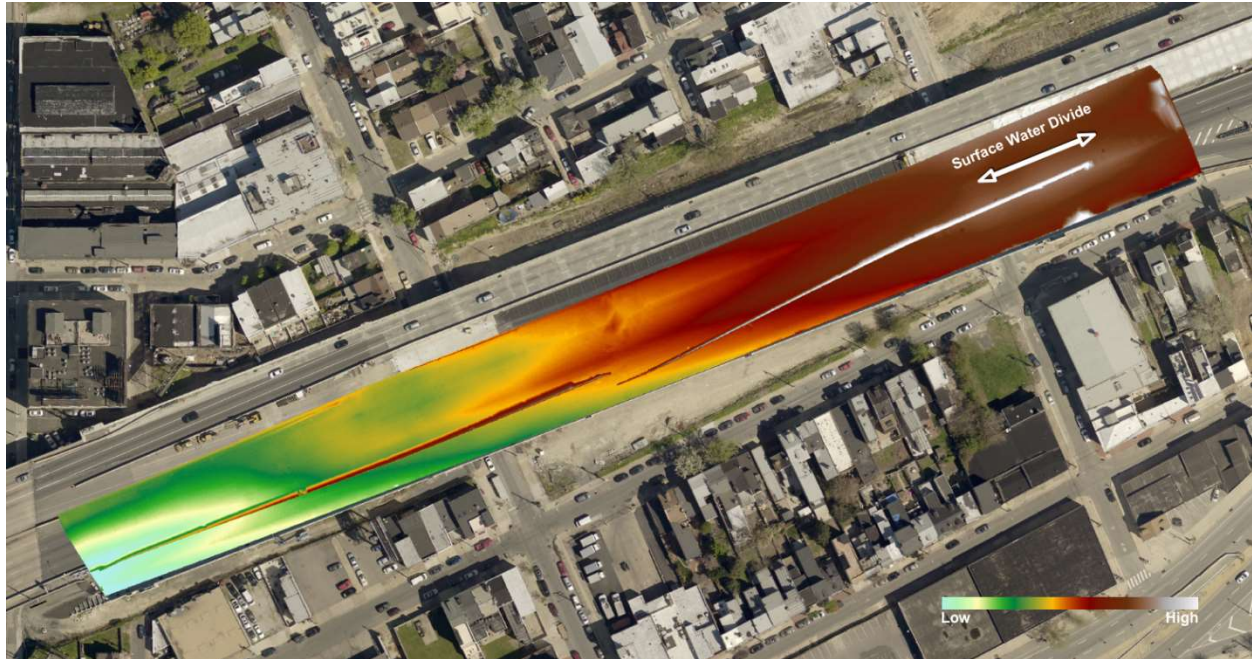


*Fig. 5.9 Color-coded DEM of the I-95 roadway surface (barrier included). A version without the barrier was also calculated. Note the surface water divide.*

The DEMs produced with and without the inclusion of the concrete barriers were imported into ArcMap (Fig. 5.9) as a basis for subsequent flow calculations. We then ran a hole-filling algorithm from the Spatial Analyst toolbox and calculated slope to simulate runoff patterns. Although the concrete road barriers have small openings beneath them to facilitate drainage (Fig 5.11), most of these opening were clogged with debris. The simulation was therefore run assuming that the barriers blocked flow completely.

Calculations of runoff flow (Fig 5.11) show that crowning in the pavement of I-95 causes much of the flow to converge on the center of the highway. Therefore, while the barriers affect drainage, removal of the barriers would not greatly increase flow to the storm drains along the southern wall. We could not map the storm drains in the center of the highway because traffic prevented the LiDAR scanner from obtaining a clear line of sight.





Fig. 5.10 Photograph showing the LiDAR scanner, concrete barriers, and their drainage openings.

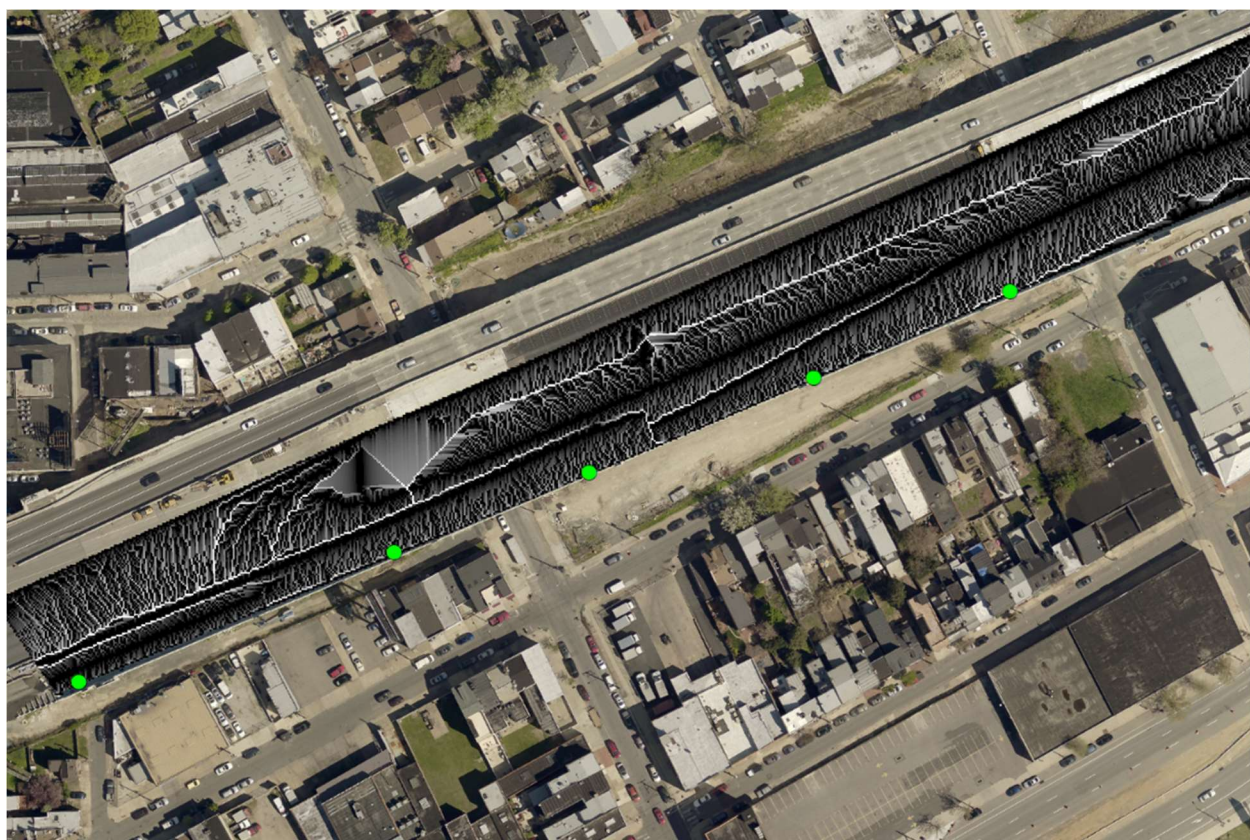


Fig. 5.11 Calculated flow accumulation ( $\log_{10}$  scale). White lines show the drainage pattern and green dots indicate storm drain locations.

Tracing the boundaries of the accumulation areas for each drain produced an estimate of the catchment area for each the five drains along the southern wall (Fig. 5-12). These areas can be used to estimate discharge into the basins in response to storms. Any flow from drains in the center of I-95 would need to be included, but their catchment areas cannot be calculated unless information on the drain's coordinates is obtained.

### **Remarks on Terrestrial LiDAR Utility**

In addition to serving as the basis of DEM construction for flow calculations, both on the highway and in the basins, the terrestrial LiDAR data was used by plant researchers to obtain coordinates of their 72 focal plants. In the future, if LiDAR data can be obtained before and after adding the amended soils to the excavated basins, it could be used for as-built verification, such as identifying areas with insufficient fill. Additionally, LiDAR data collected at regular intervals after plant installation could be used to monitor plant growth and canopy structural change (see Chapter 7).



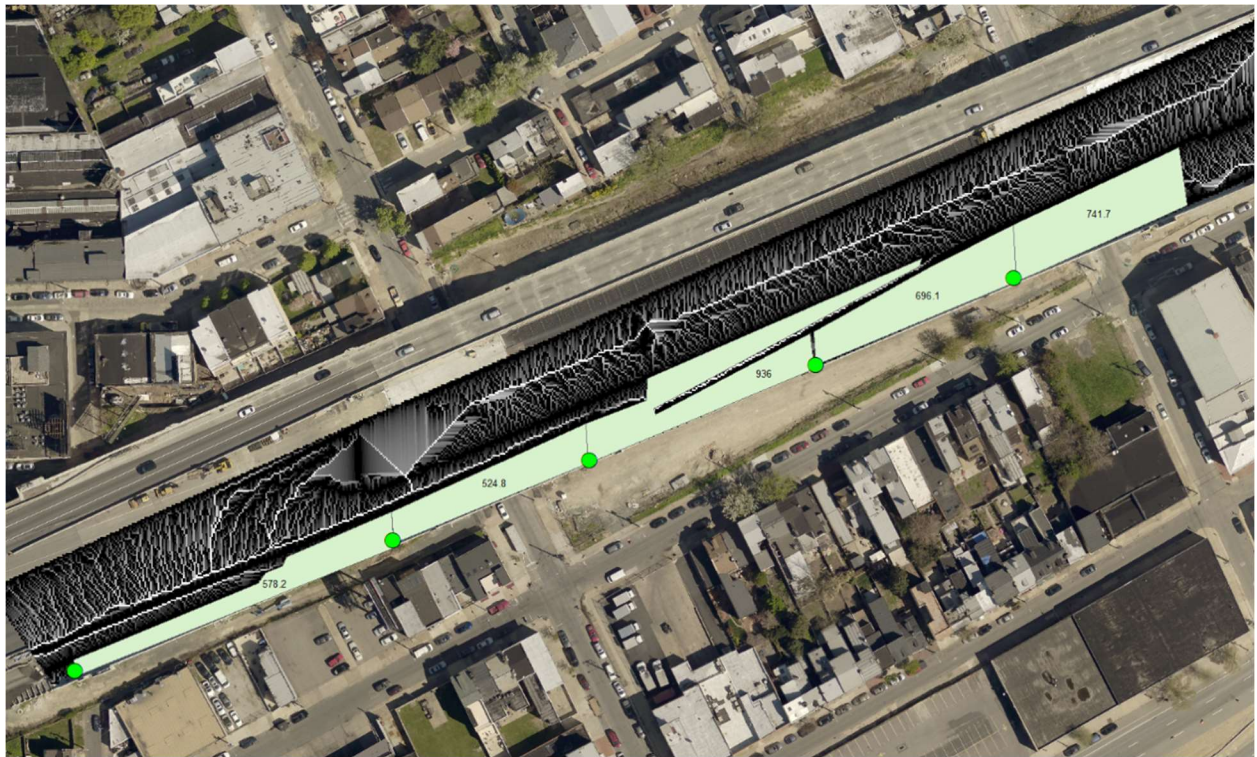


*Fig. 5.12 Polygons digitized from the flow accumulation map indicating highway surfaces that flow into each storm drain (green dots). Estimate of catchment areas (sq. meters) assume no flow under the barriers.*

## Chapter 6: SMP Computer Modeling

### Introduction

The overarching goal of Task 6 is to carry out and calibrate computer modeling of the water quantity and quality in SMPs. Computer modeling will be initiated to estimate performance capacities of alternative SMPs and groups of SMPs and simulate performance according to alternative SMP designs. The model selection was based on a literature review. Ground-based Light Detection and Ranging (LiDAR) data was obtained through use of a laser scanner to provide more accurate characterizations of SMPs, their capture areas for modeling, and related data on roadway configurations and land use (see Chap 5).

### Methods

#### *SWMM Modeling*

The USEPA Stormwater Management Model (SWMM; Rossman 2015) was selected to model the bioswales due to its singular ability to model:

- the complex hydraulics of transportation systems
- the infiltration and runoff from stormwater management practices
- both water quality and water quantity
- continuous simulation

EPA classifies SWMM as a “dynamic hydrologic-hydraulic water quality simulation model” (US EPA 2017). SWMM is used for this research project because of its physically based qualities that allow it to model the hydraulics of complex transportation systems with water quantity, quality, continuous simulation, and multiple types of SMP devices (Wang and Altunkaynak 2012). SWMM can encompass the entire water budget. It can model water and

material flows through the atmosphere (precipitation and pollutant buildup), land surface (subcatchments where precipitation and pollutants fall), groundwater (infiltration through soil), and transport systems (conveyance system of pipes, channels, and treatment systems) (Rossman 2015). SWMM is widely used for planning, analysis and design purposes, and is a reputable program for modeling drainage systems in urban areas (Cambez et al. 2008; US EPA 2017). Additionally, it is made available to the profession at no charge by the EPA. SWMM is incorporated in the current Pennsylvania Stormwater Management Manual, and is used by the Philadelphia Water Department for their GI planning and monitoring.

The model that is the focus of this report was created by Schmidt (2017) for SMP C, D, and G, and is heavily copied from her thesis. The three linearly adjacent SMP's and their drainage areas are modeled in SWMM as a series of subcatchments, conduit links, and storage nodes. The modeling schematic entered in SWMM is shown in Figure 6-1. Note that the modeling of SMP A is under development, and follows the same approach.

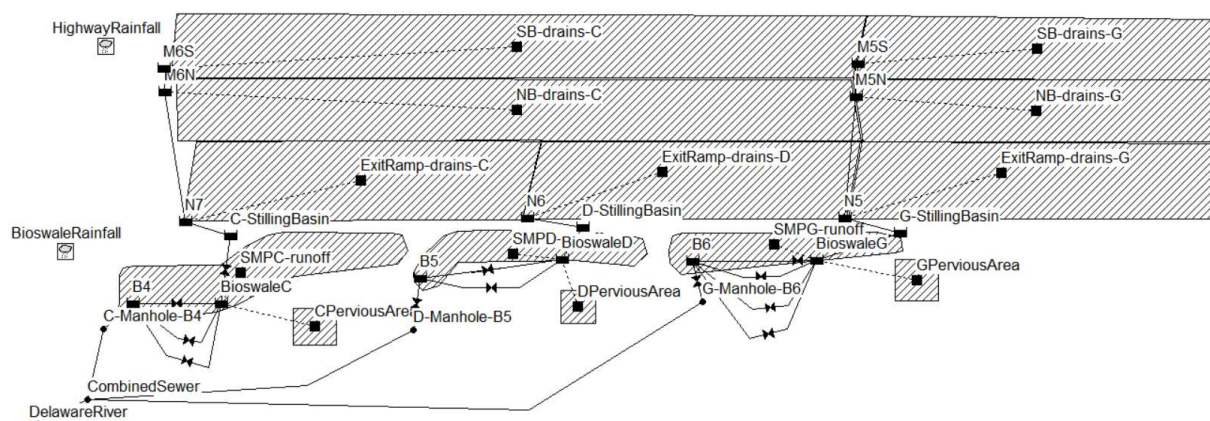


Figure 6-1: SWMM schematic of SMP C, D, and G

### Watershed Input Parameters

Input parameters for the SWMM model were determined using AECOM's plan sets, field measurements, and calculations. Dimensions and material variables were based off plan sets provided by AECOM. If a dimension or other value could not be found within the provided documentation, a value was estimated based on literature and other known values, or a value was chosen that made logical sense. This model was created with pre-construction design plan sets, so the initial parameters are accurate for the design specifications. The As-Built plan sets are not yet available, so the measurable variables will be adjusted when the plans are made available. Other data collected includes ground-based Light Detection and Ranging (LiDAR) data, which was collected by Temple University with a laser scanner to provide more accurate characterizations of SMPs, their capture areas for modeling, and related data on roadway configurations and land-use. Additional discussion of LiDAR can be found in Chapter 5. Results from the LiDAR imaging can also be used in the future to verify values for the SWMM model.

### Weather Data

Precipitation is provided in SWMM as two separate gauges with external continuous files, one for the road surface and one for the bioswales. The two rain files are used due to the spatial variability discussed in Chapter 3. Rain falling on the roadway is not significantly affected by the sound wall, so the rain falling on the weather station is assumed to be a good representation of the rainfall in the drainage area for SMP C, D, and G. Precipitation on the bioswales is provided by the rain gauge on the pole between SMP C and D. Both precipitation files are provided in five-minute increments and in a volume format (volume of rain that fell within the time increment). Due to a clogging of the rain gauge on the pole near SMP C and D in March and April of 2017, the precipitation from the weather station was used for both pervious

and impervious subcatchments. Since the pervious area is a much smaller contributing area, the spatial variability is assumed to be minimal. Future calibration should use the two separate files to minimize the propagation of errors through the model.

Evapotranspiration (ET) is a significant portion of the water budget. It also is a significant factor in SMP function and can account for between 35 and 63 of the water budget in a rain garden (Hickman 2011). Thus, accurately accounting and calculating the ET of a system is critical. A file containing the minimum and maximum daily temperatures from the weather station between SMP C and D, as well as the latitude of the bioswales locations (39.967°) is used to calculate evaporation in SWMM. Potential evapotranspiration is calculated in SWMM using the Hargreaves method (Hargreaves and Samani 1985) in Equation 6-1,

$$E = 0.0023(R_a/\lambda)T_r^{\frac{1}{2}}(T_a + 17.8) \quad 6-1$$

where  $E$  is evaporation rate (mm/day),  $R_a$  is the water equivalent of incoming extraterrestrial radiation (MJ/m<sup>2</sup>d),  $T_r$  is the average daily temperature range for a period of days (°C),  $T_a$  is average daily temperature for a period of days (°C),  $\lambda$  is latent heat of vaporization (MJ/kg) (2.5-0.002361  $T_a$ ) (Rossman and Huber 2016). The extraterrestrial radiation is calculated using the latitude, solar declination, sunset hour angle, Julian day, and the relative earth sun distance (Rossman and Huber 2016). The daily minimum and maximum temperature data is averaged over seven days in SWMM to provide accurate results as specified by Hargreaves and Merkle (1998), who specified a five day running average minimum (Rossman and Huber 2016). SWMM uses wind data to calculate the melting rate of snow during precipitation (Rossman and Huber 2016). Wind data is not used in this model, nor was snow melt, since we do not have a heated rain gage to measure snow volume.



## Drainage Area

In SWMM, subcatchments are used to delineate different areas that have their own hydrological characteristics and unique rainfall-runoff processes (Ji and Qiuwen 2015). The drainage area and subcatchments for each bioswale are split into the three different lanes, Northbound, Southbound and the Girard Street exit ramp as seen in Figure 6-1. SMP C has all three lanes draining into the N7 inlet. SMP D has just a section of the exit ramp draining to inlet N6, and SMP G has 3 lanes draining into inlet N5. The drainage area of the different lanes was delineated per the AECOM plan set. Runoff generated on the roadway flows to surface inlets, which are PennDOT Standard Type M Boxes. For SMP C and G once runoff flows to the surface inlet it travels 80-90 feet in a pipe connecting the roadway inlets to the inlet on the edge of the highway that drains to the bioswale from a pipe at the bottom of the box.

The inlets were simulated in SWMM as storage nodes, due to their ability to store water within a defined area and volume. The volume of the inlet is crucial for this model to determine flooding and flow into the piping system. Storage nodes were also chosen to model the three bioswale inlets as they had the ability to simulate fully vertical pipes by defining the area of storage. The storage node only represents the pipe drop, not the 90-degree bend and pipe to the rock bed, thus the pipe is input in SWMM as a link that is attached to the inlet storage node. The schematic of the inlet structure is shown in Figure 3-11 and the storage curves entered into SWMM representative of the inlet structure are shown in Table 6-1. The storage unit for the inlets are also designed to have a very wide shallow top section to simulate where flooding may occur, since storage nodes are not technically allowed to flood. The entire system is also allowed to pond to simulate very large storms that might cause flooding of the roadway and storage nodes. This is a valuable feature of SWMM; if the system was not able to pond, any water that

went over a node would disappear from the system. By allowing ponding, water above the maximum depth of any junction or node is held until the system can receive more water.

*Table 6-1: SWMM Inlet Storage Curves*

Storage Curves - Inlets					
N7-C		N6-D		N5-G	
Depth (ft)	Area (ft <sup>2</sup> )	Depth (ft)	Area (ft <sup>2</sup> )	Depth (ft)	Area (ft <sup>2</sup> )
0.00	3.14	0.00	1.77	0.00	1.77
5.71	3.14	7.33	1.77	6.10	1.77
5.72	1.77	7.34	0.79	6.11	0.79
10.71	1.77	12.33	0.79	11.1	0.79
10.72	14.31	12.34	14.31	11.11	14.31
17.13	14.31	18.75	14.31	17.52	14.31
17.14	10000	18.76	10000	17.53	10000

Table 6-2 shows the assumed subcatchment properties prior to calibration for each bioswale. Drainage areas and width of each subcatchment were delineated and measured by AECOM. The default slope in SWMM and PennDOT's minimum slope for roadways is 0.5 percent (PennDOT 2015), which was used as the base assumption for the roadway. The exit ramp and some of the travel lanes are made of concrete, the other travel lane surface is asphalt. The entire roadway surface was assumed to be asphalt during the calibration process (Manning's roughness coefficient of 0.015). The difference in material changes the initial abstractions for some of the subcatchments, but only will be noticeable during small precipitation events.

Table 6-2: SWMM Subcatchment values

Subcatchment	Area (ac)	Width (ft)	% Slope	% Imperv	N- Imperv	N- Perv	Dstor- Imperv (in)	Dstore- Perv (in)
SB-drains-C	0.36	37.76	0.5	100	0.015	0.1	0.0102	0.05
NB-drains-C	0.36	37.76	0.5	100	0.015	0.1	0.0102	0.05
ExitRamp-C	0.23	47.96	0.5	100	0.015	0.1	0.0102	0.05
ExitRamp-D	0.22	47.96	0.5	100	0.015	0.1	0.0102	0.05
NB-drains-G	0.13	37.76	0.5	100	0.015	0.1	0.0102	0.05
SB-drains-G	0.13	37.76	0.5	100	0.015	0.1	0.0102	0.05
ExitRamp-G	0.16	47.96	0.5	100	0.015	0.1	0.0102	0.05
CPerviousArea	0.29	920	0.5	0	0.010	0.1	0.05	0.05
DPerviousArea	0.16	548	0.5	0	0.010	0.1	0.05	0.05
GPerviousArea	0.01	1855	0.5	0	0.010	0.1	0.05	0.05
SMPC-runoff	0.06	33	0.5	100	0.100	0.01	0.05	0.05
SMPG-runoff	0.06	25	0.5	100	0.100	0.01	0.05	0.05
SMPD-runoff	0.06	26	0.5	100	0.100	0.01	0.05	0.05

The pervious area surrounding the bioswales is separated out into different subcatchments (shown in Table 6-3), which drain to each bioswale. The pervious area width surrounding each bioswale was estimated by measuring an average length of flow around each bioswale. The slope of the surrounding pervious area was assumed to be the default of 0.5 percent and was modified during the calibration process. Storage nodes do not pond water or allow precipitation, so each bioswale needed an additional subcatchment with the surface area of the bioswale to capture the precipitation that falls on the bioswale during a storm event. The pervious area of the bioswale itself is routed directly to the storage node, but is not allowed to infiltrate and is considered impervious, as all the infiltration for the bioswale will occur in the storage node. The width of the bioswale runoff was estimated based on the length of flow that would occur to get to the outlet structure, where the actual measurement is read. The slope of the bioswales is 0.5 percent as specified in design documents.

Surface runoff occurs when the initial abstractions or depression storage are filled, or when the total precipitation amount is greater than the initial abstractions for the specific surface. The depth of initial abstractions is only significant during small storms, when the precipitation amount and depth of initial abstractions are similar. Initial abstractions are input in SWMM as “Dstore-Imperv/Perv” for depth of depression storage on impervious or pervious area in inches (the entire system is entered in US units due to the design documents). Initial abstractions for the roadway surface were calculated based on the Soil Conservation Service (SCS) runoff equation, shown in Equation 6-2 (Bedient et al. 2013).

$$Q = \frac{(P-I_a)^2}{(P-I_a)+S} \quad 6-2$$

where,  $P$  is rainfall (in),  $I_a$  is initial abstractions (in), and  $S$  is potential maximum retention after runoff begins (in) (Cronshey 1986). Traditionally, initial abstractions are calculated with  $I_a = 0.2*S$  and  $S=1000/CN - 10$ , where  $CN$  is the dimensionless runoff curve number of the surface (Bedient et al. 2013; Hawkins et al. 2003).  $CN$  is a function of land use, antecedent soil moisture and other runoff and retention watershed factors (Mays 2011). A study by Hawkins et. al (2003) found that 0.2 (initial abstraction ratio =  $I_a/S$ ) was over estimating initial abstractions and a more appropriate value of 0.05 provides a more accurate fit to the data. Thus, this value was used to calculate initial abstractions for the impervious and pervious areas. A value of 0.0102 inches was calculated for impervious depression storage based on a curve number of 98, an initial value of 0.333 inches was calculated based on an average Curve number value of 60 for the bioswale, and an initial value of 0.176 inches was calculated based on a Curve number of 74 for the pervious area surrounding the bioswale. The values for pervious initial abstractions were varied during the calibration process. The percentage of zero impervious, which is the percent of

impervious area with no depression storage, was set to zero for all subcatchments. All parts of the drainage area were assumed to have depression storage.

### Conduit Links

The concrete pipes under the highway that carry the runoff to the bioswales were created as links in SWMM. SWMM classifies links as pipes, channels, pumps, or flow regulators (orifices, weirs, or outlets) that link nodes together (Rossman and Huber 2016). SWMM has a minimum elevation drop between conduit end nodes of 0.01 feet. All sections of conduit were above this value except for the conduit between the South and Northbound sections draining to SMP G. The roadway inlet surface and invert out were specified by AECOM in their PCSM to be at the same elevations, so there was a zero change in elevation of the inlet and outlet ends of the link. Thus, SWMM used an assumed elevation drop of 0.01 feet to calculate the slope of the conduit for this section (this creates a warning notice every time the model is run). Conduit links route flow from the storage node of each roadway elevation inlet to the next inlet and eventually to the stilling basin prior to flowing to each bioswale. A table of the dimensions of each pipe link entered into SWMM is shown in Table 6-3. The length from the manhole to the sewer was estimated by measuring on the AECOM design files the estimated length of pipe until it reaches the larger combined sewer pipe.

Table 6-3: Conduit properties entered in SWMM. All links are circular pipes.

Conduits	Max. Depth (ft)	Length (ft)	Roughness	Inlet Offset (ft)	Outlet Offset (ft)
C-SB-to-NB	1.500	2.002	0.012	0.000	0.090
G-SB-to-NB	1.500	2.000	0.012	0.000	0.000
C-NB-to-N7	1.500	87.032	0.012	0.000	12.230
G-NB-to-N5	1.500	78.707	0.012	0.000	14.200
N7Inlet-to-BioswaleC	2.000	6.000	0.024	0.000	1.833
N6Inlet-to-BioswaleD	1.500	6.000	0.024	0.000	1.160
N5Inlet-to-BioswaleG	1.500	6.000	0.024	0.000	1.160
C-Manhole-to-Sewer	1.500	48.000	0.012	0.000	0.000
D-Manhole-to-Sewer	1.250	231.000	0.012	0.000	0.000
G-Manhole-to-Sewer	1.250	405.000	0.012	0.000	0.000
Sewer-to-River	2.000	323.000	0.012	0.000	0.000

### Conduit/Link Routing

SWMM transports runoff through the system by routing through pipes, channels, storage/treatment devices, pumps, and regulators (Rossman and Huber 2016).

There are three options that the model provides to calculate routing through the piping system: steady flow, kinematic wave, and dynamic wave flow routing. For kinematic and dynamic wave flow routing, the continuity and momentum equations for gradually varied and unsteady flow are used to route runoff through conduits and the continuity equation solves for volume at each node (Rossman 2015). The routing method chosen for this model is kinematic wave flow routing. Kinematic wave routing solves the partial one-dimensional Saint Venant flow equations (continuity and momentum equations), where the friction slope is assumed to equal the bottom slope along a conduit (Niazi et al. 2017). Dynamic wave flow routing solves the full

Saint Venant equations, allowing the system to handle backwater effects, pressurized flow, flow reversals, and entrance/exit losses that the other two methods are incapable of handling (Rossman and Supply 2006). The kinematic wave flow routing was chosen due to the high numerical errors that occurred while running the model with Dynamic wave flow routing. This creates limitations on model results, due to not being able to measure backwater effects that might be occurring in the piping system.

### Runoff Routing

Prior to routing through conduits, the kinematic wave for overland flow, shown in Equation 6-3 is used in SWMM to calculate and route runoff from each subcatchment.

$$q = \frac{k_m}{n} \sqrt{S_0} y^{5/3} \quad 6-3$$

where  $q$  is overland flow,  $k_m$  is 1 or 1.49 for metric or US units respectively,  $S_0$  is slope, and  $y$  is mean depth of overland flow (Bedient et al. 2013; Sturm 2001). Subarea routing within each subcatchment determines how flow leaves pervious and impervious sections within each subcatchment. Within this model, the subarea routing is set to the outlet, as each subcatchment is composed of only pervious (grass around gardens) or impervious (roadway surface) surfaces.

### Bioswale Modeling

Once the water leaves the highway piping system and flows through inlets N5, N6 and N7, it enters a rock stilling basin to dissipate energy. This is also entered as a storage node to represent the shape accurately, as well as to store and measure water entering the rock stilling basin. Each of these rock stilling basins is lined with a Class 2, Type A geotextile to prevent erosion and keep the stones in place. The stilling basin stones are R-3 sized stones, which a type of rip-rap rock that is three to six inches in diameter. The design drawings and dimensions of the stilling basins are shown in Figure 6-2. The stilling basin in SMP C (N5), shown in Figure 6-3,



was altered in construction to be much larger than the designed size. This was to create a path for the water to get to the bioswale and to prevent scour from the large drainage area and predicted flow. To simulate the transition from the rock stilling basin to the vegetated bioswale, a wide trapezoidal weir was entered, with the bottom of the weir at a middle elevation of the bioswale. The estimated parameters of these weirs are shown in Table 6-4.

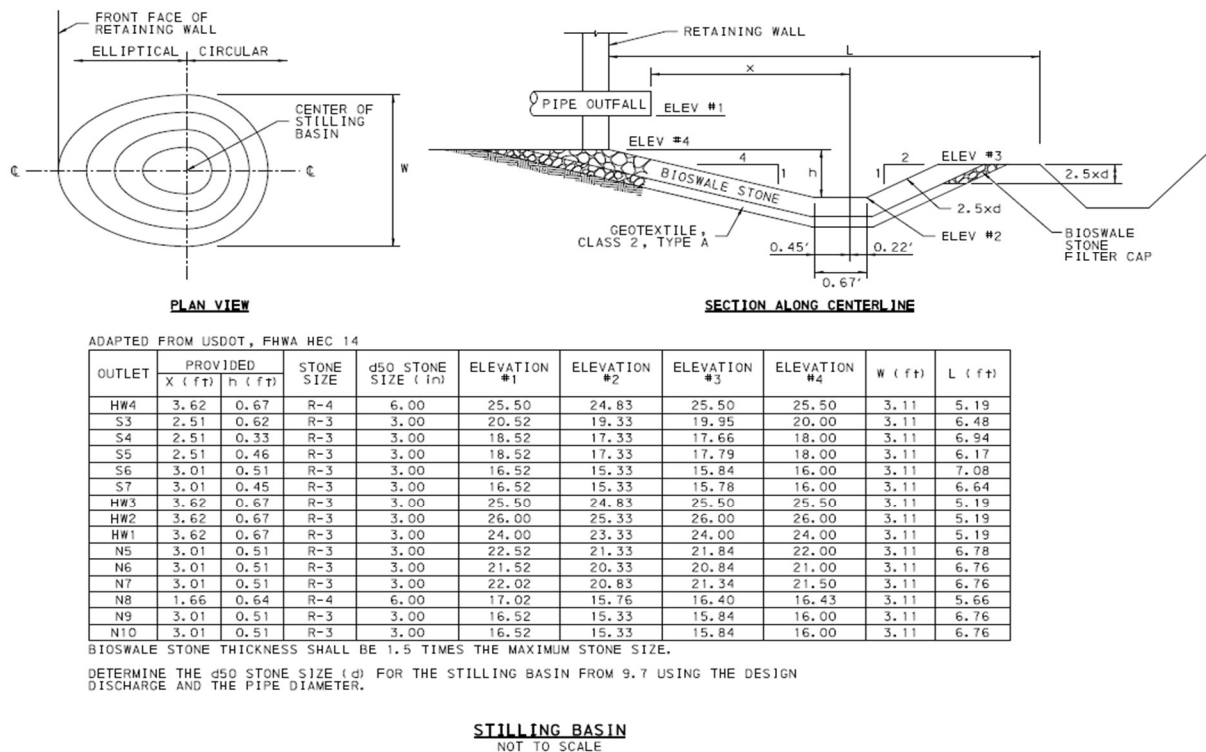


Figure 6-2: Stilling Basin Dimensions (AECOM/URS 2015)



*Figure 6-3: SMP C Rock Stilling Basin during May 5, 2017 Storm*

*Table 6-4: Weirs entered in SWMM to translate water from rockbed to bioswale*

Weirs	Type	Height (ft)	Length (ft)	Side Slope	Inlet Offset (ft)
Rockbed-to-BioswaleC	Trapezoidal	1.75	21	1	0.64
Rockbed-to-BioswaleD	Trapezoidal	0.68	7	1	1.50
Rockbed-to-BioswaleG	Trapezoidal	1.50	6	1	20.75

Storage units were chosen to model each of the bioswales due to the limitations and limited research into the validity of SWMM's LID controls. LID controls were added to SWMM in 2010 and research utilizing LID controls has yet to be highly published. A significant limitations of LID controls is that they do not allow piping or weirs to enter the LID, since they are set up through the subcatchment function in SWMM. Storage units have been used in other Villanova modeling projects as well as in the City of Philadelphia to model GI. Storage units in

SWMM have the option to have a tabular or functional curve that describes the shape and surface area of the storage unit. A tabular curve was used, since the water surface elevation level (WSEL) and corresponding area was provided for each bioswale by AECOM. The storage curves entered in SWMM for each bioswale are listed in Table 6-5 and SWMM representation is shown in Figure 6-4.

Table 6-5: SWMM Bioswale Storage Curves

Storage Curves - Bioswales					
SMPC		SMPD		SMPG	
Depth (ft)	Area (ft <sup>2</sup> )	Depth (ft)	Area (ft <sup>2</sup> )	Depth (ft)	Area (ft <sup>2</sup> )
0.00	30	0.00	30	0.00	30
0.39	1643	0.18	329	0.45	952
0.64	2674	0.68	1581	1.20	1498
0.89	3705	0.85	1688	1.45	1680
1.06	3837	1.51	2102	1.78	1878
1.39	4093	1.68	2207	2.41	2254
2.39	4889	2.18	2529	2.45	2278
				2.95	2587

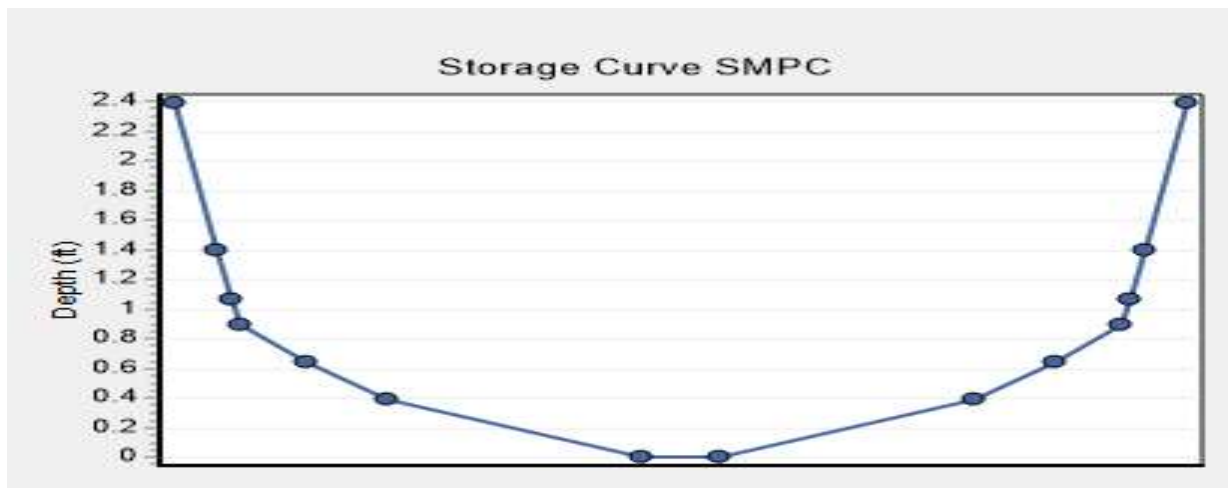


Figure 6-4: Storage curves for bioswales as represented in SWMM.

## Infiltration

All infiltration that occurs through the pervious areas of the SWMM model uses the modified Green-Ampt method, which is a model that uses continuous simulation to process infiltration using soil moisture and other environmental processes (Lee et al. 2013). Green-Ampt infiltration is often used in models, as it is simple and easy to estimate soil type parameter based on tables from Rawls et al. (1981) (Lee et al. 2013). The original Green-Ampt equation is presented in Equation 6-4,

$$Kt = F - n\psi_f \ln\left(1 + \frac{F}{n\psi_f}\right) \quad 6-4$$

where,  $K$  is hydraulic conductivity (cm/hr),  $\psi$  is the wetting front capillary pressure head (cm); and  $n$  is the available porosity, which is calculated as the effective porosity,  $\theta_e$  (total porosity,  $\phi$ , minus residual saturation,  $\theta_r$ ), minus initial soil water content (Rawls et al. 1983). A version of the Green-Ampt equation was modified by Mein and Larson (1973). This was chosen to model infiltration in this SWMM model, as it does not initially deplete the moisture deficit of the top soil layer during low rainfall (Rossman 2015). The modified method uses the soil's initial moisture deficit, hydraulic conductivity, and the suction head at the wetting front to approximate the solution to the Richards equation (Richards 1931). This approximation uses the “physics of saturated and unsaturated flow through porous media” to calculate infiltration (Lee et al. 2013).

Hydraulic conductivity is a function of suction head, which is a function of moisture content, which mean that they both change as ponding occurs (Mays 2011). Suction head varies with moisture content due to the energy from the soil suction forces which binds water to soil particles through surface tension (Mays 2011; Rossman and Huber 2016). The variable suction head is not represented in SWMM, since the value used in SWMM is an average suction along the wetting front (Rossman and Huber 2016). The variability in hydraulic conductivity change is

accounted for by calculating the hydraulic conductivity using the current soil moisture content and the provided value of saturated hydraulic conductivity (Rossman and Huber 2016).

Lee et al. (2013) found that the tables provided by Rawls et al. (1981) for Green-Ampt parameters produce extremely conservative infiltration rates and are not able to reproduce actual high infiltration rates. Thus, care must be taken in choosing values, so that correct or close values for Green-Ampt parameters are used in the model. The values used for the infiltration were based on the specified amended soil used within the rain gardens (maximum of two feet above the native soil layer), which was classified between a sandy loam and a loamy sand. AECOM specified the amended soil in the bioswales was between 72-85 percent sand and less than 10 percent clay. Soil properties entered in SWMM are based on the AECOM design specifications in combination with Rawls et al (1981) table values and the Soil Water Characteristics standalone module from the Soil Plant Atmosphere Water (SPAW) model. The SPAW model takes the data provided and models the hydrologic budget and is mainly used for agricultural fields and pond purposes (Saxton 2009). The Soil Water Characteristics module, shown in Figure 6-5, estimates the soil water holding characteristics using soil water tension and conductivity relationships with moisture (Saxton and Willey 2005). The properties entered into the module were a loamy sand soil with an average value for percent sand between the values given by AECOM. The wilting point, field capacity, available water, saturated hydraulic conductivity and a few other soil parameters are calculated and shown. The graph shows that the matric potential is significant when the soil moisture is low, but exponentially drops off as saturation occurs, then the hydraulic conductivity takes over.

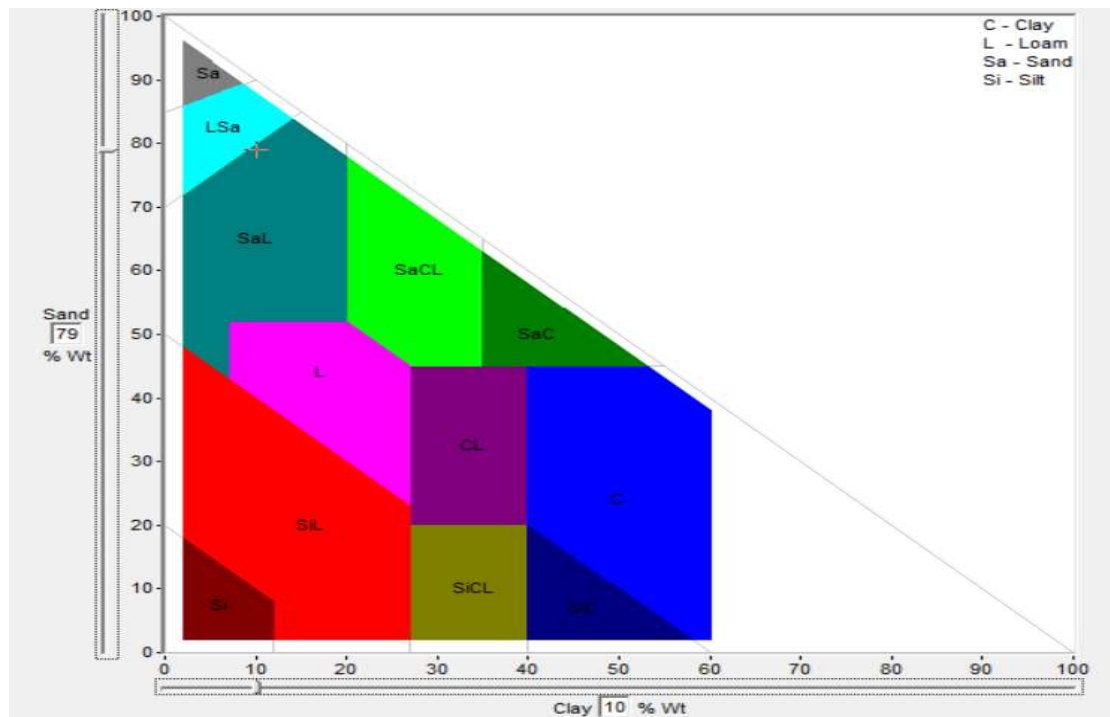


Figure 6-5: Loamy sand with 79% sand and 10% clay (75-82% sand and less than 10% clay as defined by AECOM) entered into the SPAW model

The initial deficit,  $M_d$ , needed for Green-Ampt calculations can be computed by subtracting the initial moisture content ( $\theta_i$ ) from the saturated moisture content ( $\theta_s$ ) (Rossman and Huber 2016). The maximum moisture deficit is most sensitive of the three Green-Ampt parameters for estimating runoff from pervious areas (Brakensiek and Onstad 1977). Since there is only a small portion of pervious surface in the research area, this value should not significantly alter the SWMM volume or timing of runoff significantly. The initial moisture content is variable depending on the antecedent conditions, thus the difference between field capacity and wilting point (available water) should be modeling as the lower bound for  $M_d$  (Bedient et al. 2013). The effective porosity provided in the tables from Rawls et al (1983) is another way of

determining the saturated moisture content ( $\theta_s$ ). The effective porosity accounts for the connected pore space between the soil particles that is available for water flow as opposed to the total porosity ( $\phi$ ) (Bedient et al. 2013). The available water provided by the SPAW model in inches/feet was subtracted from the effective porosity defined by Rawls et al (1983) to get the initial deficit for the soil type. This method was used to determine the value of the initial deficit of the soil. The initial values, and data sources, for all three Green-Ampt parameters for the bioswale and pervious surrounding area are shown in Table 6-6. The soil comprising pervious area around the bioswales was not defined by AECOM, thus the initial soil was assumed to be similar to the bioswale. The Green-Ampt values were chosen from the Rawls et al (1983) tables for a soil between Sandy loam and Loamy Sand.

*Table 6-6: Initial values entered in SWMM model and the data source/method used to determine the value*

	Bioswale	Pervious Area	Data Source
Suction Head (in)	2.41	3.00	Rawls et al (1983)
Saturated Hydraulic Conductivity (in/hr)	2.84	0.50	SPAW
Initial Deficit (a fraction)	0.33	0.40	Rawls et al (1983) & SPAW

Dry periods during continuous simulation are used to recover soil moisture, with the recovery rate empirically related to the hydraulic conductivity (Rossman 2015). Antecedent dry days were specified in SWMM as five days, but every calibration storm was run with a month of data analysis prior to reporting the storm to have an accurate assessment of the antecedent conditions of the soil. Not knowing the exact soil type and the spatial variation of this value



further complicates the estimation of the antecedent soil moisture conditions, as this estimation is based on soil properties and evapotranspiration rates (Lee et al. 2013)

### Outlet/Overflow structures

Water overflows the bioswale into an outlet structure, which is simulated in SWMM by another storage node of known area and height. A diagram of the outlet structure is shown in Figure 6-6 and the dimensions entered as storage curves into SWMM for the outlet structures are shown in Table 6-7. All the outlet structures have varying orifices and weirs to control the outflow from each bioswale to regulate the flow entering the sewer system. SMP C and SMP D have one orifice and SMP G has two orifices. All three outlets have an open rectangular weir on the same side as the orifices and then the top of the box is open and designed to overflow on all four sides during the 100-year flood. Table 6-8 shows the orifices and weirs for the outlet structures and their dimensions, inlet offsets and discharge coefficients.

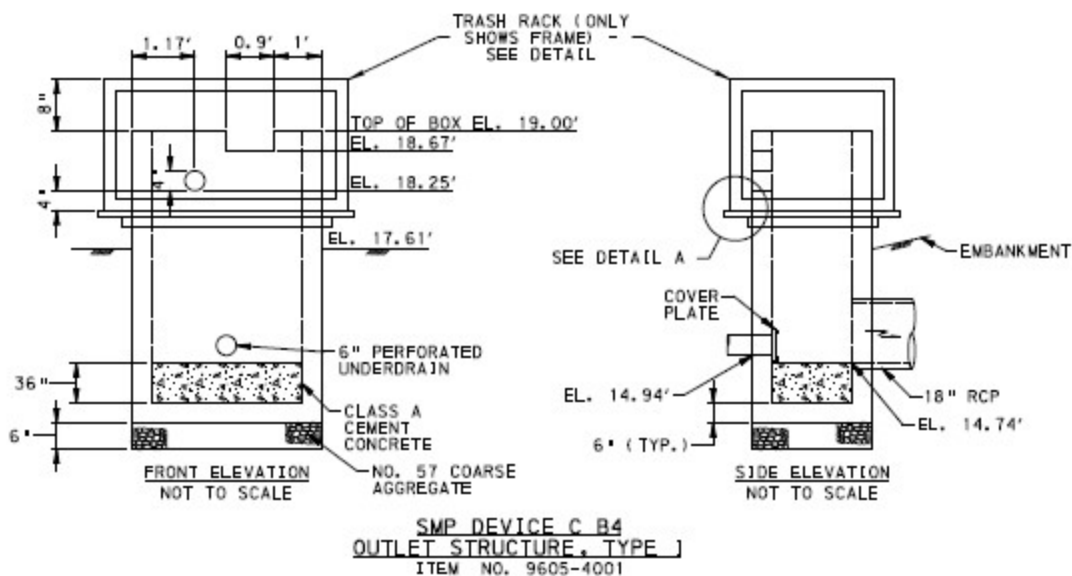


Figure 6-6: Outlet structure schematic for outlet B4 in SMP C.

Table 6-7: Storage Curves for each bioswale outlet structure

Storage Curves - Outlets					
B4-C		B5-D		B6-G	
Depth (ft)	Area (ft <sup>2</sup> )	Depth (ft)	Area (ft <sup>2</sup> )	Depth (ft)	Area (ft <sup>2</sup> )
0	5.62	0	4.69	0	4.69
0.04	7.54	0.08	7.54	0.42	7.54
4.14	7.54	4.17	7.54	5.13	7.54

The water leaving the outlet structure is measured as described previously, with a v-notch weir and pressure transducer. The weir is entered in SWMM with the same elevations and dimensions as the actual structure. Weir flow is calculated with the v-notch weir. After flowing over the weir, water runs to a manhole and then to a junction node where all the overflow from the three SMPs combine and flow goes to the outfall of the system. This outfall is meant to model the CSO pipe outfall to the Delaware River that all three outlet structures are assumed to be piped to during extreme weather events. The outfall parameters are estimated as no data was provided on the pipes and location of the outfall. To date, there has been very minimal overflow, so it is estimated that overflow is not a critical modeling parameter except for in extreme events. The outfall in SWMM defines the downstream boundary needed for kinematic wave flow routing (Rossman 2015). Only a single node/link can be connected to an outfall, which is why there is an extra node in the SWMM model before the outfall itself. A profile plot of the links and nodes in SMP C is shown in Figure 6-7. SMP D and G look similar, with D lacking the first two (right most) storage nodes and long pipe connecting to the exit ramp inlet.

Table 6-8: SWMM Side Orifices and weirs in the outlet structures

Orifices	Shape	Height (ft)	Width (ft)		Inlet Offset (ft)	Discharge Coeff.
CircularOrifice-C	Circular	0.33	0		3.51	0.65
ClosedRect-D	Rect_Closed	0.25	0.8		3.72	0.65
CircularOrifice-G	Circular	0.25	0		4.07	0.65
ClosedRect-G	Rect_Closed	0.25	0.4		4.32	0.65
Weirs	Type	Height (ft)	Length (ft)	Side Slope	Inlet Offset (ft)	Discharge Coeff.
TopBoxC	Transverse	1	12.88	0	1.39	3.33
OpenRectangular-C	Trapezoidal	0.33	0.9	0	1.06	3.33
TopBox-D	Transverse	1	15.54	0	1.51	3.33
TopBox-G	Transverse	1	14.79	0	2.41	3.33
OpenRectangular-G	Trapezoidal	0.63	0.75	0	1.78	3.33

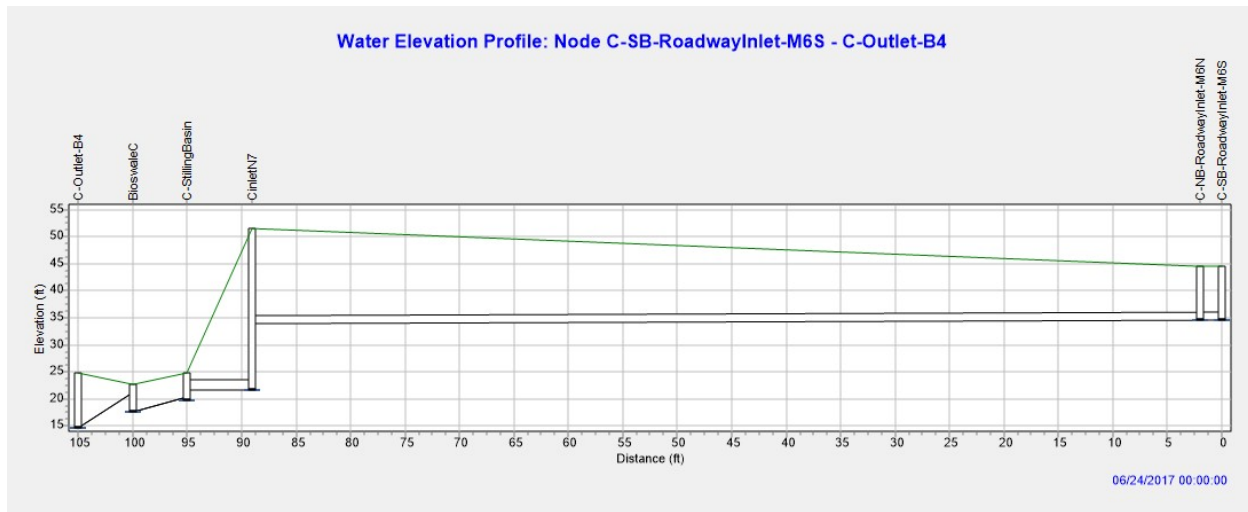


Figure 6-7: SWMM Profile Plot of SMP C

### Model Calibration Procedure

Model calibration attempts to quantitatively evaluate a “model’s ability to reproduce historic and future watershed behavior” (Krause et al. 2005). Using an uncalibrated model entails a certain risk, as uncalibrated models can produce similar results to predicted/recorded values or they can be off by a large factor (Urbonas 2007). This SWMM model was calibrated to create a

model that is “verifiable and truly representative of the physical system” (Sangal and Bonema 1994).

The design storm method and unit hydrographs have been the generally accepted way of modeling runoff for specific size storms. This methodology has been found to pose problems in modeling, as the results are not necessarily very accurate for regions that have spatial rainfall variability (Urbonas 2007), as well as the nonlinear dynamics between rainfall and runoff (Wang and Altunkaynak 2012). Thus, a continuous record of data was chosen, as it is more useful when creating a watershed model. When calibrating a model, having a continuous data record has been shown to produce more accurate calibration values, as the long record allows the initially assumed soil conditions to become negligible (Tan et al. 2008).

The calibration was event-based, meaning that the parameters were modified and calibrated to specific storms, following a common approach used in other studies (Niazi et al. 2017). A study by Tan et al. (2008) found that small watersheds can be calibrated on a per storm basis if there are a variety of different storm events that have varying peak flow, total runoff volume, and initial soil moisture conditions. It was also found that a continuous record calibration process produces more accurate runoff volumes and an event based calibration produces better overall hydrograph shape (Tan et al. 2008). This study shows that newly instrumented sites with limited data records can be calibrated with relative effectiveness.

The calibration method follows that of the standard calibration of many watershed models of manual calibration (Niazi et al. 2017). The model was calibrated by changing one parameter at a time and observing the modeled versus observed results for measured storms. Typically, the measured parameters are assumed to be accurate and fixed values, and only estimated or inferred values should be altered during calibration (Choi and Ball 2002). However,

due to error in both measured and estimated values, some “known” parameters are often altered during model calibration (Temprano et al. 2005).

The model was calibrated so that a comparison could be made between the model results and the design expectations. This was used to evaluate the model’s suitability for use in predicting performance. First the goal was to match the volume of runoff from impervious area entering each of the basins through the system of pipes. This was followed by calibrating the timing of the impervious runoff inflow hydrograph. The third calibration was to calibrate the basin ponding, which included the timing of the pervious runoff and the basin properties. Calibration of this SWMM model for the three different calibration tasks was conducted by adjusting the soil infiltration parameters, drainage areas, flow pathways and more, to minimize the error between the modeled and observed values. These results will be used to evaluate the storm hydrographs for their timing, peaks, volumes and limbs of the hydrograph (Krause et al. 2005). To calibrate the model, the most sensitive parameter was chosen first to modify, i.e. for inflow volume, the area was the most sensitive parameter and was hypothesized to be considerably less than the design standard based on the amount of inflow measured. After calibrating for area, the model was calibrated for less sensitive variables until the model achieved a high enough statistical relationship (described below).

The calibration storms that the model was calibrated against were ideally larger than one inch (but one calibration storm was less than one inch), since the design standards are supposed to capture the one-inch storm without having overflow into the sewer system. The storms used to calibrate the model are shown in Table 6-9. Since we had a relatively short period of continuous data (Starting in March 2017) with only a few storms above or around the desired one inch storm volume, only five storms were considered to calibrate the model. Two storms were used to verify

the model as verification is important to validate the model performance holds up outside of the calibration period (Niazi et al. 2017).

*Table 6-9: Calibration and Verification Storm values*

	<b>Storm Date</b>	<b>Total Rainfall (mm)</b>	<b>Total Rainfall (in)</b>	<b>Duration (hr)</b>	<b>Max Intensity (mm/5min)</b>
Calibration Storm 1	3/30/17	42.42	1.67	28.9	1.02
Calibration Storm 2	4/25/17	18.03	0.71	23.1	1.78
Calibration Storm 3	5/5/17	28.45	1.12	6.3	1.78
Calibration Storm 4	5/13/17	48.26	1.90	19.1	1.27
Calibration Storm 5 *	5/25/17	19.81	0.78	6.9	1.02
	5/25/17	23.62	0.93	5.9	9.65
Verification Storm 1	6/6/17	14.48	0.57	2.2	3.30
Verification Storm 2	6/24/17	27.94	1.10	8.5	8.64

*\* indicates a back to back storm, where 6 hours of no precipitation occur before the start of a new storm within the same day*

### Inflow Volume

The Directly Connected Impervious Area (DCIA) runoff volume was calibrated against the Blue Siren area velocity flow meters installed in the inlets for flow and depth as discussed in Chapter 3. Using Table 10 storms, the goal was to first match the volume of runoff from SWMM to the measured amount from the Blue Siren Area Velocity sensors. The volume of runoff from the drainage area of each subcatchment was varied by changing the percentage of original DCIA design area. Normally drainage area, in a scenario like this would be a fixed value, but due to the observed flows it was hypothesized that the drainage area was different than designed because of ongoing construction. For each calibration storm, the percentage of DCIA contributing to each bioswale was adjusted individually until the volume was close to the recorded volume of flow.

### Inflow Timing

After calibrating the DCIA of each bioswale for each storm, other parameters were varied to get the timing of the hydrograph to match the recorded hydrograph. An extensive literature review was conducted by Niazi et al. (2017) and they found that SWMM models are usually sensitive to impervious surface parameters, such as: percentage impervious, impervious depression storage, and the impervious Manning's roughness coefficient. Width, slope, and the impervious Manning's roughness coefficient are inputs in the Manning's equation (Equation 3), which SWMM uses to compute overland flow and velocity (Niazi et al. 2017). Thus, altering these values have direct impacts on the runoff flow timing. Impervious width, slope, Manning's roughness coefficient ( $n$ ), along with depression storage, were altered in SWMM even though the estimated parameters should be standard for newly designed roadway. The depression storage influences the volume of runoff, but was included in the timing calibration to affect the initial timing of the storm.

### Pond Depth and Timing

When the inflow volume and timing were calibrated, the bioswale pond was calibrated. This included altering the Green-Ampt parameters (saturated hydraulic conductivity, suction head, and initial deficit), slope of the pervious runoff, Manning's roughness coefficient, and impervious abstractions/depression storage for the bioswale and the pervious subcatchment. Short and high intensity storms are noted to be more useful when calibrating impervious surfaces. Table 6-10 shows the ponding in SMP C and D for storms available at the time of calibration. SMP G is not included due to the leakage observed during the Simulated Runoff Test (SRT) on July 19<sup>th</sup>, 2017, which was discussed in Chapter 3.



*Table 6-10: Pond Calibration Data for SMP C and SMP D. The storm on 3/30/17 was not used as it is considered an outlier. The storm on 5/13/17 was not used for calibration, but the values are shown since ponding was significant.*

	<b>Date</b>	<b>Total Rainfall (mm)</b>	<b>SMP C Max. Depth (mm)</b>	<b>SMP D Max. Depth (mm)</b>
Storm 1	3/30/17	42.4	118.5	11.0
Storm 2	5/13/17	48.3	92.0	--
Verification Storm	5/25/17	43.4	65.1	82.9
Calibration Storm	6/24/17	27.9	--	105.6

Long and steady rainfall is more important when calibrating pervious and infiltration parameters, due to the significant infiltration occurring during these events (Wreck Pond Brook Watershed Technical Advisory Committee 2008). Ideally, the pond should first be calibrated to storms that have rainfall intensities under the infiltration amount, so that all ponding that occurs is directly linked to the impervious runoff (Sangal and Bonema 1994). If the model depth is less than the measured, then the infiltration capacity should be decreased, and the values should be increased if the model produces higher values than the measured amount (Sangal and Bonema 1994). After calibrating the pond area, then storms with higher intensities than the precipitation rate can be used to calibrate the inflow from the pervious areas. Due to the limited amount of measured ponding (shown in Table 6-10) and small record of storms, the pond was not calibrated as described above. Any storm with significant ponding was used to calibrate the bioswale parameters. A third calibration could occur for any overflow that leaves the system based on the v-notch weirs, but as of this date no overflow has occurred, except for the SRT on July 19<sup>th</sup>, 2017.

### *Model Evaluation*

An evaluation of a hydrologic model is needed to assess a model's ability to reproduce past and future estimates of a watershed behavior (Krause et al. 2005). It is also necessary to use

a method which indicates the effect of changing model parameters on the model results. To minimize errors, the model results and the measured performance storm hydrographs were calibrated by first comparing subjectively using a visual inspection (Krause et al. 2005). Then, the relative “closeness” of the model to reality was compared quantitatively or objectively using total volume differences and efficiency criteria. Efficiency criteria are mathematical comparisons of model simulation and measured/observed data (Beven 2001). Most types of efficiency criteria use the squared absolute sum of the difference between the model results and the observed results at defined times steps, which are then “normalized by a measure of the variability in the observations” (Krause et al. 2005). This places higher emphasis on the larger errors due to the squared function. Thus, using this type of efficiency criteria causes model calibration to place higher emphasis on fitting the larger flow values (Krause et al. 2005). The calibration and efficiency criteria used in are discussed below.

To test the relationship between the model accuracy and the actual performance of the bioswales, a statistical analysis using Nash-Sutcliff Efficiency (NSE) and the coefficient of determination ( $r^2$ ) was used. Nash and Sutcliff proposed an equation for efficiency, where NSE is the “proportion of the initial variance” accounted for in the model, shown in Equation 6-5 (Krause et al. 2005; Nash and Sutcliffe 1970),

$$NSE = 1 - \frac{\sum_{i=1}^n (O_i - P_i)^2}{\sum_{i=1}^n (O_i - \underline{O})^2} \quad 6-5$$

where  $O$  is the observed values,  $\underline{O}$  is the observed average value, and  $P$  is the predicted values. The range of efficiency, NSE, values is between  $-\infty$  and 1, with 1 being a perfect fit. Anything less than zero indicates that the average observed value is a better predictor than the model and that the model is producing unacceptable results (Krause et al. 2005; Santhi et al. 2001). NSE

values are calculated by squaring the differences, resulting in overestimation of larger values and underrepresentation of lower values (Legates and McCabe Jr. 1999). Legates and McCabe Jr. (1999) suggested that the NSE coefficient was a better measure for goodness of fit for hydrologic models than correlation based methods such as  $r^2$ . Equation 6-6 states the coefficient of determination ( $r^2$ ) equation, with  $O$  and  $P$  as the observed and predicted values (Krause et al. 2005).

$$r^2 = \left( \frac{\sum_{i=1}^n (O_i - \bar{O})(P_i - \bar{P})}{\sqrt{\sum_{i=1}^n (O_i - \bar{O})^2} \sqrt{\sum_{i=1}^n (P_i - \bar{P})^2}} \right)^2 \quad 6-6$$

The range of values is between 0 and 1, with 1 describing a perfect match between observed and predicted dispersion values.  $R^2$  values predict dispersion, thus systematic over or under predictions will still have high  $r^2$  values (Krause et al. 2005). Many model evaluations use a combination of methods to evaluate the effectiveness of their hydrologic models. We used the Nash Sutcliff efficiency (NSE) and the coefficient of determination ( $r^2$ ). A previous study found that values over 0.5 are acceptable for NSE and values over 0.6 are acceptable for correlation coefficients to measure of accuracy of a hydrologic model (Santhi et al. 2001).

#### *Site Data to Date*

The start of data collection was designed to test the instrumentation. During this initial data collection period there were times when instrumentation was not performing to standard. This required replacement, calibration, or manual changes to the sensors and data. Though this period was a challenge, we could collect individual events for each bioswale to use for calibrating the SWMM model. For example, there were challenges with one brand of pressure transducers and the blue siren area velocity meter which caused data inaccuracies. In several cases, sensors had to be returned to the manufacturer several times for correction. One sensor

added to support our partners drew too much power and drained the battery. This extended the initial test data collection period, but each issue was resolved.

## **SWMM Results**

The model calibration results are presented in four sequential sections, following the process described previously: methods, inflow volume, inflow timing, and pond depth. Each calibration step is sequential and builds on the previous calibration step, so that the final calibration completes the calibration for the entire model.

The range of storms that the SWMM model used for calibration are shown in Table 6-12 and Figure 6-8. There were two larger storms, March 30<sup>th</sup> and May 13<sup>th</sup>, a large back-to-back storm in one day, and the rest of the storms were clustered around each other ranging from 0.6 inches (15 mm) to 1.2 inches (30 mm). The April 25<sup>th</sup> storm along with the March 30<sup>th</sup> and May 13<sup>th</sup> had longer durations than the other five storms. This range of duration, precipitation and intensity storms is a good basis to calibrate a watershed model. The volume of inflow measured by the inlet area velocity sensors are also provided in Table 6-11. SMP C has the largest recorded volumes, ranging from 4,130 to 51,410 liters, and SMP D and G have much smaller volumes that never exceed 10,000 liters.

Table 6-11: Calibration/Validation storm properties

	Precipitation (mm)	Intensity (high or low)	Duration (Long or Short)	Measured Volume (l)		
				SMP C	SMP D	SMP G
<b>March 30th</b>	42.42	Low	Long	4,130	9,100	660
<b>April 25th</b>	18.03	Low	Long	8,820	6,320	1,230
<b>May 5th</b>	28.45	Low	Short	23,450	6,880	3,420
<b>May 13th</b>	48.26	Low	Long	51,410	3,420	4,030
<b>*May 25<sup>th</sup></b>	43.43	High	Short	43,700	2,470	5,330
<b>June 6th</b>	14.48	High	Short	8,470	890	1,830
<b>June 24th</b>	27.94	High	Short	13,660	1,480	3,920

\* indicates a back to back storm, where 6 hours of no precipitation occur before the start of a new storm within the same day

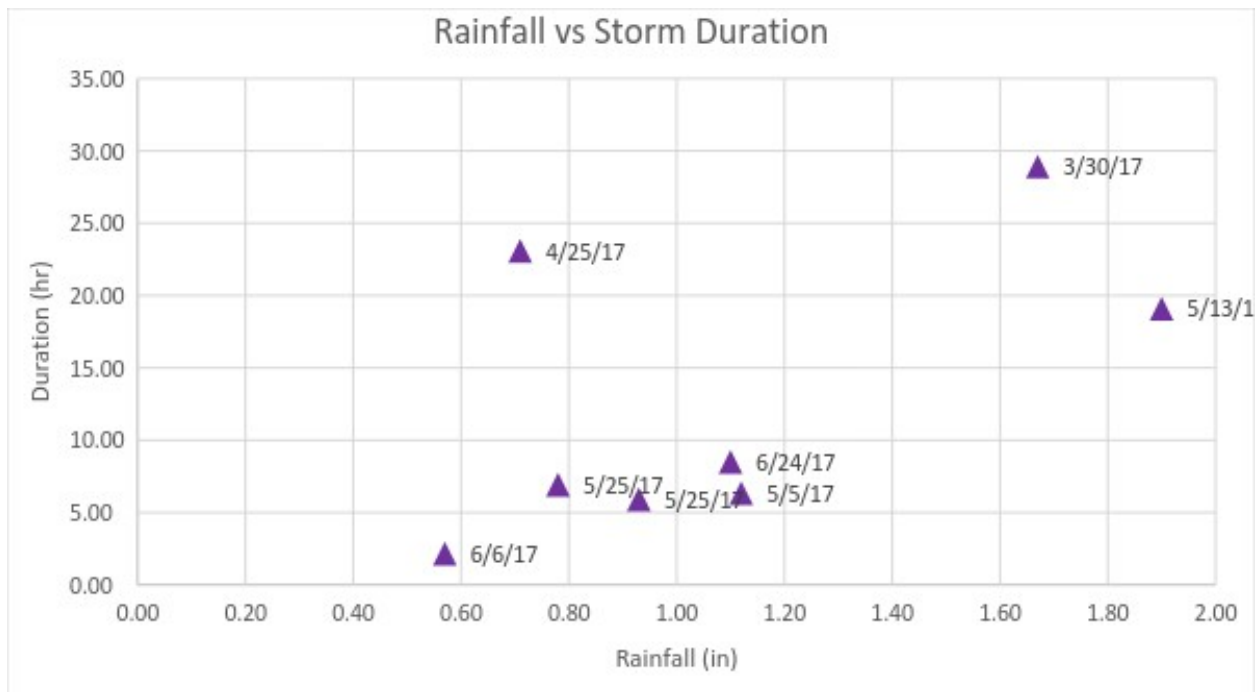


Figure 6-8: Rainfall versus Duration of a storm event (including the 6 hours after the last measured precipitation)

### Inflow Calibration

The inflow calibration was split into two steps: volume and timing. The measured inflow from the area velocity sensors was used to calculate total runoff and inflow into the rock stilling basin. Calibration was accomplished by varying the DCIA until the modeled volume matched the

measured inflow volume. Following the area calibration, the timing of the modeled inflow hydrograph was calibrated to match the timing, shape and peak of the measured hydrograph discharging to rock stilling basin for each bioswale. Results are given for the two calibration processes and then a discussion follows.

### Inflow Volume Calibration Results

The first step was to calibrate the volume of inflow captured from the highway and piping system underneath I-95. As the rainfall to runoff changed significantly between storms, the percent of original area of DCIA was varied for each subcatchment until the volume of runoff from the SWMM model matched the inflow volume measured by the Blue Siren Area Velocity sensor. This uncertainty will be discussed later in the chapter. Table 6-12 shows the percent of contributing area calculated for each storm based on the measured volume. The storm on March 30<sup>th</sup>, 2017, for example, has a much smaller percentage of contributing area than any other storm for SMP C and G, despite the large size of the storm (42.42 mm) and much larger contributing area for SMP D. Due to this observation the storm on March 30<sup>th</sup>, 2017 is treated like an outlier for the rest of the calibration process.

*Table 6-12: Percent of original area calibrated for each storm*

	Precipitation (mm)	Intensity (high or low)	Duration (Long or Short)	Volume - Calibrated % of Area		
				SMP C	SMP D	SMP G
<b>March 30th</b>	42.42	Low	Long	2	36	1
<b>April 25th</b>	18.03	Low	Long	14	47	5
<b>May 5th</b>	28.45	Low	Short	24	33	8
<b>May 13th</b>	48.26	Low	Long	30	13	5
<b>May 25th - B2B</b>	43.43	High	Short	28	7	7
<b>June 6th</b>	14.48	High	Short	20	10	7
<b>June 24th</b>	27.94	High	Short	14	7	8

Only SMP G shows reasonable variance in contributing drainage area between each storm. The variance is only three percentage points, between five and eight percent of the design area. SMP D is noted to have the widest variance in contributing impervious drainage area. The percentage varies between 47 percent and 7 percent of the DCIA. This means that the volume of flow recorded is between 57 and 93 percent less than what was expected when using the original drainage area. SMP C, which has the largest designed drainage area, has the largest average percentage of area contributing (between 14 and 30 percent) of the three bioswale drainage areas.

The graphical representation of Table 6-12 is shown in Figure 6-9, comparing the precipitation amount to the percent of DCIA contributing for each storm. SMP D's contributing area can be seen in orange there does not seem to be a significant trend in the data based on precipitation. SMP C looks like it has a positive relationship, with larger storms having a larger contributing area, but more data is needed to confirm this trend. The percentage of DCIA for SMP G does not change significantly based on precipitation, an expected result at the start of analysis. The drainage area is expected to stay constant over a calibration period, producing runoff volumes in accordance to rainfall amounts.

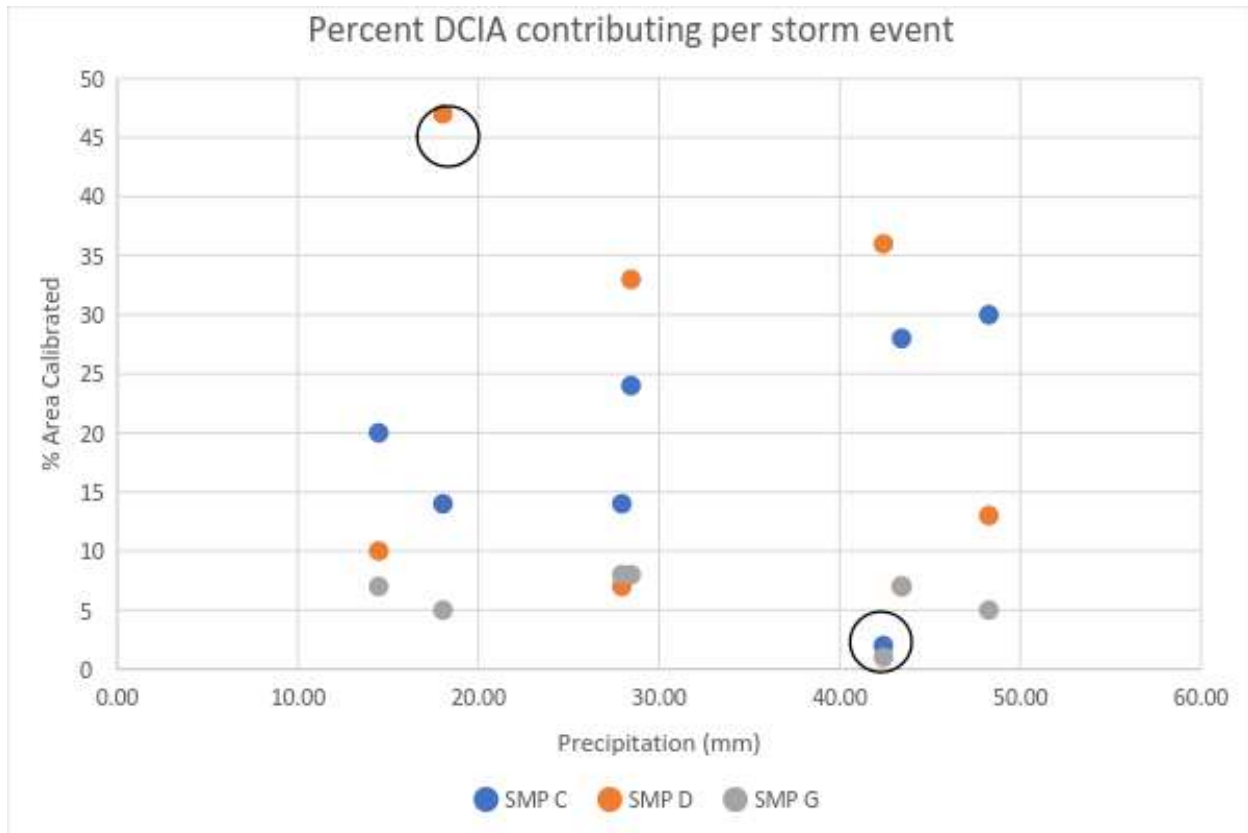


Figure 6-9: Percent of contributing area of SMP C, D, and G for each storm. The March 30th storm is circled and considered to be an outlier.

One hypothesis based on the reduced volumes measured for each storm was that only the exit ramp subcatchment area was contributing to each of the inlets. Exit ramps are 24 percent of the DCIA for SMP C, 100 percent for SMP D, and 39 percent for SMP G. The volume reduction seen could explain SMP C's calibrated area, but not SMP D or G. SMP D and SMP G both have contributing areas significantly under the exit ramp drainage area, meaning there must be another reason for the significant change in DCIA. The SWMM model was altered to only include the exit ramps to explore this idea and Table 6-13 shows the percent of area captured by the new model. SMP D and G measure significantly more with only the exit ramps in the model than was actually measured. SMP C varies less than the other bioswales, but still is not consistent in its



variation. Thus, using only the exit ramp drainage area does not entirely explain the runoff volume discrepancy.

*Table 6-13: SWMM Volume percentage of measured volume with only Exit Ramps*

	<b>SWMM Volume Percent of Measured</b>		
Date	<b>SMP C</b>	<b>SMP D</b>	<b>SMP G</b>
4/25/2017	72	112	62
5/5/2017	2	236	377
5/13/2017	19	980	588
5/25/2017	14	1345	404
6/6/2017	72	1322	422
6/24/2017	83	1552	378

### Inflow Timing Calibration

After calibrating the contributing impervious drainage area entering through the inlet pipe it was determined that each storm needed to be calibrated for area prior to any other calibration due to the wide variance of DCIA. The method used for calibrating the DCIA hydrograph timing was the Nash Sutcliff Efficiency (NSE) and the coefficient of determination ( $r^2$ ) as discussed previously. The parameters changed for all the bioswales that resulted in the best NSE and coefficient of determination values for the inflow were: reducing the Manning's roughness coefficient from 0.015 to 0.014, reflecting the incorporation of the concrete (0.014) exit ramp to the asphalt (0.015) travel lanes; increasing conduit roughness from 0.012 to 0.024 for the pipes under the highway to match the pipe roughness provided by AECOM for the pipe discharging in the bioswale; decreasing the slope of the subcatchment from 0.5 to 0.25 percent to push back the peak of the hydrograph; and decreasing the width each of the subcatchments to 80% of the design width, to slightly shift the peak of the hydrograph. The results compared to the

uncalibrated model of the four calibration storms, excluding the March 30<sup>th</sup>, 2017 storm (deemed an outlier for volume), are shown in Table 6-14.

*Table 6-14: Original versus Calibrated Volume percent captured, NSE and  $r^2$  values*

	SMP C			SMP D			SMP G		
	<b>Vol % Diff</b>	<b>NSE</b>	<b><math>r^2</math></b>	<b>Vol % Diff</b>	<b>NSE</b>	<b><math>r^2</math></b>	<b>Vol % Diff</b>	<b>NSE</b>	<b><math>r^2</math></b>
4/25/2017 Original	0.7	-15.970	0.052	3.5	-0.49	0.181	3.5	-3.26	0.15
4/25/17 with timing	0.7	-13.101	0.072	5.6	-2.35	0.18	76.7	-0.46	0.11
5/5/17 Original	0.1	-2.277	0.472	1.5	0.092	0.563	6.5	0.144	0.516
5/5/17 with timing	2.2	-1.548	0.553	7.4	0.46	0.66	3.5	0.425	0.605
5/13/2017 Original	16.5	-0.544	0.592	236.9	-4.622	0.668	61.3	-0.081	0.754
5/13/17 with timing	0.4	-1.014	0.637	63.6	-0.528	0.653	1.1	0.777	0.789
5/25/2017 Original	5.2	-11.839	0.07	8.4	-4.879	0.01	4.3	-9.029	0.023
5/25/17 with timing	6.8	-8.916	0.092	8.4	-8.940	0.010	8.6	-5.106	0.045

Table 6-14 shows that only one storm for one basin could obtain a NSE value of over 0.5 as recommended by Santhi et al. (2001), which was the May 13<sup>th</sup>, 2017 storm for SMP G. A few storms achieved the  $r^2$  of greater than 0.6 as recommended by Santhi et al. (2001); May 5<sup>th</sup>, 2017 for SMP D and G; and May 13<sup>th</sup>, 2017 for SMP C, D, and G. SMP C was unable to achieve positive NSE values for any storm, with the calibrated NSE varying between -13 to -1.0. Some storms even had a negative response to calibration, with the storm on May 13<sup>th</sup>, 2017 changing from -0.544 to -1.014 NSE for SMP C (but the coefficient of determination values increased, indicating better performance). SMP G had the best response to timing calibrations, which was expected as it had the least variable drainage area. This indicates that there was potentially very

similar or constant roadway and instrumentation conditions during the period of calibration (more discussion below). Figure 6-10 shows the hydrograph for the calibrated storm with the best NSE value on May 13<sup>th</sup>, 2017 for SMP G. The calibrated model does not match the peak flow rate measured by the sensor, but matches the volume and general shape/timing of the hydrograph.

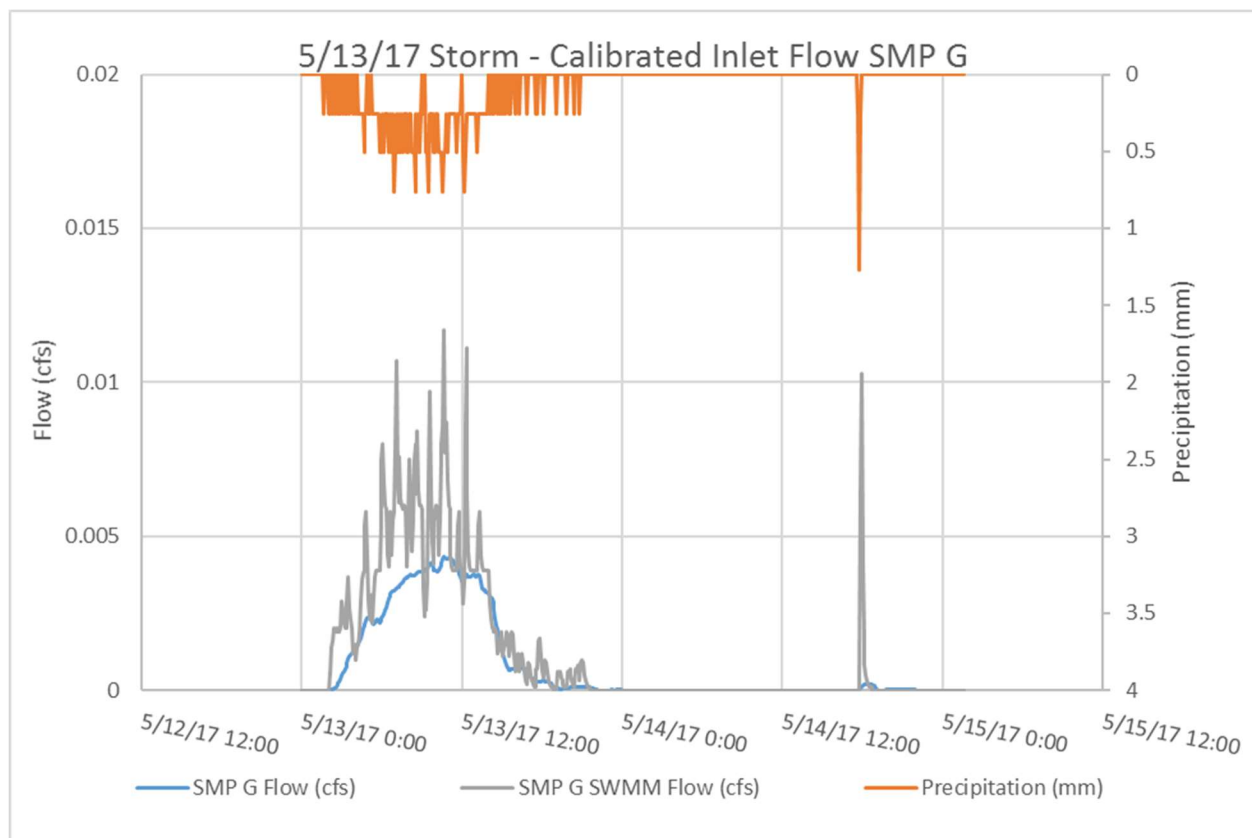


*Figure 6-10: SMP G measured versus calibrated inflow during 5/13 storm (48.26 mm precipitation)*

### Inflow Results Discussion

The variability of the inflow volumes suggest that the system is much more variable and complex than originally thought. Many of the possible reasons that the DCIA inflows differ in volume and hydrograph timing are linked. As discussed in Chapter 5, the existing topography

results in much of the runoff converging on the center of the highway, rather than flowing toward the storm inlets. The highway is currently still in a construction state, with lanes shifted until the final highway is complete. The section before and after the research site are under active construction (to the north) or slated for construction in the next 5-10 years (to the south). This resulted in the semi-permanent installation of New Jersey Barriers lining the new construction of the Girard Street Exit ramp as seen in Figure 6-11. It is hypothesized that these barriers are affecting the drainage area per storm and altering the shape of the hydrograph. The openings under the barriers can clog and thus, could be changing the amount of water getting through to the inlet based on cleaning schedules. There are two types of openings in the barriers, the one that is shown in Figure 6-11 is more frequently used and has one opening that is 30.75 inches (781 mm) long by 1.75 inches (44 mm) high. The second and more infrequently seen type of barrier has two openings in the bottom that are 24 inches (610 mm) by 4.25 inches (108 mm) high. In addition, the New Jersey barriers are assumed to be placed in a location where the flow stream lines would naturally travel past the openings in the barriers and flow would be carried through the openings to continue their natural flow path. As commonly seen in the field, debris could also affect the inlets themselves, since they are on the roadway and could cause bypass of the runoff to the next inlet. The limited size in addition to deposition of trash and sediment is hypothesized to be impeding and slowing the flow that gets to the inlets. It is also assumed that the barriers are infrequently maintained, so deposition can accumulate, further impeding the flow over time.



*Figure 6-11: New Jersey Barriers defining the temporary travel lanes. The opening is circled to show where flow can get through.*

It is concluded that the flow path within the drainage area has been changing in an inconsistent way, which is affecting the volume and timing of inflow to the bioswales. To attempt to match the results, the catchment slope was decreased to 0.25 percent to smooth the hydrograph by slowing the flow to the inlet, but this did not change the hydrograph significantly. The SWMM model has extreme peaks, which follow the precipitation trends. The curve number of the roadway is very high since it is all impervious, thus the Manning's equation (Equation 7) for overland flow will produce runoff very soon after the precipitation falls. The 'flashiness' in the hydrograph shape makes sense for before the runoff enters the drop inlet, but not for after it drops in elevation and reaches the stilling basin below. The inlets to the bioswales have a significant drop and visual inspection during the SRT in SMP A showed that there is significant energy dissipation in the drop inlets. Thus, it is possible that the piping system is not modeled in SWMM correctly and/or may not have the capabilities to be modeled easily or accurately. Since dynamic wave flow routing created large continuity errors, kinematic wave routing was used. Kinematic wave routing is incapable of modeling energy losses in conduit or links. SWMM also does not have a way of measuring energy loss in storage nodes, so using dynamic wave flow

routing would not solve a significant portion of the energy loss, which is needed to smooth out the hydrograph shape.

The barriers were hypothesized to be changing the timing and volume of runoff, thus on May 28<sup>th</sup>, they were moved from a straight line to the configuration shown in Figure 6-12. Visual inspection of the barrier movement, as seen in Figure 6-12, show that the barriers moved are immediately upstream of the inlet which drains to SMP C (N7). It is unclear if there is enough space for the flow path to get to the inlet, or if the water still bypasses the structure. To see if the change in barriers had any effect on the volume and timing of inflow to SMP C, two storms were simulated in SWMM, July 6<sup>th</sup>, 2017 (14.48 mm) and July 24<sup>th</sup>, 2017 (27.94 mm). The movement of the barriers did not have a noticeable effect on the volume or timing of runoff. Both the storms after the movement of the barriers were high intensity precipitation storms, which plays an impact on the NSE of the calibration. SWMM predicts much faster time to peak than the measured performance. The measured results do not have a notable response to high intensity precipitation, where the SWMM model does. The size of the opening in the barriers could affect the flow through them at different intensity and duration storms. The higher intensity storms could be creating a flow path that is bypassing the New Jersey barrier openings due to their limited size. This muting and transposition of the peak flow in high intensity storms could also be a factor of the Blue Siren area velocity sensor measurements, which average multiple point measurements. Thus, the sensor could be averaging out the peak flow values. Figure 6-10 shows that there was a high intensity rainfall peak after the main rainfall that occurred on May 13<sup>th</sup>, 2017. SWMM estimates a large inflow peak for this brief high intensity rain, but the measured results barely register the flow.



*Figure 6-12: Barriers moved from single line, to form an opening in front of SMP C exit ramp inlet (shown on the right edge of photo, indicated with the blue arrow)*

The logical response for an impervious surface would be to have a response relative to the precipitation. Thus, as previously hypothesized, there is a secondary system that is dampening the measured result of precipitation on the roadway, which is potentially pipe losses not accounted for in SWMM. To mimic the New Jersey barriers and this secondary muting response, the model was artificially changed by lengthening and increasing the roughness of the inlet pipes as well as the roughness and width of the subcatchment. None of these alterations provided a significant improvement in the SWMM hydrograph modeling of the system.

SMP D also had some storms that had negative response to calibration, but the large discrepancy in volume and timing seen in SMP D could be due to the roadway surface construction zone setting. Figure 6-13 shows the only inlet draining to SMP D is currently (August 2017) blocked by a station built to rinse construction machinery, which would be changing the flow path to the drainage area for SMP D. The amount of time that this structure has been here is unknown, but could explain the extreme variance in drainage area and timing discrepancies seen in SMP D. A similar structure has recently (as of August 2017) been erected

in front of SMP G, so future storms may be impacted. These structures and accompanying activity would explain any flow that the Area Velocity sensors record during times when there is no precipitation. Note that these stations have been removed as of September 2017.



*Figure 6-13: Inlet draining to SMP D, with construction blockade immediately upstream shown by the big yellow arrow. The smaller arrow is pointing to the construction blockade recently installed next to the inlet to SMP G.*

SMP D only has one drainage subcatchment, which is comprised of a section of the Girard Street exit ramp. The New Jersey barriers (in addition to the constructed structure) could be clogging the flow as previously discussed, which would cause the excess flow to go to either SMP C or SMP G (depending on the slopes). This variation could result in the large variation of 10-50% of contributing area that is seen going into SMP D on various storms. This could also be the reason that SMP C has a varying contributing area, if the excess flow from SMP D is



rerouted to SMP C. If flow from a different drainage area enters SMP C, it would decrease the NSE values, as the variable inflow is not represented by the model. The negative response to calibration seen for a few storms could be for this reason. Different storms will cause drainage in different places that alter timing as well as volume, which make a very difficult calibration process.

The March 30<sup>th</sup> storm, which was considered an outlier, had significantly different volume that could be due to flow from C being captured by SMP D or the depth sensor in the area velocity sensors being calibrated the week before. Flow meters have a range of resolution, which can slightly skew results. The goal of any flow meter monitoring is that the skew is small enough that the data can still be used to provide analysis of how a system is working. The Blue Siren sensor is sensitive to low depth, therefore errors during low depth in the pipe could be contributing to unacceptable skewed results. Due to the previously discussed sensitivity to low water depth, low intensity and small precipitation events would be the most effected with this sensor. Also, previously mentioned is the way that the sensor averages velocity values that are used to calculate SWMM. If the average is occurring over too large of a time interval, the timing and peak of the flow will be skewed. A calibrated SWMM model could provide a more accurate representation of the small/low intensity storms than the flow meter, by using the Manning's equation to calculate flow for intensities and depths.

After analyzing the depth data read by the Blue Siren sensors, it was noticed that the sensors read zero depth immediately after calibration, but gradually crept above zero during times of non-precipitation. This drift in the zero reading for depth was especially noticeable for SMP C, where the depth gradually read up to around 30 millimeters (1.18 inches). This high of a reading when it should be reading zero is outside the resolution stated by the manufacturer. This

complication could be contributing to the low NSE and  $r^2$  values calculated for this bioswale, as the recorded depth may be creating flow exceeding actual flow. This could explain Figure 6-14, where the measured flow extends for hours after the model predicts, where the flow does not extend that long in SMP D or SMP G (Figure 6-11). Due to the challenges in determining the drainage area, calibration of this site would normally not occur. Errors with low depth readings are not something that is expected to be an issue during calibration in the future as a larger data set will allow calibration to occur with larger storm events. Additionally, when the drainage area has been returned to the designed area, the volume of runoff will be much higher, so low depth in the inlet pipes will be less significant.

Another concern found, was a leaking bridge joint on Shackamaxon Street overpass, which is shown in Figure 6-15. Although the leak is occurring over the drainage area for SMP A, it illustrates that there are construction errors that can change the research landscape. Leaks in the wall above SMP A were also detected during the August SRT.

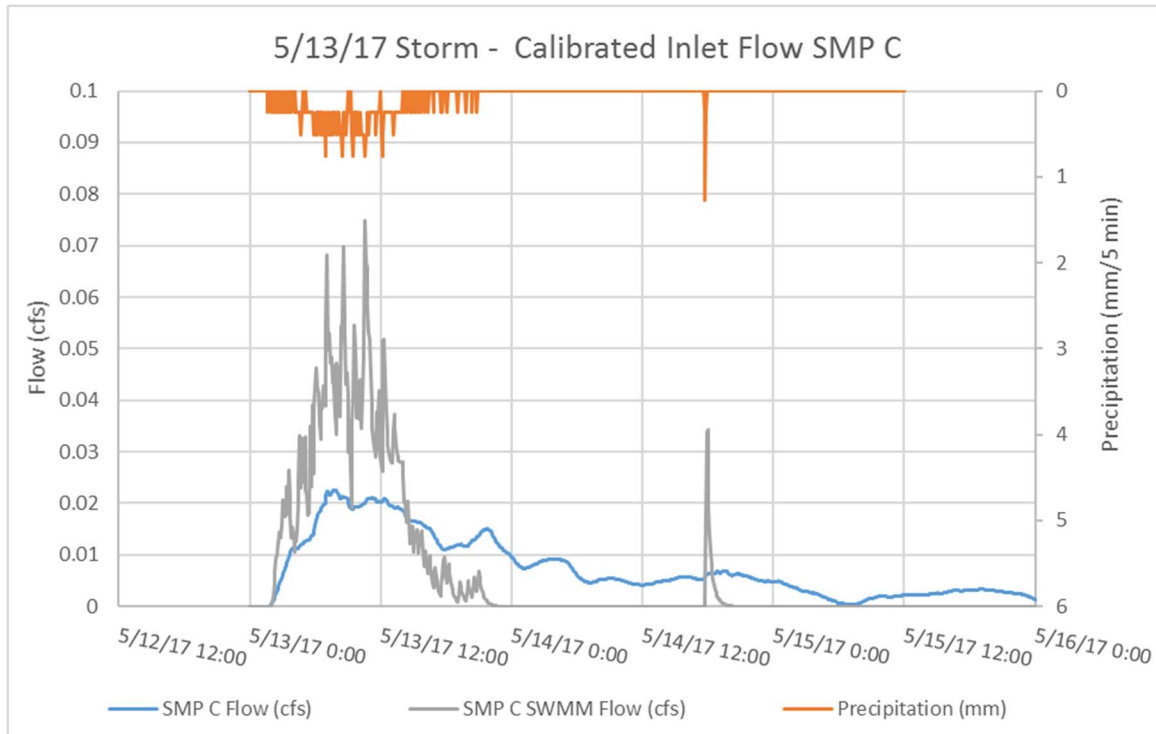


Figure 6-14: SMP C calibrated for timing and area – 5/13/17 Storm (48.26 mm precipitation)

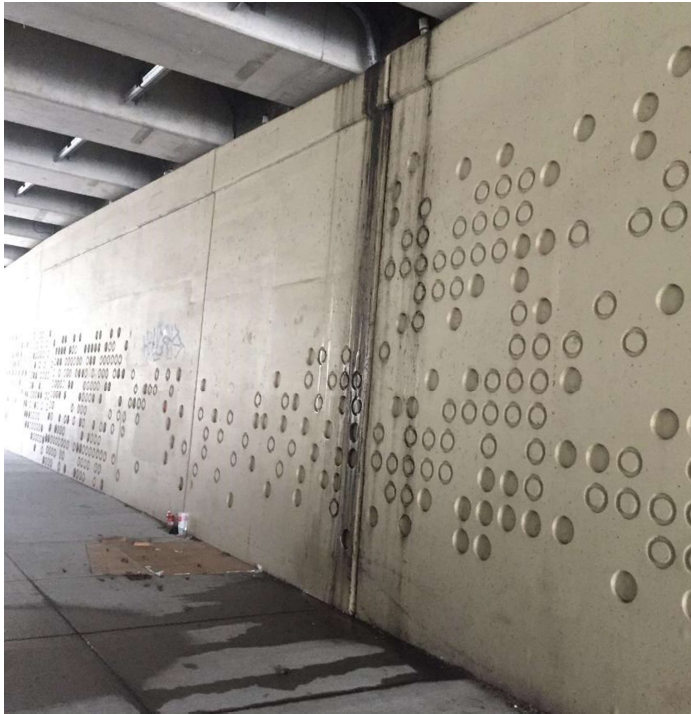


Figure 6-15: Shackamaxon Street overpass leak under drainage area for SMP A during July 6th storm (1.65 mm of precipitation had occurred in 1.5 hours at the time of this photo).

### Inflow Results Summary

Despite the variable and changing watershed area and flow path for each bioswale, the timing and runoff volume were balanced by using different DCIA for each bioswale per storm event. This alteration is a first approximation. However, it would not be sufficient to explore watershed performance to show regulatory compliance or verify drainage area/inflow designs.

### *Pond Calibration and Discussion*

The pond calibration involved many more parameters as calibration had to take into consideration the bioswale itself, the rock stilling basin, the pervious area around the bioswale, and the subcatchment representing the surface area of the bioswale. After modifying and calibrating the inflow volume, the ponding and outlet depth were calibrated. Due to reduced drainage area, there were very few storms with significant ponding depth that were acceptable to use in the calibration process, which limited the scope of the calibration. Therefore, the SRT was heavily relied upon in this work.

The flow from the SRT was entered into SWMM in the rock stilling basin as a lateral inflow into the storage node, since water did not flow over the flow meter and was instead placed on the rock bed. The model was calibrated during the SRT for Green-Ampt parameters in the bioswale storage unit and the rock bed storage unit. In the Figure 6-16, the calibrated pond depth is compared to the measured data as well as the uncalibrated SWMM depth prediction. The model with the best NSE and  $r^2$  values had a suction head of 2.0 inches for the bioswale and 3.0 inches for the rock bed; a saturated hydraulic conductivity ( $k_s$ ) of 3.5 in/hr for the bioswale and 9.0 in/hr for the rock bed, and an initial deficit fraction of 0.4 for the bioswale and 0.3 for the rock bed.

As previously mentioned, the Green-Ampt method uses the saturated hydraulic conductivity to base its recovery time, so increasing this value would increase the slope of the recession rate and decrease peak ponding as desired in the model. The calibrated saturated hydraulic conductivity for the rock bed is very high, but was used as it decreased the peak ponding depth in the bioswale and the outlet to match the recorded level. The rock bed has a significant amount of void space rocks, but is mainly used for conveyance of the runoff to the bioswale and is expected to not contribute to infiltration removal due to siltation from the runoff. The rock stilling basin's large value of  $k_s$  points out the limitations of the model and future studies/calibrations are needed to achieve a more reasonable number for this property of the rock bed. The measured data had a sharper peak in pond depth initially that was not seen in the calibrated model. Since suction head plays a larger role prior to saturation of the soil, this value could be one of the reasons for the difference in the ponding values before the peak depth. While the peak depth was matched, the model calibration was not able to match the high recession limb infiltration. This means that the bioswale is performing better than expected and has more capacity than designed as shown by the SWMM model.

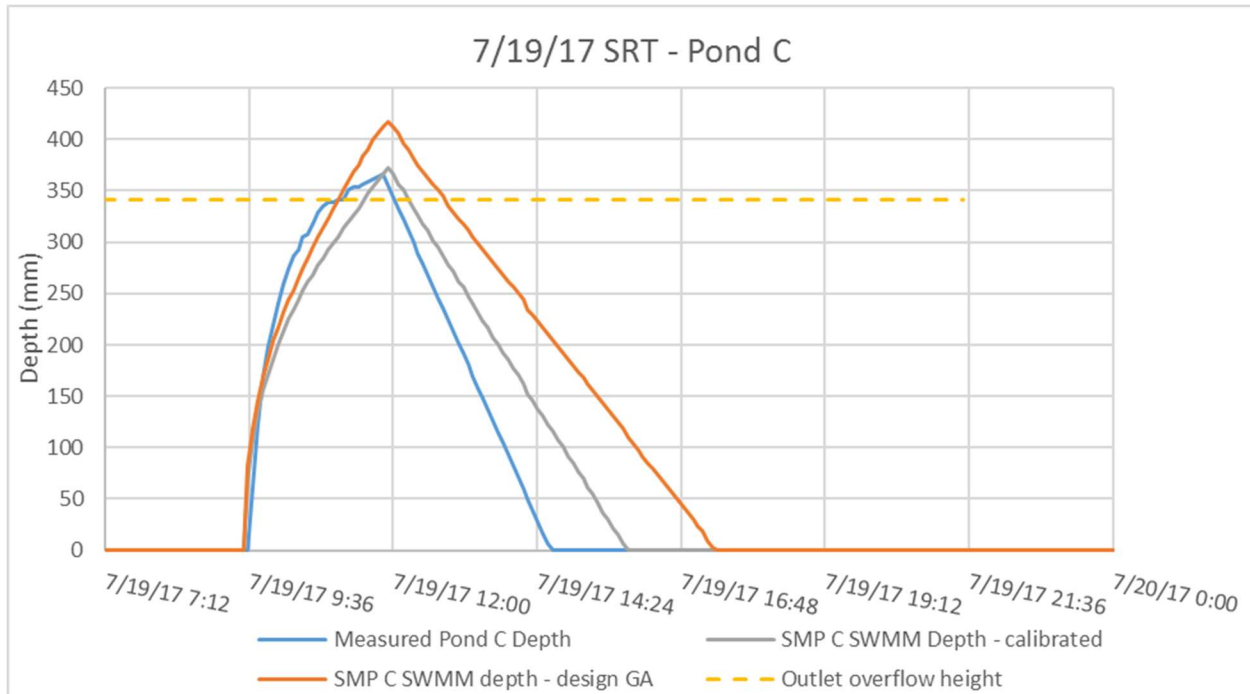


Figure 6-16: Pond C calibration for depth during SRT on 7/19/17 compared to the non-calibrated and measured pond depths. The dotted line is the depth when overflow first occurs.

In Figure 6-17, the calibrated outlet data is compared to the measured data and shows that there was water depth in the outlet before overflow from the pond occurred. This indicates that the box is leaking and not sealed correctly (although a complete seal is difficult to achieve). The leaking was minimal, so it was permissible to use the data for the test and all the previously recorded data. Additionally, water quickly decreased after the test, when the SWMM model indicates that the recession limb should be almost horizontal when the outlet depth is below the crest of the weir. With the alteration to the rock stilling basin to have higher saturated hydraulic conductivity, the model could accurately estimate the maximum depth in the outlet as well as the relative time this occurred. The low NSE and  $r^2$  values are low due to the unaccounted leak in the outlet structure. This leak can be quantified by measuring the volume change in the outlet prior to the overflow of the pond.

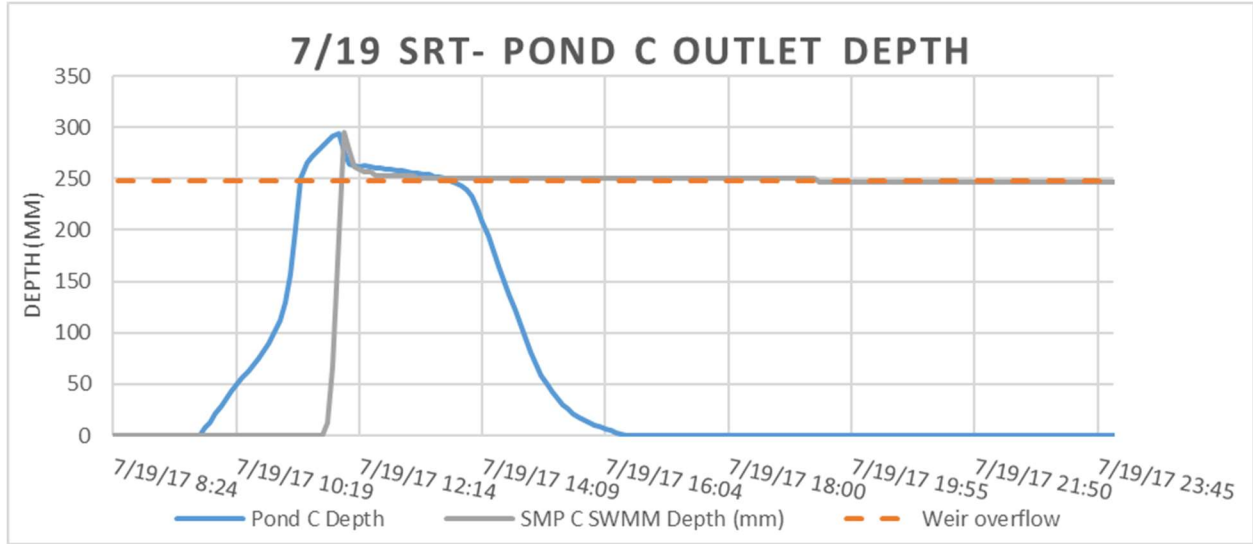


Figure 6-17: Outlet depth for SMP C during the 7/19/17 SRT

When comparing the ponding depth in SMP C during the SRT to the soil moisture volumes, shown in Figure 6-18, we see that ponding and the spike in soil moisture occur around the same time. The sensor at 10 cm peaks the fastest and highest, due to its shallow emplacement. The deepest sensor at 60 cm has a slow increase and then peaks suddenly after the flow into the bioswale has stopped for almost an hour. This peak and then sudden dip back down in soil moisture could be due to the water making its way down to the deepest layer and peaking only for a short time due to the pond emptying at roughly the same time.

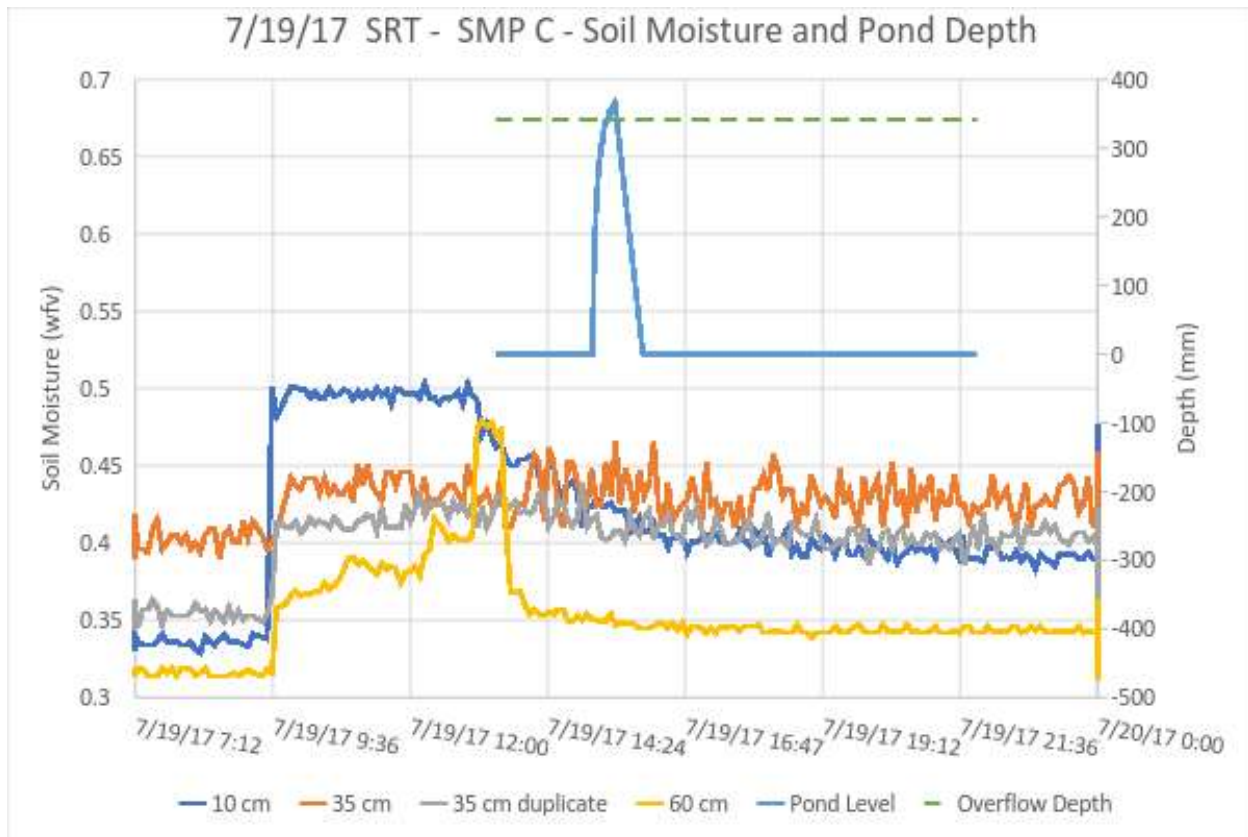


Figure 6-18: Soil moisture readings in SMP Pond C during SRT on 7/19/17

Since the SRT on SMP C was a simulated storm, there was no overland flow on the pervious area around the bioswale. Hence, the pervious area surrounding the bioswale had to be calibrated with an actual storm. Due to the way storage nodes are set up in SWMM, they do not allow precipitation to fall on them, so the bioswale has a separate subcatchment to capture rainfall. This subcatchment also had to be calibrated with an actual storm event. June 24<sup>th</sup> storm had a medium amount of precipitation of 27.94 mm (1.1 inches). This precipitation amount is a good amount for calibrating a SMP with the design drainage area, but these bioswales have variable drainage area that is significantly smaller. Due to drainage area change, the storm event on June 24<sup>th</sup> provided minimal ponding in all three bioswales, but still had the most ponding of



any storm event. SMP D had the most ponding of 106 mm (4.2 inches), therefore it was used to calibrate the pervious areas of the bioswales following the calibrations using the SRT.

Figure 6-19 shows the results from the uncalibrated versus the calibrated pond depths for the storm on June 24<sup>th</sup>, 2017. The parameters that provided the best efficiencies were: two percent catchment slope, 0.04 manning's roughness coefficient, 0.05 inches of impervious abstractions for the bioswale subcatchment. The values chosen for the pervious subcatchment area around the bioswale are: two percent slope, 0.3 manning's roughness coefficient, 0.05 inches of initial abstractions. The Green-Ampt parameters for the pervious area were calibrated to 3.0 inches of suction head, 1.0 in/hr saturated hydraulic conductivity, and 0.40 initial deficit. The NSE for the pond depth during the June 24<sup>th</sup>, 2017 storm is -0.418 and the coefficient of determination is 0.372. The value for both NSE and  $r^2$  are not acceptable, but the recession limb of the measured data is 18 inches an hour, which is a value that is higher than SWMM will model. This recession rate could indicate better infiltrating soil than can be modeled due to some underlying process. This recession limb could also indicate leaking, like that observed in SMP C and G, where the underdrain plate is not tightly sealed, which caused the basin to drain faster. Another discrepancy between the modeled and measured data is the peak of the hydrograph is offset, with the modeled peak occurring later. Further calibration and testing against larger storms is needed to attempt to get the peaks to match.

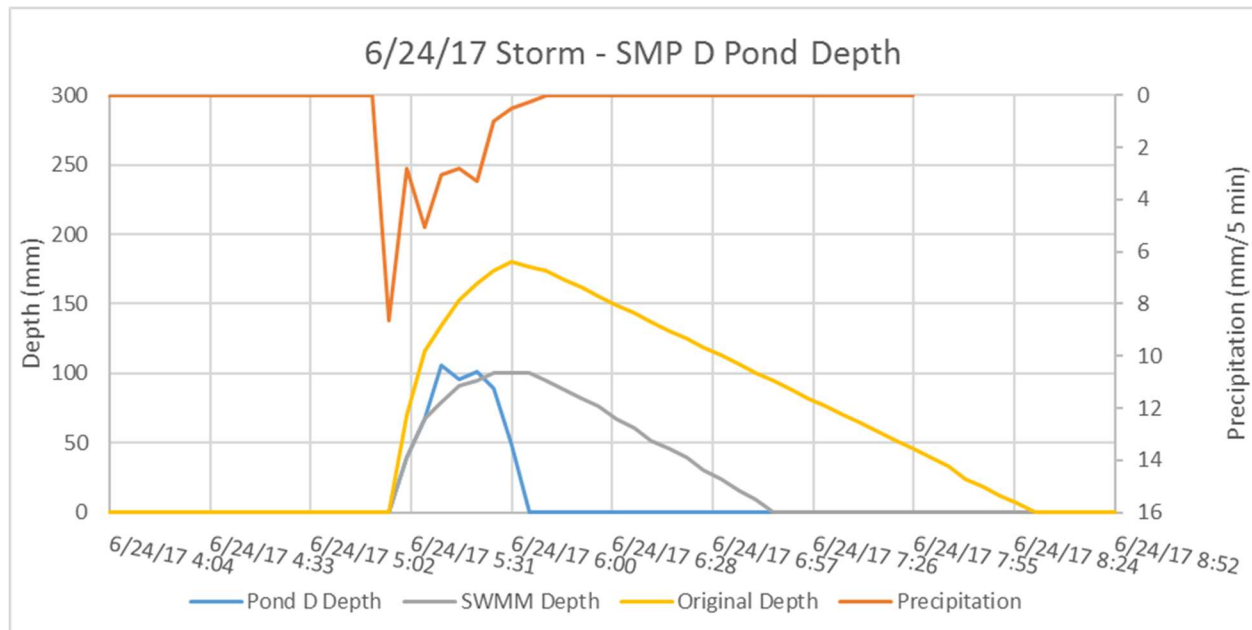


Figure 6-19: SMP D pond calibration versus measured depths for 6/24 Storm (27.94 mm precipitation)

After calibrating the pervious areas of the bioswale in SMP D, the calibration was applied to another storm to verify the parameters chosen. The storm on May 25<sup>th</sup> was a back-to-back storm, meaning that there were two storms that occurred one right after the other, separated by at least six hours. The storm had a precipitation amount of 43.43 mm (1.71 inches), which is an appropriate size storm for calibrating a model, but again due to the drainage area reduction, ponding depths were minimal. Figure 6-20 shows the measured pond depth (blue) versus the modeled depth (gray) plotted against the two storms that occurred that day. The figure shows that the SWMM model consistently under predicts the pond depth, but the general trend in ponding and recession are almost identical. This model verification provided the best correlation of any storm or bioswale, with a NSE of 0.873 and a  $r^2$  value is 0.966. These values indicate that the model predicts the actual performance very well.

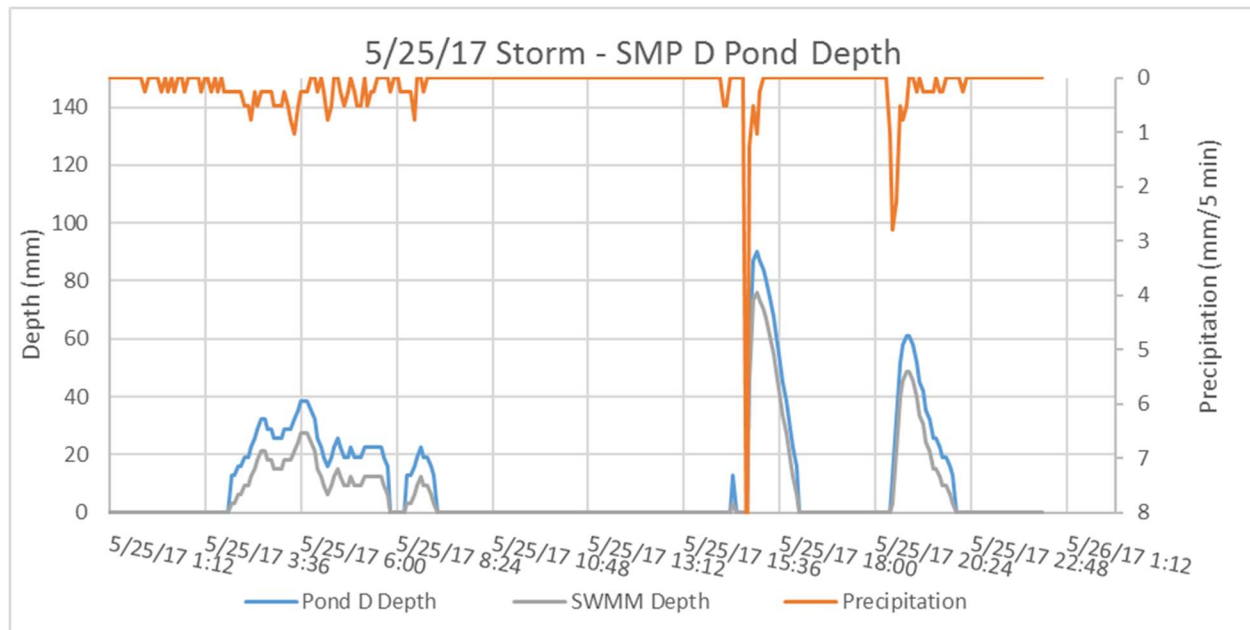


Figure 6-20: SMP D Pond Depth Calibration applied to May 25th, 2017 Storm (43.43 mm precipitation)

### Pond Results Summary

The observed ponding depth in all three bioswales has been minimal, which is partially due to the unexpectedly low inflow volumes. Due to the volume change and numerous small precipitation storms, there were only a few events that the bioswales could be calibrated against. The results from the SRT on July 19<sup>th</sup>, 2017 and the storm on June 24<sup>th</sup>, 2017 both indicate that the bioswales themselves are performing as predicted and have better than predicted recession rates. The outlet structures were noted to have significant leaks in SMP G, which meant that bioswale could not be calibrated without accounting for the flow in the outlet structure. SMP C had minor leaks, thus all three bioswale underdrains were sealed after the discovery of the leak. The verification storm of May 25<sup>th</sup>, 2017 showed that the model does a very good job at estimating the ponding depth for SMP D, even with the limitations to the drainage area.

### *SWMM Modeling Conclusions*

Despite the limitations of the data record for the three bioswales, conclusions can be drawn based on the data collected and model calibration experience. During the modeling process, it was found that all three bioswales are receiving significantly less flow than predicted due to the changes caused by on-going construction along the elevated highway. The volume variance was not uniform per storm, so each storm was calibrated for percentage of original DCIA prior to any other calibration. Based on the seven storms analyzed, SMP C is receiving 14-30 percent of the expected volume, SMP D is receiving 7-36 percent, and SMP G is receiving 5-8 percent of the predicted volume. The inflow hydrographs showed a variation of responses to volume and timing calibrations. The Nash Sutcliff Efficiency (NSE) values ranged from -13.1 to -1.0 for SMP C, -8.9 to 0.46 for SMP D, and from -5.1 to 0.78 for SMP G. The coefficient of determination ( $r^2$ ) values ranged from 0.07 to 0.64 for SMP C, from 0.01 to 0.66 for SMP D, and from 0.045 to 0.79 for SMP G.

These results indicate that it is difficult to test design performance when there is uncertainty in the contributing drainage area. Although we can identify a volume of inflow runoff absent from the bioswales we have yet to pinpoint the exact location of the source or the pathway of the “missing” runoff. The calibration process occurred with some small sized storms due to the limited storm record. The runoff from small storms is more affected by the observed volume change, because initial abstractions play a larger role during small precipitation events, and lower flow measurements are difficult to capture. Despite these challenges, we have discovered several factors influencing the discrepancy between expected and recorded runoff specific to each SMP.

Interstate 95 is currently under construction and the roadway drainage plans did not reflect the temporary configuration. Since the final roadway surface of the travel lanes has not been completed, the New Jersey barriers and slope of the highway are different from the design documents. This is hypothesized as the major reason for the volume variation for SMP C and G, which both have inlets in the center of the current northbound travel lanes, and are influenced by the New Jersey barriers. After the final grading and configuration of the highway has been completed, it is expected that the flow paths will change to match the proposed/designed areas which will validate this hypothesis. The implications due to this unplanned construction change is that some SMPs receive higher flows. Additional material and labor may be required to restore the bioswales that have been overloaded.

The hydrographs for all three bioswales created by the SWMM model had irregular sharp peaks following the precipitation trend, where the measured flow was smooth and much more muted compared to the predicted trend. The timing of the hydrograph was altered to attempt to push the peak later and reduce it. While the timing and general shape of the storm hydrographs were matched, the model was unable to replicate the smooth peaking hydrograph that was recorded. The timing and volume results showed that the higher NSE and  $r^2$  values were for lower intensity with medium to high precipitation storms. The higher intensity and short duration storms (no matter the rainfall amount) had much lower correlation and NSE values. This difficulty in matching the peak flows and smooth hydrograph shape is hypothesized to be caused by challenges in hydraulic modeling of the elevated piping system within SWMM and possibly measurement error. The piping system model was unable to replicate the energy dissipation occurring within the drop inlet. Additionally, the flow meters might be averaging out the peaks in flow due to the way they are programmed, thus smoothing and lowering peak flow.

This change in NSE for the higher intensity short storms can be partially be explained by the configuration of the New Jersey barriers between the north and southbound travel lanes and the barriers lining the Girard Street exit ramp. The barriers are expected to pass runoff through the openings at the bottom of the barriers. Instead, they are hypothesized to be a factor changing the flow rate and volume of runoff entering each bioswale. The opening size causes sediment clogging, which changes the volume and timing of flow entering the inlet. Additionally, if the flow path does not slope or naturally flow to the gap under the barriers, the flow will bypass the barriers and move to another location, also changing both volume and timing of runoff. The barrier openings and consequent clogging, change the flow path and thus the way overland flow is calculated in SWMM with kinematic wave.

SMP C never achieved a NSE value over zero, indicating that the average value of measured flow does a better job predicting flow than the model does. This is in large part due to the storm sizes used and the drainage area being significantly smaller than predicted. The flow for all storms is greatly reduced exiting the culvert that is designed for the original drainage area. The limitations of modeling the piping system, coupled with flow measurement error, mean that efforts to improve the hydraulic model await future studies and data from larger storms. SMP D had large variability in the total volume per storm, which is influenced by the placement of a temporary tool cleaning structure constructed ten feet from the only drainage inlet into the bioswale sometime during the monitoring period. This structure has been removed, but its implications for modeling results were substantial. SMP G was the only bioswale that was consistent in the area contributing to inflow for each storm.

The bioswale ponding depths and timing could be replicated by the SWMM model well. The slope of the recession limbs was steeper than what SWMM can model, indicating better than

expected soil infiltration for SMP C. For SMP G, the testing discovered leaking underdrain seals, which have been sealed tighter following the SRT on July 19<sup>th</sup>, 2017. The leaking underdrains can be modeled if the leak is quantified. Thus, the leak in SMP G, discovered during the SRT on July 19<sup>th</sup> is still able to be modeled at a future date so that the bioswale can be calibrated and verified. The rock stilling basin was calibrated using the SRT data from SMP C and the saturated hydraulic conductivity value was higher than reasonable, but used as it provided the best pond and outlet depth correlations. During the SRT on SMP C, the bioswale could approximately capture the two-year storm volume and exfiltrate over 40 percent of the water before overflow occurred. The ponding during the SRT and the few ponding events recorded up to July of 2017 receded at a much higher rate than could be modeled in SWMM, showing above average/expected soil properties. The ponding that occurred during the SRT shows that the bioswale is meeting the regulatory requirements, that it capture a minimum one-inch storm and design parameters of the two year, 24-hour storm before overflow. It also met the regulatory requirement of infiltrating and/or evaporating the ponded water in under 72 hours. The soil properties would be easier to model using SWMM's LID controls, but due to the piping of the system and definition of LID controls in SWMM (LID controls are set up through the subcatchment property and pipes/links are not allowed to flow onto a subcatchment), it is not possible without large modification to the model setup.

The combination of monitoring and modeling these SMP's resulted in significant discoveries for the operation of both the watershed area and the bioswales themselves. The watershed area is underrepresented and has repercussions for the areas receiving the extra runoff. Additionally, the effect of temporary construction changes and roadway installations have runoff flow and quantity implications on the bioswales. The bioswales were found to be performing at

or above design expectations, but did have leakage short circuited the design. It should be noted that without monitoring and modeling, this would not have been discovered or corrected.

### **Coupling the Hydrologic Model with the Fate of Contaminants**

#### *Observed Pollutant Removal Rates*

During the period of observation (October 2016 to March 2017), no stormwater discharge was observed flowing from SMP C into the storm sewer. However, precipitation event analysis conducted with the *hydromad* R package (Andrews et al. 2011) indicates that 51 precipitation events occurred during this period. Rainfall received during these events has ranged from 0.01 to 0.95 inches (Figure 6-21). The lack of discharge from SMP device C to the storm sewer likely indicates that SMP C is relatively efficient at infiltrating storm runoff. Ponding of water on the surface of SMP C during storm events has been minimal (Fig. 6-22), which would be consistent with relatively rapid infiltration rates. The relatively fast infiltration of storm water is further suggested by the analysis of baseline monitoring wells described in Chapter 4. Water levels in well MW2, which is located next to SMP device C, responded relatively quickly to medium and high volume precipitation events, which is suggestive of a relatively fast infiltration. Thus, at present, the removal rates of TSS, TN, and TP must be 100%, as no effluent has been observed discharging from SMP device C to the storm sewer.



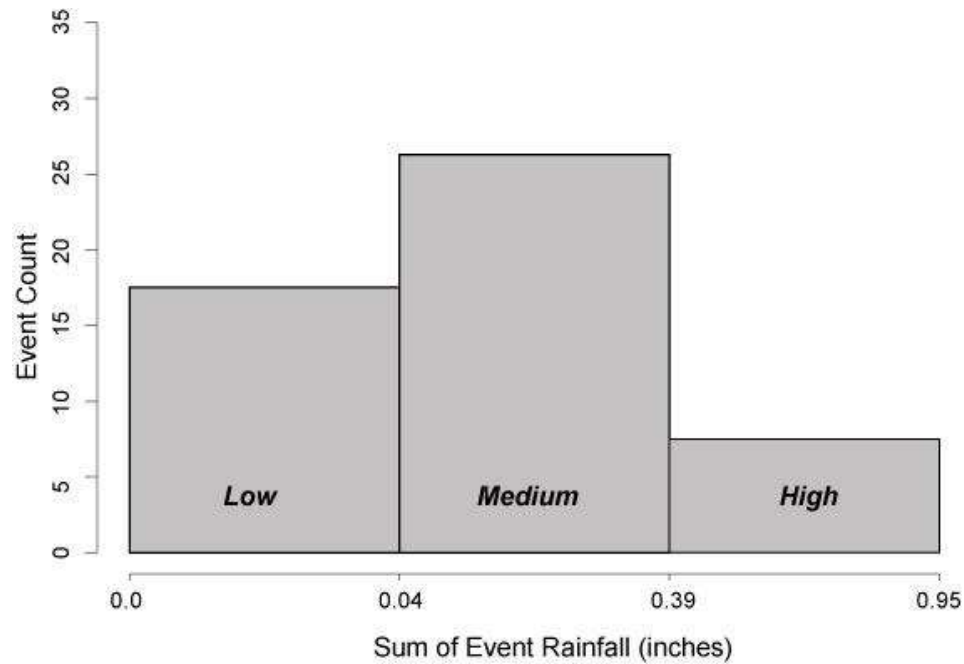


Fig. 6-21. Frequency histogram of precipitation events occurring between October 2016 and March 2017.



Fig. 6-22. Photo of the extent of ponding on SMP device C. This photo was taken on 31 March 2016 during a 1.54-inch rainstorm. Note that the height of ponded water is still well below the outlet drain (red arrow).

While the lack of discharge to the storm sewer is promising in the context of minimizing road-borne pollutant loadings to the storm sewer system, the absence of physical data complicates the construction of the appropriate pollutant removal algorithms for SMP device C. Consequently, a thorough meta-analysis of the literature pertaining to stormwater BMP devices has been conducted (Table 6-15). Based on this review, the consistency of removal rates appears to be influenced by site heterogeneity. However, a wide review of similar bioretention systems should nonetheless provide reasonable, scientifically backed, removal algorithms to utilize in future modeling.

*Table 6-15. Percent mass or event mean concentration reduction rates of total suspended solids (TSS), total nitrogen (TN), and total phosphorus (TP) taken from existing literature. Negative values indicate an export from the SMP device.*

Study location	TSS	TN	TP	Study
	<b><u>% Mass Reduction</u></b>			
Greenbelt, MD		49	65	Davis et al., 2006
Largo, MD		59	87	Davis et al., 2006
University of Maryland	56.5		78	Davis, 2007
Greensboro, NC	-170	40	-240	Hunt et al., 2006
Chapel Hill, NC		40	65	Hunt et al., 2006
College Park, MD	96		-36	Li & Davis, 2009
Silver Spring, MD	99		100	Li & Davis, 2009
Haddam, CT		51	-108	Dietz & Clausen, 2006
Haddam, CT		32	-110.6	Dietz & Clausen, 2005
Greenbelt, MD			65	U.S. EPA, Office of Water, 2000
Landover, MD			87	U.S. EPA, Office of Water, 2000
McDowall, Queensland	93	37	86	Hatt, Fletcher, & Deletic, 2009
Monash, Victoria	76	-7	-398	Hatt, Fletcher, & Deletic, 2009

Louisburg, NC		33	30	Sharkey, 2006
Louisburg, NC		47	-61	Sharkey, 2006
Mean	42	38	-19	
Median	85	40	65	
<b><u>Event Mean Concentration Reduction</u></b>				
Charlotte, NC	60	32	31	Hunt et al., 2008
Alamance County, NC		54	63	Passeport et al., 2009
Alamance County, NC		54	58	Passeport et al., 2009
Mean	60	47	51	
Median	60	54	58	

#### *Total Suspended Solids Removal Algorithm*

A removal algorithm for total suspended solids (TSS) will be based on the fundamental filtration model (Yao et al. 1971). Existing literature suggests that TSS removal by a bioretention device is due to settling and filtration in the bioretention area (Li & Davis 2008a; Li & Davis 2008b), and, as such, the fundamental filtration model, as shown in Equation 6-7 would be an appropriate descriptor of steady state particulate matter removal:

$$TSS_{eff} = TSS_{in} \exp\left[-\frac{3}{2} \frac{(1-\varepsilon)}{d_c} \alpha \eta_o L\right] \quad 6-7$$

where  $TSS_{eff}$  is the mass of TSS the effluent water (in kg),  $TSS_{in}$  is the mass of TSS the influent water (in kg),  $\varepsilon$  is the filter porosity (unitless),  $d_c$  is the collector diameter (in m),  $\alpha$  is the sticking coefficient (unitless),  $L$  is the bed depth (in m), and  $\eta_o$  is the overall collector efficiency, which is the sum of the sedimentation ( $\eta_s$ ) (Equation 6-8), interception ( $\eta_i$ ) (Equation 6-9), and diffusion ( $\eta_D$ ) (Equation 6-10) efficiencies:

$$\eta_s = \frac{[(\rho_s - \rho) \times g d_p^2]}{18\mu v} \quad 6-8$$

$$\eta_i = \frac{3}{2} \left( \frac{d_p}{d_c} \right)^2 \quad 6-9$$

$$\eta_D = 0.9 \left[ \frac{(kT)}{(\mu d_p d_c v)} \right]^{\frac{2}{3}} \quad 6-10$$

where  $\rho_s$  is the density of the suspended sediment (in kg/m<sup>3</sup>),  $\rho$  is the density of water (1 kg/m<sup>3</sup>),  $g$  is the acceleration due to gravity (9.81 m/s<sup>2</sup>),  $d_p$  is the particle diameter (in m),  $\mu$  is the dynamic viscosity of water (1.002 Ns/m<sup>2</sup>),  $v$  is the flow velocity (m/s),  $k$  is the Boltzmann's constant (1.38 x 10<sup>-23</sup> m<sup>2</sup>kg/s<sup>2</sup>K), and  $T$  is the absolute temperature (in K).

#### *Total Phosphorus Removal Algorithm*

In general, the physical transport mechanisms of TP and TSS during runoff events are closely linked. Specifically, P is primarily transported by sorption to soil particles during urban rainfall-runoff (Berretta & Sansalone 2011), likely because the transport of dissolved forms of P is retarded by sorption to Fe and Al oxy-hydroxides or clay minerals (Walkers & Syers 1976). Unsurprisingly, studies have attributed TP removal to the removal of TSS within a bioretention area (e.g., Sharkey & Hunt, 2004). However, TP removal can be complicated by the P content of bioretention media. For example, in a field study of the performance of a bioretention device in North Carolina, Hunt et al. (2008) attributed their observed P removal rates to the low P content of the bioretention media. Likewise, Sharkey (2006) concluded that P removal in a bioretention system is highly dependent on the P content of bioretention media, and Debusk & Wynn (2011) attributed high TP concentrations in outflow to relatively P-rich mulch used in the bioretention media. However, these observations are not directly comparable to SMP device C, as we have recorded no flow exiting the SMP. Thus, TP removal in SMP device C is likely governed by the

physical movement of sediments, and linking TP removal to TSS removal should be a suitable strategy to model TP removal.

#### *Nitrogen removal algorithm*

A removal algorithm for total nitrogen (TN) will be based on Masi (2011). In this thesis research, Masi used SWMM-5 to model nitrogen removal in a proposed bioretention system in Venice, Florida. Ultimately, Masi created two nitrogen removal algorithms which were tailored to the two main layers of this system, a 12 inch nitrification layer (Equation 6-11) and 6 inch denitrification layer (Equation 6-12):

$$TKN_{eff} = TKN_i e^{-k_1 HRT1} \quad 6-11$$

$$NO_{3,eff} = [NO_{3,i} + (R_TKN_i)]e^{-k_2 HRT2} \quad 6-12$$

where  $TKN_{eff}$  is the mass of total kjeldahl nitrogen in the effluent water (in lbs),  $TKN_i$  is the mass of total kjeldahl nitrogen in the influent water (in lbs),  $NO_{3,eff}$  is the mass of nitrate in the effluent water (in lbs),  $NO_{3,i}$  is the mass of nitrate in the influent water (in lbs),  $R_TKN_i$  is the mass of  $TKN_i$  reacted (equal to  $TKN_i - TKN_{eff}$ ),  $k_1$  and  $k_2$  are estimated rate coefficient values for nitrification, and  $HRT1$  and  $HRT2$  are the hydraulic residence times of the nitrification and denitrification layers, respectively. Hydraulic residence times were calculated using Equation 6.13.

$$HRT = V/(Q \times \eta) \quad 6-13$$

where  $V$  is the volume of the layer (in ft<sup>3</sup>),  $Q$  is the flow rate through the layer (in cfs), and  $\eta$  is the porosity of the layer (unitless).

Moving forward, we plan to alter the nitrogen removal algorithm created by Masi (2011) to account for the differences between our study site and Masi's site. In particular, because SMP device C does not have a specifically designed denitrification layer, we will not use equation (6-6) to describe nitrate removal via a denitrification layer. Instead, we plan to utilize equation (6-5) to model nitrogen removal in SMP device C. Depending on the success of future storm samplings, an appropriate rate coefficient value can be calculated from empirical data or will be calculated from data synthesized from the literature.

No additional analysis or simulation of pollutant concentrations or treatment has been conducted now due to the lack of overflow events in the SMPs. However, future work can focus, in part, on analyzing additional data to confirm the validity of the algorithms discussed in the May 2017 report and then implementing them. This includes assessing the results of the SRTs and lysimeter data discussed in Chap 4.

Our focus remains on utilizing the SWMM code for modeling water quality. This can be accomplished in several ways. First, the SWMM GUI allows for water quality modeling in which the pollutant reduction is a function of one or more specific parameters (hydraulic residence time, flow, depth, or surface area). As noted previously, Masi (2011) has found that TKN removal can be modeled as an exponential decay function of hydraulic residence time. For TSS, the removal function is more complex. This function may be incorporated directly into the SWMM model by editing the source code, or alternatively, a MATLAB code may be written which extracts TSS influent loads from SWMM, calculates TSS reduction using the method of Li and Davis (2008a, 2008b) and then feeds the TSS effluent load back to SWMM. These effluent loads will then be used to model TP removal as a function of TSS removal.

## Evaluation of Computational Water Quality Models

In addition to the 1-D SWMM, a literature review of 2D and 3D models that could potentially be used to simulate SMP performance was conducted. This initial review focused on several EPA-supported models (WASP, EFDC, AQUATOX, SWMM) and one proprietary model (Infoworks ICM). In addition, one programming platform (MATLAB) has been reviewed. Each of these can simulate both hydrodynamics and water quality. The benefits and drawbacks of each are discussed below.

### *SWMM (Storm Water Management Model)*

SWMM is a well-accepted model used in countless studies of stormwater runoff. It is a 1D model with capabilities of simulating pollutant build up and wash off from land surfaces as well as pollutant removal via user-defined algorithms which relate pollutant concentrations to one or more model variables such as inflow concentration, water depth, hydraulic residence time, etc. (Rossman and Huber, 2016). The flexibility and functionality of SWMM for both water quality and quantity modeling make it a very attractive choice even though it is limited to 1D modeling.

### *WASP (Water Quality Assessment Program)*

WASP is a highly flexible model that can simulate water quality processes in 0D, 1D, 2D or 3D. It was originally developed for the US EPA in the mid-1980s (Di Toro et al. 1982) and has been updated and expanded several times since then. The current stable version is WASP7 (Ambrose & Wool 2009) and WASP8 is being beta tested (<http://epawasp.twool.com/>). The model incorporates water column and benthic processes and can estimate concentrations of several pollutants including nitrogen, phosphorus, sediment, metals, and organics. Modeling of

nutrients requires a full specification of the eutrophication process, including nutrient speciation, dissolved oxygen concentrations, and sediment interactions. Pollutant removal modeling for other parameters is limited to simple speciation and first order decay. WASP requires an external input of pollutant loads, for example, from a database or from a model such as SWMM. The model requires extensive data to be parameterized. This model will continue to be considered for use, with the decision contingent on whether field data collection yields sufficient information to proceed.

### *AQUATOX*

This model was developed by the EPA and first released in 1990 (Park 1990); in 2000 a Windows-based version was released (Park & Clough 2000). The most recent version, Release 3.1+ (Park & Clough 2014), is designed to simulate ecosystem processes in surface waters. Nutrients, sediment, and organic loads are input from external sources and pollutant transformations such as absorption, decomposition, partitioning, and bioaccumulation are then simulated to model the movement of these pollutants through various ecosystem compartments (sediment, water column, plants, fish and invertebrates). AQUATOX models hydraulics via linked ‘segments’ in which water and pollutants move between segments through advection, diffusion, drift, or bedload movement. The model has the potential to simulate stormwater management practices; however, many of the included ecosystem compartments would be dormant or dry much of the time in our system given the fast infiltration rates of the SMPs. This model could be considered in more detail should the SMPs perform in such a way that standing water becomes commonplace.



### *EFDC (Environmental Fluid Dynamics Code)*

EFDC is has highly complex and flexible code base that can be used to model waterbodies in 1D, 2D, or 3D. It was first developed in 1992 (Hamrick 1992), but was later updated to include eutrophication (Park et al. 1995) and sediment and contaminant transport (Tetra Tech 2007). It has been used to model lakes, rivers, reservoirs, and other waterbodies, and can potentially be used to model SMPs. It is computationally similar to the Chesapeake Bay Model. It may be suitable for 2D or 3D modeling because it can simulate the wetting and drying cycles typically observed in SMPs. However, the degree of complexity of the model and its data requirements make it more suitable for large waterbodies such as the Delaware River, rather than individual SMPs.

### *Infoworks ICM (Integrated Catchment Model)*

The propriety model published by Innovyze ([www.innovyze.com/products/infoworks\\_icm](http://www.innovyze.com/products/infoworks_icm)) can simulate catchment runoff and subsurface flow. It was developed originally to model urban infrastructure and later expanded to include natural channels. The model simulates pollutant loads in runoff based on an assumed exponential buildup, whereas wash off is simulated as a function of rainfall intensity and sediment mass. Channel routing uses 1D advection without dispersion and floodplain modeling is accomplished in 2D. The usefulness of this model is limited since (a) the 1D SWMM model is more flexible with respect to buildup and wash off and (b) Infoworks ICM uses the SWMM LID modules to simulate SMPs.

### *MATLAB*

MATLAB ([www.mathworks.com](http://www.mathworks.com)) is not a water quality model per se. Instead, it is a programming language widely used for data analysis and algorithm development. Its flexibility

allows for ease of use in a wide variety of fields, including water quality modeling. Use of MATLAB will be further investigated as a tool for modeling TSS and linking the results with SWMM.

## **Water Quality Modeling Summary**

### *Computational Models*

The WASP model appears to be the most appropriate multi-dimensional model for describing contaminant transport. It is flexible enough to be useful at the hydrologic scale of an SMP and to model the water quality parameters of interest (e.g., nutrients, sediment, and toxics). However, the need for multi-dimensional modeling of the SMPs is not demonstrated from the current water quality monitoring data or literature review. Generally, 2D or 3D modeling is required when vertical or lateral variation in water quality results in localized areas of concern. The SMPs are generally not deep enough, not do they retain water long enough, to suggest vertical stratification would become an issue. In addition, any significant lateral variation in forward flow velocity which might result in hydraulic or pollutant ‘dead zones’ can be addressed with proper planting as suggested in Chapter 7. While this issue can be revisited if future monitoring data suggest that the SMPs exhibit important vertical or lateral variation in pollutant concentrations, at this time we intend to use SWMM and MATLAB for water quality modeling.

### *Refinement of Algorithms for Water Quality Modeling*

Future efforts can be focused on collecting data needed to construct simple, yet effective, descriptor of TSS removal. Specifically, future field work can be conducted to sample ponded water on the surface of SMP device C during storm events. The collection and analysis of these samples, collected across multiple storm events, will allow for the creation of a mathematical expression that describes the TSS mass removal in SMP device C. If sampling of TSS in ponded

water is not possible due to shallow ponding depths, a TSS removal algorithm based on the fundamental filtration model (Equation 6-1) will be added to the model. Values needed to satisfy equations 6-1 through 6-4 (e.g., water flow velocity) will be taken from the hydraulic SWMM model, field data (e.g., bed depth), and/or from values published in the literature (e.g., collector diameter) that are specific to bioretention systems (Davis & McCuen 2005).

To establish the relationship between the masses of TSS and TP in the inflow to SMP device C, regression analysis of storm runoff samples will be conducted (see Chap 4). The resulting mass ratio will be used to create a TP removal algorithm in the SWMM model. Specifically, a TP removal algorithm will be entered as a percentage of the calculated TSS removal, thereby enabling a coupled prediction of TSS and TP removal rates.

In the coming months, the nitrogen removal algorithm created by Masi (2011) will be incorporated and adjusted to account for the differences between our study site and Masi's site. Specifically, SMP device C does not have a denitrification layer, and analysis of baseline monitoring wells does not suggest that the lower depths of SMP device C are saturated. As such, creating a removal function to describe nitrate removal via a denitrification layer would not be appropriate. Thus, equation 6-6 is not recommended in future water quality modeling.

Consequently, we plan to utilize equation 6-5 to model nitrogen removal in SMP device C. The hydraulic residence time for the SMP will be calculated from the hydraulic portion of the SWMM model. However, due to the lack of outflow data, we do not know the mass of total nitrogen in the effluent, and thus cannot solve for the appropriate rate coefficient value. If future sampling efforts are successful in generating data that describe effluent chemistry, then this coefficient can be calculated using those empirical data.

If there continues to be a lack of effluent from SMP device C, then the rate coefficient value will be calculated using data synthesized from the current literature. Specifically, inflow and outflow masses of TN in published studies exploring SMPs will be regressed against the process variables used by SWMM (e.g., inflow rate, water depth, hydraulic residence time, and surface area of the bmp). The process variable(s) selected will be the variable(s) that are most widely reported in the literature to ensure a maximally robust algorithm.

#### *Model Calibration and Comparison to Design Expectations*

Calibration of the SWMM model will be conducted by adjusting the soil infiltration parameters, drainage areas, flow pathways, and pollutant removal algorithms to minimize the error between modeled and observed values. The model will be compared to that of the design expectations, to evaluate its suitability for use in predicting performance.

#### **References**

- Ambrose, R.B. & Wool, T.A. (2009). WASP7 Stream Transport – Model Theory and User's Guide, supplement to water quality analysis simulation program (WASP) user documentation, Athens, GA.
- Andrews, F.T., Croke, B.F.W. & Jakeman, A.J. (2011). Hydrological Model Assessment and Development. *Environmental Modelling & Software*, 26(10), pp.1171–1185
- Bedient, P. B., Huber, W. C., and Vieux, B. E. (2013). Hydrology and Floodplain Analysis. Pearson, Upper Saddle River, NJ.
- Berretta, C. & Sansalone, J. (2011). Speciation and transport of phosphorus in source area rainfall-runoff. *Water, Air, and Soil Pollution*, 222(1–4), pp.351–365.
- Beven, J. K. (2001). Rainfall-Runoff Modelling - The Primer. John Wiley & Sons Ltd., Chichester.

- Brakensiek, D. L., and Onstad, C. A. (1977). "Parameter Estimation of the Green-Ampt Equations." *Water Resources Research*, 13(6), 1009–1012.
- Cambez, M. J., Pinho, J., and David, L. M. (2008). "Using SWMM 5 in the continuous modelling of stormwater hydraulics and quality." 11th International Conference on Urban Drainage, Edinburgh, Scotland, UK.
- Choi, K., and Ball, J. E. (2002). "Parameter estimation for urban runoff modelling." *Urban Water*, 4(1), 31–41.
- Cronshey, R. (1986). *Urban hydrology for small watersheds*. US Dept. of Agriculture, Soil Conservation Service, Engineering Division.
- Davis, A.P. (2007). Field Performance of Bioretention: Water Quality. *Environmental Engineering Science*, 24(8), pp.1048–1064.
- Davis, A.P. et al. (2006). Water Quality Improvement through Bioretention Media: Nitrogen and Phosphorus Removal. *Water Environment Research*, 78(3), pp.284–293.
- Davis, A.P. & McCuen, R.H. (2005). *Stormwater Management for Smart Growth*, New York: Springer Science.
- Debusk, K.M. & Wynn, T.M. (2011). Storm-Water Bioretention for Runoff Quality and Quantity Mitigation. *Journal of Environmental Engineering*, 137(9), pp.800–809.
- Dietz, M. & Clausen, J. (2005). A Field Evaluation of Rain Garden Flow and Pollutant Treatment. *Water, Air, & Soil Pollution*, 167(1), pp.123–138.
- Dietz, M.E. & Clausen, J.C. (2006). Saturation to improve pollutant retention in a rain garden. *Environmental Science and Technology*, 40(4), pp.1335–1340.
- Di Toro, D.M., Fitzpatrick, J.J. & Thomann, R.V. (1982). *Water Quality Analysis Simulation*

- Program (WASP) and Model Verification Program (MVP) - Documentation, Duluth.
- Hamrick, J.M. (1992). A three-dimensional environmental fluid dynamics computer code: Theoretical and computational aspects, Gloucester Point, VA
- Hargreaves, G. H., and Merkle, G. P. (1998). Irrigation Fundamentals. Water Resources Publications, LLC, Highlands Ranch, CO.
- Hargreaves, G. H., and Samani, Z. A. (1985). "Reference Crop Evapotranspiration from Temperature." *Journal of Agricultural Safety and Health*, 1(2), 96.
- Hatt, B.E., Fletcher, T.D. & Deletic, A. (2009). Hydrologic and pollutant removal performance of stormwater biofiltration systems at the field scale. *Journal of Hydrology*, 365(3–4), pp.310–321.
- Hawkins, R. H., Jiang, R., Woodward, D. E., Hjelmfelt, A. T., Van Mullem, J. A., and Quan, Q. D. (2003). "Runoff curve number method: examination of the initial abstraction ratio." World Water & Environmental Resources Congress 2003, 1–10.
- Hickman, J. M. (2011). "Evaluating the Role of Evapotranspiration in the Hydrology of Bioinfiltration and Bioretention Basins Using Weighing Lysimeters." MS Thesis, Villanova University.
- Hunt, W.F. et al. (2006). Evaluating Bioretention Hydrology and Nutrient Removal at Three Field Sites in North Carolina. *Journal of Irrigation and Drainage Engineering*, 132(6), pp.600–608.
- Hunt, W.F. et al. (2008). Pollutant Removal and Peak Flow Mitigation by a Bioretention Cell in Urban Charlotte, N.C. *Journal of Environmental Engineering*, 134(5), pp.403–408.
- Ji, S., and Qiuwen, Z. (2015). "A GIS-based subcatchments division approach for SWMM." *Open Civil Eng. J*, 9(1), 515–521.

- Krause, P., Boyle, D. P., and Bäse, F. (2005). "Comparison of different efficiency criteria for hydrological model assessment." *Advances in Geosciences*, 5, 89–97.
- Lee, R. S., Traver, R. G., and Welker, A. L. (2013). "Continuous Modeling of Bioinfiltration Storm-Water Control Measures Using Green and Ampt." *Journal of Irrigation and Drainage Engineering*, 139(12), 1004–1010.
- Legates, D. R., and McCabe Jr., G. J. (1999). "Evaluating the use of 'goodness-of-fit' measures in hydrologic and hydroclimatic model validation." *Water Resources Research*, 35(1), 233–241.
- Li, H. & Davis, A.P. (2008a). Urban Particle Capture in Bioretention Media . I : Laboratory and Field Studies. *Journal of Environmental Engineering*, 134(6), pp.409–418.
- Li, H. & Davis, A.P. (2008b). Urban Particle Capture in Bioretention Media . II : Theory and Model Development. *Journal of Environmental Engineering*, 134(6), pp.409–418.
- Li, H. & Davis, A.P. (2009). Water Quality Improvement through Reductions of Pollutant Loads Using Bioretention. *Journal of Environmental Engineering*, 135(8), pp.567–576.
- Masi, M. (2011). A SWMM-5 Model of A Denitrifying Bioretention System to Estimate Nitrogen Removal from Stormwater Runoff. University of South Florida.
- Mays, L. W. (2011). *Water Resources Engineering*. John Wiley & Sons Ltd., Hoboken, NJ.
- Mein, R. G., and Larson, C. L. (1973). "Modeling Infiltration During a Steady Rain." *Water Resources Research*, 9(2), 384–394.
- Nash, J. E., and Sutcliffe, J. V. (1970). "River Flow Forecasting through Conceptual Models Part I - A Discussion of Principles." *Journal of Hydrology*, 10, 282–290.

- Niazi, M., Nietch, C., Maghrebi, M., Jackson, N., Bennett, B. R., Tryby, M., and Massoudieh, A. (2017). "Storm Water Management Model: Performance Review and Gap Analysis." *Journal of Sustainable Water in the Built Environment*, 3(2), 04017002.
- Park, K., Kuo, A., Shen, J., and Hamrick, J.M. (1995). A three-dimensional hydrodynamic eutrophication model (HEM3D): description of water quality and sediment processes submodels, Gloucester Point, VA.
- Park, R.A. (1990). AQUATOX, a Modular Toxic Effects Model for Aquatic Ecosystems., Corvallis, OR.
- Park, R.A. & Clough, J.S. (2014). AQUATOX (Release 3.1 plus) Modeling Environmental Fate and Ecological Effects in Aquatic Ecosystems, Washington, D.C.
- Park, R.A. & Clough, J.S. (2000). AQUATOX for Windows, A Modular Fate and Effects Model for Aquatic Ecosystems, Release 1, Washington, D.C.
- Passeport, E. et al. (2009). Field Study of the Ability of Two Grassed Bioretention Cells to Reduce Storm-Water Runoff Pollution. *Journal of Irrigation and Drainage Engineering*, 135(4), pp.505–510.
- PennDOT. (2015). "PennDOT Drainage Manual." Pennsylvania Department of Transportation.
- Rawls, W. J., Brakensiek, D. L., and Miller, N. (1983). "Green-Ampt infiltration parameters from soils data." *Journal of hydraulic engineering*, 109(1), 62–70.
- Richards, L. A. (1931). "Capillary conduction of liquids through porous mediums." *Physics*, 1(5), 318–333.
- Rossman, L. (2015). "Storm Water Management Model User's Manual Version 5.1." US EPA.
- Rossman, L. A., and Huber, W. C. (2016). "SWMM Manual Volume 1 - Hydrology.pdf." US EPA.



- Rossman, L.A. and Huber, W.C. (2016). Storm Water Management Model Reference Manual  
Volume III-Water Quality, US EPA
- Rossman, L. A., and Supply, W. (2006). Storm water management model, quality assurance  
report: dynamic wave flow routing. US Environmental Protection Agency, Office of  
Research and Development, National Research Management Research Laboratory.
- Sangal, S. K., and Bonema, S. R. (1994). “A methodology for calibrating SWMM models.”  
Journal of Water Management Modeling, (R176-24), 375–387.
- Santhi, C., Arnold, J. G., Williams, J. R., Dugas, W. A., Srinivasan, R., and Hauck, L. M. (2001).  
“Validation of the SWAT Model on a Large River Basin with Point and Nonpoint  
Sources.” Journal of the American Water Resources Association, 37(5), 1169–1188.
- Saxton, K. E. (2009). “SPAW Field & Pond Hydrology.”  
<<https://hrsl.ba.ars.usda.gov/SPAW/Index.htm>> (Aug. 4, 2017).
- Saxton, K. E., and Willey, P. H. (2005). “The SPAW model for agricultural field and pond  
hydrologic simulation.” Mathematical modeling of watershed hydrology, 401–408.
- Schmidt, N. (2017). “Bioswale Modeling in a Transitive Urban Transportation Setting: Green  
Infrastructure Instrumentation, Challenges, And Lessons.” MS Thesis, Villanova  
University.
- Sharkey, L.J. (2006). The Performance of Bioretention Areas in North Carolina: A Study of  
Water Quality, Water Quantity, and Soil Media. North Carolina State University.
- Sharkey, L.J. & Hunt, W.F. (2004). Case studies on the performance of bioretention areas in  
North Carolina. In *Proceedings of Putting the LID on Stormwater Management*. College  
Park, MD.
- Sturm, T. (2001). Open Channel Hydraulics. McGraw Hill, New York, NY.

- Tan, S. B., Chua, L. H., Shuy, E. B., Lo, E. Y.-M., and Lim, L. W. (2008). “Performances of rainfall-runoff models calibrated over single and continuous storm flow events.” *Journal of Hydrologic Engineering*, 13(7), 597–607.
- Temprano, J., Arango, Ó., Cagiao, J., Suárez, J., and Tejero, I. (2005). “Stormwater quality calibration by SWMM: A case study in Northern Spain.” *water SA*, 32(1), 55–63.
- Tetra Tech. (2007). *Theoretical and computational aspects of sediment and contaminant transport in EFDC*, Fairfax, VA.
- Urbonas, B. (2007). “Stormwater Runoff Modeling; Is it as Accurate as We Think?” Keynote, International Conference on Urban Runoff Modeling, Humboldt State Univ., Arcata, CA
- US EPA Office of Water. (2000). *Low Impact Development (LID): A Literature Review*
- US EPA. (2015a). “What is Green Infrastructure?” US EPA, Overviews and Factsheets, <<https://www.epa.gov/green-infrastructure/what-green-infrastructure>> (Jun. 30, 2017).
- US EPA. (2017a). “Summary of the Clean Water Act.” Overviews and Factsheets, <<https://www.epa.gov/laws-regulations/summary-clean-water-act>> (Mar. 31, 2017).
- US EPA. (2017b). “Storm Water Management Model (SWMM).” Data and Tools, <<https://www.epa.gov/water-research/storm-water-management-model-swmm>> (Apr. 21, 2017).
- US EPA. (2017c). “Enforcement.” Announcements and Schedules, <<https://www.epa.gov/green-infrastructure/enforcement>> (May 16, 2017).
- US EPA, O. (2015b). “Combined Sewer Overflows (CSOs).” US EPA, Overviews and Factsheets, <<https://www.epa.gov/npdes/combined-sewer-overflows-csos>> (Aug. 22, 2017).

- US EPA. (n.d.). “Storm Water Management Model (SWMM).” Data and Tools,  
<<https://www.epa.gov/water-research/storm-water-management-model-swmm>> (Apr. 14,  
2017).
- Walkers & Syers. (1976). The fate of phosphorus during pedogenesis. *Geoderma*, 15(1), pp.1–  
19.
- Wang, K.-H., and Altunkaynak, A. (2012). “Comparative Case Study of Rainfall-Runoff  
Modeling between SWMM and Fuzzy Logic Approach.” *Journal of Hydrologic  
Engineering*, 17(2), 283–291.
- Wreck Pond Brook Watershed Technical Advisory Committee. (2008). Wreck Pond Brook  
Watershed Regional Stormwater Management Plan, Book 1: Watershed Characterization.  
Monmouth County Planning Board, Freehold NJ, 253.
- Yao, K., Habibian, M.T. & O’Melia, C.R. (1971). Water and Waste Water Filtration: Concepts  
and Applications. *Environmental Science & Technology*, 5(11), pp.1105–1112.

## **Chapter 7: Plant monitoring**

### **Introduction**

The Pennsylvania Department of Transportation (PennDOT) has integrated several hectares of vegetated stormwater infiltration basins into their plans for the Interstate 95 (I-95) renovation in northeast Philadelphia. However, selecting plants and designing landscaping plans for these basins presents a number of challenges. In particular, it is unclear how resilient various plant species will be to the unique stressors in these systems, including species that have proven to be suitable in smaller stormwater infiltration basins or adjacent to smaller roadways. For example, to be successful, plants at the lowest elevations of the SMPs (i.e., in the stormwater flow paths) will need to be tolerant of episodic inundation by water containing heavy metals and salts, extended periods of dry weather, and elevated temperatures (Table 7-1). Information useful for guiding species selection and placement is therefore critical to maximizing plant performance (i.e., survival, growth, health, and flowering). In addition, with appropriate information, vegetation planning and management could be done in such a way that it increases the provisioning of ecosystem services by the plant community (Lovell and Taylor 2013). For example, plants could be selected and placed for optimal heavy metal uptake, water export (via transpiration), pollinator habitat, and/or aesthetics.

The research described in this report is being carried out to inform the design of stormwater infiltration basins adjacent to I-95 by PennDOT in the coming 25 years. In particular, it focuses on SMPs installed during the first phase of this long-term project, such that successes and failures can be improved upon in future phases, and the ecosystem services provided by the SMPs can be optimized. The overarching goals of the plant monitoring program described here are to (a) evaluate plant health and soil conditions, (b) assess plant contributions to contaminant

uptake and stormwater management, and (c) inform the future selection of plant species. The specific components of this task include:

- a) Conducting inventories of plant species to determine survival rates and general patterns in plant health in the first two years following installation.
- b) Evaluating patterns of plant health as a function of topographic position using metrics of canopy size and leaf-level physiology (e.g., features of photosynthesis, stomatal conductance of water, and fluorescence).
- c) Identifying spontaneously occurring plant species, particularly in the minimally managed stormwater infiltration basin (SMP A).
- d) Measuring plant sorption and uptake of heavy metals and nutrients.
- e) Measuring heavy metals and other chemical constituents in the soil.

**Table 7-1.** Species with particularly high tolerance of inundation and/or salts. Group indicates functional group: G = graminoid, HP = herbaceous perennial, TS = tree or shrub. Salt denotes salt tolerance if a T is present

Species	Common name	Group	Light	Elevation	Salt
<i>Acorus calamus</i>	Sweetflag	G	sun to part shade	lower	
<i>Ammophila brevigulata</i>	Beach grass	G	sun	middle to upper (w/ sandy soil)	T
<i>Carex stricta</i>	Tussock sedge	G	sun to part shade	lower to middle	
<i>Juncus effusus</i>	Common rush	G	sun	lower	
<i>Panicum amarum</i>	Bitter panic grass	G	sun	middle to upper	T
<i>Panicum virgatum</i>	Switch grass	G	sun to part shade	lower to upper	T
<i>Scirpus cyperinus</i>	Woolgrass	G	sun to part shade	lower	
<i>Chelone glabra</i>	Turtlehead	HP	shade	lower	
<i>Helianthus angustifolius</i>	Swamp sunflower	HP	part shade	lower	
<i>Hibiscus moscheutos</i>	Rose mallow	HP	sun	lower to middle	T

<i>Lobelia siphilitica</i>	Great blue lobelia	HP	sun to part shade	lower to middle	
<i>Physostegia virginiana</i>	Obedient plant	HP	sun	middle	
<i>Pycnanthemum virginiana</i>	Virginia mountain mint	HP	sun	lower to middle	
<i>Solidago sempervirens</i>	Seaside goldenrod	HP	sun	lower to middle	T
<i>Baccharis halimifolia</i>	Eastern baccharis	TS	sun		
<i>Clethra alnifolia</i>	Sweet pepperbush	TS	sun to part shade	lower to middle	T
<i>Myrica pensylvanica</i>	Bayberry	TS	sun to part shade	middle to upper	T
<i>Physocarpus opulifolius</i>	Ninebark	TS	sun to part shade	middle to upper	
<i>Prunus maritima</i>	Beach plum	TS	sun	middle to upper	T
<i>Rhododendron viscosum</i>	Swamp azalea	TS	part shade	lower to middle	
<i>Rhus copallinum</i>	Winged sumac	TS	sun to part shade	middle to upper	T
<i>Rosa palustris</i>	Swamp rose	TS	sun	lower to middle	
<i>Salix discolor</i>	Pussy willow	TS	sun to part shade	lower to middle	T
<i>Salix nigra</i>	Black willow	TS	sun to part shade	lower	
<i>Sambucus canadensis</i>	Elderberry	TS	sun to part shade	lower to middle	T

## Methods

### *Plant Survival and General Health*

Several inventories of the intentionally planted vegetation were conducted in GR2, basins A, C, D, G, and E (as well as part of F). The vast majority of species were inventoried twice: first in mid-October 2016, approximately one year after planting, and again in late May 2017, after the plants had experienced two winters in the SMPs. All individuals from species that had leaves at the time of surveys were included in the inventory; the exceptions were two bulb species as they produce leaves only in early spring. To ensure that at least one of the bulb species would be represented in our dataset, we conducted a third inventory in early April 2017 that focused

exclusively on *Narcissus* ‘ice follies’. Additional observations, such as the presence of plant pests, were also made during the inventories.

Inventories were conducted by identifying spatially contiguous groups of plants from a single species (as mapped in the Landscaping Plan) and counting the number of living individuals in each group. Plants within each group were counted by two or three observers simultaneously, with discrepancies in counts triggering recounts until a consensus number was reached. In a few cases, it was not initially clear if small plants or small clusters of stems were (a) individuals that had been planted initially but were not thriving or (b) if new plants had been generated by clonal reproduction or growth from seed. These were dealt with on a case by case basis; a clear determination was reached in the majority of cases in October 2016. However, an increasing number of unclear cases became evident during the May 2017 survey, where plants growing as multi-stem clones had grown together such that it was not possible to identify even groups of stems belonging to a single individual. *Monarda didyma* was arguably the most challenging such case. We provide below our best estimates of counts, but recommend use cover-based assessments rather than counts in the future to avoid this and other complicating issues.

While we could directly account for dead plants that were present, we made the assumption that all plants that were missing (i.e., in the Landscape Plan but not present) had died since the time of installation and had not gone missing for other reasons (e.g., theft). At the outset of our first inventory we sought to verify that missing plants had, in fact, been planted originally and were not absent simply because they were never planted. Evidence of truly missing plants included incisions in the landscaping fabric or gaps in the mulch where a plant was likely to have been placed. These often occurred in locations that were likely to be stressful

for plants (e.g., in the primary flow path of stormwater). In the end, we found high fidelity between the Landscaping Plan and the estimated number of installed plants, and only one clear case in which an insufficient number of plants was installed. There were several cases in which counts of living plants slightly exceeded the number we expected to find, so we adjusted our ‘planted’ counts accordingly. We concluded that designating all missing plants as dead would lead to a negligible number of inaccuracies in survival rates. We later determined that there were a few cases where root systems remained alive despite shoot systems senescing; further information is provided below.

There were several cases in which we located clusters of plants during one of the two primary inventories but not the other. These were due to human error associated with visually identifying clusters of plants on the Landscaping Plan or in the field; they occurred in ~10 of the 500 attempts to locate plant clusters. Nevertheless, we infilled missing data in these cases by assuming that plant numbers had not changed between the two surveys. Another issue became apparent during the May 2017 inventory, namely that some individuals of a few species (e.g., *Geranium maculatum*) had senesced prior to our October inventory, such that we had overcounted dead plants. These few cases therefore show spurious increases in living plants from first to the second inventories. These were not adjusted as we felt it was more important for data on health class fractions (described subsequently) to remain accurate.

In addition to counting the total number of living plants, we rated plant health on a 0-3 scale, determining the number of individuals within each group that fell into each category. The criteria for the four health ratings were as follows:

- Class 3: Apparently healthy and either full sized or minimally stunted growth.
- Class 2: Some evidence of reduced health (e.g., more than a few dead leaves) and/or moderately stunted growth ( $\leq 50\%$  of full-size).



- Class 1: Visually unhealthy (e.g., many dead leaves) and/or having severely stunted growth ( $\leq 25\%$  of full-size).
- Class 0: Dead or presumed dead (see below).



Figure 7-1. Examples of health rating classes 1-3. The remaining class (designated 0) is assigned to dead plants. The species shown is *Calamagrostis* × *acutiflora* ‘Karl Foerster’, which is one of the most abundant species in the study area.

### Gradient Approach

We took a combined approach in addressing subtasks on plant health (*b*), plant contaminant uptake (*d*), and soil conditions (*e*). The approach took advantage of the planting design, which frequently located groups of plants from a single species (or alternating rows of plants from two species) on slopes. Given that all plants from a given species were similar in size when planted, this configuration provided a means of assessing the effects of elevation on numerous aspects of plant health. In this setting, variation in elevation is likely to be associated

with several co-occurring factors: soil saturation or flooding during and after precipitation events (with increased soil moisture for some period after), physical disturbance from infrequent but high-velocity stormwater inflows, and exposure to any salts, heavy metals, or other contaminants in the stormwater. While a controlled experiment would be necessary to determine the extent to which these factors influence variation in plant health, the gradient approach is a well-established method for inferring how environmental conditions *likely* affect plants (Whittaker 1967). Moreover, our initial observations suggested that plants from a number of species had more strongly stunted growth when they were closer to the bottom of the basins (Figures 7-1 and 7-2). In addition, individuals of some species changed color and senesced earlier when growing at lower elevations (e.g., *Viburnum trilobum*).

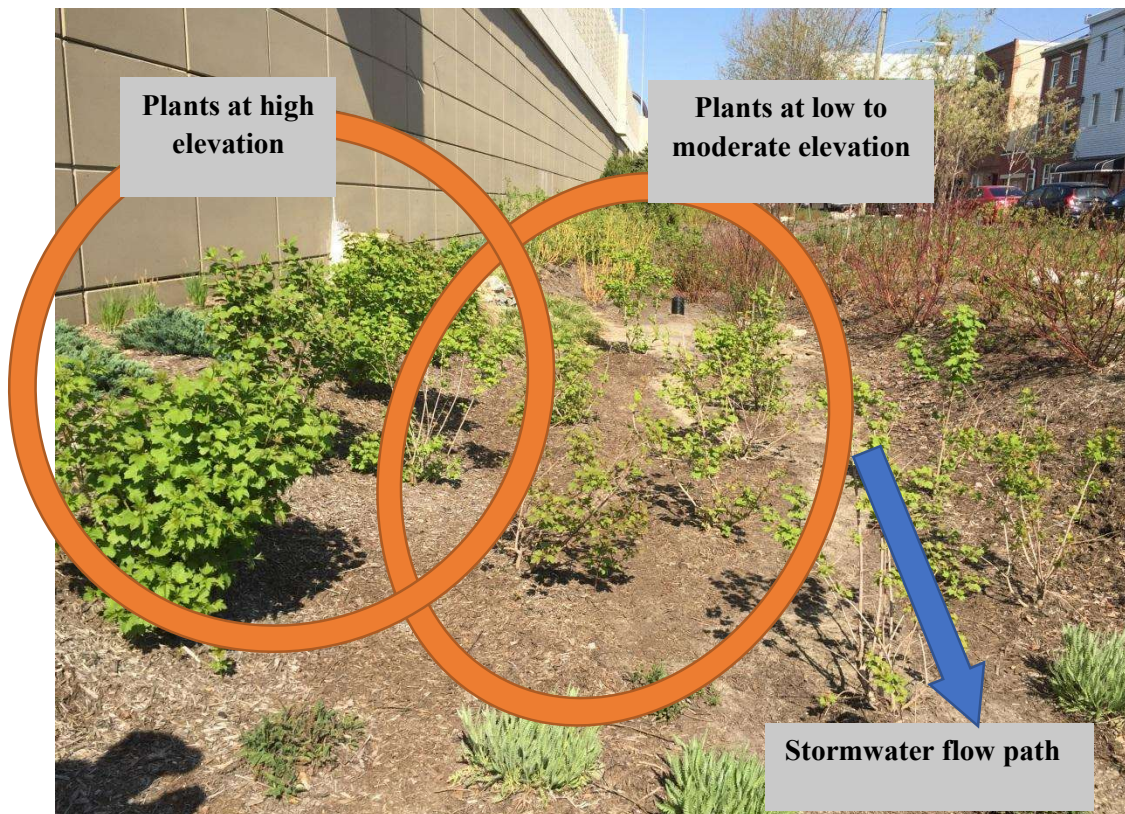


Figure 7-2. Example of plant health differing by elevation. The species shown is *Viburnum trilobum* 'Wentworth'; the photo was taken in April 2017.

Using a set of 72 plants spanning the elevation gradient in SMPs A, C, and D, we conducted three field campaigns during the 2017 growing season (in June, July, and August) and plan to conduct another in October. These campaigns were undertaken to provide the physiological field data, leaf samples, and soil samples needed to complete subtasks b, d, and e. During each campaign we (a) collected measurements from 8 individuals from 9 focal species (Table 7-2) and (b) collected soil and leaf tissues for further analysis. The eight plants from each species were selected in pairs or triads distributed across the combined length of the SMPs (Fig. 7-3). Each field campaign was conducted over 2-3 consecutive days when weather was clear. The measurements and samples taken during each round of field visits included the following; methodological details are provided in the corresponding sections below:

- Plant canopy size
- Leaf-level physiology
- Soil sampling
- Leaf samples

To characterize plant position along the elevation gradient and its implications for soil moisture, we precisely determined elevations for each of the 72 focal plants and measured the water content of soil. Plant elevations were determined from the LiDAR dataset collected in October 2016 (see Chapter 5). Once each plant was identified in the LiDAR point cloud, the XYZ coordinates of points at the base of each plant were extracted. Local elevation baselines were then subtracted from the mean of the two Z coordinates for each plant, such that final elevation values reflected distances above the local topographical low. In most cases, this was the base of the outlet box or weir nearest the plants.



Volumetric soil moisture content was measured at three locations near the base of each plant on each of the same days that leaf physiology measurements were taken. Measurements were made using a time-domain reflectometry (TDR) probe that penetrated to 20 cm depth (FieldScout TDR 100, Spectrum Technologies, Aurora, IL).



**Plant locations overlaid on 3-inch aerial photography from 2015**

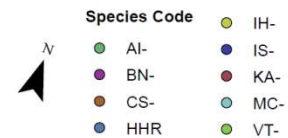


Figure 7-3. Locations of the 72 focal plants used in this investigation. Soil samples were collected from these locations as well. Species codes are defined in Table 7-2. Note that locations are approximate, as the LiDAR scans from which they were determined have not been precisely registered in real space.

Table 7-2. Species selected for in-depth studies of plant ecophysiology.

Species code	Scientific name	Common name
HHR	<i>Hemerocallis</i> 'Happy returns'	Happy returns daylily
CS	<i>Cornus sericea</i> 'Cardinal'	Red-osier dogwood
BN	<i>Betula nigra</i> 'Heritage'	Heritage river birch
VT	<i>Viburnum trilobum</i> 'Wentworth'	American cranberrybush

IS	<i>Iris sibirica</i> 'Caesar's brother'	Caesar's brother iris
MC	<i>Monarda didyma</i> 'Cambridge scarlet'	Cambridge scarlet beebalm
AI	<i>Asclepias incarnata</i> 'Ice ballet'	Swamp milkweed
KA	<i>Calamagrostis x acutiflora</i> 'Karl Foerster'	Karl Foerster's feather reed grass
IH	<i>Itea virginica</i> 'Little Henry'	Virginia sweetspire dwarf

### *Topographic Variation in Plant Health*

This sub-task entailed measuring a suite of characteristics in order to evaluate plant health, in particular the ability of commonly used species in the SMPs to tolerate inundation by stormwater and the contaminants it contains. To accomplish this, we collected data on canopy size (in August) and leaf-level physiology (in June, July, and August) from each of the 72 focal plants (8 individuals from each of 9 species), with individuals within each species spanning the highest to lowest elevations within the SMPs. All measurements were repeated during the monthly field campaigns; this was necessary because several factors change through time, including antecedent precipitation conditions, ambient temperature, leaf development and senescence, and herbivore pressure.

### Canopy Size

Plant heights and the widths of their canopies were measured immediately after the August field campaign. Heights were measured directly for small plants (i.e., using a measuring stick), with measurements made in triplicate (at the tallest point and two additional points where the canopy was more dense). Widths were measured across the widest axis of each plant's canopy and in the direction perpendicular to that. The edge of the canopy was taken to be where the plant covered approximately 50% of the observer's visual field. Canopy size was then calculated as the volume of an elliptical cylinder using mean height and width values. To

facilitate comparisons across species, canopy volumes were rescaled by subtracting the appropriate species mean from each value and dividing by the corresponding standard deviation.

### Leaf-level Physiology

We measured features of both gas exchange (i.e., water export through transpiration and carbon dioxide (CO<sub>2</sub>) fixation through photosynthesis) and fluorescence (which is particularly well suited for identifying stress-induced damage to chlorophyll). With a state-of-the-art instrument for measuring gas exchange and fluorescence simultaneously (an LI-6800, LI-COR Biosciences, Lincoln, NE), we recorded data for one leaf from each of the 72 plants in sequence, spanning morning through mid-day. To remove the influence of diurnal changes in environmental conditions we had the instrument maintain an irradiance of 1000  $\mu\text{mol photons m}^{-2} \text{ s}^{-1}$ , a constant temperature (20°, 30°, and 28° C in June, July, and August, respectively), a reference CO<sub>2</sub> concentration of 400 ppm, and a relative humidity level of 70%. Note that irradiance was specifically that of photosynthetically active radiation (PAR) and most appropriately referred to as photosynthetic photon flux density (PPFD).

Measurements of gas exchange included rates of net carbon assimilation (hereafter, photosynthesis or  $A_{\text{net}}$ ) and stomatal conductance to water ( $g_s$ ). Stomatal conductance is derived from transpiration ( $E$ ), but scales  $E$  to the evaporative demand of the air surrounding the leaf. Stomatal conductance thus reflects plant control of water loss directly, whereas measurements of transpiration are additionally influenced by environmental conditions. We note that, under the controlled conditions of the LI-6800's leaf chamber, these two measures remain highly correlated. We additionally calculated water use efficiency, calculated as  $A_{\text{net}}/E$ , which describes the amount of carbon gained per unit water lost. Fluorescence measurements made with the LI-6800 simultaneous with gas exchange used the multi-phase flash (MPF) method to determine

light-adapted maximum and basal fluorescence yields ( $F_m'$  and  $F$ , respectively). These values were used to calculate  $\Phi_{\text{PSII}}$ , the quantum efficiency of PSII-mediated electron transport [ $\Phi_{\text{PSII}} = (F_m' - F) / F_m'$ ].

We used four additional photosynthesis systems (LI-6400XT, LI-COR Biosciences, Lincoln, NE) to measure an additional set of biophysical parameters. These instruments were loaned to Temple by Rutgers University, Bryn Mawr College, and the Smithsonian Environmental Research Center; a colleague from Rutgers was also sub-contracted to assist with data collection (Dr. Allyson Salisbury) as she has the expertise to run two of the instruments simultaneously. The leaf chambers of the LI-6400XTs were set to  $\text{CO}_2$  and temperature conditions matching those of the LI-6800, but relative humidity cannot be controlled as tightly with these instruments and was allowed to vary between 60-80%. This range is above the threshold at which most plants restrict stomatal conductance and below the threshold at which water can condense in the instrument. It is therefore a widely used humidity range for conducting these kinds of gas-exchange measurements.

The determination of biophysical parameters with LI-6400XTs relied on a technique called photosynthetic light response curves (or simply 'light curves'). Light curves entail altering PPFD from saturating to absent and measuring gas exchange at each PPFD level. They allow several key biophysical parameters to be determined, specifically once they are fitted with a mathematical function describing the light-dependence of the physical and biochemical processes that most strongly limit photosynthesis at a given PPFD. We recorded light curves on each of the 72 focal plants during our three field campaigns using the PPFD sequence: 2000, 1500, 1000, 500, 200, 100, 50, 20, 0  $\mu\text{mol m}^{-2} \text{s}^{-1}$ . We then fit a well-established non-rectangular hyperbolic function to the resulting data from each sequence of measurements (Prioul and

Chartier 1977) using the *nls* function in the statistical computing software R version 3.4 (R Project for Statistical Computing, Vienna, Austria). This yielded each of the following parameters:

- **A<sub>sat</sub>**: light-saturated photosynthesis (asymptotic maximum rate of carbon fixation rate that the leaf is capable of)
- **R<sub>d</sub>**: dark respiration (rate of CO<sub>2</sub> release from the leaf due to basal metabolic processes)
- **QY**: quantum yield (moles of CO<sub>2</sub> fixed per mole of photons incident on the leaf)
- **k**: convexity (transition rate from light-limitation of photosynthesis to biochemical limitation)

In addition, we calculated several additional parameters:

- **LCP**: light compensation point (the light level at which CO<sub>2</sub> intake through photosynthesis is equal to CO<sub>2</sub> lost through respiration).
- **A<sub>1k</sub>**: photosynthesis rate at PPFD = 1000  $\mu\text{mol m}^{-2} \text{s}^{-1}$  (determined as the mean of the pair of values collected with the LI-6800 and the LI-6400XT on a given day).

### *Spontaneous Vegetation*

The identity of spontaneously occurring plants (a.k.a. weeds) present in GR2 bioswales were noted when they were encountered during field visits. A list of these taxa (typically identified to species, but to genus in some cases) was compiled subsequently.

### *Contaminant Uptake*

We used leaves collected from the 72 focal plants during each of the field campaigns for analysis of heavy metals and select other elements. Depending on leaf sizes, between 5 and 25 leaves were collected per plant or, in the cases of a few small plants, neighboring plants from the



same species at the same elevation. Leaves were sealed in plastic bags and kept cool until they could be processed. Processing took place in the lab and involved weighing, counting, scanning for leaf area, rinsing in nanopure water, drying, reweighing, crushing, and mixing. A subsample ( $0.5 \pm 0.01$  g) was later digested in concentrated, trace metal grade nitric acid. Digestion was performed in a microwave digester following the CEM protocol for plant tissue (CEM 2016a). We are in the process of analyzing elemental concentrations in digests via inductively-coupled plasma mass spectrometry (ICP-MS).

Combining concentration data for leaf tissue with that from soils (see subtask *e*), we will determine bioconcentration factors (BCFs) for the 9 focal species, as well determine which metals accumulate in leaf tissues of each species through the growing season. BCFs are the ratios of an element in living tissue vs. in the soil, and are a commonly used for assessing the accumulation of contaminants in biota (e.g., Zhuang *et al.* 2007; Gobas *et al.* 2016).

### *Soil Contaminants*

Soil to be used for elemental analysis was collected from three locations beneath the canopies of each of the 72 focal plants. Samples came from the upper 5 cm of soil; if necessary, we temporarily removed mulch and landscape fabric to gain access to the soil itself. Acid-washed scoops were used to minimize potential for contamination. Samples were composited, sealed in plastic bags, and chilled until further processing could be completed. In the lab, samples were divided for (a) elemental analysis, (b) nutrient analysis, and (c) microbial characterization.

Subsamples intended for elemental analysis were weighed, dried, reweighed, and sieved to 2 mm. Contact with metal was avoided throughout this process (e.g., sieving was done using acid-washed polyethylene mesh). Subsamples ( $0.5 \pm 0.01$  g) were subsequently subjected to

microwave extraction in concentrated, trace metal grade nitric acid (EPA method 3051a; CEM 2016b) and diluted for elemental analysis using an ICP-MS (Agilent Technologies, Santa Clara, CA). At the time of writing, the samples collected during the July field campaign have been analyzed via ICP-MS.

Given that pH influences the availability of most heavy metals in soil, we measured pH in one set of our soil samples, namely those from the July field campaign ( $n = 72$ ). Measurements were made after making a 1:1 slurry with water using a PC 700 pH/conductivity meter (Oakton, Vernon Hills, IL). We opportunistically measured conductivity simultaneously, as soil conductivity is often correlated with soil salinity and could therefore be an indicator of road-salt residuals in the soil. However, soil conductivity measurements are also influenced by ions in the soil from other sources, and are not definitive.

We are evaluating X-ray fluorescence (XRF) as an alternative means of measuring heavy metal concentrations in soil samples. Although XRF is an indirect measure of elemental concentrations, it is less expensive and higher-throughput than ICP-MS and there are many precedents its use with soils (e.g., Peterson 2014; Kondo *et al.* 2016). Samples from the June and July rounds of sample collection have been measured with an XRF, and we are in the process evaluating the accuracy and repeatability of XRF measurements. If data prove to be highly consistent with those measured via ICP-MS, future efforts can focus on XRF.

## **Results and Discussion**

### *Plant Survival and General Health*

The inventory we conducted accounted for 8,124 plants (Table 7-2). The majority of these (54%) were herbaceous perennials, i.e., species whose root systems remain alive through winter but whose shoots senesce. The second most common functional group was that of

graminoids (i.e., grasses, sedges, and similar; these are referred to as Ornamental grasses in the Landscaping Plan), followed by shrubs and bulbs. Trees were the least common functional group planted, which could be expected based on their size. A species-specific summary of the number of individuals planted and the number that we found alive during each of our inventories appears in Figure 7-4.

Of the 8,124 plants originally in the inventoried SMPs, 6,438 survived until May 2017 (Table 7-3). In other words, 79.2% of plants lived through two winters in the SMPs, which was an increase relative to the 6,102 plants identified as living in October 2016. As described above, the reason for the upward revision was that all aboveground organs had senesced in a number of plants by October (in particular, 359 individuals of *Geranium maculatum*), more than compensating for the number of plants lost during the winter of 2016-17. However, there was a decline in health for a number of species during that winter. While 2.0% of plants were noted as being severely unhealthy or having severely stunted growth (class 1) in October 2016, 5.4% of plants had that status by May 2017. Further, 5.7% of plants were reduced in size or modestly unhealthy (class 2) in October, whereas 12.3% were in that category the following May. As a result of these declines, the fraction of plants that appeared to be healthy (class 3) declined from 92.3% to 82.3% during the winter of 2016-17. We note that the above values were highly variable across plant functional groups, with perennials having substantially lower survival than the other functional groups (Table 7-3). The fraction of individuals in health rating classes 1 and 2 was also notably greater for perennials than for other functional groups.

*Table 7-3. Survival and health ratings for plants in GR2 during the two inventories conducted. Note that Bulbs only includes Narcissus ‘ice follies’ and was surveyed separately from other species due to its early-season life cycle.*

Inventory	Functional	Planted	Living	Survival	Mortality	Class 1	Class 2	Class 3
-----------	------------	---------	--------	----------	-----------	---------	---------	---------

	group							
Oct 2016	<i>Bulbs</i>	600	494	82.3%	17.7%	0.0%	0.0%	100.0%
	<i>Graminoids</i>	1804	1620	89.8%	10.2%	0.5%	4.8%	94.8%
	<i>Perennials</i>	4414	2745	62.2%	37.8%	3.6%	9.3%	87.1%
	<i>Shrubs</i>	1179	1122	95.2%	4.8%	1.0%	1.1%	98.0%
	<i>Trees</i>	127	121	95.3%	4.7%	0.8%	5.0%	94.2%
	<b>Total</b>	<b>8124</b>	<b>6102</b>	<b>75.1%</b>	<b>24.9%</b>	<b>2.0%</b>	<b>5.7%</b>	<b>92.3%</b>
May 2017	<i>Bulbs</i>	600	494	82.3%	17.7%	0.0%	0.0%	100.0%
	<i>Graminoids</i>	1804	1620	89.8%	10.2%	4.3%	14.0%	81.7%
	<i>Perennials</i>	4414	3110	70.5%	29.5%	7.9%	15.6%	76.6%
	<i>Shrubs</i>	1179	1089	92.4%	7.6%	2.2%	7.0%	90.8%
	<i>Trees</i>	127	125	98.4%	1.6%	4.8%	6.4%	88.8%
	<b>Total</b>	<b>8124</b>	<b>6438</b>	<b>79.2%</b>	<b>20.8%</b>	<b>5.4%</b>	<b>12.3%</b>	<b>82.3%</b>

Within functional groups, survival rates and plant health differed considerably by species (Figures 7-4 and 7-5). Variation was greatest for perennials, with a number of species losing <10% of individuals by May 2017 (e.g., *Hemeroacallis* spp.) while other perennials had among the highest mortality rates at the site:

- *Cimicifuga ramosa* ‘hillside black beauty’ (87%)
- *Matteuccia struthiopteris* (50%)
- *Geranium maculatum* (48%)
- *Monarda didyma* ‘Cambridge scarlet’ (40%)
- *Echinacea purpurea* (38%)
- *Asclepias incarnata* ‘ice ballet’ (30%)
- *Rudbeckia fulgida* var. *sullivantii* ‘Goldsturm’ (28%)

- *Hosta* ‘royal standard’ (27%)
- *Liatris spicata* (26%)

We found relatively high rates of suboptimal health in all of the aforementioned species as well (often 30-40% of those still living), potentially indicating that they were not planted in suitable locations. It is also possible that the plant material was unhealthy when delivered or that these species were preferentially damaged by pathogens or herbivores after installation. In one case, namely that of *Asclepias incarnata* ‘ice ballet’, we did observe excessively high numbers of aphids on the plants in July 2017.

Although first-year survival rates were relatively high for bulbs, graminoids, shrubs, and trees, there were several species that had mortality >10% in May 2017 (Figure 4-3):

- *Narcissus* ‘ice follies’ (18%, bulb)
- *Pennisetum alopecuroides* ‘Hameln’ (30%, graminoid)
- *Carex vulpinoidea* (14%, graminoid)
- *Forsythia suspensa sieboldii* (83%, shrub)
- *Kerria japonica* (32%, shrub)
- *Thuja occidentalis* ‘Holmstrup’ (13%, tree)

Percentages of plants in health classes 1 and 2 (i.e., those with distinctly suboptimal health) increased for a number of species between the October 2016 and May 2017 inventories. Although health ratings are not fully comparable between the two surveys (having taken place at different times of year) the general expectation is that plants would be less healthy in fall than in spring. Given that the situation was reversed in most cases, it would appear that increases in ratings of 1 and 2 correspond to increasing growth limitation or ill health for a number of species through time. Among the most prominent such cases are those of *Achillea*

*millefolium* 'fireland' (a perennial), *Calycanthus floridus* (a shrub), *Viburnum trilobum* 'Wentworth' (a shrub), and *Crataegus phaenopyrum* (a tree). There were a few cases in which plants that appeared to be dead in the October 2016 inventory were found to be living the following May (e.g., *Geranium maculatum*, *Picea pungens*, and *Thuja occidentalis* 'emerald green'). All of the above cases warrant further observation to determine if they are in decline at the site and, if so, for what reasons.

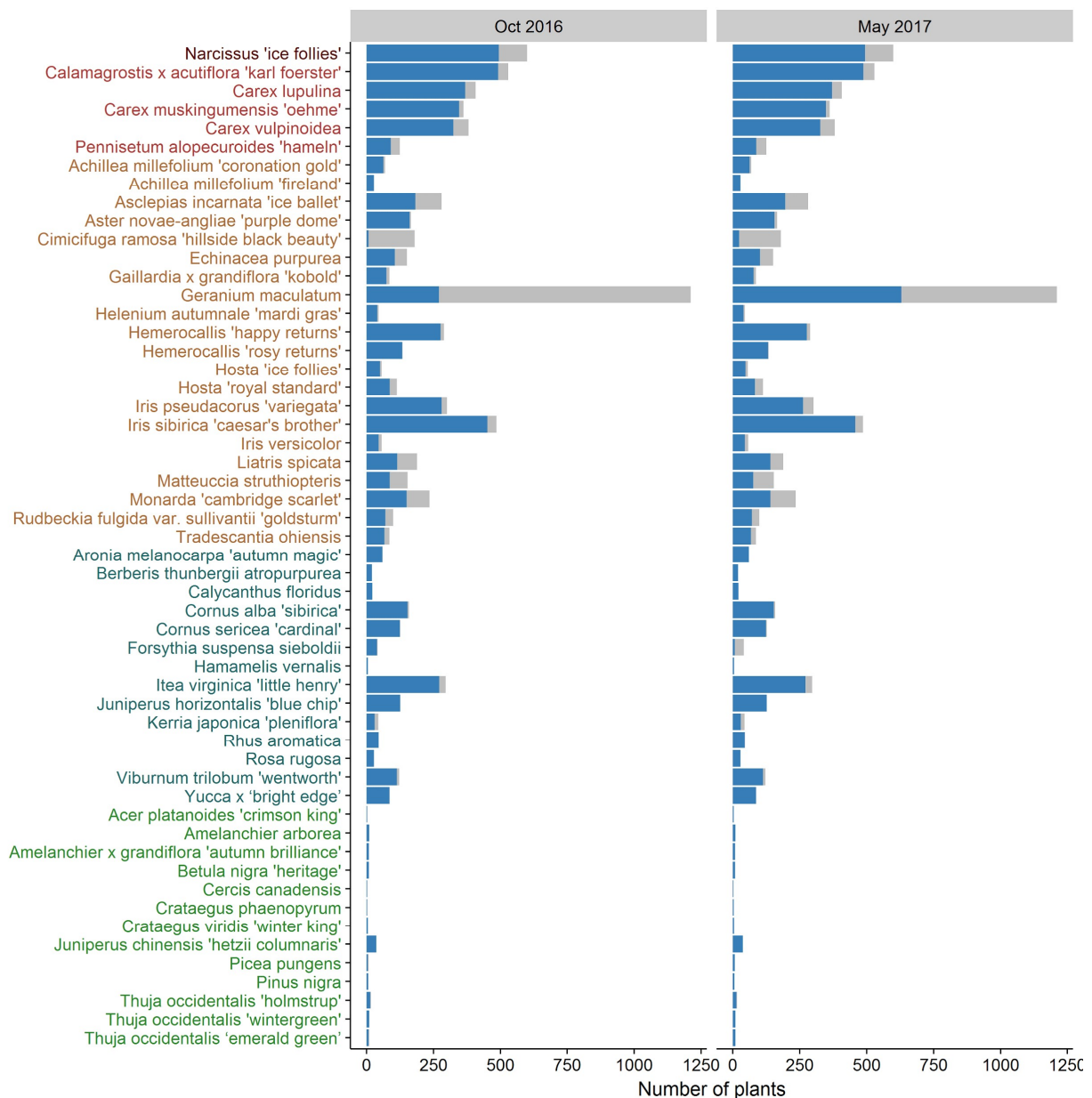


Figure 7-4. The number of plants of each species found living during surveys (blue bars), and the total number planted (gray bars). Coloration of species names corresponds to functional groups: bulbs (dark red), graminoids (light red), perennials (brown), shrubs (blue), trees (green).

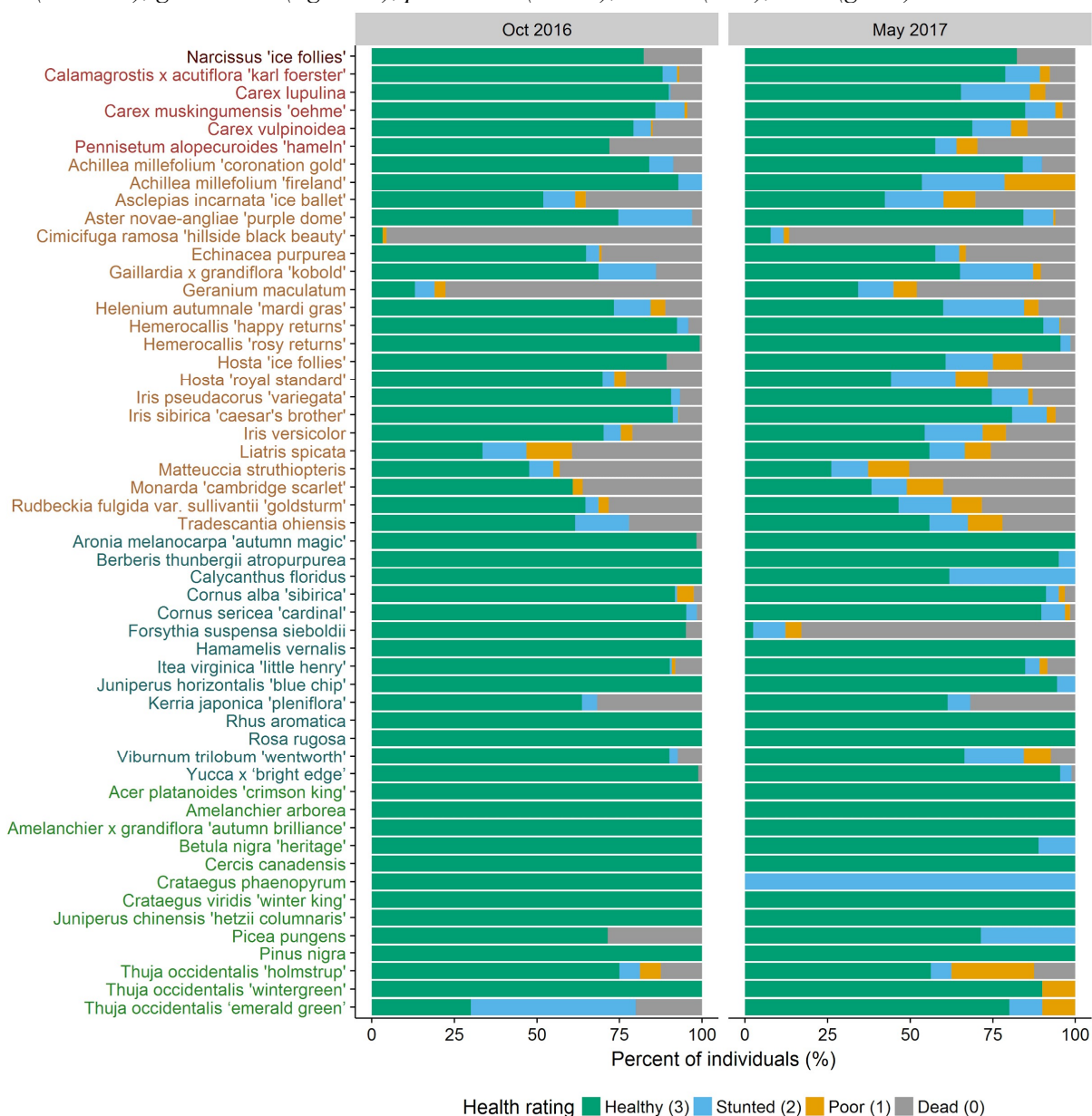


Figure 7-5. The percentage of plants of each species falling into each of four health rating classes. See text for a more detailed explanation of the criteria used to rate plant health. Coloration of species names corresponds to functional groups: bulbs (dark red), graminoids (light red), perennials (brown), shrubs (blue), trees (green).

### *Taxonomic Discrepancies*

While there was typically agreement between the taxonomic identity of plants in the Landscaping Plan and those ultimately planted, there were a few discrepancies. With the exception of *Lindera benzoin*, we have not altered the names used in this report.

- A group of 21 *Lindera benzoin* plants (spicebush, a native Northeast forest shrub) was slated for installation in basin E. An equal number of plants of a different shrub species (*Calycanthus floridus*) was planted in their place. It is likely that a lack of availability of the species from the supplier led to the replacement; while *L. benzoin* is a common native in Northeast forests, few nurseries propagate it because it is slow growing and has low survival rates in greenhouse settings. It is also possible that a decision was made to deviate from the plans due to *L. benzoin* being known as an understory/shade plant, as the location for which it was intended had relatively high exposure.
- One of the three species of *Carex* at the site, namely *C. lupulina* appears to have been replaced by a congener (different organism within the genus), *Carex flacca* (cultivar ‘Blue Zinger’). The plants used throughout all basins where the Landscaping Plan indicates that these were to be planted appear to have been consistently replaced.
- The species listed as *Cimicifuga ramosa* ‘hillside black beauty’ is likely a congener, or at the least, a different cultivar. Note that this taxon had the highest mortality rate at the site.
- The species listed as *Cornus sericea* ‘Cardinal’ is likely another *Cornus* species, as *C. sericea* has red stems, whereas the planted taxon has yellow-green stems.
- The species listed as *Kerria japonica* ‘pleniflora’ is the straight species *Kerria japonica*, not the ‘pleniflora’ cultivar.



## Spontaneous Vegetation

A total of 26 species were observed growing spontaneously in GR2 during field visits (Table 7-4). All are common species in urban areas of the Northeast (Del Tredici 2010). Among these, *Senecio vulgaris* has become the most abundant in the 1.5 years since the SMPs were completed. Two other species that are particularly likely to spread, and therefore become serious management concerns, are *Aretmisia vulgaris* and *Cirsium arvense*.

Table 7-4. Species of spontaneously occurring plants in GR2.

Species	Common name	Family
<i>Amaranthus hybridus</i> L.	Pigweed	Amaranthaceae
<i>Arctium</i> sp.	Burdock	Asteraceae
<i>Artemisia vulgaris</i> L.	Common wormwood, mugwort	Asteraceae
<i>Bidens frondosa</i> L.	Beggar-ticks	Asteraceae
<i>Capsella bursa-pastoris</i> (L.) Medik.	Shepherd's purse	Brassicaceae
<i>Cardamine</i> sp.	Bitter-cress	Brassicaceae
<i>Cirsium arvense</i> (L.) Scop.	Canada thistle	Asteraceae
<i>Convolvulus arvensis</i> L.	Field bindweed	Convolvulaceae
<i>Conyza canadensis</i>	Horseweed	Asteraceae
<i>Coronopus didymus</i> (L.) Sm.	Wartcress, swinecress	Brassicaceae
<i>Echinochloa muricata</i> (P.B.Eauv.) Fernald	Barn-yard grass, cockspur	Poaceae
<i>Erigeron philadelphicus</i> L.	Daisy fleabane	Asteraceae
<i>Galium aparine</i> L.	Bedstraw, cleavers	Rubiaceae
<i>Juncus effusus</i> L.	Soft rush	Juncaceae
<i>Lactuca serriola</i> L.	Prickly lettuce	Asteraceae
<i>Malva neglecta</i> Wallr.	Common mallow, cheeseweed	Malvaceae
<i>Oenothera perennis</i> L.	Sundrops	Onagraceae
<i>Persicaria lapathifolia</i> (L.) S.F. Gray	Willow-weed	Polygonaceae
<i>Rumex obtusifolius</i> L.	Bitter dock	Polygonaceae
<i>Securigera varia</i> (L.) Lassen	Crown vetch	Fabaceae
<i>Senecio vulgaris</i> L.	Groundsel	Asteraceae

<i>Setaria faberi</i> Herrm.	Giant foxtail	Poaceae
<i>Setaria viridis</i> (L.) P.Beauv.	Green foxtail	Poaceae
<i>Stellaria</i> sp.	Chickweed	Caryophyllaceae
<i>Taraxacum officinale</i> F.H. Wigg.	Common dandelion	Asteraceae
<i>Trifolium campestre</i> Schreb.	Low hop-clover	Fabaceae

### *Topographic Variation in Plant Health*

#### Canopy Size

For the majority of species, canopy volumes became progressively smaller as plants were positioned lower in the SMPs (Fig. 7-6). This was the case for *Asclepias incarnata*, *Calamagrostis x acutiflora*, *Hemerocallis*, *Iris sibirica*, and *Monarda didyma*. Two of the exceptions to this pattern (*Cornus sericea* and *Viburnum trilobum*) instead had reduced canopy sizes at both low and high topographic positions. *Betula nigra* appeared to be reduced in size when growing at the lowest elevation, but was otherwise unaffected by topographic position.

When evaluated as a function of soil water content, canopy volumes again showed linear changes, with reduced growth apparent in the wettest soils (Fig. 7-7). In fact, two of the species for which the relationship with elevation was non-linear (*Cornus sericea* and *Betula nigra*) had notably linear relationships with soil water. However, the relationship for *Calamagrostis* × *acutifolia* and *Viburnum trilobum* were less clear with respect to the soil water gradient than they were with respect to elevation.

Given the evidence currently available, we suspect that the primary factor contributing to size reductions with decreasing elevation is soil saturation. Although there are exceptions, lower elevations typically correspond to longer durations of saturation, which can have several implications for plants. For one, roots are active sites of aerobic

respiration in terrestrial plants, and aerobic respiration cannot take place in flooded conditions when oxygen is unavailable, ultimately limiting growth. Also, soil microbial communities can be strongly influenced by soil saturation, with mycorrhizal fungi frequently less able to survive and provide roots with nutrients. Instead, pathogenic fungi and bacteria are more likely to kill and decrease the health of root systems. As many terrestrial plants can withstand prolonged periods of minimal rainfall, albeit with reduced growth, those that are not specifically adapted to wet environments can be more strongly impacted by prolonged soil saturation.

Finding correlations between plant size and elevation and/or soil water content does not rule out the possibility that salts, heavy metals, or other contaminants could be affecting plant health in the lower topographic positions of the SMPs, or that they could affect plant health in the future. However, we do not yet see evidence of heavy metals or salts/conductivity varying with elevation, nor have we measured problematically high levels of those factors (see subtask *e*). Unless and until there is evidence for chemical limitations to plant growth, we tentatively conclude that inundation is the strongest factor limiting to plant growth in the SMPs currently.

We note that, in interpreting canopy size to equate to growth, we have assumed that all plants within each species were the same size when planted. Although there was certainly some variation in the plant material provided by the original source, batches of nursery-grown plants typically have consistent sizes. Therefore, the magnitude of size variation at the time of planting was likely to be far smaller than the magnitude of differences over the elevation gradient reported here, and not a confounding factor in this analysis.

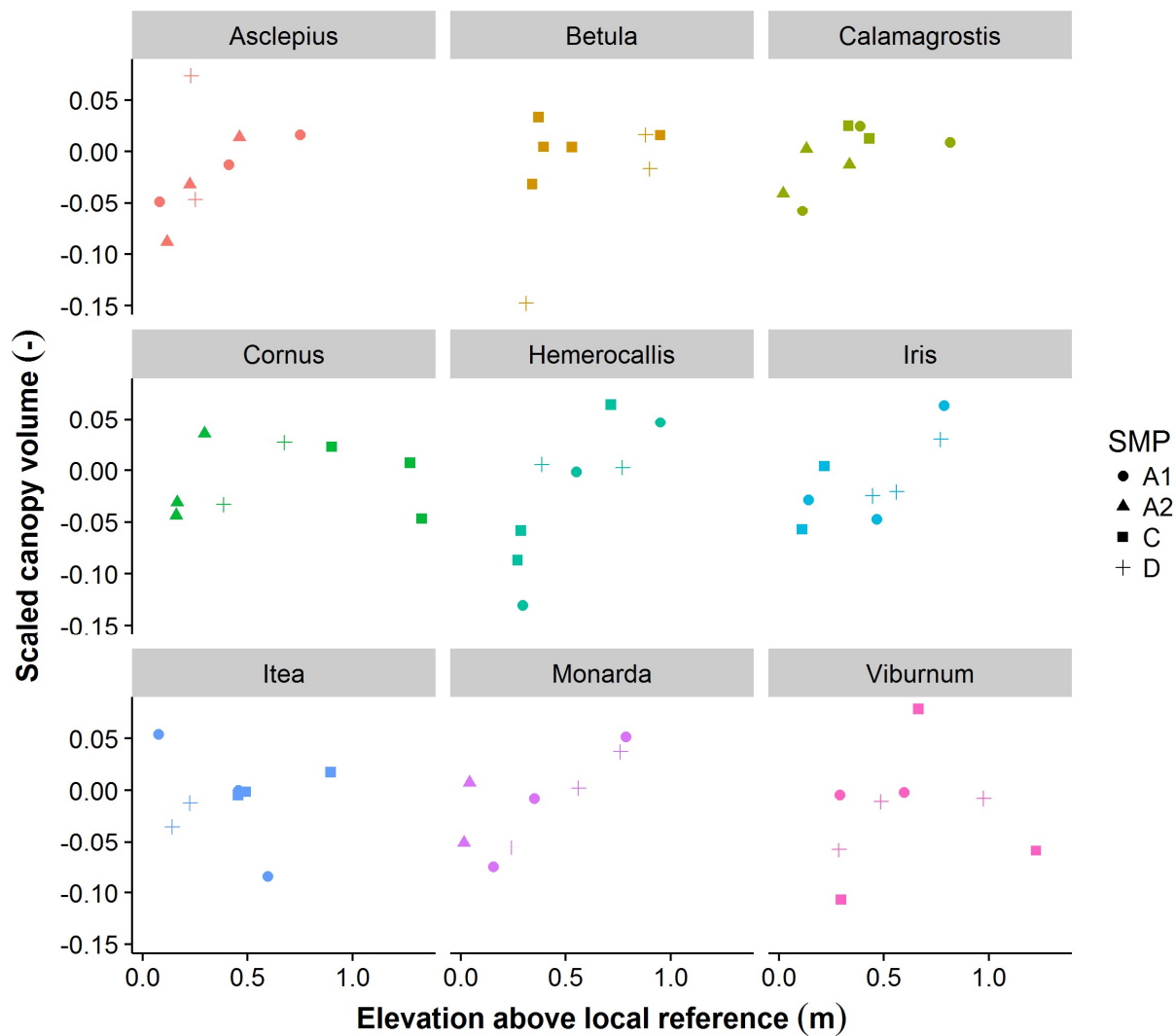


Figure 7-6. Canopy size (scaled according to the species mean and standard deviation) as a function of topographic position. Note that elevations are likely proportional to related metrics like the total numbers of hours that soils are saturated.

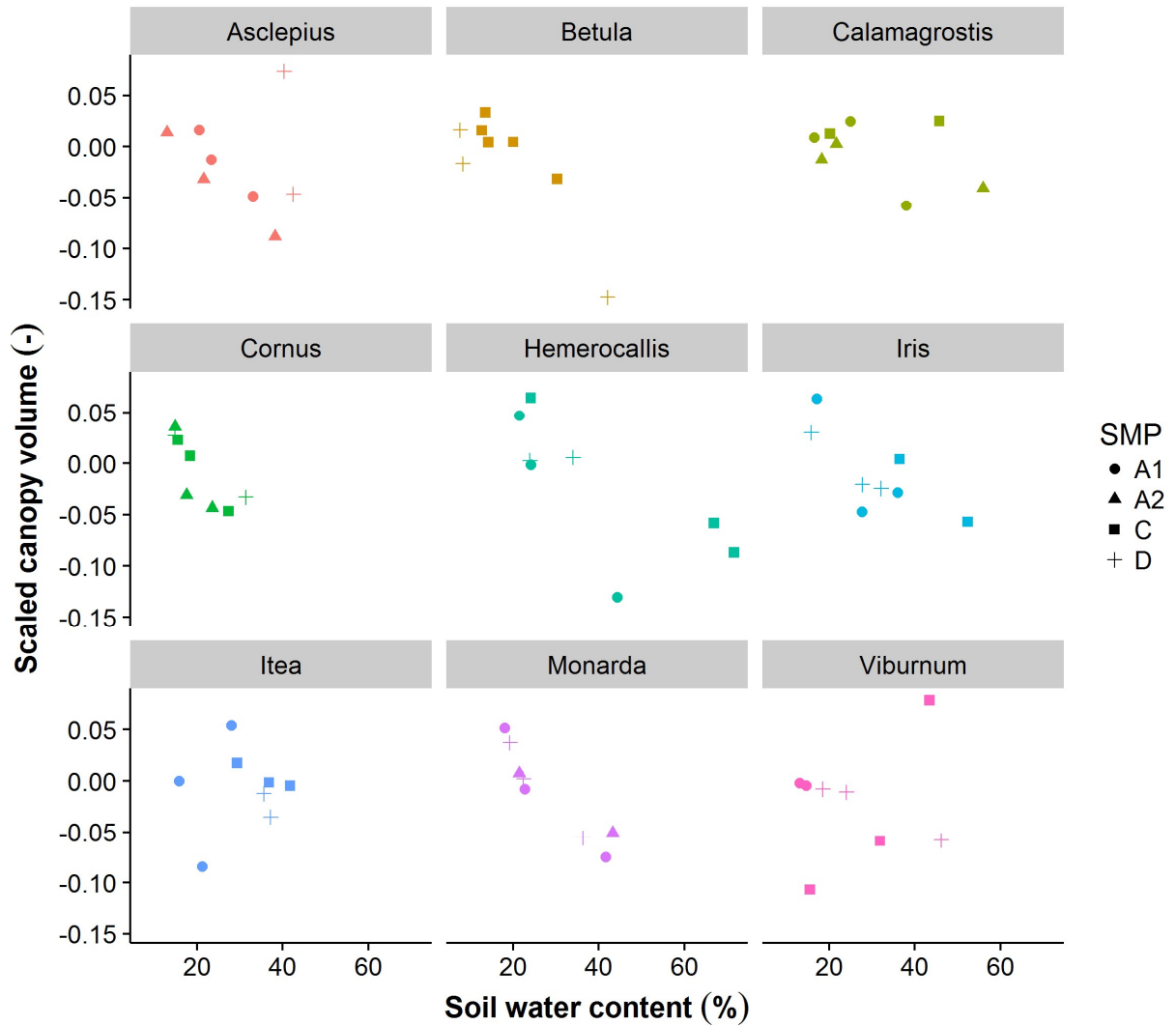


Figure 7-7. Canopy size (scaled according to the species mean and standard deviation) as a function of soil water content. Note that soil water content values depict means of measurements taken during our field campaigns, but are likely proportional to related metrics like the total numbers of hours that soils are saturated.

### Leaf-level Physiology

We present here a subset of the biophysical parameters we measured or calculated, as some exhibited few discernible patterns with soil moisture (e.g., LCP and  $k$ ) and some were similar to others that we characterized more reliably (e.g.,  $A_{1k}$  was similar to  $A_{sat}$  but  $A_{1k}$  was calculated from twice the number of measurements). However, we found considerable variation among species in physiological change across the topographic gradient, so we present the data

for each of the nine species independently. Because relationships were frequently nonlinear, we used smoothing to aid in the identification of patterns and optimal soil moisture levels (via R's *loess* function).

In nearly all species, the most pronounced ecophysiological pattern was that gas exchange rates were increasingly limited by insufficient water availability below a species-specific maximum (Figures 7-8 through 7-16). This primarily manifested as positively-sloped relationships between photosynthesis and stomatal conductance vs. soil water content over at least part of the measured range (panels A and B). Several other physiological parameters exhibited similar patterns (e.g.,  $\Phi_{PSII}$  in *Hemerocallis*, Figure 7-11F), suggesting some of the underlying mechanisms, but these were highly species-specific. Nevertheless, water limitation appears to be a prominent abiotic constraint on photosynthesis in plants at higher elevations in these SMPs. It is important to note that, given our methodology, the patterns expressed can be interpreted as the result of acclimation to the conditions present at each plant's location and not simply to the soil water conditions present at the time measurements were made. In other words, water content values should be interpreted as proxies for topographic position and thus long-term exposure to stormwater; plants cannot be expected to shift along these curves if hydrological conditions change.

In some cases, there was clear evidence of physiological inhibition at greater soil water levels as well, such that the slope of the relationship became negative as soils became saturated (particularly *Hemerocallis* 'happy returns', Figure 7-11 and *Asclepias incarnata*, Figure 7-13). There were also several cases in which the slope was positive at low to moderate soil moisture levels but not discernable from zero in wetter soils (e.g., *Viburnum trilobum* 'Wentworth', Figure 7-14 and *Betula nigra*, Figure 7-15). However, there were several additional cases in which

plants never occurred locations where the mean soil water content was sufficiently high for us to capture a changeover (e.g., *Monarda didyma*, Figure 7-8). Using the available data, we are therefore able to estimate the optimum soil moisture level for each of the 9 focal species, but are limited by the range of the data in some cases (Table 7-5). We note that *Calamagrostis* × *acutiflora* had no discernable change in physiological performance over the elevation gradient (possibly suggesting that it is well adapted to the full range of topographic positions), precluding an optimum from being estimated.

That gas exchange rates would vary along the elevation gradient in a direction that was, in most cases, exactly opposite to that of canopy and leaf sizes was unexpected. One explanation consistent with the data is that plants at lower elevations initially had a reduced time over which to photosynthesize (because they were inundated) and had to allocate a greater fraction of the energy harnessed in photosynthesis to metabolize the byproducts of anaerobic respiration and possibly deal with greater pathogen loads. Therefore, they may have grown more slowly, producing fewer and smaller leaves, but with highly functional photosynthetic apparatus. Plants at higher elevations may have produced leaves less capable of exchanging water and CO<sub>2</sub> per unit leaf area, but, in being able to allocate a greater fraction of their photosynthate to additional stems and leaves, plants would have experienced strong positive feedbacks in whole-plant carbon gain, overcoming the limitations of reduced water availability.

Table 7-5. Estimated optimum soil moisture levels for each of the species in the study. Note that optimum soil water content indicates the level experienced when we collected data (i.e., 1-2 days after a modest storm).

Species	Optimum soil water content	Figure
<i>Monarda didyma</i> 'Cambridge scarlet'	>50%	7-8
<i>Iris siberica</i> 'Caesar's brother'	50%	7-9
<i>Itea virginica</i> 'Little Henry'	>40%	7-10
<i>Hemerocallis</i> 'happy returns'	40%	7-11
<i>Cornus sericea</i> 'Cardinal'	>30%	7-12
<i>Asclepias incarnata</i> 'ice ballet'	30%	7-13
<i>Viburnum trilobum</i> 'Wentworth'	30%	7-14
<i>Betula nigra</i> 'Heritage'	30%	7-15
<i>Calamagrostis</i> × <i>acutiflora</i> 'Karl Foerster'	None	7-16



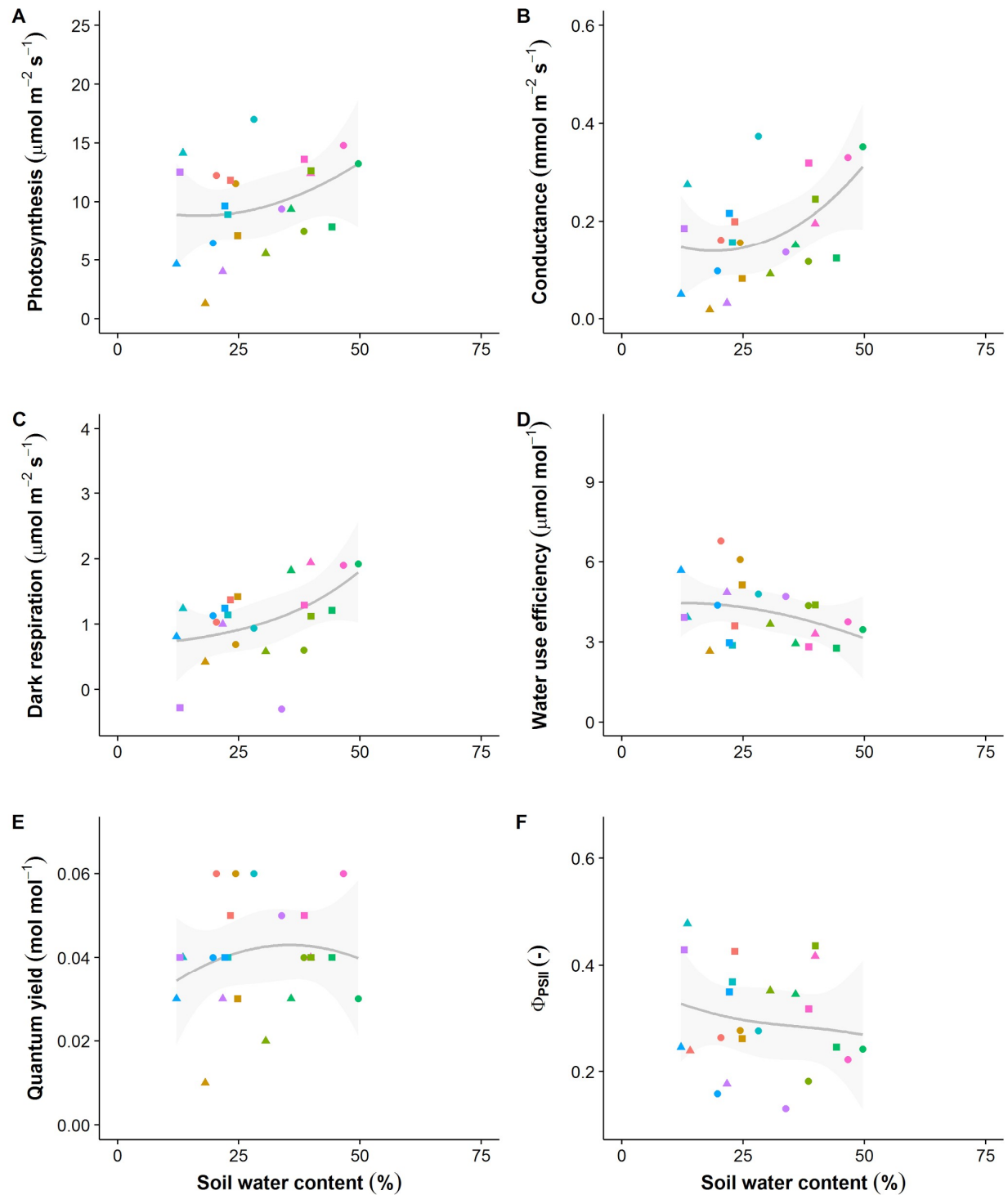


Figure 7-8. Physiological rates and efficiencies for *Monarda didyma*. Photosynthesis is the rate at PPFD =  $1000 \mu\text{mol m}^{-2} \text{s}^{-1}$  and Conductance is stomatal conductance to water; see text for further description of biophysical parameters. Colors indicate individual plants while shapes indicate measurement rounds. The line and shaded area were generated by loess smoothing ( $\pm 1$  standard error).

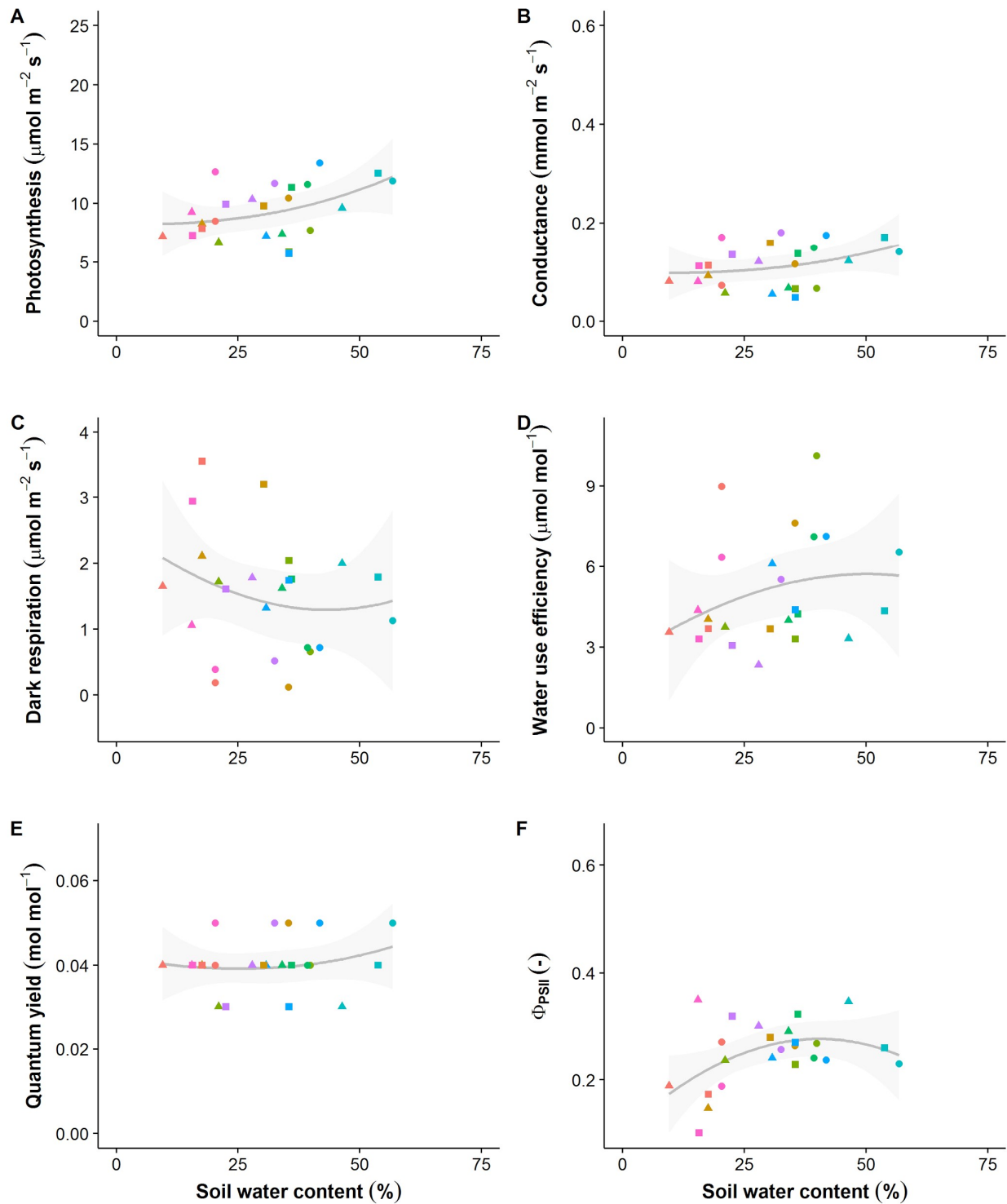


Figure 7-9. Physiological rates and efficiencies for *Iris siberica*. Photosynthesis is the rate at  $\text{PPFD} = 1000 \mu\text{mol m}^{-2} \text{s}^{-1}$  and Conductance is stomatal conductance to water; see text for further description of biophysical parameters. Colors indicate individual plants while shapes indicate measurement rounds. The line and shaded area were generated by loess smoothing ( $\pm 1$  standard error).

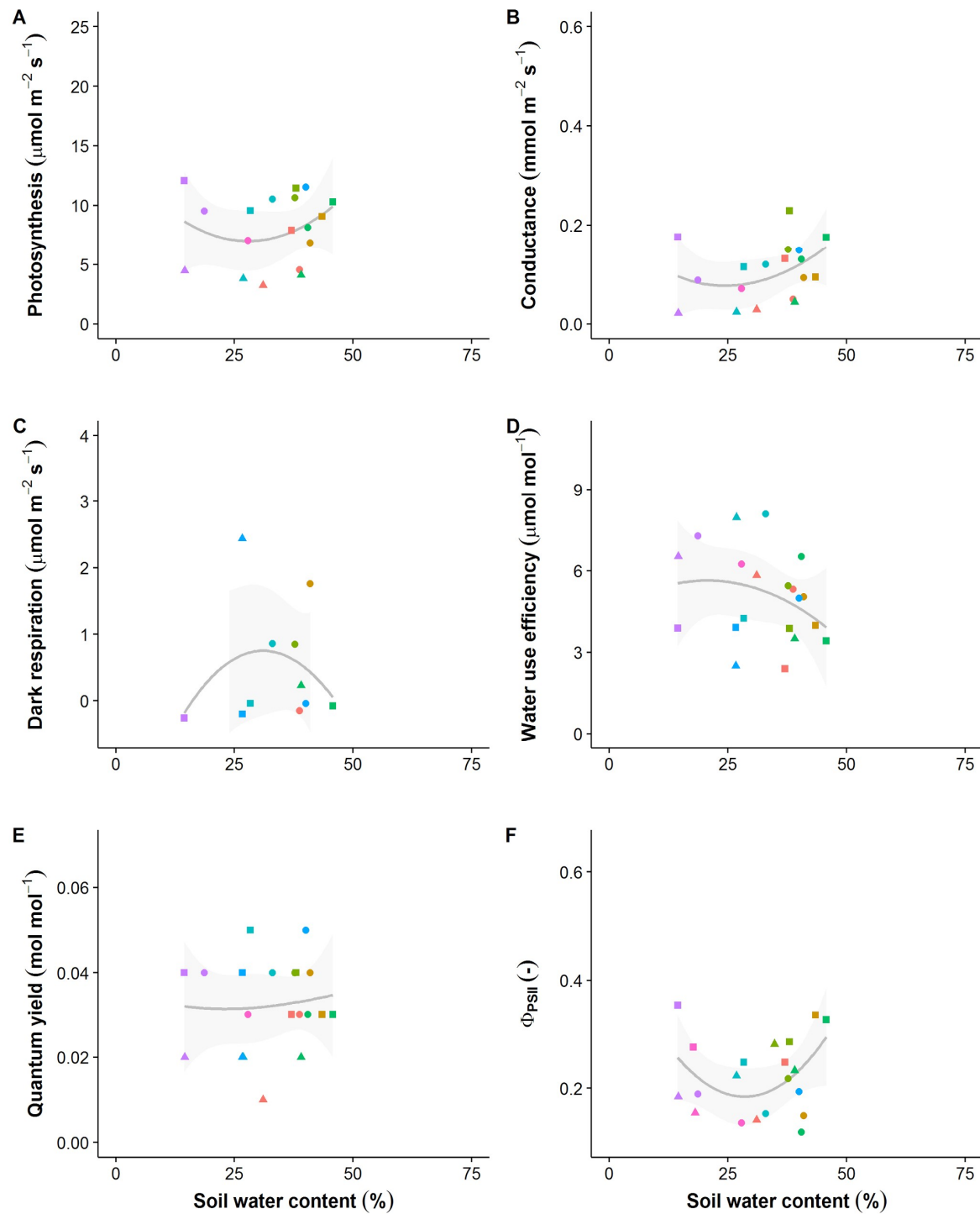


Figure 7-10. Physiological rates and efficiencies for *Itea virginica* 'Little Henry'. Photosynthesis is the rate at  $\text{PPFD} = 1000 \mu\text{mol m}^{-2} \text{s}^{-1}$  and Conductance is stomatal conductance to water; see text for further description of biophysical parameters. Colors indicate individual plants while shapes indicate measurement rounds. The line and shaded area were generated by loess smoothing ( $\pm 1$  standard error).

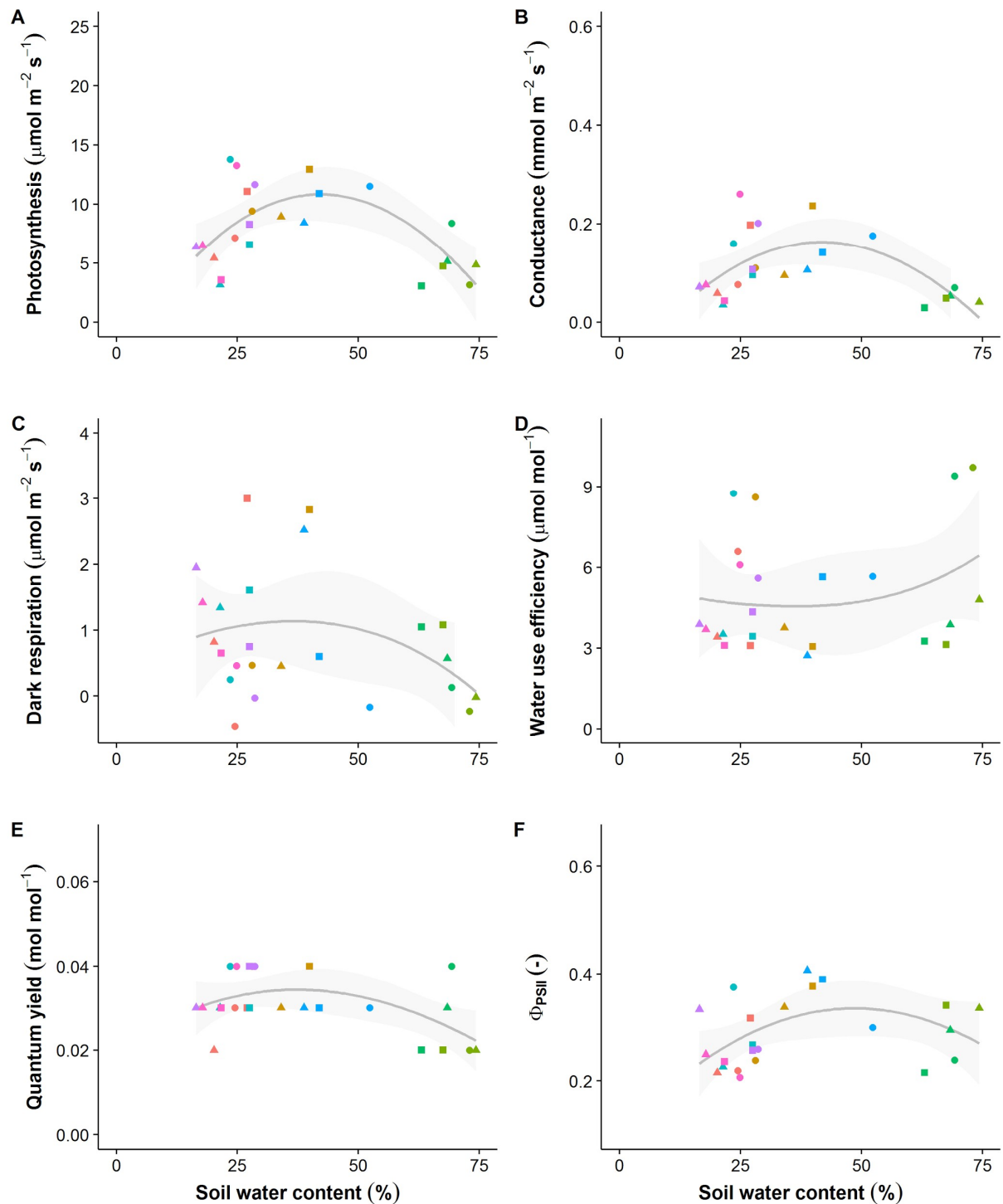


Figure 7-11. Physiological rates and efficiencies for *Hemerocallis* 'happy returns'. Photosynthesis is the rate at  $\text{PPFD} = 1000 \mu\text{mol m}^{-2} \text{s}^{-1}$  and Conductance is stomatal conductance to water; see text for further description of biophysical parameters. Colors indicate individual plants while shapes indicate measurement rounds. The line and shaded area were generated by loess smoothing ( $\pm 1$  standard error).

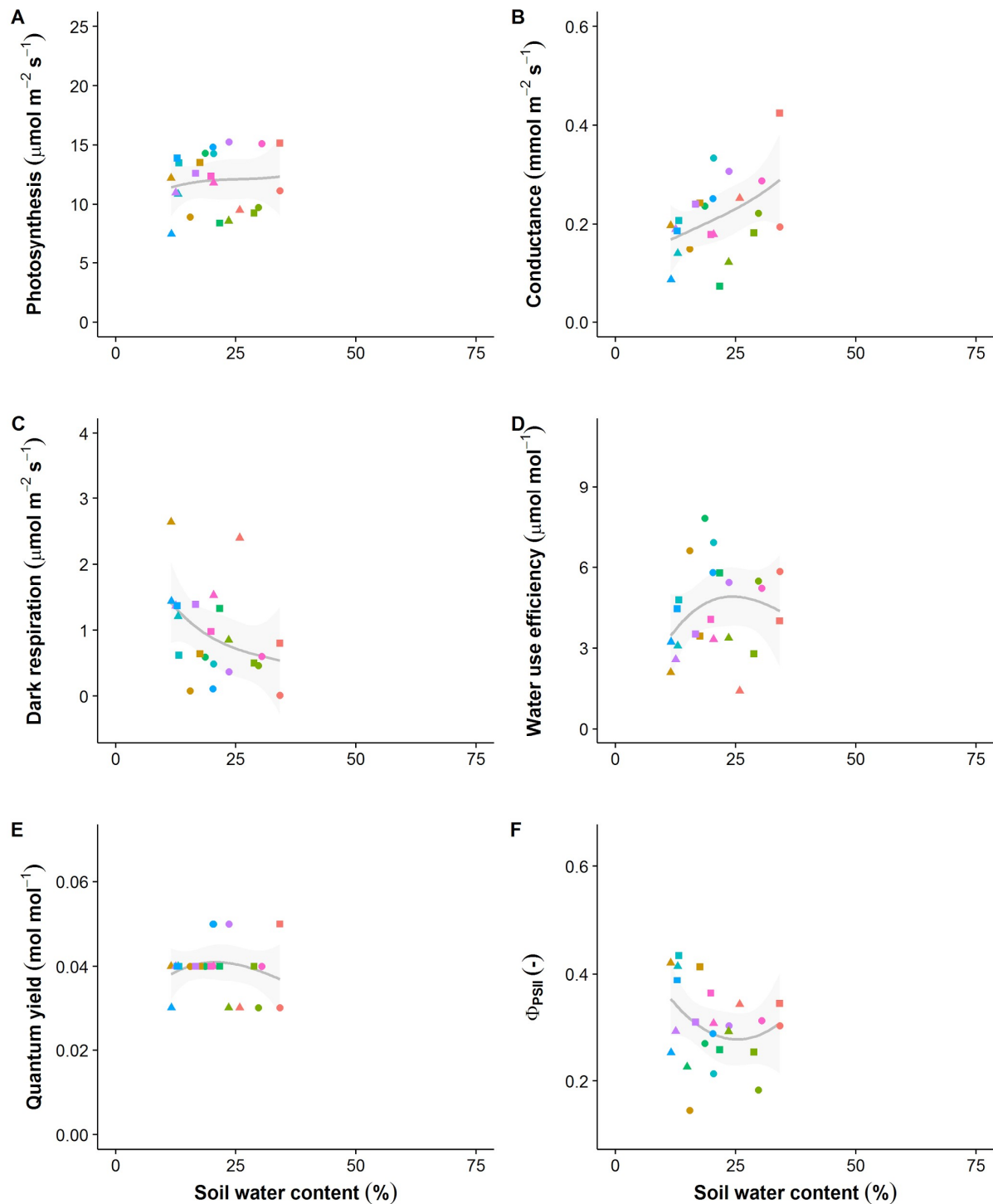


Figure 7-12. Physiological rates and efficiencies for *Cornus sericea* 'Cardinal'. Photosynthesis is the rate at PPFD =  $1000 \mu\text{mol m}^{-2} \text{s}^{-1}$  and Conductance is stomatal conductance to water; see text for further description of biophysical parameters. Colors indicate individual plants while shapes indicate measurement rounds. The line and shaded area were generated by loess smoothing ( $\pm 1$  standard error).

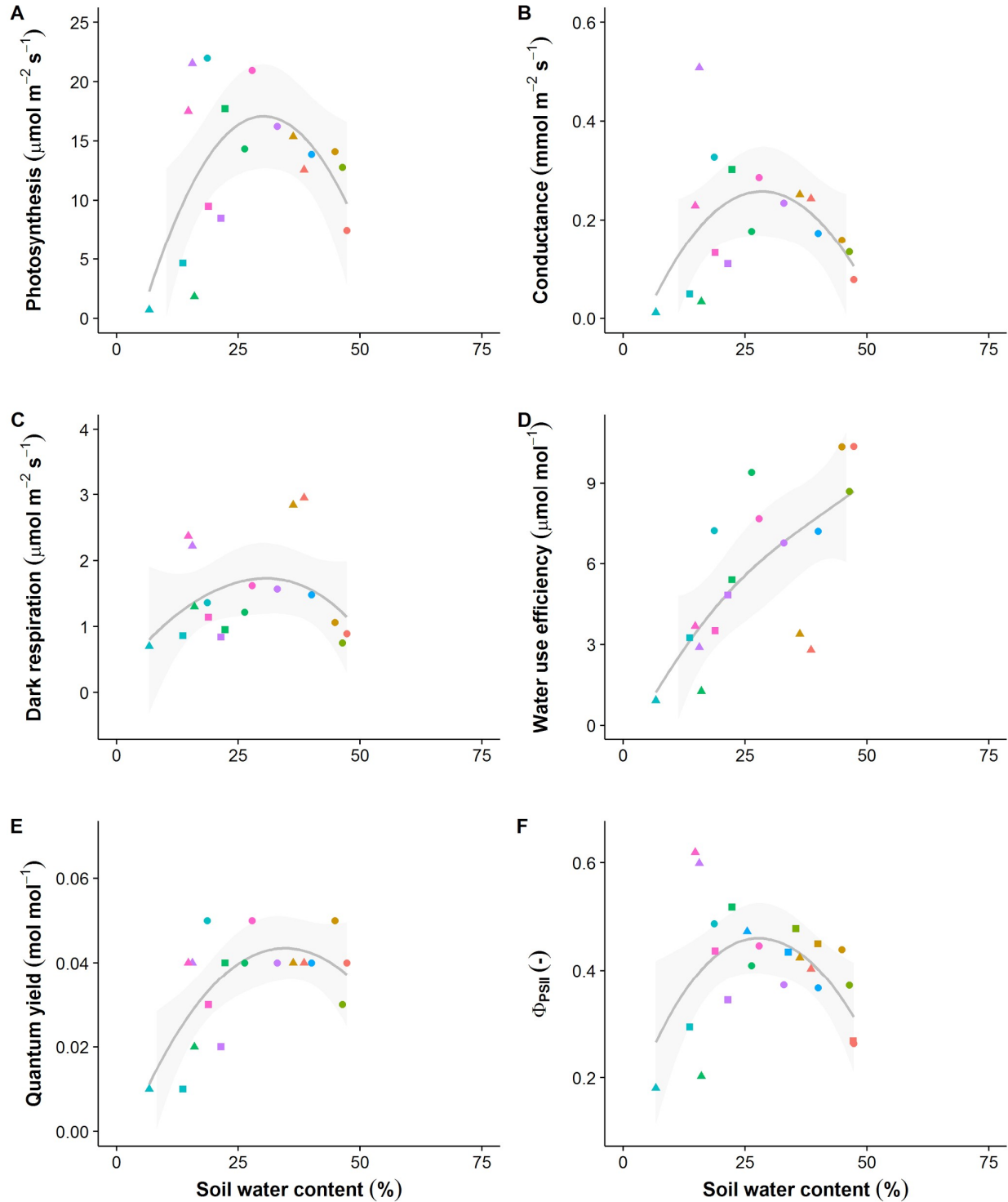


Figure 7-13. Physiological rates and efficiencies for *Asclepias incarnata* 'ice ballet'. Photosynthesis is the rate at PPFD =  $1000 \mu\text{mol m}^{-2} \text{s}^{-1}$  and Conductance is stomatal conductance to water; see text for further description of biophysical parameters. Colors indicate individual plants while shapes indicate measurement rounds. The line and shaded area were generated by loess smoothing ( $\pm 1$  standard error).

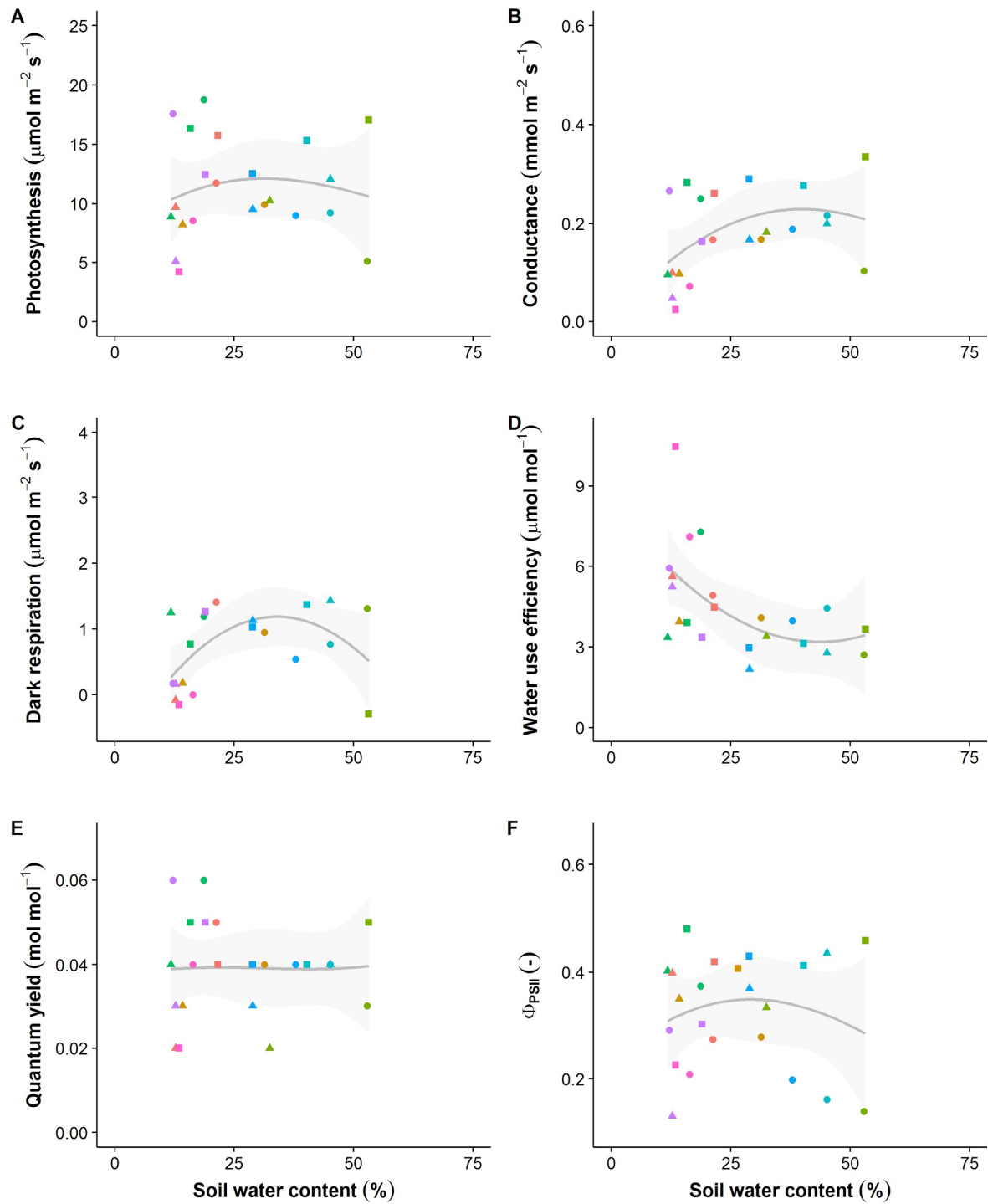


Figure 7-14. Physiological rates and efficiencies for *Viburnum trilobum*. Photosynthesis is the rate at PPFD =  $1000 \mu\text{mol m}^{-2} \text{s}^{-1}$  and Conductance is stomatal conductance to water; see text for further description of biophysical parameters. Colors indicate individual plants while shapes indicate measurement rounds. The line and shaded area were generated by loess smoothing ( $\pm 1$  standard error).

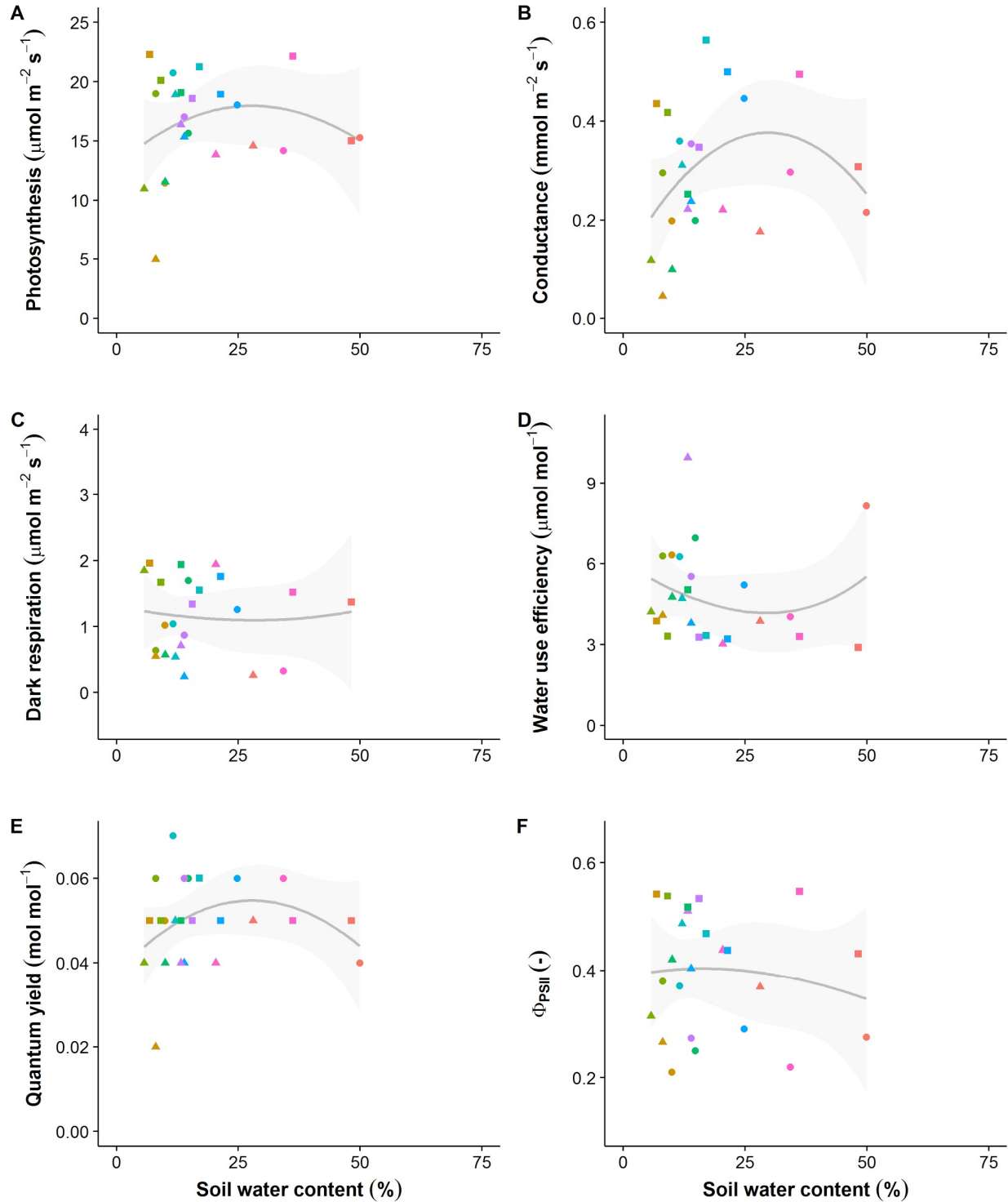


Figure 7-15. Physiological rates and efficiencies for *Betula nigra*. Photosynthesis is the rate at  $\text{PPFD} = 1000 \mu\text{mol m}^{-2} \text{s}^{-1}$  and Conductance is stomatal conductance to water; see text for further description of biophysical parameters. Colors indicate individual plants while shapes indicate measurement rounds. The line and shaded area were generated by loess smoothing ( $\pm 1$  standard error).



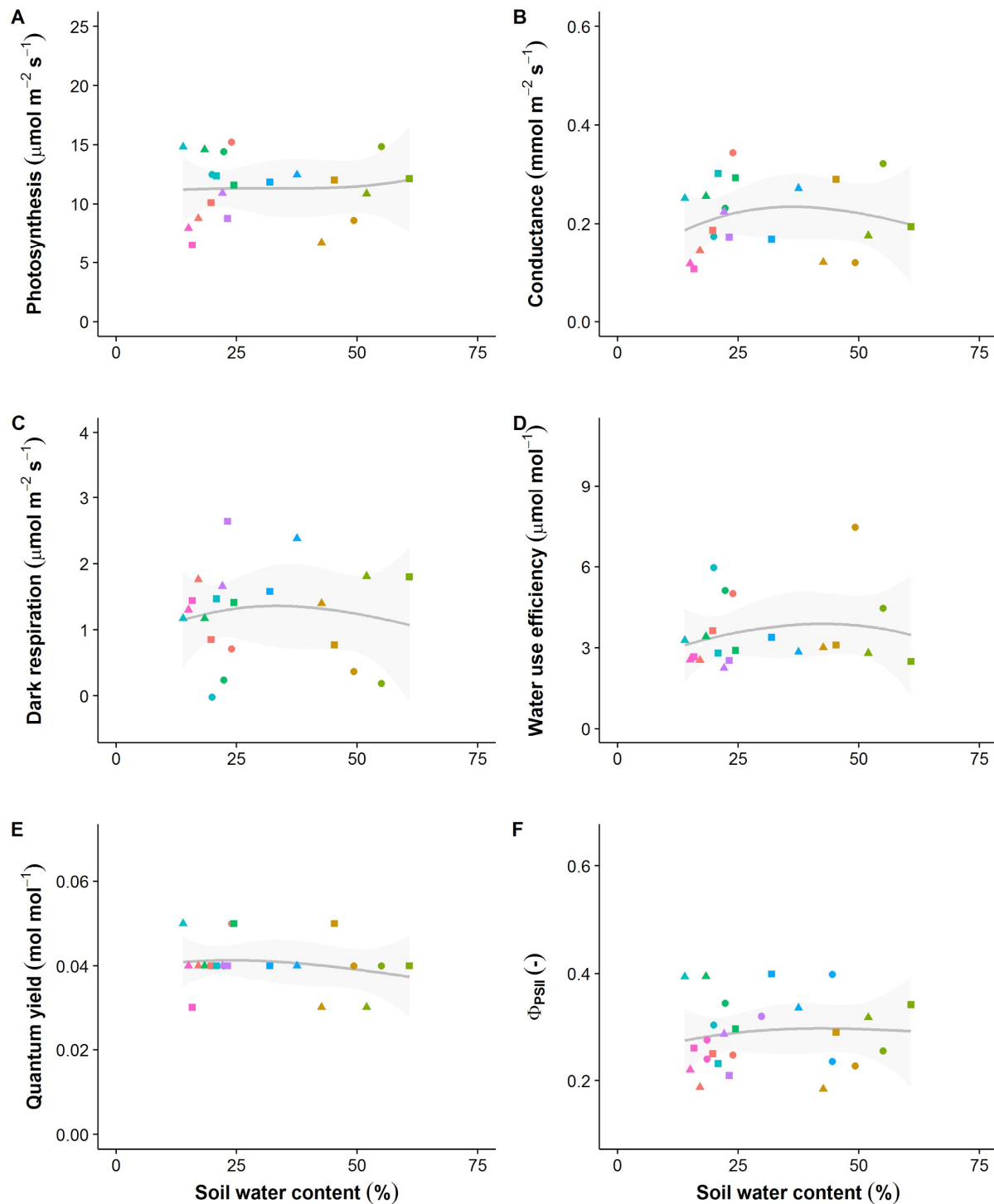


Figure 7-16. Physiological rates and efficiencies for *Calamagrostis* × *acutiflora* 'Karl Foerster'. Photosynthesis is the rate at  $\text{PPFD} = 1000 \mu\text{mol m}^{-2} \text{s}^{-1}$  and Conductance is stomatal conductance to water; see text for further description of biophysical parameters. Colors indicate individual plants while shapes indicate measurement rounds. The line and shaded area were generated by loess smoothing ( $\pm 1$  standard error).

## *Soil Contaminants*

Heavy metals were near or below background levels reported for Pennsylvania soil in the vast majority of cases (Table 7-6; US-EPA 2003). Concentrations occasionally reached levels exceeding those that the Pennsylvania Department of Environmental Protection (PADEP) lists as warranting remediation in residential circumstances (PADEP 2016), though we did not find cases where levels exceeded remediation thresholds for non-residential circumstances. Examples include the single greatest values of cadmium (Cd) and lead (Pb) that we measured in separate soil samples (Figure 7-17). SMP soils in GR2 therefore appear to have developed mild and localized ‘hotspots’ for some heavy metals within their first two years of use.

We note that the PADEP guidelines pertain to direct human contact, whereas levels inducing health effects in organisms living in or around the soil (e.g., insects) may be considerably lower. Comparisons of metal concentrations in SMP soils with guidelines for freshwater sediments (Table 7-6; MacDonald 2000) indicates that concentrations of some elements may regularly exceed ‘threshold effect concentrations’ (TECs), which are levels above which some deleterious health effects might be found. This was the case for copper (Cu), lead (Pb), and zinc (Zn). However, levels did not exceed probable effect concentrations (PECs), which are levels above which deleterious health effects are likely to occur.

While it is not possible to definitively determine the sources of the heavy metals found in SMP soils with these data, some likely originated in the amended soil itself. Some elements may have other sources unrelated to stormwater, such as lead (Pb), for which a number of Philadelphia soils have concentrations above the statewide background (Peterson 2014). However, a subset of elements exhibited increased concentrations in wetter areas within the SMPs; this finding is consistent with stormwater transporting the metals from the I-95 roadway

(Figure 7-17). Therefore, while soil heavy metal concentrations are not yet a cause for concern, the metals are likely to accumulate, reaching substantially greater concentrations after years to decades.

Soil pH was  $7.34 \pm 0.03$  (mean  $\pm$  SE); it was between 7 and 8 in all but three samples, and was  $>6$  in those cases. These pH values are similar to those observed in the lysimeter samples, as expected, and suggests that the mobility of metals will not be driven by pH differences, though this is based on a single time point assessment. Also, mean soil conductivity was  $778 \pm 35$   $\mu$ S, which is similar to lysimeter values observed along the edge of SMP C but considerably lower than values observed in the central flow path. These values are well below levels that one would expect if deicing salts were present. However, given that our soil sampling took place in the summer, salts may have been present in the SMPs during the winter but were subsequently washed out. Additional measurements taken during the winter would be needed to better characterize the influx of salts to the SMPs.

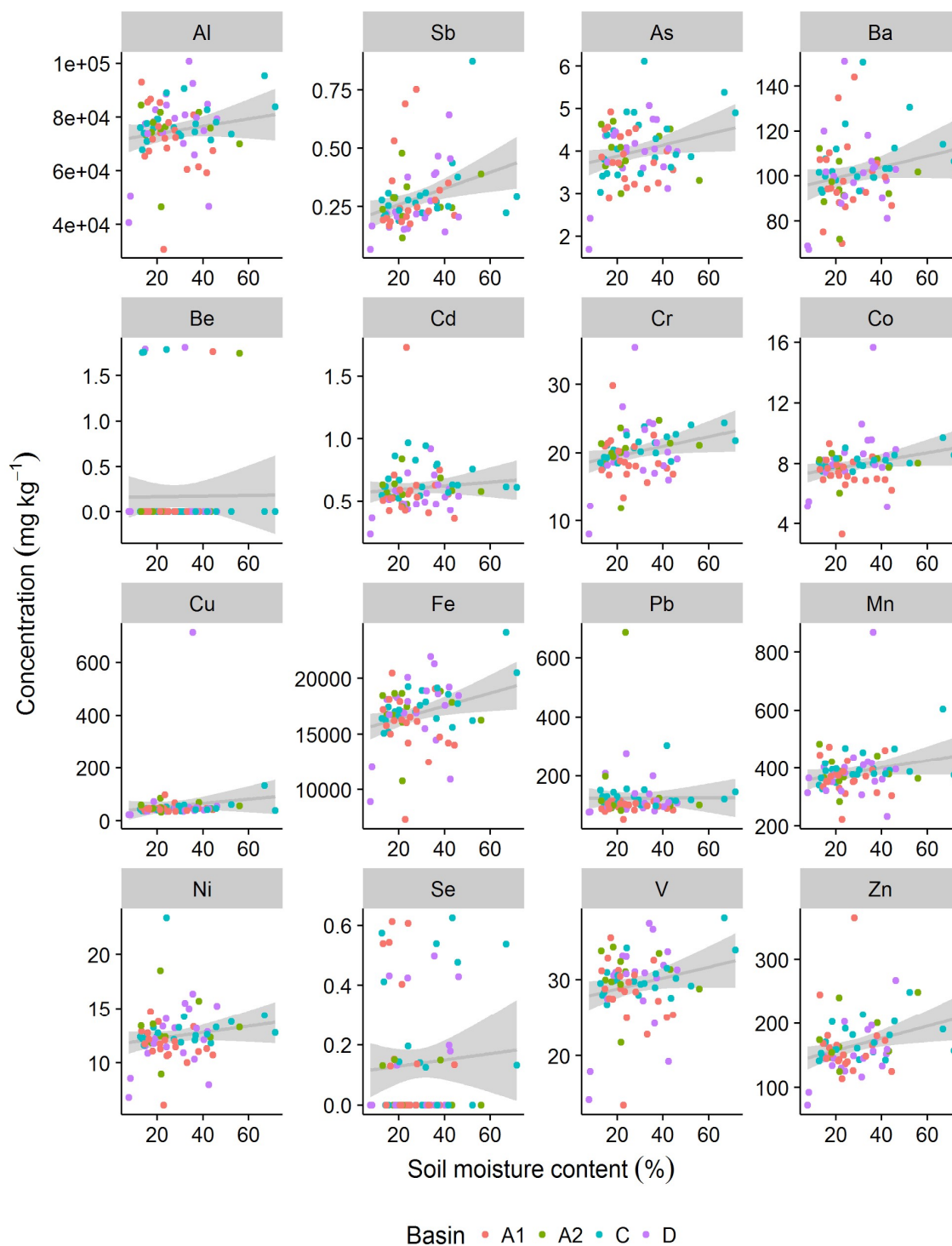


Figure 7-17. Concentration of heavy metals found in soils of SMPs A, C, and D. Soil moisture content is used as a metric of topographic position, with greater moisture levels indicating where soil presumably have greater contact time with stormwater. Regression lines ( $\pm 1$  standard error) are shown in gray.

Table 7-6. Reference concentrations ( $\text{mg kg}^{-1}$ ) for select heavy metals. Background concentrations are averages for Pennsylvania soil (US-EPA 2003). MSC indicates ‘medium specific concentrations’ for inorganic regulated substances in soil, with values pertaining to direct contact (PADEP 2016). These are designated separately for residential (Res) and non-residential (Non-res) settings. TEC and PEC are threshold and probable effect concentrations for organisms in freshwater settings, respectively (MacDonald 2000).

Element	Symbol	Background	MSC Res	MSC Non-res	TEC	PEC
Aluminum	Al	63438	190000	190000		
Antimony	Sb	1	88	1300		
Arsenic	As	13	12	61	9.79	33
Barium	Ba	366	44000	190000		
Beryllium	Be	1.4	2	11		
Cadmium	Cd		1.2	6	0.99	4.98
Chromium	Cr	52.8	4	220	43.4	111
Cobalt	Co	15	66	960		
Copper	Cu	37	8100	120000	31.6	149
Iron	Fe	36063	150000	190000		
Lead	Pb	23	500	1000	35.8	128
Manganese	Mn	609	10000	150000		
Nickel	Ni	24	4400	64000	22.7	48.6
Selenium	Se	0.5	1100	16000		
Vanadium	V	80	15	220		
Zinc	Zn	81	66000	190000	121	459

## References

- CEM (2016). MARS 6 method note: microwave digestion of plant tissue.  
[http://cem.com/media/contenttype/media/literature/MetNote\\_MARS6\\_Plant\\_Tissue.pdf](http://cem.com/media/contenttype/media/literature/MetNote_MARS6_Plant_Tissue.pdf)
- CEM (2016). MARS 6 method note: microwave digestion of US EPA 3051.  
[http://cem.com/media/contenttype/media/literature/MetNote\\_MARS6\\_US\\_EPA\\_3051.pdf](http://cem.com/media/contenttype/media/literature/MetNote_MARS6_US_EPA_3051.pdf)
- Del Tredici, P. (2010). *Wild urban plants of the northeast*. Cornell University Press.
- Gobas, F.A.P.C., Burkhard, L.P., Doucette, W.J., Sappington, K.G., Verbruggen, E.M.J., Hope, B.K., Bonnell, M.A., Arnot, J.A. and Tarazona, J.V. (2016). Review of existing terrestrial bioaccumulation models and terrestrial bioaccumulation modeling needs for organic chemicals. *Integrated Environmental Assessment and Management*, 12, 123-134.
- Kloeppel, B.D. and Abrams, M.D. (1995). Ecophysiological attributes of the native *Acer saccharum* and the exotic *Acer platanoides* in urban oak forests in Pennsylvania, USA. *Tree Physiology*, 15, 739-746.
- Kondo, M.C., Sharma, R., Plante, A.F., Yang, Y. and Burstyn, I. (2016). Elemental Concentrations in Urban Green Stormwater Infrastructure Soils. *Journal of Environmental Quality*, 45, 107-118.
- Loriaux, S.D., Avenson, T.J., Welles, J.M., McDermitt, D.K., Eckles, R.D., Riensche, B. and Genty, B. (2013). Closing in on maximum yield of chlorophyll fluorescence using a single multiphase flash of sub-saturating intensity. *Plant, Cell and Environment*, 36, 1755-1770.
- Lovell, S.T. and Taylor, J.R. (2013). Supplying urban ecosystem services through multifunctional green infrastructure in the United States. *Landscape Ecology*, 28, 1447-1463.
- MacDonald, D.D., Ingersoll, C.G. and Berger, T.A. (2000). Development and Evaluation of Consensus-Based Sediment Quality Guidelines for Freshwater Ecosystems. *Archives of Environmental Contamination and Toxicology*, 39, 20-31.
- Peterson, S.P. (2014). The geologic, geomorphic, and geographic influence on lead and other heavy metal concentrations in the soils of Fairmont Park, Philadelphia. MS Thesis, Temple University.

- PADEP (2016). Statewide health standards, medium specific concentrations. Table 4a - MSCs for Inorganic Regulated Substances in Soil: Direct Contact Values.  
<http://www.dep.pa.gov/Business/Land/LandRecycling/Standards-Guidance-Procedures/Pages/Statewide-Health-Standards.aspx>
- PFAF (2017). Plants for a future: a resource and information centre for edible and otherwise useful plants. <http://www.pfaf.org/user/Default.aspx>.
- Prioul, J.L. and Chartier, P. (1977). Partitioning of transfer and carboxylation components of intracellular resistance to photosynthetic CO<sub>2</sub> fixation: a critical analysis of the methods used. *Annals of Botany*, 41, 789-800.
- Silander, J.A. and Klepeis, D.M. (1999). The invasion ecology of Japanese barberry (*Berberis thunbergii*) in the New England landscape. *Biological Invasions*, 1, 189-201.
- US-EPA (2003) Guidance for Developing Ecological Soil Screening Levels. OSWER Directive 9285.7-55. Washington, DC.
- Whittaker, R.H. (1967). Gradient analysis of vegetation. *Biological Reviews of the Cambridge Philosophical Society*, 42, 207-264.
- Zhuang, P., Yang, Q., Wang, H. and Shu, W. (2007). Phytoextraction of heavy metals by eight plant species in the field. *Water, Air, and Soil Pollution*, 184, 235-242.

## **Chapter 8: Maintenance and SMP Functionality**

### **Introduction**

SMPs are subject to alteration by the erosive forces of water, the effects of which may impact the functionality of the structures over time. Additionally, a bioswale with a highly ornamental, garden-like design will require a certain amount of upkeep to maintain the plantings. The purpose of this task is to monitor the changes in the structure and function of BMPs within GR2, while providing maintenance support for all GR2 bioswales. In addition, maintenance requirements for SMPs will be evaluated, options to improve function and maintenance procedures will be outlined, and changes to SMP design and maintenance approaches will be recommended. This task includes the following specific activities:

- a) Provide functional support for GR 2 bioswales.
- b) Track site function and its relationship to performance.
- c) Evaluate maintenance requirements for SMPs and outline options to improve maintenance.
- d) Recommend changes to Philadelphia Water Department (PWD) and PennDOT maintenance manuals.

### **Methods**

SMP maintenance and evaluation are being conducted according to the guidelines and schedules contained in the I-95 GIR Phase 2 Landscape Maintenance Plan (summarized in Tables 1&2). This detailed manual has explicit instructions for all aspects of maintaining SMPs, including Landscape Areas Maintenance, General Landscape Maintenance Tasks, SMP Maintenance, SMP Devices and Components, and SMP Inspection and Maintenance. The landscaping and arboriculture firm, Terraquarbor, has been contracted to maintain the SMPs in



GR2. This firm is based in Kensington and is therefore readily available to assess SMP conditions and perform maintenance tasks at the required times.

The maintenance of GR2 SMPs consists of numerous responsibilities including:

- *Turf*: mowing maintenance, lawn establishment, lawn repair.
- *General Landscape Maintenance Tasks*: weeding, plant health inspection, watering (as needed), fertilizing (as needed), pruning (as needed), mulch replacement, removal of tree stakes.
- *SMP Maintenance*: SMP devices must be routinely inspected and have the required maintenance performed on them to be certain that they continually function as designed.

Observations made at the time of inspection, maintenance actions performed, and remediation actions carried out are documented using the Maintenance Reporting Requirements and Inspection Form. During the planning phase of the project it was decided that SMP A would be "let go" to determine if a lack of maintenance impacts functionality of the system. This included no weeding, trash collection, or repairs or alterations to the inlets, outlets, vegetation, or soil.

*Table 8-1. Timetable for SMP landscape maintenance.*

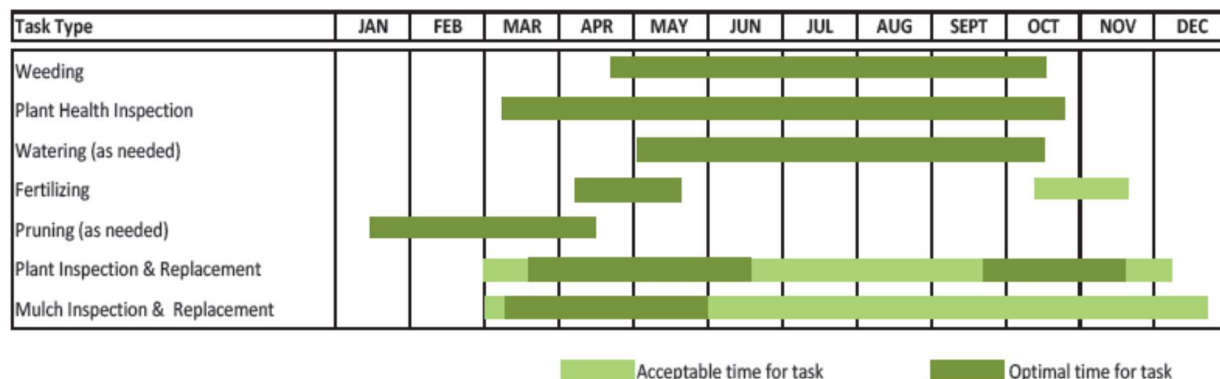
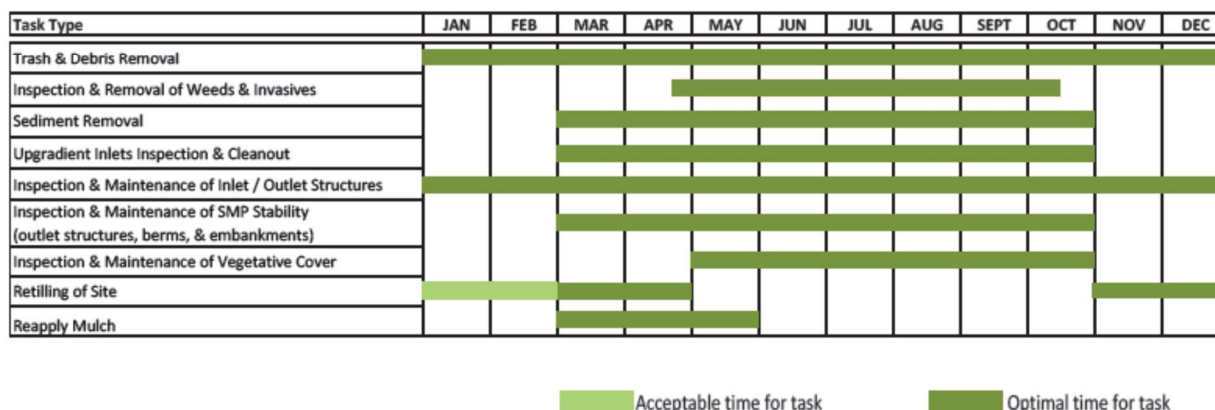


Table 8-2. SMP maintenance schedule.

Task Type	Monthly	2x / Year	4x / Year	Annually	After Storm Event	Other
Trash & Debris Removal	X				X	
Inspection & Removal of Weeds & Invasives	X					
Sediment Removal		X			X	Every 2 years or when 2 inch has accumulated
Upgradient Inlets Inspection & Cleanout		X			X	
Inspection & Maintenance of Inlet /Outlet Structures			X		X	
Inspection & Maintenance of SMP Stability (outlet structures, berms, & embankments)			X		X	
Inspection & Maintenance of Vegetative Cover			X		X	
Inspection & Maintenance of Fencing & Gate Areas				X		
Retilling of Site						Once every 5 years
Reapply Mulch				X		



In addition to the maintenance reporting form documentation, numerous site visits have been conducted and photos of the relevant issues have been taken to document functionality and maintenance issues that are developing in the SMPs.

## Results

### *Maintenance requirements and evaluation*

The landscaping and arboriculture firm, Terraquarbor, has been contracted to maintain the SMPs in GR2. Twelve maintenance reporting forms have been submitted thus far; they cover the time period spanning 12/1/2016 – 8/31/2017. The most significant issues that these forms have documented are slow drainage in SMP I, increasing erosion near inlets I and J (as well as

inlet E, but to a lesser extent), minor rill erosion in most of the bioswale bottoms, an abundance of trash, and loss and erosion of mulch. Also, they note that considerable weeding, cutting back of perennials, and mulch replacement are required to maintain these landscapes.

During the planning phase of the project it was decided that SMP A would not receive maintenance to determine how that impacts the functionality of the system. By November 2016, it was evident that the amount trash accumulation in SMP A was beyond the acceptable level (based on appearance) and that all SMPs will need regular trash collection. It is worth noting that SMP A is fenced, suggesting that direct littering is a minimal source of trash, and that wind-blown plastic is much more significant problem. Also note that a community member has regularly collected trash from SMPs C, D, and G. Since these are within the unfenced areas, they are readily traversed by people and animals.





*Figure 8-1. SMP A is showing signs of erosion along the lower edge of the gabion (a), along the lowest elevation of the basin (b). There is also an accumulation of large (c) and small (d) trash items.*





*Figure 8-2. SMP C. This basin has a particularly large area and has developed signs of erosion from stream-like flow that occurs during precipitation events (a, d). This has had a scouring and slight channelizing effect. Placing plants in rows parallel to the flow of water may exacerbate this process. The basin edge (b) and sloped sides of the basins (c) show significant loss of mulch.*



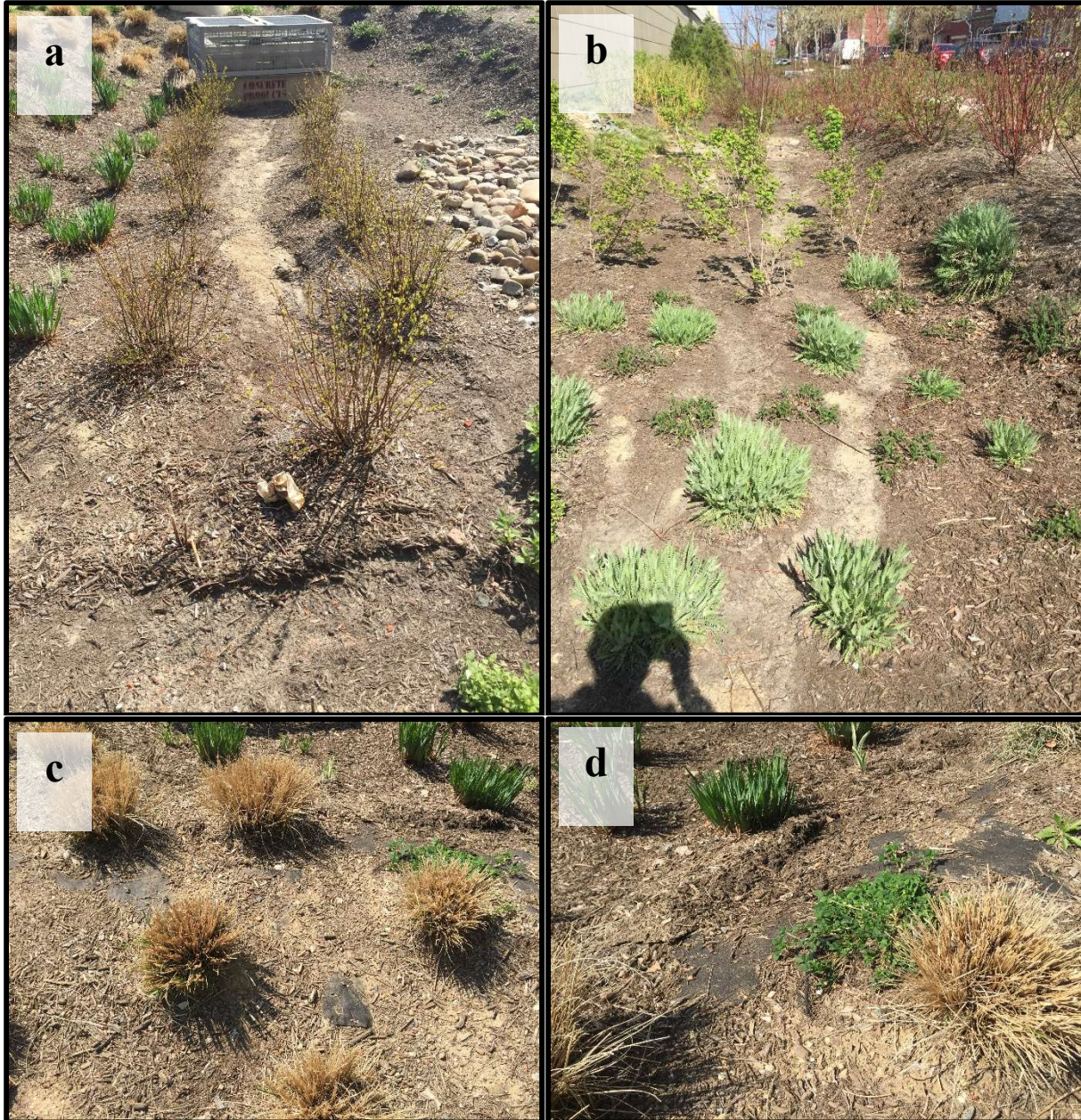


*Figure 8-3. SMP D shows evidence of rill erosion (a, b) and mulch loss (c, d).*





*Figure 8-4. Erosion in SMP E consists of scour and soil loss at the edges of inlet rip rap (a, b). Large amounts of small trash accumulates in the rip rap (b).*





*Figure 8-5. SMP H. Photos were taken 4-14-2017, a week after the last precipitation event (4-7-2017), and there is still a small amount of standing water in the SMP (a, b, c). There is also significant scour near the inlet and soil loss near the outlet (a, b, c, d).*



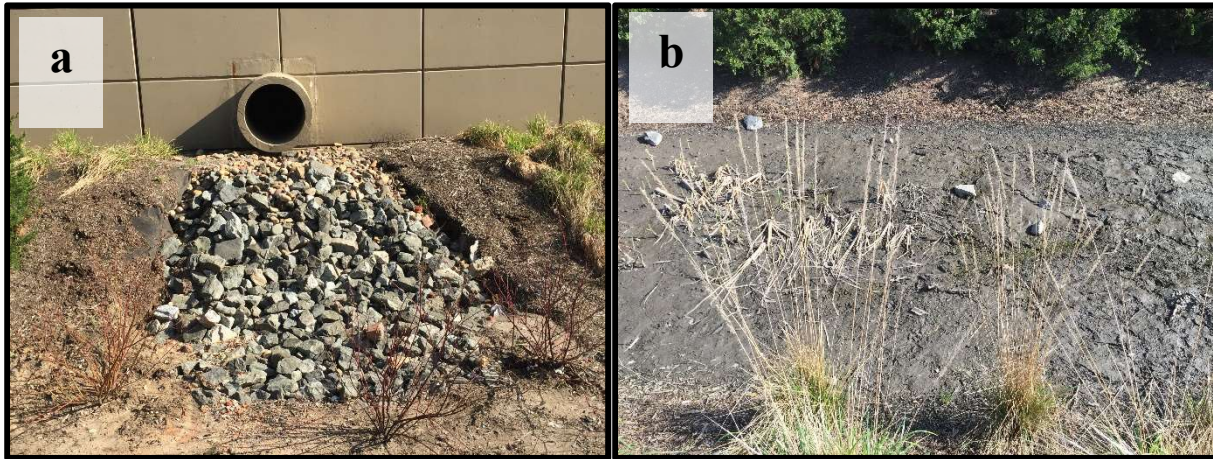


*Figure 8-6. SMP I has erosion occurring on the margins of the inlet rip rap (a). The basin does not drain properly and is being colonized by the obligate wetland plant Typha [cattail] (b).*



*Figure 8-7. SMP J has severe erosion of the soil around the inlet and is experiencing failure of the rip rap support structure.*

### *Drainage and erosion*

Improper drainage is an obvious issue in SMP I and, to a lesser extent, in SMP H. SMP I does not drain after 72 hours and the lowest part of the basin is being colonized by *Typha sp.* (cattail), which is not part of the planting design (Figure 8-6). This is an obligate wetland species, and is a clear sign of poor drainage. In future installations, we recommend that a more thorough evaluation of sub-soil conditions should be conducted prior to the installation of amended soil. Multiple infiltration tests should be conducted in both the sub soil and the amended soil layers. Minor soil erosion is evident in most of the SMPs in GR2. Erosion typically occurs in the lowest parts of the basins where flowing water scours the bottoms of the SMPs, and channels have started forming in some areas (Figs. 8-1 through 8-4). The soil below inlets in SMPs E, H, I, and J are also showing signs of erosion (Figs 8-4 through 8-7). In SMP J, this is causing rip rap displacement. In these cases, it is clear that modifications to the inlet spillways are necessary. The mulch on the sloped sides of the basins is prone to erosion, exposing the underlying landscape fabric in numerous areas. The erosion of mulch primarily occurs in two areas within the bioswales: in the low-lying areas that are subject scouring and on the steep side walls of the basins (Figs 8-1 through 8-3). Because SMPs C, D, G, and I are not fenced, they have become a popular place for community members to walk their dogs. It is common to see people and dogs entering the basins and walking through the bioswales, and there is clear evidence that pedestrians and dogs have caused significant disturbance to the mulch on these steeper slopes.

### *Trash issues*

It was determined that the amount of trash accumulation in SMP A was beyond the acceptable level and that the SMPs will need regular trash collection. Another issue is the lack of

public trashcans in the vicinity of the SMPs. Also, there is a substantial amount of dog excrement around and in the unfenced bioswales. These observations suggest that it is not sufficiently convenient for pedestrians to discard trash or dog waste. In addition to larger pieces of trash that accumulate in the SMPs, a significant amount of small trash enters with the stormwater from the roadway. The rocks below the inlets have become filled with small pieces of trash that eventually washes through the basins. In SMP A there are distinct deposits along the low-lying gabion. In addition to regular trash collection and maintenance by Terraquarbor, a community member has regularly collected trash from SMPs C, D, and G (which are unfenced), and collects 2 large Ikea bags full of trash on a biweekly basis.

#### *Soil amendments*

We suggest evaluating the use soil amendments to improve plant health and infiltration. These could include amendments of biochar or metal oxides, as these may have a beneficial effect on contaminant sequestration. Biochar is a product of the pyrolysis of organic material and is becoming increasingly popular as a soil amendment. Different biochars impart varying properties to the soil in which they are added; some increase pH and macronutrients while others contribute more significantly to enhanced carbon sequestration and contaminant absorption (Dai et al., 2013). The reported benefits of biochar incorporation were reviewed by Sohi *et al.* (2010), and include carbon sequestration, microbial stimulation, and improved soil chemical and physical characteristics. Biochar is emerging as an ameliorant to reduce the bioavailability of contaminants in the environment, with additional benefits of soil fertilization and mitigation of climate change (Sohi, 2012). Biochar has recently been shown to be a promising area in environmental remediation (Cao *et al.* 2011; Ahmad *et al.* 2014). Biochar has shown to be efficacious in the adsorption of heavy metals, as well as organic compounds, from soil and water

(Ahmad et al., 2014; Beesley et al 2015; Hale et al, 2015; Silvani et al., 2017). A variety of metal oxides have been evaluated to enhance contaminant adsorptive removal. Generally, either aluminum and iron oxides have been used, and manganese oxide has also been employed. In many studies, phosphorus has been the contaminant of interest, though metals (Cu, Zn, Cr, Co, Ni, and Pb) have also been targeted. In the current work, iron oxide was selected for further consideration; aluminum oxide was eliminated due to potential plant toxicity concerns and manganese-oxide wasn't considered due to a dearth of data. Previous research efforts on iron-oxide base approaches have used a variety of amendment materials, including: steel wool, steel shavings, or water treatment residual (WTR). Amendment rates have generally ranged from 1-10%. In our proposed approach, we are investigating small diameter ( $\sim <0.25$  in) steel options that will be incorporated at a 5% amendment level.

## References

- Ahmad M, Rajapaksha AU, Lim JE, Zhang M, Bolan N, Mohan D, Vithanage M, Lee SS, Ok YS. (2014). Biochar as a sorbent for contaminant management in soil and water: a review. *Chemosphere* 99:19–33.
- Beesley L, Moreno-Jiménez E, Fellet G, Carrijo L., Sizmur T. (2015). Biochar and heavy metals. pp. 563-594. *In Biochar for environmental management: science, technology and implementation*. Lehmann J, Joseph S (editors). Routledge.
- Hale S, Cornelissen G, Werner D. (2015). Sorption and remediation of organic compounds in soils and sediments by (activated) biochar. pp. 625-654. *In Biochar for environmental management: science, technology and implementation*. Lehmann J, Joseph S (editors). Routledge.
- Dai Z, Meng J, Muhammad N, Liu X, Wang H, He Y, Brookes PC, Xu J. (2013). The potential feasibility for soil improvement, based on the properties of biochars pyrolyzed from different feedstocks. *J. Soils Sediments* 13:989–1000.
- Silvani L, Vrchotova B, Kastanek P, Demnerova K, Pettiti I, Papini MP. (2017). Characterizing biochar as alternative sorbent for oil spill remediation. *Sci. Rep.* 7.
- Sohi, S. P. (2012). Carbon storage with benefits. *Science*, 338:1034–1035.

Sohi SP, Krull E, Lopez-Capel E, Bol R (2010). A review of biochar and its use and function in the soil. *Adv Agron* 105:47–82. doi:[http://dx.doi.org/10.1016/S0065-2113\(10\)05002-9](http://dx.doi.org/10.1016/S0065-2113(10)05002-9)

## Chapter 9:

### Recommended Changes to Future SMP Designs and Placement Plan

This task includes recommendations for design, location, and installation of SMPs, and advisement regarding soil mixes and plant palates for future construction phases based on the preliminary monitoring since project inception in the fall of 2016. The report is divided into four sections: hydrologic design, contaminant mobility, plants, and basin maintenance, followed by a final summary statement.

### Recommendations on Hydrologic Design

#### *Watershed drainage design – temporary phases*

Stormwater management practices (SMPs) are designed to receive water from a specific drainage area. When this drainage area is altered after temporary phases are completed the SMPs will not operate as designed. For example, GR-2 bioswales C, D, and G were completed several years before the highway above will receive final grading, and temporary New Jersey barriers were added to define temporary lanes during construction phases. During this period, SMPs C, D, and G are receiving runoff from only a small fraction of what will be the contributing drainage area. These changes in drainage area substantially alter the amount of runoff entering the SMPs, potentially resulting in both overuse and underuse during different phases. The ultimate result could be failure to meet design expectations and erosion or sedimentation damage could occur in completed SMPs. We recommend that drainage system design include consideration of performance during the intermediate construction stages, and not just the final design requirements.

In addition, stormwater can become diverted for unexpected reasons. For example, concrete tool washing basins were observed blocking flow to inlets for short periods. This type

of blockage is assumed to be due to a contractor's error and not PennDOT's activities, but reinforces the need to ensure that drainage pathways are protected during construction.

#### *Capture of runoff from travel lanes and detection of highway drainage patterns*

Contributing watershed areas from travel-ways can be altered substantially by slight changes of grade when stormwater is directed to inlets in the travel-way or shoulder. This sensitivity to grade is problematic given that slopes of highways always have some imperfections, and may change slightly over time due to settling or repaving. The watershed drainage capture area is affected such that it becomes difficult to assess the SMP's performance.

We recommend that designers locate inlets where slight changes of slope will not cause stormwater to bypass inlets. In addition, inlets with larger openings could be installed and oriented perpendicular to the drainage path (double inlets or trench drains). It was observed that the inlets on the elevated highway were offset from the sound wall; this created a path that would allow flow to bypass inlets, and resulted in the buildup of trash. Given that small volumes of trash can dramatically alter drainage patterns, inlets could be integrated into the walls, or be sumped slightly.

Drainage patterns from highway surfaces are not easy to identify visually, so it is difficult to determine watershed boundaries or surface slope patterns. We found that both high-density LiDAR scans and monitored rainfall events were good methods for evaluating watershed drainage areas. We recommend that LiDAR and monitoring be used to validate that constructed surfaces are within tolerance before project acceptance.

#### *SMP construction evaluation*

Evaluation of SMP construction is difficult because SMPs are built for infrequent rainfall events and errors are not visually evident. By monitoring rainfall events and conducting

simulated runoff tests (SRTs), we quickly identified construction issues such as leaking underdrains and inlets, differences in elevations of outlet weir structure from design specifications, and suspect grading. SRTs also made it possible to evaluate infiltration capabilities. We recommend that SRTs or rain event monitoring be required as part of SMP acceptance.

#### *Instrumentation in support of SMP monitoring*

When planned prior to construction, instrumentation housing for inspection monitoring and research can be integrated into designs for a minimal cost. Housing for pressure transducers, staff gages, weir plates in outflow structures, and elevated inflow pipes (to allow measurement) will all be implemented in the next phase of the I-95 monitoring project. We recommend that instrumentation be routinely included to support temporary monitoring of performance and maintenance activities.

#### *Observations on hydrologic monitoring and modeling*

The reduced drainage capture area limits our ability to make substantive recommendations on monitoring or modeling. Note that this work will continue in the next phase of the project and will include the removal of the NJ Barriers and eventually, repaving. However, the use of SRTs and a few larger storms do provide some preliminary observations.

First, the SRT confirmed that the volume capture capacity of SMP C is greater than the design volume. Evaluation of the capacity of SMP A is underway and results will be added for the final report. Second, lessons were learned on monitoring equipment placement and configuration to guide future monitoring for both research and performance. Third, SWMM modeling reproduced the general pattern and volume of runoff inflow, and depths through calibration. As the inlet flowmeter is not accurate at low depths, a combination of monitoring



and flow data is needed to recreate storm events. It was also clear that the SWMM model underestimated the rate of infiltration after the storm event ended, which would potentially impact performance expectations. Finally, the model should be able to be used to evaluate the impact of construction errors, and to identify whether changes would be required to meet performance criteria. These observations further confirm the benefits of using SRT for future basin evaluation.

### **Recommendations on Contaminant Accumulation and Mobility**

It should be noted that observations on contaminant mobility are made based on a limited data set and for a new SMP (~one year of use). To date, there have not been any natural storm events resulting in water exiting the outlet structure. This highlights the need for water quality modeling to predict SMP performance under extreme events. Current observations on contaminant dynamics in SMPs were evaluated using a mass balance approach and data collected from lysimeters, grab samples of storm water in the basin and nearby wells, and the SRT.

In the context of stormwater management, decisions can be made regarding what media to use, and how frequently it should be removed and replaced with fresh media. In the current study, only one medium was investigated, so current evaluations are based only on that medium. As mentioned, media characteristics can also affect contaminant mobility; future research efforts can evaluate the effect of media amendments and maintenance practices specifically selected to limit contaminant mobility.

Thus, the contaminant mobility recommendations will be addressed more after longer term studies. Based on the data collected to date, some limited observations on contaminant fate and transport have been made; these are provided below with potential management strategies.

### *Contaminant remobilization*

Evaluating the SMPs with a mass balance approach, the current influent and lysimeter sample data suggest that the SMPs are accumulating contaminants, likely in the soil media near the surface. In a large storm, the water entering the SMP could remobilize some of the stored contaminants via two potential pathways: 1) resuspension of SMP basin sediment particles due to elevated stormwater velocities, thus increasing the suspended solid concentration and corresponding particle-associated contaminant concentrations, or 2) desorption of contaminants from SMP basin sediments, thus increasing the dissolved contaminant concentrations in the water. In either scenario, if a large storm event were to exceed the basin capacity, releasing storm sewer via the outlet, then there is the potential that the exiting water could be more contaminated than the stormwater entering the SMP.

Based on the SRT, the preliminary ponded water sample data suggests that sediment is not being significantly resuspended, and metals are not desorbing from basin sediments, which was evaluated based on suspended solids, total metals, and dissolved metals concentrations.

Based on these observations, contaminants stored in the SMP media are not likely to be remobilized and released into the storm sewer or adjacent waterway during large events.

Accordingly, SMP media can be replaced or managed to prioritize infiltration performance and underlying water quality rather than concerns of remobilization within the SMP. The current lysimeter data suggest that some metals are migrating into the soil media and are generally observed at low concentrations in the soil pore water; if contaminant mobility were deemed a

risk (i.e., increased concentrations, or high priority groundwater), the risk could be managed through replacement of the soil media or incorporation of a sorbent material.

Although contaminants accumulated in sediments are unlikely to be remobilized during large rain events, we observed during the SRT in SMP A that a large quantity of debris was floating at the surface of the ponding water, covering almost the entire surface of the water in some places. This debris likely originated from plant material and mulch. It is anticipated that such floating material would escape the SMP through the outfall and reach the combined sewer system during particularly large storm events.

#### *Preferential flow paths in SMPs and lesson from the use of tracers*

Observation of water flows in SMPs C, G, and A during the simulated runoff tests (SRTs) using the fluorescent tracer fluorescein indicated that water does not travel at a homogenous velocity throughout the basins. Preferential flow paths and turbulence could be clearly observed, making the flow complex. Obstacles such as plants and rocks significantly affected the flow path of the water. This observation may have implications for the distribution of the contaminants in the SMPs such that they become highly heterogeneous. Hotspots of higher contaminant concentrations could form in regions of still water where sedimentation and infiltration are higher, or erosion when plants are planted parallel to the flow path. Observations during the SRT also suggests that some locations in the SMP basins may be more susceptible to erosion and the formation of water channels. The observations of preferential flow emphasizes the importance of planting vegetation in the basins to reduce preferential flow paths and render the flow more turbulent, thereby increasing mixing and reducing the magnitude of surface water hotspots.

## Recommendations on Planting Designs

As of May 2017, survival in GR2 was 79% overall and 70% for perennial species. Further, 18% of surviving plants exhibited moderately to severely stunted growth. A number of actions may increase the number of plants that live beyond the initial 1-2 year period when mortality is greatest and improve the growth of plants after establishment.

### *Avoid intolerant plants*

Many species had disproportionately high mortality rates or stunted growth when located in the areas most frequently exposed to stormwater. This was the case for a number of herbaceous perennials and shrubs; examples of intolerant species from the set we monitored intensively include *Betula nigra*, *Cornus sericea*, *Monarda didyma*, and *Asclepias incarnata*. Based on patterns over the first two years, areas where these species are in decline are likely to become increasingly devegetated and subject to weed incursion. While elevated mortality and reduced growth are likely unavoidable in hydrologically active areas, these issues can likely be reduced by tailoring the planting design in the primary stormwater flow paths to better accommodate extreme hydrological conditions. In addition to avoiding the use of flood-intolerant species in these areas, plants could be placed more densely, and designs could incorporate species that are specifically adapted to wet soil conditions (see the plant tolerance table in Chapter 7). We note that using flooding intolerant species at the edges of low elevation areas could be viable if size reductions are deemed acceptable.

Based on the plant survival data collected thus far, there are three species whose use should be avoided or reserved for shaded and minimally stressful regions of the SMPs. These are *Cimicifuga ramosa*, *Geranium maculatum*, and *Matteuccia struthiopteris*. In the wild, these species are often found in forest understories, and may therefore be maladapted to the level of

exposure many of them are experiencing. Although *C. ramosa* is likely a different taxon than currently labeled, it may be prudent to avoid placing any *Cimicifuga* species in exposed areas or in stormwater flow paths. We note that several specimens of *G. maculatum* that had no living shoots in October 2016 were growing well and producing flowers in May 2017. It may therefore be possible for this species to spread clonally from these successful individuals. However, even if this proves to be the case, it is likely that far more individuals would need to be planted than would survive to overcome low first-year survival rates.

#### *Expand the use of stress-tolerant plants*

It is possible that species particularly tolerant of inundation, salts, and heavy metals could prove to be suitable in problematic low-elevation areas. Examples of such species are provided in the table in Chapter 7. Among the species currently used in GR2, several appear to have a relatively high tolerance of inundation by stormwater. For example, of the nine species whose sizes we measured, *Calamagrostis* × *acutiflora*, *Iris sibirica*, and *Hemerocallis* spp. were reduced in size but had relatively low mortality rates in the most hydrologically active areas; all had >90% survival in the SMPs overall. Among the species whose sizes we did not measure specifically, the three *Carex* species currently used widely in GR2 stood out as being relatively well-suited to the hydrologic conditions. Like *Carex* spp., members of the genus *Juncus* are often found in wetlands and are frequently incorporated into bioswale designs. *Juncus* species do not appear to have been used in GR2, but several species would likely be readily available, including *J. effusus*. We have also observed that the grass *Echinochloa muricata* has colonized low elevation areas of several SMPs. It is native and adapted to wet soils, so its growth could be allowed rather than it being removed during weeding events. Given the difficult growing

conditions found at the lowest elevations within SMPs, we recommend planting additional species that are known to tolerate periodic inundation.

### *Overplanting*

In some contexts, such as low-lying areas where mortality is particularly high for perennial species, it may be reasonable to install plants at a greater spatial density. For one, overplanting in this way will align planning expectations with the probability that a significant fraction of plants will inevitably fail in certain locations. Moreover, packing plants more tightly in hydrologically active areas may dissipate the energy of rapidly moving stormwater, reducing scour and direct damage to plants. Even dead stems and roots will continue to stabilize soil and reduce water velocities until they are dislodged or removed. We suspect that a large cluster of *Forsythia* that did not survive through the winter of 2016/17 is preventing mulch and soil erosion on the hillside in SMP E. Eventually, dead plants may need to be removed for aesthetic or other reasons, but their presence may improve the habitat quality for living plants long enough for them to fully establish.

### *Other recommendations*

We identified several individual plants that were unlikely to survive from the start, likely because plant material was unhealthy when delivered or because plants were not installed sufficiently deeply (this was clearly the case for several trees and shrubs in SMPs C and E). Regardless of the reason, many installers will replace individuals that die within a year of planting; we recommend that this provision be noted when contracting with installers and that it be enforced.

We recommend avoiding the use of known invasives in SMP plantings. For example, there are individuals of *Berberis thunbergii* and *Acer platanoides* in GR2. Not only is it possible

that these species will spread within the SMPs themselves, but they may also serve as a seed source for nearby natural areas. Perhaps equally important, their presence will be noticed and frowned upon by conservation-minded citizens who pass by the site.

### *Alternative design strategies*

The vegetation in all of the SMPs in GR2 were designed in a highly-landscaped style. While this is desirable in highly visible areas, landscaped SMPs are expensive to install and to maintain. For example, this design approach tends to include many open areas between plants; this allows for weed colonization even when soil is covered by mulch. We estimate that weeding would have been necessary at least every two weeks during wet years like 2017 to prevent weeds from reaching undesirable levels. We recommend considering alternative vegetation designs for future SMPs in which plants are more densely spaced, such as meadow-like plantings in fenced SMPs. In this type of installation, light and soil resources are relatively inaccessible and weeds are likely to colonize much more slowly. While weeding would still be required, the frequency (and therefore cost) could be reduced.

In addition, when the planting patterns in the stormwater flow path are aligned with the direction of flow, it can cause channelized flow and erosion (as observed in SMP C). In contrast, areas in which vegetation is planted more densely or in irregular patterns, erosion was substantially reduced. We recommend that dense and less regular planting patterns be used and that plants be staggered and massed to slow runoff velocities, and extend flow paths. Additionally, it may be prudent to install clusters of rocks or small gabions much more commonly in low-lying areas to disperse the energy of high-velocity stormwater.

We have frequently observed or found evidence of members of the public entering the vegetated areas of SMPs. We recommend accommodating foot traffic in the design strategy to

reduce erosion, soil compaction, and damage to plants. Installing pathways that allow for directed travel through the SMPs would be the primary way to accomplish this.

#### *Improvements to the amended soil*

While alternative soil mixes will be evaluated in the context of GR 3-4, we identified several areas in GR2 where the amended soil was quite thin (<20 cm). This was particularly the case on slopes and at the highest elevation areas of the SMPs. Soil moisture was frequently 10-15% in these areas shortly after rain events compared to 40-50% in low-lying areas, and we sometimes found when inserting our probes that the underlying soil was highly compacted. These conditions are not amenable to plant growth, and would likely be improved considerably if the amended soil was at least as deep as specifications require. We recommend that the depth of amended soil in upper areas of SMPs be increased, either by increasing the soil thickness specified or ensuring that the current specification is enacted.

One way to verify that the application of amended soil meets design specifications is to perform terrestrial LiDAR scans. This could be done immediately after excavation and again after adding amended soil to the basins. Areas with insufficient fill would be immediately apparent upon differencing the digital elevation models. This procedure could be tested during the construction of the next bioswale to determine whether detecting areas of uneven fill thickness justifies the expense of additional LiDAR scans.

### **Recommendations for SMP Maintenance**

#### *Weed removal*

The PennDOT maintenance manual currently states that weeds are to be removed from SMPs monthly. This is insufficient, especially where the landscaped planting design of SMPs like those in GR2 is used. Based on observations of weed colonization and growth both in SMP



A where weeding did not occur, and SMPs C, D, and G where it was scheduled to occur monthly, many weed species were able to grow prolifically in a month's time. In addition, several neighbors commented to us that weeds were growing unacceptably rapidly along their fence lines. We recommend that weeding be conducted every two weeks, and that the maintenance manual be updated to reflect this. This frequency could be reduced in years in which rainfall is substantially lower than it was in 2017. However, frequent weeding (perhaps even weekly) along the fences of neighboring residences and businesses could be an important way to maintain positive relations with neighbors.

The maintenance manual currently prohibits the use of motorized weeding devices and herbicides. Mechanized tools can cut large plants far faster than manual tools and are therefore much more efficient and cost effective. Hand pulling can also induce erosion on slopes when root systems are removed and can leave an area unsightly. For example, weed removal has removed the mulch and exposed the landscaping fabric in several locations along the mow line in SMP C/D/G. Motorized tools could be particularly useful for controlling weed infestations that are relatively large or inaccessible. Targeted herbicide applications using appropriately selected herbicides, surfactants, and delivery methods could also be a safe and effective means of reducing weed control costs. Pre-emergent herbicides could slow the growth and spread of weeds well into the growing season. We recommend that motorized weeding devices be allowed during restricted hours of the day in certain cases where weed removal is prohibitively difficult with manual tools and hand pulling and that targeted herbicide application be used.

#### *Removal of litter and dog waste*

The approaches for removing litter that accumulates in the SMPs will need to differ for large versus small items, mainly because it is impractical to collect numerous small pieces by

hand (e.g., the cigarette butts in SMP A likely number in the thousands). Most small trash enters with the stormwater from the roadway; some collects in the rocks below the inlets while others wash through the basins. A pretreatment catchment would be helpful in preventing the dispersal of these small but abundant pieces of trash. More specifically, the elevated inlet pipes provide an opportunity to develop a low-cost trash collection system where the flow enters the SMP. This will extend the lifespan of SMPs and reduce maintenance costs. We recommend that inflow pipes continue to be elevated, and that a low-cost, maintenance-friendly trash collection system be developed.

Large trash is currently scheduled for monthly removal by Terraquarbor, but a community member regularly collects trash from SMPs C, D, and G. Even with this additional effort, litter accumulates far faster than it is being removed. The maintenance manual currently specifies that litter and debris should be removed monthly, which we recommend increasing to at least every two weeks.

The vegetation in the SMPs within GR2 seems to make the adjacent sidewalk highly attractive for dog walking. This has had the side effect of considerable amounts of dog waste being left in the lawns and in the low-lying areas of the SMPs themselves. Adding signage about dog waste negatively impacting water quality would inform the community and making it as easy as possible for dog owners to collect and dispose of their dog's waste could also help mitigate the problem, e.g., by installing community-sponsored bag dispensers and trash cans. Incorporating a more obvious pedestrian pathway within the design may also prevent the SMPs from appearing to be “out of the way” areas where dog waste will go unnoticed.

### *Erosion reduction*

Minor soil erosion is evident in most of the SMPs in GR2 and channels have started

forming in some areas. Erosion typically occurs in the lowest parts of the basins where flowing water scours the bottoms of the SMPs. For example, the soil below inlets in SMPs E, H, I, and J have experienced notable erosion (in SMP J, the riprap has been largely displaced). We recommend modifying inlet spillways to be able to withstand greater water velocities. For example, increasing the area (length and width) of riprap at the inlets may help to mitigate erosion, as may increasing the size of stones used. It may also be appropriate to modify the specifications for the soil used under the riprap and the landscape fabric layer such that it remains stable (e.g., using gravel). A further preventative measure may be installing additional stone barriers in areas further from the inlets to buffer the erosive energy of incoming stormwater. We note that, in agricultural settings, grassed waterways and contour strip cropping (planting rows of plants perpendicular to the flow of water as vegetation barriers) are used to reduce scour and rill erosion; these practices may likewise be beneficial in bioswale applications like those in GR2.

There is also significant mulch movement on slopes. We recommend decreasing the slopes of SMP sidewalls when they are initially dug out. This may further help plants to establish on the slopes. Adding pathways with steps where appropriate could also decrease erosion.

### *Drainage*

Several areas within the SMPs in GR2 are not draining well. In future installations, we recommend that a more thorough evaluation of subsoil conditions be conducted prior to the installation of amended soil. Multiple infiltration tests should be conducted in both the subsoil and the amended soil layers.

## **Recommendations of Community Adoption**

Actively engaging the community in SMP management could be an effective strategy for both increasing the person-hours dedicated to maintaining the vegetation and litter in BMPs and decreasing the labor costs. For instance, an ‘adopt a bioswale’ program could be initiated much like those in place for PennDOT’s highways. High school environmental groups, community associations, and youth groups like boy/girl scouts could all potentially assist in the maintenance of these community assets. In fact, a New Jersey based environmental group called Re-Youth has expressed interest in collaborating in cleanup efforts. They are interested in expanding volunteer activities to Philadelphia and to increase community awareness of environmental issues. In tandem with engaging the community in SMP management, we recommend soliciting feedback from neighbors and community members on proposed SMP designs and ongoing issues once they are installed.

Neighbors clearly value the green infrastructure in their neighborhood. We have seen them add bird feeders, and scarecrows at Halloween, remove trash, and regularly walk dogs. Neighbors from one SMP also petitioned the city for no parking signs. However, there are issues associated with homeless utilizing the sites and the neighbors periodically contact the police to have them relocated. Overall, PennDOT’s communication with the residents is a success story. It is recommended that District 6 continue these communication efforts but that amenities for community members such as walking paths, doggie bag stations, etc., be added to future designs.

## **Final Observations**

The SMPs in GR2 have proven to be successful in many ways. They are capturing stormwater together with the contaminants it carries, thereby preventing either from entering the municipal stormwater system and being released into the Delaware River. Moreover, much of

the vegetation has successfully established and promises to beautify the neighborhood for years to come. Our data-intensive investigation has highlighted several ways in which the design and maintenance of SMPs can be improved while minimizing the associated costs. The analyses and recommendations provided here are an initial synthesis of our ongoing effort; we expect the empirical and modeling processes that we have developed to facilitate many further insights and suggestions that can be put into practice in future phases of SMP design, installation, and management.

## Appendix 1: Baseline well drilling logs

*Table A1. Description of the sedimentology in each monitoring well. The depth range is the depths (in ft) below the land surface, the unit thickness is the thickness of the recorded sedimentological unit (in ft), and the elevation is the elevation (in ft above sea level) of the top of the sedimentological unit. Well log provided by Susquehanna Civil, Inc.*

MW1					
Depth Range (ft)		Unit Thickness (ft)	Elevation (ft asl)	Description	USCS Classification
0	0.4	0.4	21.2	Concrete	
0.4	8.8	8.4	20.8	Sandy silt (fill)	ml
8.8	15.5	6.7	12.4	Well sorted sand with gravel (alluvium)	sp
15.5	18	2.5	5.7	Clayey sand (alluvium)	sc
18	22	4	3.2	Well sorted fine sand (alluvium)	sp
22	29.6	7.6	-0.8	Silty fine sand with clay (alluvium)	sp-sm
29.6	30	0.4	-8.4	Sandy silt (alluvium)	ml
MW2					
Depth Range (ft)		Unit Thickness (ft)	Elevation (ft asl)	Description	USCS Classification
0	3	3	19.7	Unsampled	
3	6.5	3.5	16.7	Sandy silt some clay (fill)	ml
6.5	10	3.5	13.2	Well sorted sand with silt, some gravel (alluvium)	sp
10	12	2	9.7	Well sorted gravel with silt and sand (alluvium)	gp
12	13.5	1.5	7.7	Poorly sorted sand with gravel (alluvium)	sw
13.5	21	7.5	6.2	Silty fine sand some clay (alluvium)	sp-sm
21	26	5	-1.3	Clayey sand (alluvium)	sc
26	30	4	-6.3	Silty fine sand (alluvium)	sp-sm
MW3					
Depth Range (ft)		Unit Thickness (ft)	Elevation (ft asl)	Description	USCS Classification
0	0.4	0.4	19	Concrete	
0.4	3	2.6	18.6	Silty gravel with slag, some coal and ash (fill)	gm
3	6	3	16	Sandy silt with clay (fill)	ml
6	7.5	1.5	13	Silty sand with gravel (alluvium)	sm
7.5	10	2.5	11.5	Poorly sorted sand with gravel and silt (alluvium)	sw
10	12	2	9	Sandy silt (alluvium)	ml
12	18	6	7	Silty fine sand clay (alluvium)	sm
18	21	3	1	Clayey fine sand (alluvium)	sc
21	30	9	-2	Silty fine sand (alluvium)	sm

**MW4**

Depth Range (ft)	Unit Thickness (ft)	Elevation (ft asl)	Description	USCS Classification	
0	0.4	0.4	14.5	Concrete	
0.4	3	2.6	14.1	Silty gravel with brick (fill)	gm
3	4.5	1.5	11.5	No recovery	
4.5	6	1.5	10	Silty fine sand (alluvium)	sm
6	9	3	8.5	Silty gravel (alluvium)	gm
9	10.5	1.5	5.5	No recovery	
10.5	12	1.5	4	Clayey sand (saprolite)	sc
12	25.5	13.5	2.5	Silty sand (saprolite)	sm

**MW5**

Depth Range (ft)		Unit Thickness (ft)	Elevation (ft asl)	Description	USCS Classification
0	9	9	16.5	Sandy sand with gravel and brick (fill)	sm
9	10.5	1.5	7.5	Well sorted sand with silt and gravel (alluvium)	sp
10.5	11	0.5	6.2	Silty clay (alluvium)	cl
11	21.5	10.5	5.7	Poorly sorted gravel with sand (alluvium)	gw
21.5	23	1.5	-4.8	Well sorted sand (alluvium)	sp
23	30	7	-6.3	Sandy silt with clay (saprolite)	sp

**MW6**

Depth Range (ft)		Unit Thickness (ft)	Elevation (ft asl)	Description	USCS Classification
0	10	10	10.6	Sandy silt with gravel, brick, coal slag, and ash (fill)	ml
10	13.4	3.4	0.6	Sandy silt (alluvium)	ml
13.4	15	1.6	-2.8	No recovery	
15	15.2	0.2	-4.4	Silty sand with mica (saprolite)	sm
15.2	18.5	3.3	-4.6	Schist	

**MW7**

Depth Range (ft)		Unit Thickness (ft)	Elevation (ft asl)	Description	USCS Classification
0	1.5	1.5	14.5	Silty sand some gravel with brick, coal, ash, and slag (fill)	sm
1.5	5.5	4	13	Well sorted gravel and sand gravel is brick (fill)	gp
5.5	10	4.5	9	Well sorted sand trace gravel (alluvium)	sp
10	22.5	12.5	4.5	Poorly sorted sand with gravel (alluvium)	sw
22.5	24	1.5	-8	Well sorted gravel with silt and sand (alluvium)	gp
24	31.5	7.5	-9.5	Well sorted sand some silt (alluvium)	sp
31.5	33	1.5	-17	No recovery	
33	36	3	-18.5	Silty clay (alluvium)	cl

## Appendix 2: Monitoring and modeling of SMP A

### Introduction

The purpose of this addendum is to update the project report for TEM 006 to capture the accomplishments to date since submission of the draft final report on October 1, 2017.

Instrumentation and analysis for SMP A was still under development, and the purpose of this addendum is to complete the project report. The primary additions are further site descriptions and storm events recorded for SMP A, summarization of monitored data records, and further comparison coupling the monitoring data, LiDAR and computer simulation analysis using SWMM. The results from this period further support the conclusions and observations previously reported.

### SMP A - Site Description

As previously presented, Villanova and Temple are currently doing research on four bioswales (SMP C, D, G and A) shown in Figure A2-1, located along the Northbound side of Interstate 95 in Philadelphia, Pennsylvania. Instrumentation and data analysis of SMP A follows the same approach of SMP C, D, and G as previously presented.

SMP A is a gated, long linear bioswale located between Shackamaxon Street and Frankford Avenue along Richmond Avenue with three culvert inlets and two outlet structures that overflow into Philadelphia's combined sewer. The surrounding area around SMP A consists of primarily small business and residential properties. SMP A has an approximate surface basin area of 4616 ft<sup>2</sup> and a design drainage area of 2.17 ac. SMP A receives runoff through three culvert inlets (N8, N9, N10), and a bypass lane that will be extended to become an on ramp in the near future. These inflows

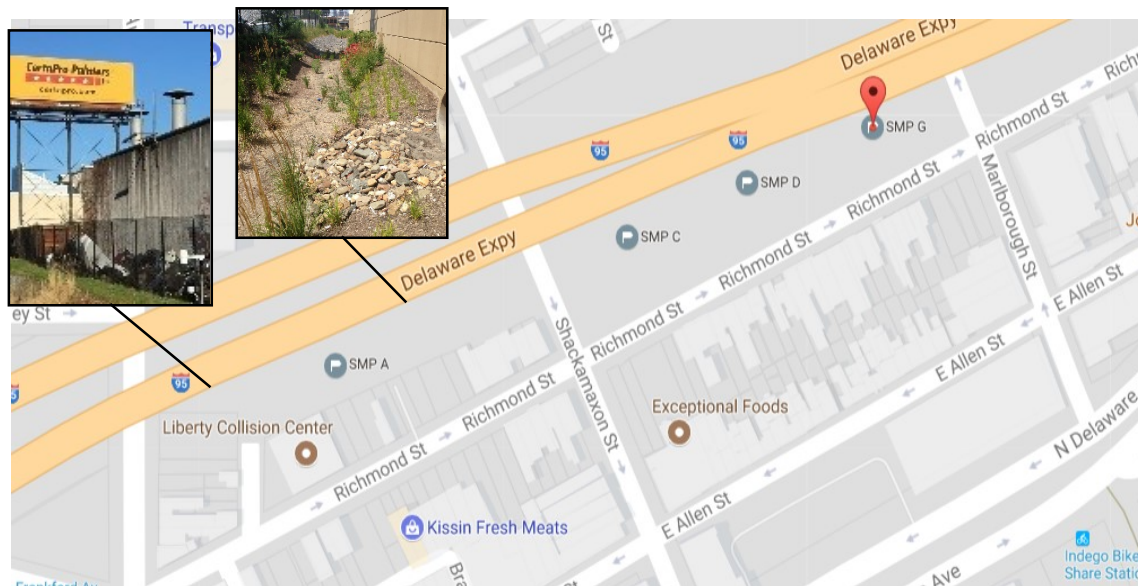


Figure A2-1: SMP A, C, D, and G Locations (Google 2017).



contribute 0.172 ac, 0.218 ac, 1.499 ac, and 0.112 ac of the impervious area, respectively. The contributing pervious area accounts for about 0.0631 ac of the design drainage area. Two outlet structures connected to the combined sewer system are termed B1 and B2. Figure A2-2 shows the as-built with corresponding inlet and outlet structures labeled.

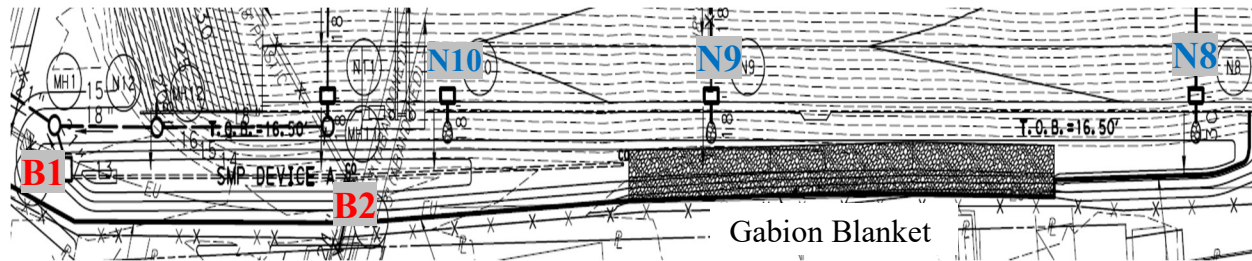


Figure A2-2: Inlet (Blue) and Outlet (Red) Structures

There is a large gabion blanket located between the first and last inlet coming into SMP A to help slow down flow and prevent erosion and sedimentation. Due to the long length of the bioswale, two 90°V-Notch weir structures were put in place upstream and downstream of the gabion. Figure A2-3 shows the upstream and downstream weirs.



Figure A2-3: (a) Upstream and (b) Downstream V-Notch Weirs

Pressure transducers are located upstream of each gabion to calculate flow over the weir. Stones, which have been replaced with permeable pavers were placed downstream of each weir to reduce erosion and sedimentation downstream.

A water quantity monitoring for SMP A is currently ongoing, and was initiated after completion of instrumentation in May 2017. A small weather station has been installed at the outlet structure B2 as shown below in Figure A2-4, to compliment the elevated weather station.



*Figure A2-4: Small Weather Station at Outlet B2*

This weather station contains the housing for the datalogger in SMP A that collects data from three inlet flow meters, six pressure transducers, and two clusters of soil moisture sensors. The meteorological monitoring includes air temperature, wind speed, and wind direction. The elevated weather station located on Frankford Ave provides rain gage data, relative humidity, and barometric data for SMP A.

Villanova is currently monitoring inflow from I-95 and outflow to the combined sewer system, while monitoring flow within the system as well. Figures A2-5 and A2-6 below display a layout of the monitoring plan that has been implemented. Figure A2-5 shows the monitoring plan upstream of the gabion blanket, and Figure A2-6 shows the monitoring plan downstream of the gabion blanket. The smaller weather station at SMP A is denoted with a gold star. All data is downloaded to the network at Villanova every 6 hours. The data is then uploaded every month to Villanova's database.

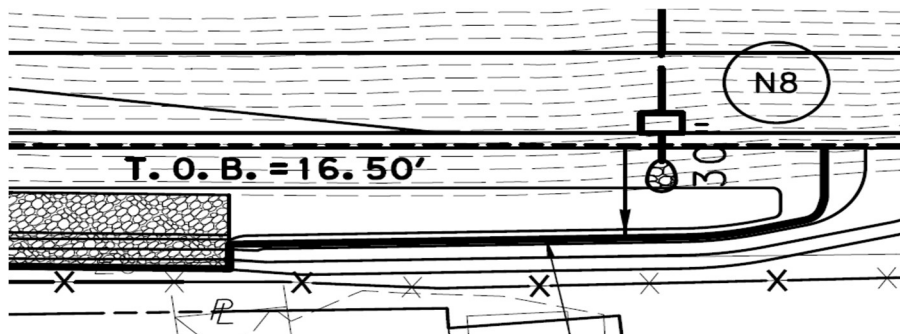


*Figure A2-5: Monitoring Plan in SMP A Upstream of the Gabion*

## SMP A - Simulated Runoff Test Results

To validate both instrumentation and the SMP performance, a simulated runoff test (SRT) was performed for SMP A on August 18, 2017. The procedures were similar to that performed at SMP C, and G previously, except the firehoses were able to access the inlet grates on I-95 immediately adjacent to the noise barrier.

Philadelphia Water Department (PWD) used firehoses to connect with a fire hydrant located on the corner of Richmond Street and Sarah Street. The test started at 10:00 AM (EST). The firehose was placed so flow entered inlet N8 for 2 hours and 15 minutes at a constant flow rate of 28 cfm. The

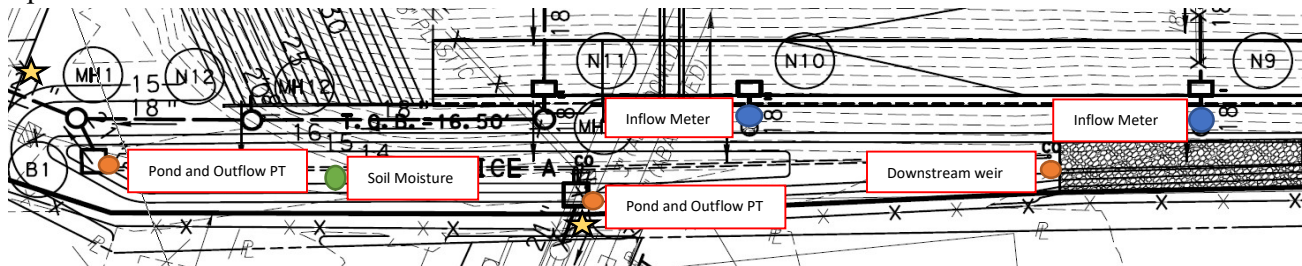


*Figure A2-6: Monitoring Plan for SMP A Downstream of the Gabion*

firehose was then moved to inlet N9 for 45 minutes at a constant flow rate of 31 cfm until 1:00 PM (EST). The water was shut off after 10 minutes of overflow entered outlet structure B1. A total of 5075 ft<sup>3</sup> of water entered the garden over a duration of 3 hours. This would correspond to a 0.64 in rain event using the original design drainage area.

The outlet structure B1 overflowed earlier than expected due to discrepancies between construction and design. Both structures were designed to overflow at the same elevation of 13.92 ft through weirs or orifices depending on the depth of flow. Post construction surveys provided by AECOM showed that the as-built elevations (top overflow) were not the same as design. The final elevation for the top of outlet B1 was approximately one foot lower than B2. Outlet structure B1 overflowed at a water surface elevation (WSEL) of 13.5 ft. While this difference in elevation was known, this result supports previous observations that SRT and instrumentation are a valuable inspection and evaluation tool. Currently the researchers are working with AECOM to discuss follow on actions, which may be as simple as plugging the orifice / weirs of outlet B1. When developed, the SWMM model of SMP A will be of use in this process.

Results of the SRT were also used to review area velocity inflow instrumentation performance. Figure A2-7 shows a graph of inflow for both inlets N8 and N9 from PWD data and that from the Blue Siren® area-velocity sensors that were installed. The flow rate that was recorded by PWD corresponded to water that was flowing through the firehose, prior to entering the inlet. This is read



from an analog dial on the flow meter. The flow rate that was recorded by the inlet area velocity sensors corresponded to water that was leaving the inlet pipes. These values are spot readings of both depth and velocity that are taken at each five-minute time stamp to match that of the PWD data. Flow is then calculated based on these measurements using the pipe dimensions. As shown in the graph, the maximum rate for the AV meter and that of the PWD flowmeter are remarkably similar, which was felt to validate the performance of the instrumentation, and match results achieved in pre-installation testing at the Villanova Fluid Mechanics Laboratory. However, there was some differences over the course of the storm. As the SRT progressed, the AV Sensor reported less flows than that as recorded by PWD.

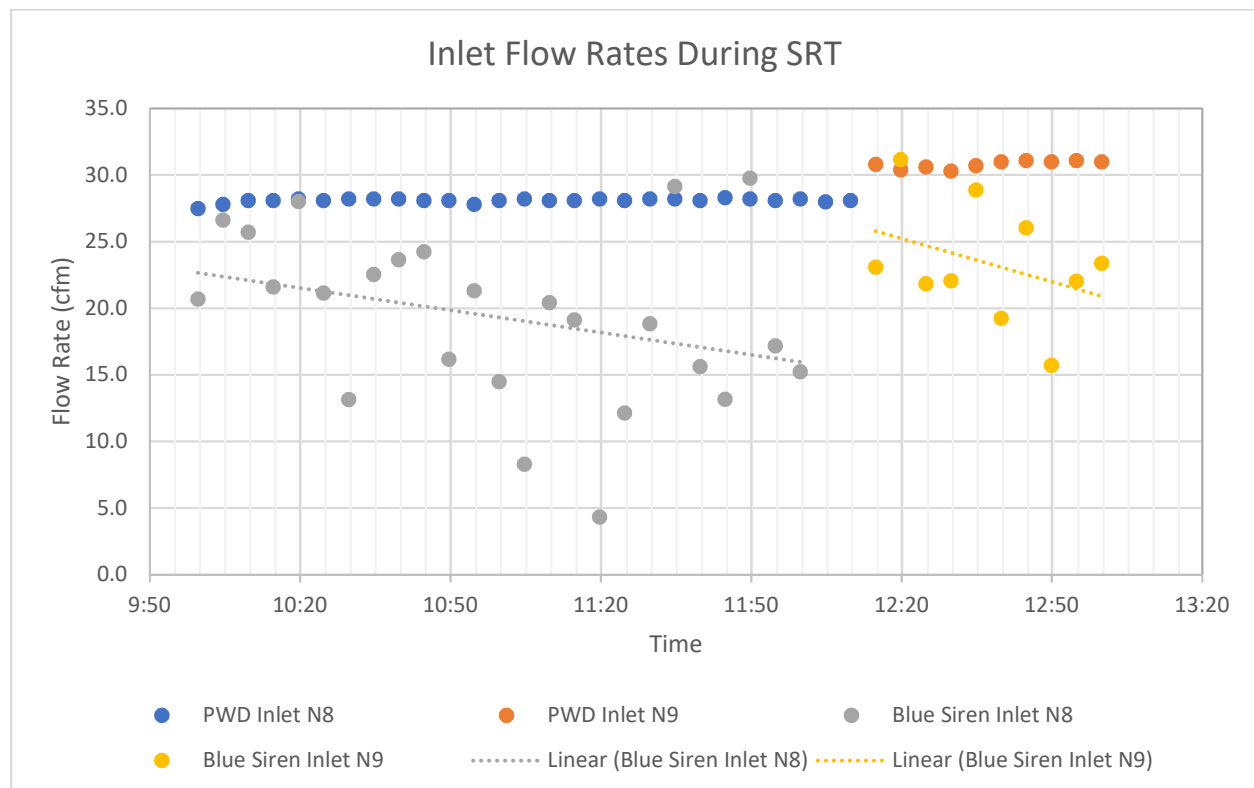
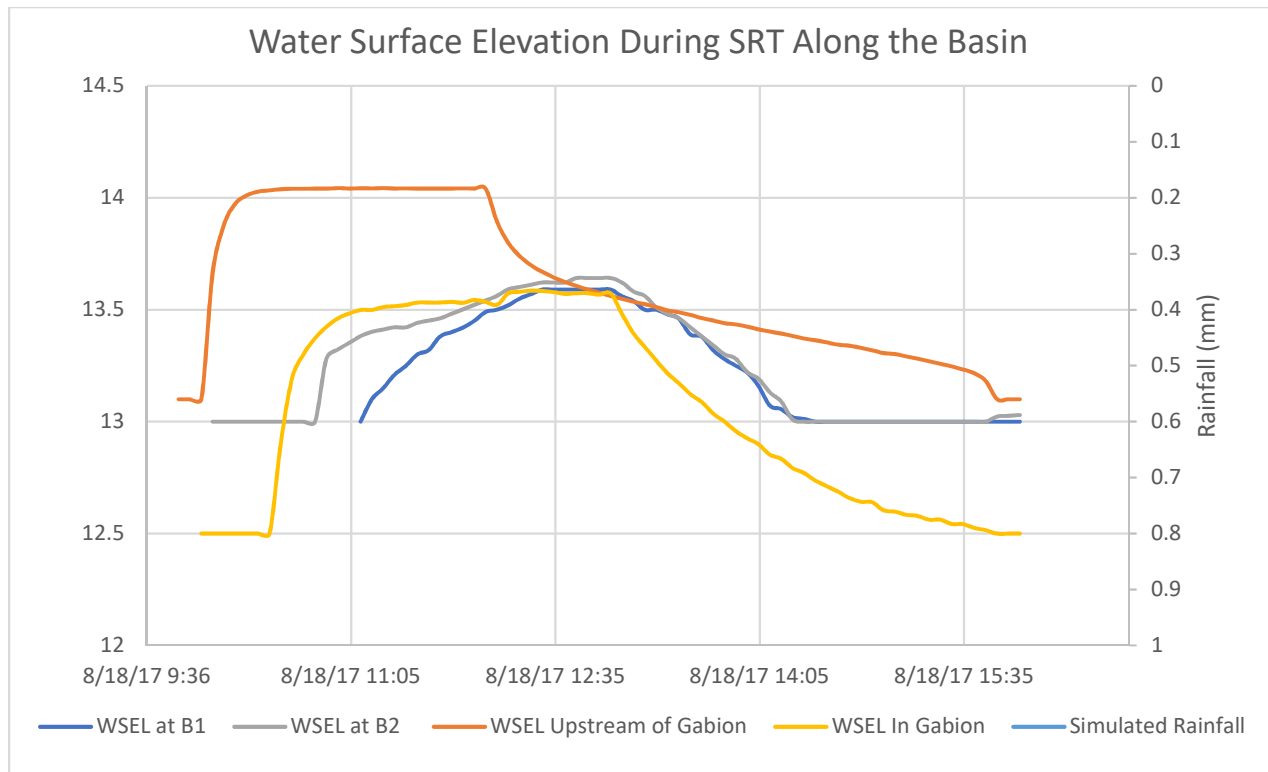


Figure A2-7: SRT Inlet Flow Rates (N8 and N9)

Part of the differences are due to the turbulence during the event; some error is expected, which is why instead of one point in time, the Area Velocity Sensors average flows over five-minute intervals. However, the chief cause of the differences is postulated to be due to pipe losses during the event. During the SRT it was apparent that there was seepage coming from the retaining wall located above the inlet pipe. The vertical pipes are not sealed, and as the fire hose concentrates a stream of water, there was loss of volume before water was conveyed through the end of the inlet pipe. This will be further investigated as the project continues past the IDEA grant end date.

Several observations can be made from review of the water surface elevations recorded during the SRT. As stated earlier, the maximum water surface elevation measured in the SMP during the SRT was 13.5 ft. Figure A2-8 shows the water surface elevation during the duration of the SRT. The PWD flow data was translated to simulated rainfall using the AECOM design drainage areas.



*Figure A2-8: Water Surface Elevations (ft) Along SMP A During the SRT*

The sharp declines seen in the WSEL curves for the gabions correspond to the water being shut off at each inlet, N8 and N9. Note that the WSEL upstream of the gabion drops earlier when the flow changes from inlet N8 to N9 which is below the upstream measurement point. The elevations suggest the differences in analysis of this type of a structure which has more of a swale configuration. At the time at which the water started to overflow outlet B1, 4763 ft<sup>3</sup> of water were pumped into the basin. At the point of overflow, 2790 ft<sup>3</sup> was held in surface storage, with 1973 ft<sup>3</sup> infiltrated. Over 40% of the flow was infiltrated during this short period which is not considered in current design practices. This may be higher than normal due to the gabion structure. Of note is that all surface water infiltrated post SRT in less than two hours. There was some limited outflow as shown in Figure A2-9.

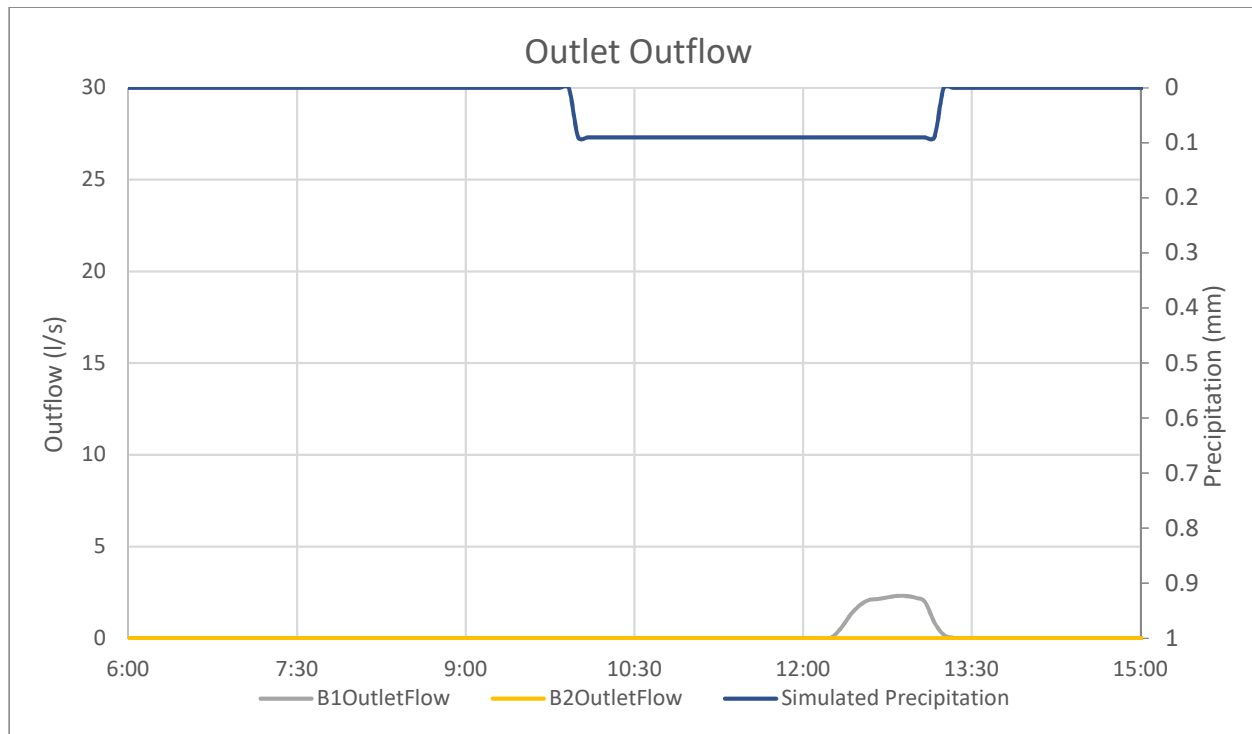


*Figure A2-9: Outlet Outflow During SRT*

The soil moisture meters upstream (Figure A2-10) and downstream (Figure A2-11) of the gabion were recorded during the event. A rainfall event occurred just prior to the SRT. The upstream data showed minimal responses, suggesting that the soil retained antecedent soil moisture, as the upper inlet captures a larger drainage area. The soil moisture downstream showed a slight increase for the sensors at 10 and 60 cm, but a drastic increase for the soil moisture at 35 cm. It is suspected that there was antecedent soil moisture at the higher depths.

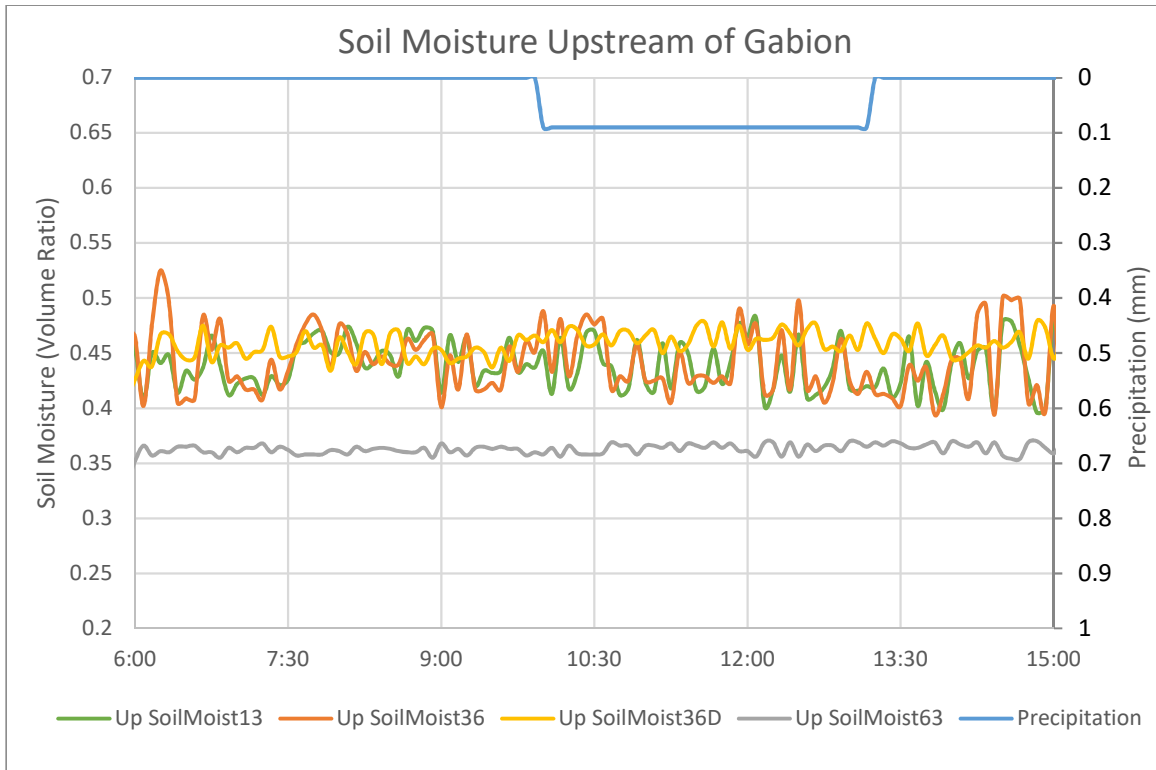


Figure A2-10: Soil Moisture Upstream of Gabion during SRT

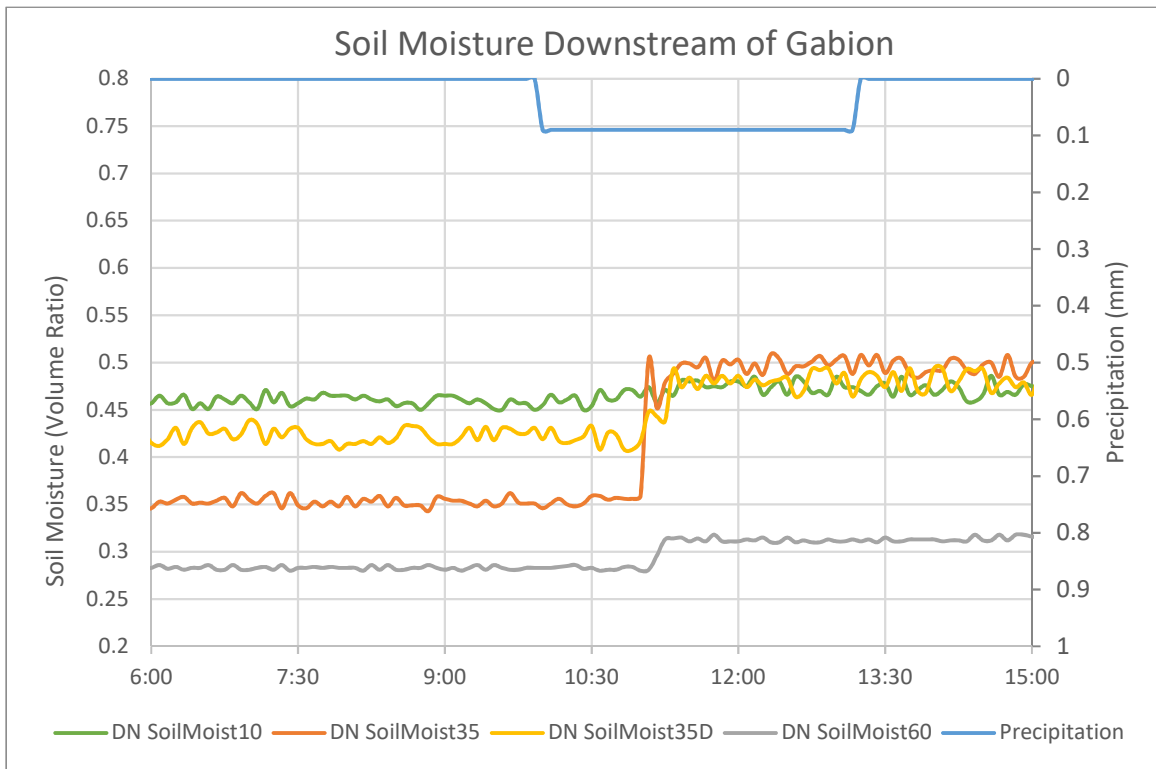
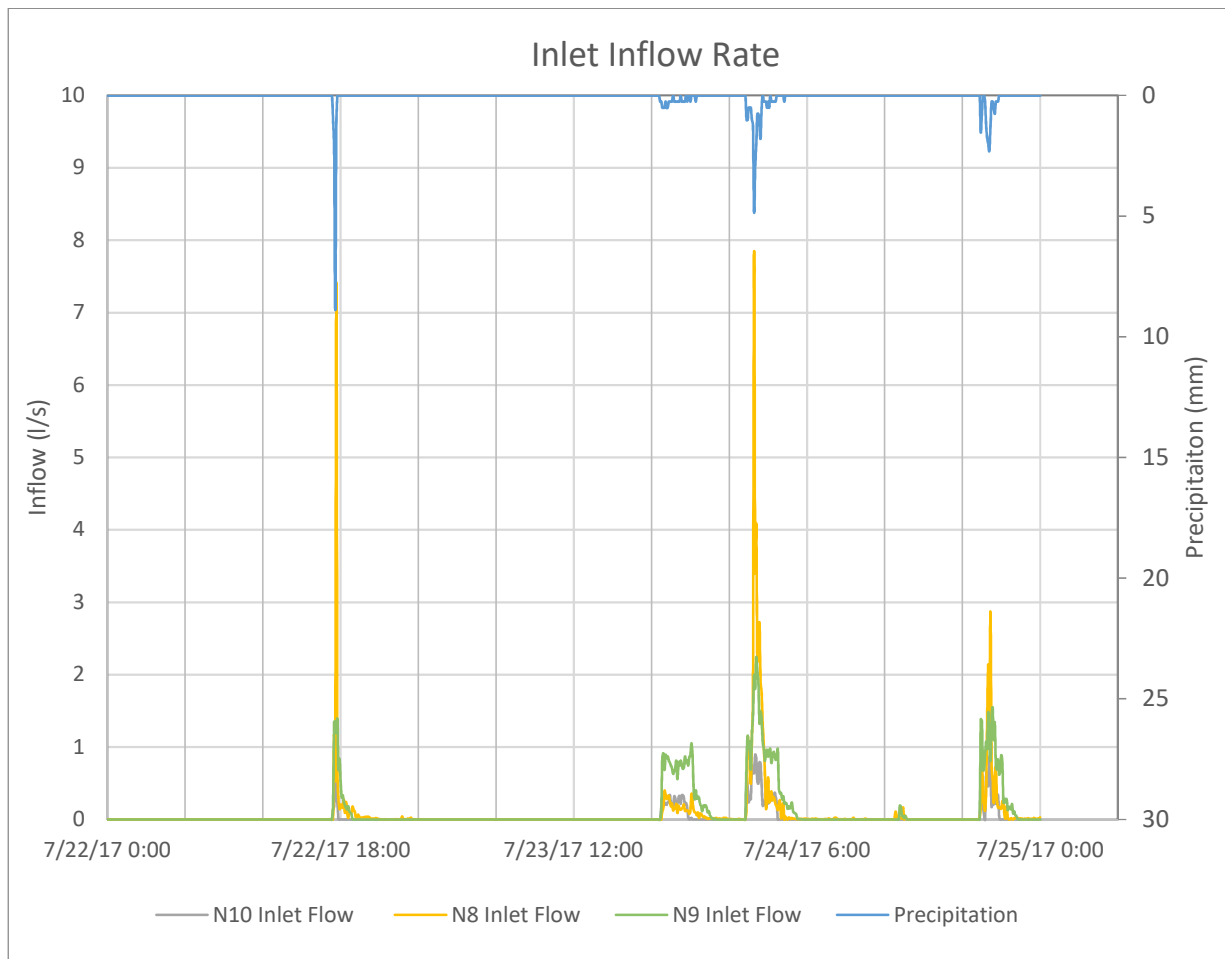


Figure A2-11: Soil Moisture Downstream of Gabion during SRT

## SMP A - Sample Storm Events

Two storm event periods were chosen to represent the site performance. The first was a series of storms occurring from July 22<sup>nd</sup> to 25<sup>th</sup> (Figure A2-12). Over this period, three storms occurred totaling 2.33 inches of rain (58.4 mm), in increments of 0.53, 1.26, and 0.54 inches respectively (or 13.5, 32, and 13.7 mm). The initial storm on the 22<sup>nd</sup> was very short with an exceptionally high intensity of over an inch an hour. The middle larger storm over the evening of the 23<sup>rd</sup> and early morning of the 24<sup>th</sup> had a double peak, and the third storm was smaller and less intense.



*Figure A2-12: 7/22-25/17 Inflow*

The outflow and soil moisture data for this period are presented in Figures A2-13 and A2-14. Note that some minor leakage is shown for B1 and B2 though the ponding depth is less than the overflow levels. This is normal for most outlet structures and not viewed as a problem. Overflow does occur during the larger event at B1. The soil moisture measurements downstream of the storm show the effects of the moisture in filling the basin. Clearly these storms are related and need to be evaluated as a series and not individual events.



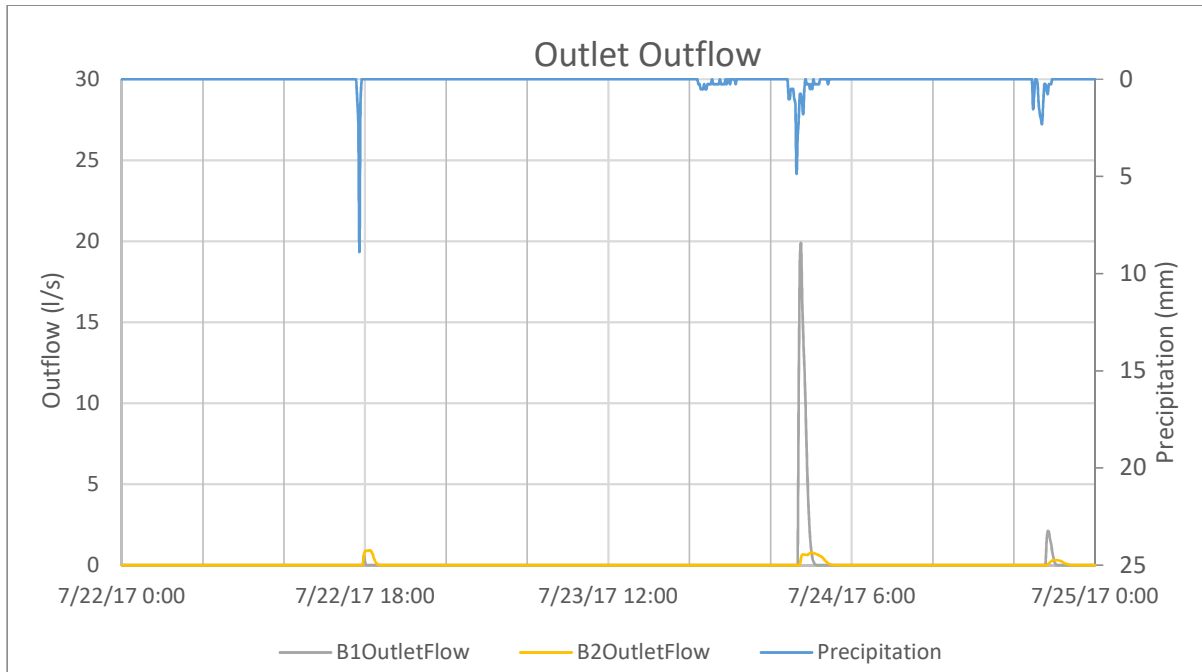


*Figure A2-5: 7/22-25/17 Outflow*

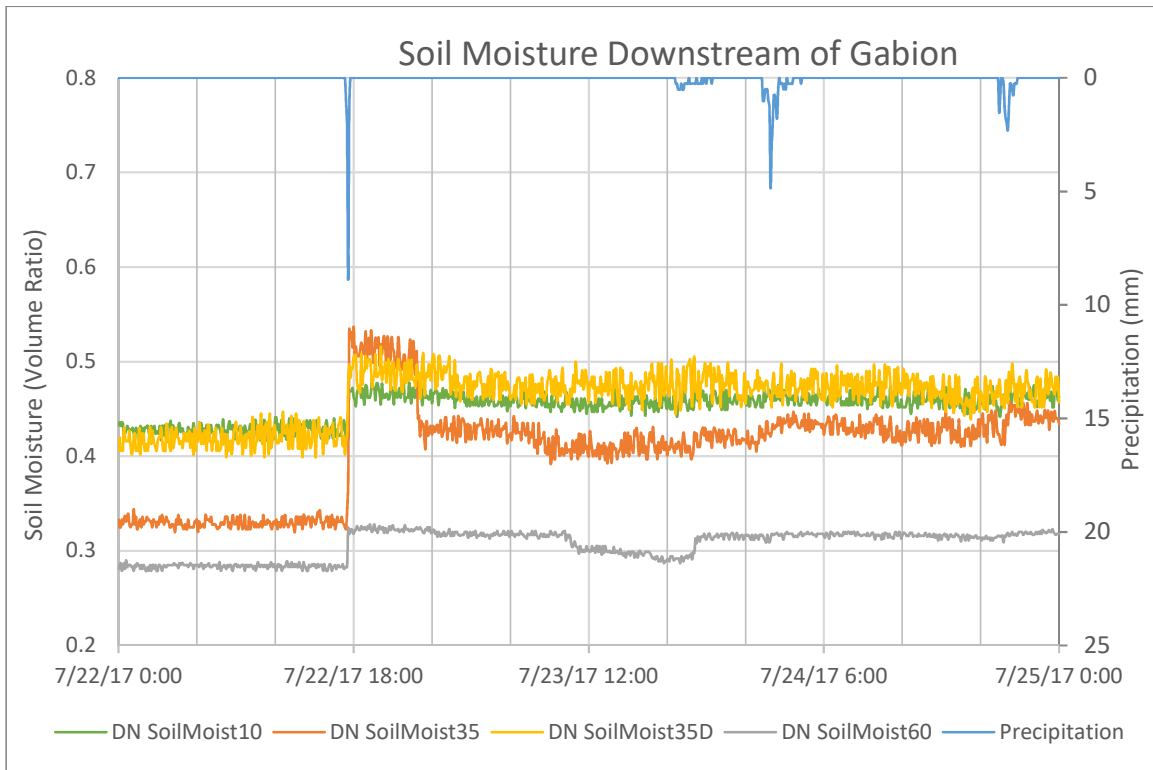


*Figure A2-6: 7/22-25 /17 Soil Moisture Downstream of Gabion*

The second example storm is from a large event of 2.33 inches (59.2 mm) on the 29<sup>th</sup> of October. The period of rain is close to 24 hours, and the storm exceeds the PWD volume reduction

expectations, and overflow was recorded. Figure A2-15 shows the inlet flow rate as recorded during the storm. The larger inflow occurs in Inlet N8 which corresponds to the larger drainage area. Figure A2-16 shows the depth as recorded at B1 and B2, showing that the reduced elevation of the riser at B1 resulted in outflow. The reader should be reminded this is a sloped channel, and the results are listed here as depth not water surface elevation. Figure 16 is also interesting, as the ponding depth quickly recedes.

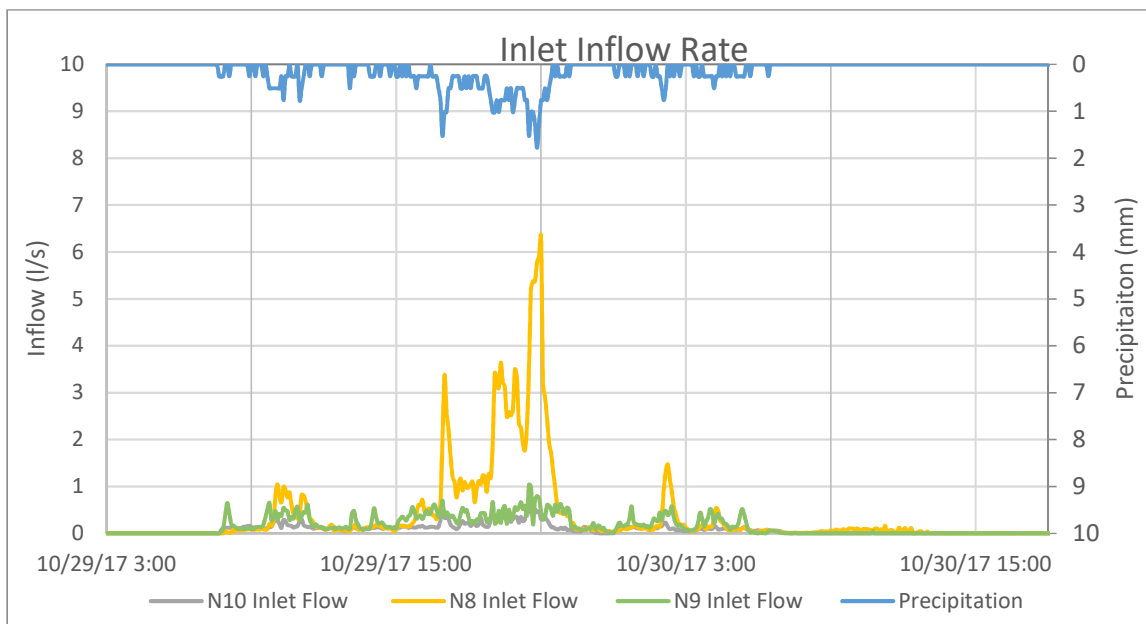


*Figure A2-15: 10/29/17 Inlet Inflows*

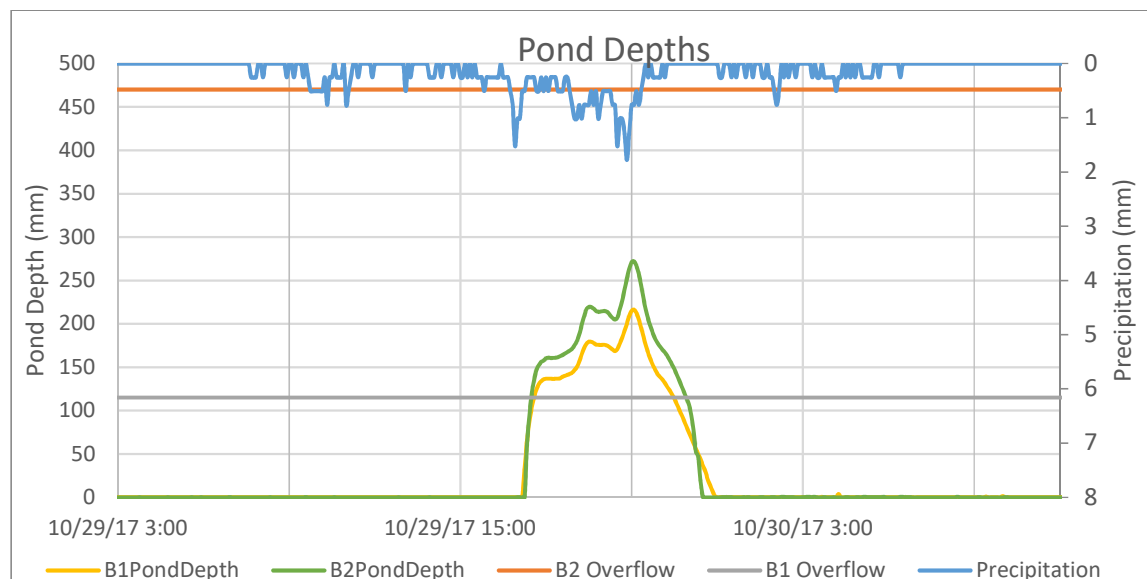


*Figure A2-16: 10/29/17 Pond Depths*

Outflow from this event are presented in Figure A2-17, and soil moisture readings upstream and downstream of the gabion structure in Figures A2-18 and A2-19. Figure A2-17 does show the

overflow for this larger event in which the rainfall exceeds PWD volume reduction expectations. The soil moisture readings in Figures 18 and 19 shows how quickly the soil void space is filled during this event.

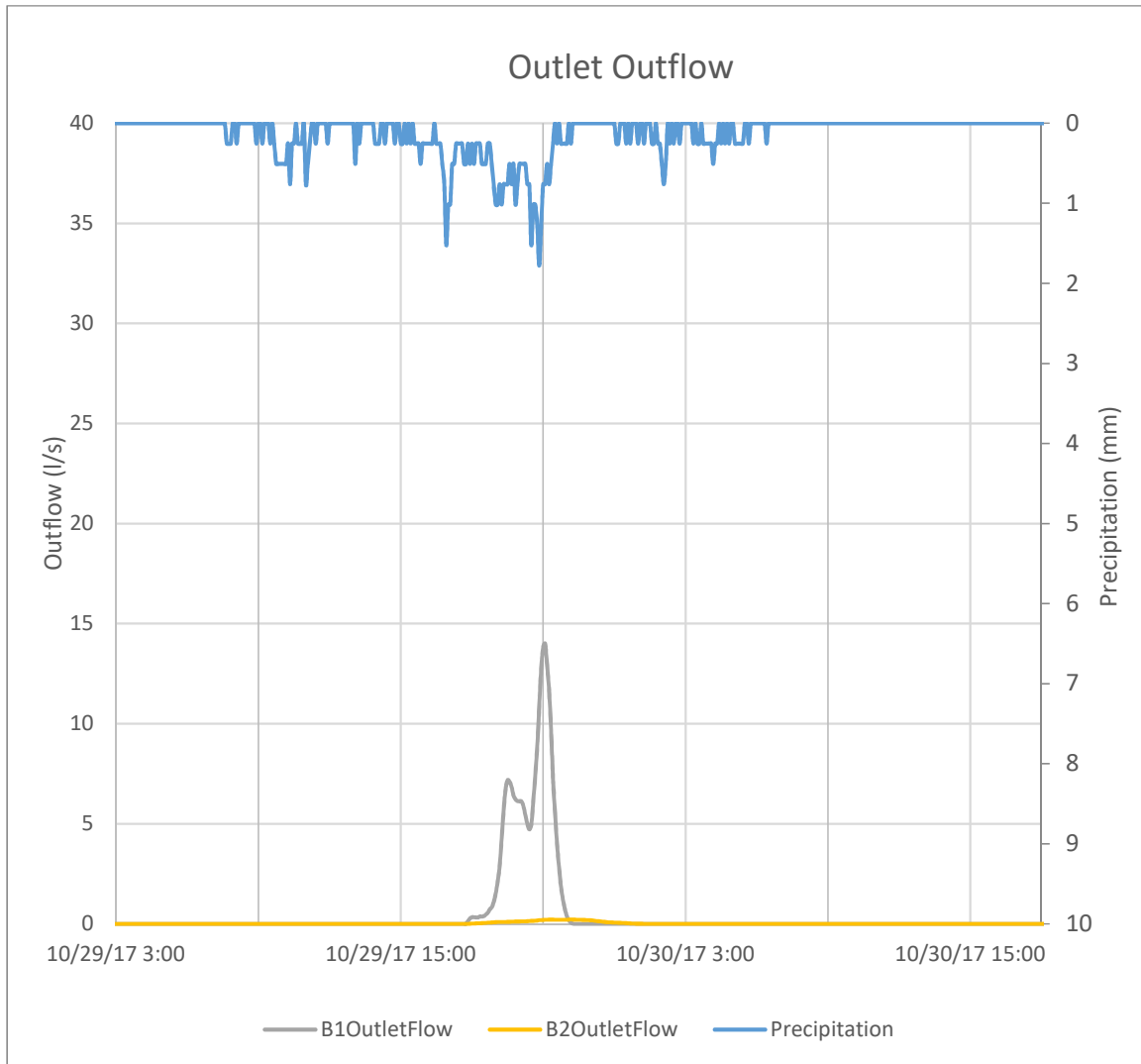


*Figure A2-7: 10/29/17 Outlet Outflows*

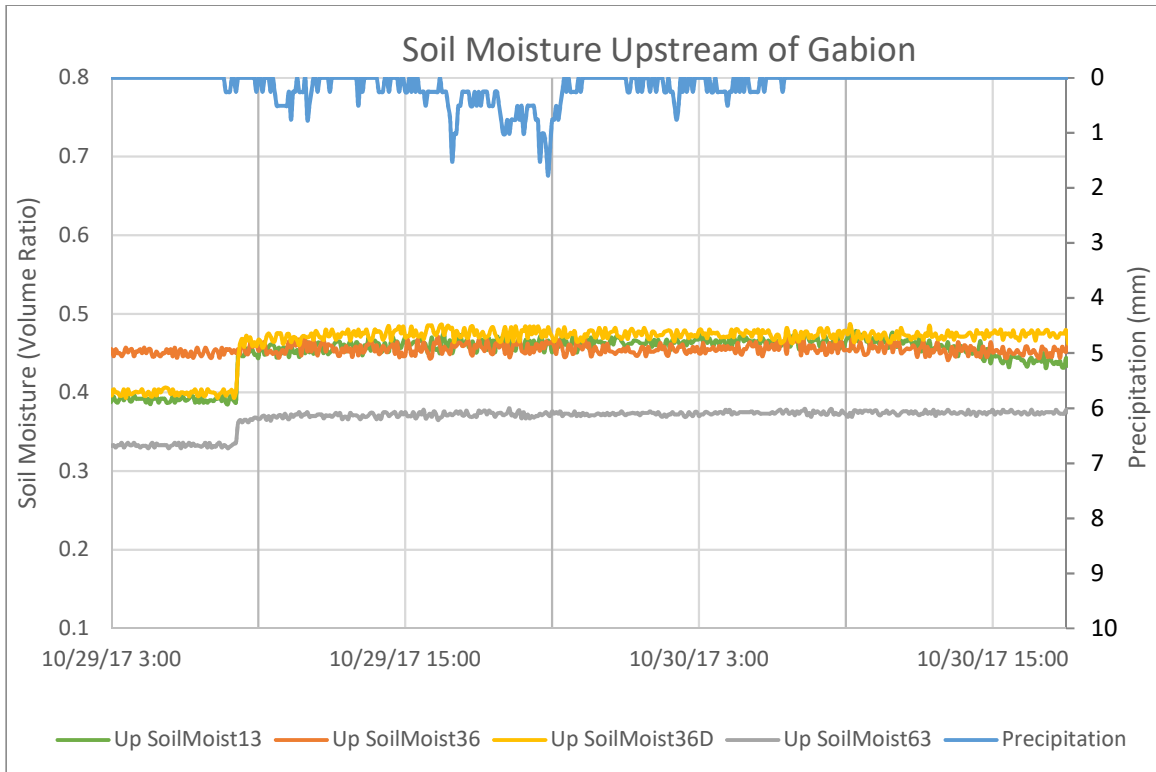


Figure A2-18: 10/29/17 Soil Moisture Upstream of Gabion

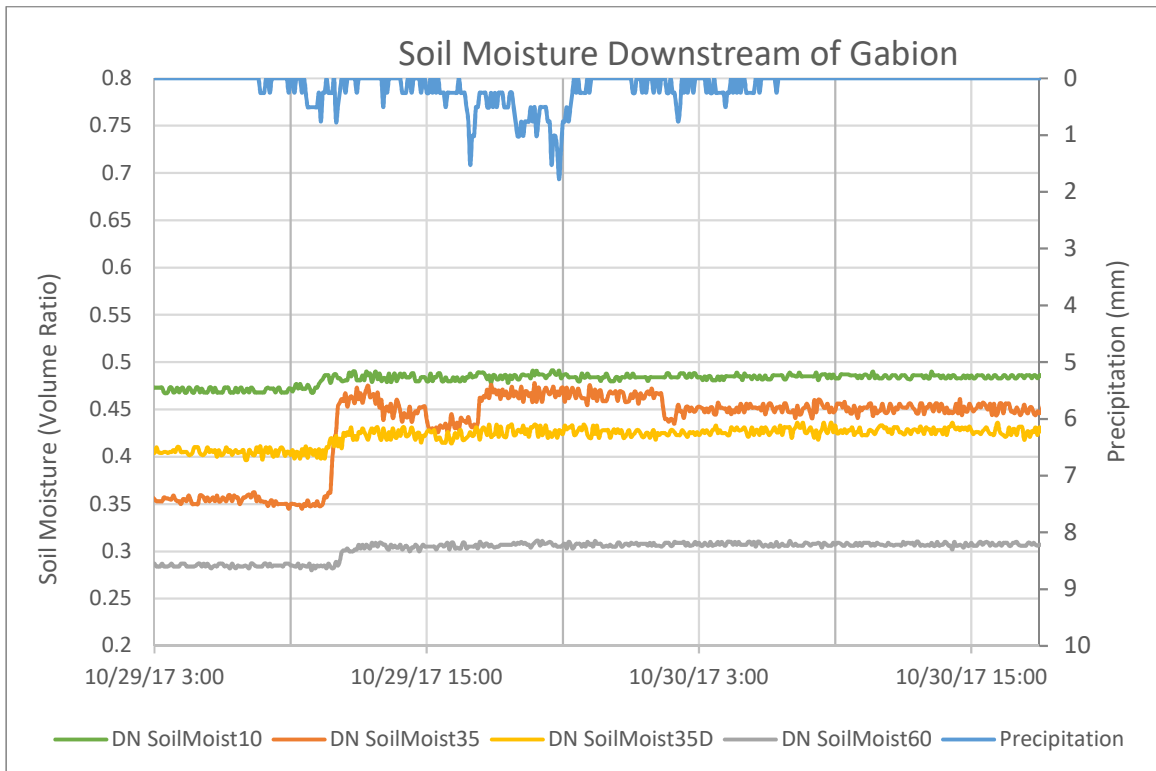


Figure A2-19: 10/29/17 Soil Moisture Downstream of Gabion

## SMP A – Recorded Storm Event Summaries

Following the SRT, twelve events were monitored through the end of October as presented in Table A2-1. The storms included some high intensity events, with the highest storm being over two inches. The highest rainfall event with no overflow was a low intensity 0.74-inch (18.90-mm) event, and the lowest with overflow was a high intensity event of 0.73 inches (18.55-mm). The results coupled with future modeling will greatly assist PennDOT with evaluating the need for retrofitting the outlet structure which is reducing potential performance of the site.

*Table A2-2: Event Statistics*

<b>Event Date</b>	<b>Precipitation Amount (inches)</b>	<b>Duration (hr)</b>	<b>Intensity (in/hr)</b>	<b>Outlet Flow?</b>
07/22/2017	0.53	0.42	1.26	No
07/23/2017	1.26	9.75	0.13	Yes
07/24/2017	0.54	1.50	0.36	No
08/02/2017	0.65	4.33	0.15	No
08/05/2017	0.94	2.42	9.87	Yes
08/18/2017	0.73	0.99	0.34	Yes
08/22/2017	0.75	3.25	0.23	Yes
08/29/2017	0.76	12.42	0.26	Yes
09/02/2017	0.41	16.42	0.02	No
09/06/2017	0.74	19.91	0.04	No
09/16/2017	1.14	2.33	0.49	Yes
10/29/2017	2.61	22.92	0.11	Yes

Similar to SMPs C, D, and G (Figure 6.12) it was found that except for N9, when inflows were related to design drainage areas, the volumes were less than expected (Table A2-2). The contributing area is simply the measured inflow volume, divided by the rainfall, and then divided by the design area. If all the rainfall reached the inlet it would be 100%. We would expect some losses in the pavement resulting in a contributing area percentage between 85 and 100 percent for storms of this size. For some events in N9, the volumes were actually larger, probably due to volumes intended for N8 being redirected to N9.

*Table A2-2: Percent Contributing Drainage Areas Based on AECOM Data*

<b>Event Date</b>	<b>N10 Contributing Area (%)</b>	<b>N9 Contributing Area (%)</b>	<b>N8 Contributing Area (%)</b>
07/22/2017	5.4	23.6	4.8

07/23/2017	8.3	28.3	1.0
07/24/2017	60.4	155.0	20.0
08/02/2017	13.2	47.9	5.2
08/05/2017	15.2	42.7	6.4
08/18/2017	16.4	31.7	2.8
08/22/2017	29.6	53.4	5.6
08/29/2017	79.9	148.1	4.3
09/02/2017	69.3	153.4	4.1
09/06/2017	60.2	138.0	6.2
09/16/2017	12.4	21.6	5.5
10/29/2017	25.7	39.7	13.8

### **SMP A – Summary**

Clearly the instrumentation and data collection in SMP A reinforces the previously made observations as to the importance in understanding how the SMP works, and as an inspection mechanism. An added benefit will be the role of monitoring and modeling in evaluating future steps in resolving any required retrofits for the SMP A outlet structure. Modifications will be evaluated to minimize the retrofit cost. Future monitoring data can support research efforts to resolve the questions about contributing areas and evaluate post-construction stormwater capture.

### **Appendix 3: Calculation of loads in SMPs C and D**

This appendix provides some details of the loading calculations conducted for the executive summary and includes updated values since the draft report. The period covered in this study includes a portion funded by a subcontract with AECOM. A closer approximation to a full year of coverage could only be achieved through the inclusion of data collected prior to the start of the TEM WO 006 project (i.e., data collected before the December 1, 2016).

Table A3-1: Loading estimates in SMP C for each storm based on LiDAR areas with barriers and based on design areas.

<b>SMP C</b>					
<b>Surface Area = 395 m<sup>2</sup></b>					
<b>Drainage Area, LiDAR = 1174 m<sup>2</sup></b>					
<b>Drainage Area, AECOM = 4023 m<sup>2</sup></b>					
<b>TSS<sup>a</sup></b>					
<b>Storm</b>	<b>Runoff, LiDAR (m<sup>3</sup>)<sup>d</sup></b>	<b>Runoff, Design (m<sup>3</sup>)<sup>e</sup></b>	<b>Avg. Concentration (g/m<sup>3</sup>)<sup>f</sup></b>	<b>Load, LiDAR (g)</b>	<b>Load, Design (g)</b>
27-Oct	0.89	3.1	81	73	249
30-Nov	5.1	17	42	211	724
20-Jan	2.0	6.8	87	172	591
7-Feb	5.7	19	142	803	2750
27-Mar	3.7	13	192	700	2397
6-Apr	0.30	1.0	43	13	44
22-May	3.7	13	75	280	958
29-Aug	3.5	12	356	1235	4231
<b>Total (g)</b>				<b>3486</b>	<b>11944</b>
<b>Annual SMP Areal Load (g/m<sup>2</sup>-yr)<sup>g</sup></b>				<b>91</b>	<b>313</b>



NO3- <sup>b</sup>					
Storm	Runoff, LiDAR (m <sup>3</sup> ) <sup>d</sup>	Runoff, Design (m <sup>3</sup> ) <sup>e</sup>	Avg. Concentration (g/m <sup>3</sup> ) <sup>f</sup>	Load, LiDAR (g)	Load, Design (g)
27-Oct	0.89	3.1	4.4	3.9	13
30-Nov	5.1	17	1.1	5.3	18
20-Jan	2.0	6.8	1.4	2.7	9.3
7-Feb	5.7	19	3.4	19	66
27-Mar	3.7	13	2.7	9.8	34
6-Apr	0.30	1.0	2.2	0.65	2.2
22-May	3.7	13	1.9	7.2	25
			Total (g)	49	168
			Annual SMP Areal load (g/m <sup>2</sup> -yr) <sup>g</sup>	1.6	5.3
TP <sup>c</sup>					
Storm	Runoff, LiDAR (m <sup>3</sup> ) <sup>d</sup>	Runoff, Design (m <sup>3</sup> ) <sup>e</sup>	Avg. Concentration (g/m <sup>3</sup> ) <sup>f</sup>	Load, LiDAR (g)	Load, Design (g)
27-Oct	0.89	3.1	0.14	0.13	0.44
20-Jan	2.0	6.8	0.23	0.46	1.6
7-Feb	5.7	19	0.27	1.5	5.1
27-Mar	3.7	13	0.55	2.0	6.9
6-Apr	0.30	1.0	0.11	0.03	0.11
22-May	3.7	13	0.22	0.81	2.8
			Total (g)	5.0	17
			Annual SMP Areal Load (g/m <sup>2</sup> -yr) <sup>g</sup>	0.23	0.79

a. TSS = total suspended solids

b. NO3- = nitrate as nitrogen

c. TP = total phosphorus

- d. Runoff volume determined using LiDAR drainage area measurement and KPNE rainfall data
- e. Runoff volume determined using design drainage area measurement and KPNE rainfall data
- f. Average concentration of samples during storm
- g. Estimation of annual load per surface area of SMP. Based on expected annual rainfall total for Philadelphia using a scaling factor of 10.3 for measured v observed storms.

Table A3-2: Loading estimates in SMP D for each storm based on LiDAR areas with barriers and based on design areas.

<b>SMP D</b>					
<b>Surface Area = 216 m<sup>2</sup></b>					
<b>Drainage Area, LiDAR = 728 m<sup>2</sup></b>					
<b>Drainage Area, AECOM = 866 m<sup>2</sup></b>					
<b>TSS<sup>a</sup></b>					
<b>Storm</b>	<b>Runoff, LiDAR (m<sup>3</sup>)<sup>d</sup></b>	<b>Runoff, Design (m<sup>3</sup>)<sup>e</sup></b>	<b>Avg. Concentration (g/m<sup>3</sup>)<sup>f</sup></b>	<b>Load, LiDAR (g)</b>	<b>Load, Design (g)</b>
<b>27-Oct</b>	0.55	0.66	70	39	46
<b>30-Nov</b>	3.1	3.7	32	100	118
<b>20-Jan</b>	1.2	1.5	43	52	62
<b>7-Feb</b>	3.5	4.2	77	272	323
<b>27-Mar</b>	2.3	2.7	94	214	254
<b>6-Apr</b>	0.18	0.22	22	4.0	4.8
<b>22-May</b>	2.3	2.7	44	102	121
<b>29-Aug</b>	2.5	3.0	314	783	931
<b>Total (g)</b>				<b>1565</b>	<b>1862</b>
<b>Annual SMP Areal Load (g/m<sup>2</sup>-yr)<sup>g</sup></b>				<b>75</b>	<b>89</b>

<b>NO3-<sup>b</sup></b>					
Storm	Runoff, LiDAR (m <sup>3</sup> ) <sup>d</sup>	Runoff, Design (m <sup>3</sup> ) <sup>e</sup>	Avg. Concentration (g/m <sup>3</sup> ) <sup>f</sup>	Load, LiDAR (g)	Load, Design (g)
27-Oct	0.55	0.66	3.3	1.8	2.2
30-Nov	3.1	3.7	0.63	2.0	2.4
20-Jan	1.2	1.5	1.0	1.2	1.4
7-Feb	3.5	4.2	1.8	6.2	7.4
27-Mar	2.3	2.7	1.7	3.9	4.6
6-Apr	0.18	0.22	1.6	0.29	0.3
22-May	2.3	2.7	1.0	2.2	2.7
			<b>Total (g)</b>	<b>18</b>	<b>21</b>
			<b>Annual SMP Areal Load (g/m<sup>2</sup>-yr)<sup>g</sup></b>	<b>1.0</b>	<b>1.2</b>
<b>TP<sup>c</sup></b>					
Storm	Runoff, LiDAR (m <sup>3</sup> ) <sup>d</sup>	Runoff, Design (m <sup>3</sup> ) <sup>e</sup>	Avg. Concentration (g/m <sup>3</sup> ) <sup>f</sup>	Load, LiDAR (g)	Load, Design (g)
27-Oct	0.55	0.66	0.16	0.09	0.10
20-Jan	1.2	1.5	0.14	0.17	0.20
7-Feb	3.5	4.2	0.31	1.1	1.3
27-Mar	2.3	2.7	0.29	0.7	0.8
6-Apr	0.18	0.22	0.09	0.02	0.02
22-May	2.3	2.7	0.16	0.37	0.44
			<b>Total (g)</b>	<b>2.4</b>	<b>2.9</b>
			<b>Annual SMP Areal Load (g/m<sup>2</sup>-yr)<sup>g</sup></b>	<b>0.20</b>	<b>0.24</b>

- a. SS = suspended solids  
b. NO3- = nitrate as nitrogen

c. TP = total phosphorus

d. Runoff volume determined using LiDAR drainage area measurement and KPNE rainfall data

e. Runoff volume determined using design drainage area measurement and KPNE rainfall data

f. Average concentration of samples during storm

g. Estimation of annual load per surface area of SMP. Based on expected annual rainfall total for Philadelphia using a scaling factor of 10.3 for measured v observed storms.

Table A3-3: Loading calculations in SI units for comparison with literature values in Table A3-4

Contaminant	Conc. measured in SMP <sup>a</sup> (mg/L) <i>median</i> <i>[min-max]</i>	Conc. reported in literature <sup>b</sup> (mg/L) <i>median</i> <i>[min-max]</i>	Load measured in SMP <sup>c</sup> (g) <i>median</i> <i>[min-max]</i>	Total load measured in SMP <sup>d</sup> (g)	Predicted annual load <sup>e</sup> (g/yr)	Annual load per surface area measured in SMP (kg/yr/ha)	Annual load per area reported in literature for urban runoff <sup>f</sup> (kg/yr/ha) <i>mean [min- max]</i>	Efficiency reported in literature <sup>g</sup> (mg/L) <i>median</i> <i>[min-max]</i>
<b>SMP C Contributing Drainage Area<sup>h</sup> = 1174 m<sup>2</sup> Basin Surface Area = 395 m<sup>2</sup></b>								
<b>Suspended Solids</b>	80 [0.0-845]	40.6 [2-1200]	245 [13-1235]	3486	36073	307.3	2000 [200-5000]	59 [-100-98]
<b>Nitrate Or TN</b>	1.83 [0.63-7.17] Nitrate	0.35 [0.06-1.2] Nitrate	5.3 [0.65-19] Nitrate	49  Nitrate	616  Nitrate	5.25  Nitrate	5 [2-20] TN	43 [0-76] Nitrate
<b>Total Phosphorus</b>	0.22 [0.066-0.83]	0.13 [0.01-2.0]	0.63 [0.03-2.0]	5.0	91	0.78	0.8 [0.25-5]	5 [-100-65]
<b>SMP D Contributing Drainage Area<sup>h</sup> = 728 m<sup>2</sup> Basin Surface Area = 216 m<sup>2</sup></b>								
<b>Suspended Solids</b>	41 [0.0-600]	40.6 [2-1200]	101 [4.0-783]	1565	16197	222.5	2000 [200-5000]	59 [-100-98]
<b>Nitrate</b>	1.07 [0.13-6.63]	0.35 [0.06-1.2]	2.0 [0.29-6.2]	18	223	3.06	5 [2-20]	43 [0-76]
<b>Total Phosphorus</b>	0.11 [0.057-0.83]	0.13 [0.01-2.0]	0.27 [0.02-1.1]	2.4	44	0.6	0.88 [0.25-5]	5 [-100-65]

See Table E-3 for footnotes (not repeated here).

Table A3-4: Literature loading values from loads per unit area reported in Burton & Pitt (2007) and Shaver (2007) multiplied by Basin C and D SMP areas<sup>a</sup>

	SMP C area g/m <sup>2</sup> /yr	SMP C area kg/ha/yr	SMP D area g/m <sup>2</sup> /yr	SMP D area kg/ha/yr
TSS	83-261	830-2610	94.7-296	947-2960
NO <sub>3</sub>	0.39-1.25	3.9-12.5	0.44-1.42	4.4-14.2
TP	0.18-0.45	1.8-4.5	0.2-0.51	2-5.1

<sup>a</sup> Note that these values are within the ranges reported in EPA 1976, so are encompassed in the values shown in table A3-3 above.